SHRP-H-644

Ice-Pavement Bond Disbonding-- Surface Modification and Disbonding

Albert F. Wuori

Keweenaw Research Center
Michigan Technological University

Strategic Highway Research Program
National Research Council
Washington, DC 1993

SHRP–H–644
Contract H-204

Program Manager: *Don M. Harriott*
Project Manager: *David Minsk*
Production Editor: *Cara J. Tate*
Program Area Secretary: *Francine Burgess*

June 1993

key words:
ice adhesion - countermeasures
ice - radiation absorption
ice control
ice removal - chemical
roads - ice control
snow removal

Strategic Highway Research Program
National Academy of Sciences
2101 Constitution Avenue N.W.
Washington, DC 20418

(202) 334-3774

350/NAP/693

Acknowledgments

The research described herein was supported by the Strategic Highway Research Program (SHRP). SHRP is a unit of the National Research Council that was authorized by section 128 of the Surface Transportation and Uniform Relocation Assistance Act of 1987.

This final report was prepared by the Keweenaw Research Center (KRC), Michigan Technological University (MTU) and the subcontractors, Midwest Research Institute (MRI), Iowa Institute of Hydraulic Research (IIHR), Cold Regions Research and Engineering Laboratory (CRREL), and Research Associates of Syracuse (RAS) under SHRP Contract H-204. The report covers the work done during 1989-90 until termination of the contract.

Mr. L. David Minsk was the SHRP Project Manager for the contract. The report was prepared by Mr. Albert F. Wuori, Principal Investigator, with assistance of the following:

Mr. Robert R. Blackburn (MRI)	-Passive Pavement Modifications
with assistance from	-Surface Texture
John B. Jones, and	-Deformable Pavement
Howard W. Christie (MRI)	
and Robert Eaton and	
Richard J. Roberts (CRREL)	
Dr. Kazuhiko Itagaki (CRREL)	-Plunger Application of Deicer
Mr. Jack Monson (RAS)	-Microwave Radiation
Dr. Wilfrid Nixon (IIHR)	-Cutting Edge Experimental Program
Dr. Michael Ohadi (MTU)	-Abrasive-Liquid Jets
Mr. Mark Osborne (KRC)	-Abrasive-Air Jets
Dr. James Rogers (MTU)	-Acoustic Waves
Dr. Carl Vilmann (MTU)	-Cutting Edge Profiles-Design Analysis

Several state highway officials lent their assistance in providing core samples of highway pavements for use in the experimental portion of the program. Special acknowledgment and appreciation are due for assistance given by key members of the highway or transportation department staffs of California, Connecticut, and New York.

TABLE OF CONTENTS

Abstract

Current techniques to remove ice and compacted snow from pavement surfaces are costly because they needlessly crush or melt most of the ice layer. Also, in many cases they do not accomplish disbonding or clear the ice to the pavement interface. In addition, deicing chemicals currently in use (salts) are environmentally objectionable. More efficient alternatives to current physical and chemical methods are needed which will apply energy selectively to the ice - pavement interface to accomplish disbonding and which are environmentally acceptable.

This research program has explored new techniques of disbonding ice. Pavement modifications included differences in surface texture or composition; one example being a rubber additive to create a more flexible pavement surface to facilitate disbonding under traffic loads. Noncontact methods included electromagnetic radiation, abrasive air and liquid jets, acoustic waves, and application of pressurized deicer directly to the ice-pavement interface. Contact techniques included analyses and experiments to develop a more energy efficient cutting edge for snow plows which may include auxiliary force augmentation.

It was concluded that several of the techniques have potential for highway use but need further development. In the pavement modifications area, changes in surface texture or geometry did create greater shear forces under traffic loads than smooth surfaces, however insufficient to disbond ice. Microencapsulation of deicers for release during icing conditions using interfacial polymerization techniques was not possible. The addition of coarse rubber aggregate to asphaltic pavement surfaces to create a deformable surface for disbonding indicated good potential for ice release. However, further investigation of pavement integrity and increased rolling resistance is necessary.

In the non-contact techniques, the use of microwave radiation to disbond ice appears feasible. However, attainment of realistic highway speeds is difficult and requires further study. Abrasive liquid and abrasive-air jet removal both appear quite feasible at realistic highway speeds. Further investigation of preventing pavement damage is necessary. The application of acoustic waves does not appear promising. The use of a spike-plunger to apply deicer to the ice-pavement interface appears somewhat promising but requires further investigation to determine the time required for ice disbonding.

In the contact area, improved geometry of cutting edges, particularily provision of a 15 to 30° rake angle, results in significant energy savings in cutting ice from pavement surfaces. The use of pretreatment such as rolling the ice surface to create cracks results in additional energy savings.

Executive Summary

The research described in this report was funded by the Strategic Highway Research Program (SHRP) under Contract SHRP-88-H-204 to the Keweenaw Research Center (KRC) of Michigan Technological University (MTU) as prime contractor in May of 1989 for a period of four years. Other performers under subcontract to MTU included Midwest Research Institute, Iowa Institute of Hydraulic Research, U. S. Army Cold Regions Research and Engineering Laboratory, and Research Associates of Syracuse. Total funding for the contract was to be approximately $1.5 million.

The program included physical pavement modifications to facilitate ice disbonding by traffic action or other external energy; application of energy by non-contact means to unmodified pavements; and contact methods such as cutting edges with optimized geometry and augmentation.

It was concluded that several of the techniques have potential for highway use but need further development. In the pavement modifications area, changes in surface texture or geometry did create greater shear forces under traffic loads than smooth surfaces, however insufficient to disbond ice. Microencapsulation of deicers for release during icing conditions using interfacial polymerization techniques was not possible. The addition of coarse rubber aggregate to asphaltic pavement surfaces to create a deformable surface for disbonding indicated good potential for ice release. However, further investigation of pavement integrity and increased rolling resistance is necessary.

In the non-contact techniques, the use of microwave radiation to disbond ice appears feasible. However, attainment of realistic highway speeds is difficult and requires further study. Abrasive liquid and abrasive-air jet removal both appear quite feasible at realistic highway speeds. Further investigation of preventing pavement damage is necessary. The application of acoustic waves does not appear promising. The use of a spike-plunger to apply deicer to the ice-pavement interface appears somewhat promising but requires further investigation to determine the time required for ice disbonding.

In the contact area, improved geometry of cutting edges, particularly provision of a 15 to 30° rake angle, results in significant energy savings in cutting ice from pavement surfaces. The use of pretreatment such as rolling the ice surface to create cracks results in additional energy savings.

After a period of one and one-half years and an expenditure of $650,000, project H-204 was terminated because it was determined that none of the approaches except for the cutting edge designs, were sufficiently developed to be put into practice during the life of the SHRP program.

Introduction

Ice and snow conditions on highway and airport pavements cause serious disruptions to transportation of goods, services, and people. Further, the annual costs of winter highway maintenance due to ice and snow removal is on the order of $1 billion annually in the United States. Included in this is the use of salt which is approaching an alarming 10 million tons per year.

Sodium chloride has been the chemical of choice because of its effectiveness at low temperatures (eutectic of -6°F [-21°C]), relatively low (first) cost, and its ready availability. However, the damaging effects of salt usage in terms of the roadside environment, water supplies, vehicles, and highway structures are of increasing concern. Current national salt usage is about $350 million. However, the National Bureau of Standards has estimated automobile corrosion costs attributable to salt use were about $1.2 billion per year. Therefore, other chemical alternatives to salt are being used at an increasing rate. Calcium Magnesium Acetate (CMA) is one such chemical which is non-corrosive and environmentally more acceptable. However, its purchase price is about 20 times that of salt.

Current mechanical techniques to remove ice and compacted snow from pavement surfaces are insufficient since they needlessly crush most of the ice layer. Also, in many cases, they do not accomplish disbonding or clear the ice completely to the pavement. Methods which will selectively apply energy to the ice-pavement interface to accomplish disbonding should prove less costly and more efficient.

The Strategic Highway Research Program (SHRP) of the National Academy of Sciences established a project in March 1989 to investigate and develop more energy efficient and environmentally acceptable methods. The contract, awarded to Michigan Tech University, sought to develop methods in three areas: (1) pavement modification to facilitate disbonding; (2) non-contact disbonding, and (3) improvement in contact (cutting-edge) techniques. The project has evaluated a number of approaches in 1989 and 1990. This final report describes the research and results and presents an evaluation of the efficacy of each approach.

Research Approaches and Results

General Research Approach

The general research approach was to first review the literature for a state-of-the-art appraisal of previous investigations. The next step was to coordinate with, and closely review the results obtained under, other ongoing SHRP investigations. This included the work conducted under SHRP Contract Nos. H-201 and H-203 which were fundamental studies on ice bond prevention and ice disbonding. Also, the work of the contractor on SHRP Contract No. H-206 in regard to cutting edge designs was coordinated with this project.

The following step in the investigation was to analytically evaluate the potential effectiveness of a broad range of possible techniques. The results of the literature review and analytical studies eliminated a number of approaches and indicated the most promising for laboratory investigations. Laboratory work was then conducted under carefully controlled conditions on a relatively small scale. The most promising techniques for pavement modification and devices for contact and non-contact disbonding of ice were then to be chosen for demonstration to SHRP. Upon approval from SHRP, two cutting edge designs (with or without augmentation by jets or other forces) were to be fabricated for the H-206 contractor. At least three pavement modification techniques would be incorporated into a field testing program as well as at least two non-contact device prototypes, provided the techniques and prototypes showed promise for implementation.

To accomplish the contract objectives, a highly structured multi-task research program was established. The multi-year research program consisted of five tasks, with each task consisting of between three and six subtasks. The five tasks were:

- Task 1--Physical Pavement Surface Modifications
- Task 2--Non-contact Disbonding Methods
- Task 3--Contact Methods
- Task 4--Field Tests on Pavement Modifications and Non-contact Disbonding Methods.
- Task 5--Final Reports and Manuals of Practice

Tasks 1, 2, and 3 continued for a period of one and one-half (1 1/2) years. At that time, it was determined that none of the approaches, except for cutting edge designs, were sufficiently developed to be put into practice during the life of the SHRP program. Therefore, they were terminated and Tasks 4 and 5 were not implemented.

Physical Pavement Surface Modifications

Introduction

The breaking and dislodging of ice on compacted snow is required only on ice/snow that has significant mechanical strength. Loose snow or sleet may present a removal problem, but it does not need to be dislodged and broken from the pavement. In the following discussion, attention is directed primarily to the thin layer that is likely to be left on the pavement after conventional plowing or snow blowing.

The solution to the ice-pavement bond disbonding problem is to produce desirable fractures in the ice/snow layer. There are two aspects to desirable fractures. Most importantly, it is necessary to cause fractures at the ice-pavement interface or in the ice very close to the interface. This type of fracture is required to obtain bare pavement conditions. The second aspect involves energy conservation. Energy requirements for breaking and dislodging are minimized when the number of fractures or fracture surfaces are minimized. (It is desirable to produce large rather than small fragments.) The efficiency of the fracturing process is also important.

It has been hypothesized that the passage of passenger car and truck tires may contribute to the breaking and dislodging of a snow/ice layer. Failure of this layer may result from the application of a single large load or from fatigue caused by the replicated application of smaller loads. Tires of motor vehicles in motion apply both vertical and horizontal (shear) loads to an ice/snow layer. No measurements of the forces imposed on snow/ice layers are readily available. Consequently, the following discussion depends on the measured forces applied to roadway pavements and the possible effects of these forces on ice/snow layers postulated by Blackburn and St. John (1).

The local pressures under the tire footprints need to be examined in conjunction with the mechanical properties of snow and ice. The highest contact pressures under treaded passenger car tires can approach the ultimate compressive stress for compacted snow. This means that uncompacted snow will yield under passenger car tires; snow density and strength will increase until ultimate strength equals the applied stress. Trucks will provide even higher stresses, leading to more compaction and strength than generated from passenger car passages. And, even without higher stresses, strength will increase as the result of metamorphic processes which include the sublimation of water from ice crystal surfaces and deposition back on other ice surfaces. The result is generally a stronger porous structure.

The stress distribution under a tire footprint is not uniform. However, the distribution does not contain point or line concentrations that would effectively initiate fractures in the ice/snow. The most pronounced concentrations are located at the sides of the footprint where the loads carried by the side walls appear. These concentrations would

probably be more elevated in isolated areas if measurements were made with tire tread patterns.

A tire imposes a load that is primarily vertical and induces primarily compressive stresses in the ice/snow. This kind of loading is relatively ineffective for producing fractures in the ice/snow layer. A tire also imposes shear stresses at the tire-ice/snow interface that could be beneficial in disbonding the ice/snow from the pavement. However, this effect may be diminished by the low friction coefficient between tire and ice/snow. The coefficient of friction will usually be less than 0.5. As a result, the pattern and magnitude of shear stresses imposed by the tire is limited by the coefficient of friction and is considerably less than the stresses indicated by tire-pavement measurements.

Passive Pavement Modifications

Objective and Scope of Work

The objective of the work dealing with passive pavement modifications was to investigate various pavement modifications that could be used in combination with passages of wheeled vehicles to break the ice-pavement bond. The scope of the work was both analytical and experimental in nature. The pavement surface modifications selected for study were not to affect the structural integrity of the pavement, nor to seriously degrade the frictional characteristics of the surface. The modifications selected for field trial were to be economical to manufacture, install and maintain, have a long service life, be nontoxic and noncorrosive, and be effective over a wide range of climate and traffic conditions. Also, the materials selected should not prevent recycling nor result in greatly increasing reprocessing costs. Finally, the ability of the pavement surface modifications to meet many of the stated requirements down to 0°F (-18°C) needed to be demonstrated in the laboratory.

A three-pronged approach was followed in an attempt to accomplish the above objective while still satisfying as many of the pavement modification requirements as possible. The first approach was an investigation of pavement surface texture features that are potentially effective in concentrating stresses and initiating cracks at the ice-pavement interface to promote disbonding under wheel passage conditions. This investigation was accomplished using finite element analysis (FEA) methods. The second approach involved the formulation of an asphalt concrete mix design that was modified to include a gradation of rubber aggregate. The third approach involved the development of laboratory equipment and the subsequent testing of the various pavement modifications considered. Each of these three approaches is described in the following sections.

1. Investigations of Surface Texture Modifications Using FEA Methods

An analytical investigation was conducted to determine if pavement surface texture modifications could be used to promote ice pavement disbonding under wheel passage loadings. The approach used finite element analysis (FEA) to determine the feasibility of destroying the ice-pavement interfacial bond with wheel passage loads. The Algor FEA software package was used to compute the interfacial compressive and shear stresses generated by a rolling tire on ice-covered portland cement and asphaltic concrete pavements.

The FEA work begun under SHRP Contract H-203 was extended by considering both vertical and horizontal (shear) loads to an ice layer of the magnitude representative of wheeled passages. Various surface texture features, similar to those used under Contract H-203, were used in the analytical investigation.

The results of the analytical studies were used to guide the development of laboratory experiments discussed later in this section. These laboratory experiments were designed to test the efficiency of using wheel passages to break the ice-pavement bond when certain pavement surface treatments and modifications are used.

The first modeling efforts with the Algor FEA software package consisted of duplicating some of the simpler analysis results achieved under SHRP Contract H-203. The duplicated runs were designed to help in the software familiarization process plus provide a check of the previous results.

The models used in this initial effort were simple two-dimensional (2-D) representations of 1/2-in. thick ice on rigid substrates with a uniformly applied shear stress of 100 psi applied to the top surface of the ice as shown in Figure 1. Both a smooth substrate (Figure 1) and a substrate with a square waveform at the interface (Figure 2) were considered in the modeling. The interfacial shear stress computed under Contract H-203 for the square wave profile and a smooth surface are presented in Figure 3. The results for a sinusoidal and a triangular waveform are also presented in Figure 3.

The interfacial shear stress results computed using the Algor software package for the square wave profile and a smooth surface are given in Figure 4 and are essentially identical to those presented in Figure 3.

More complex 3-D models were then developed. These 3-D models described the resultant stresses in the ice layer and at the ice-pavement interface that were induced by the tire's compressive and shear forces applied to the surface of the ice. The stresses at the tire-ice interface varied with the location in the footprint area. The 3-D models were designed to be representative of the small area of ice located directly beneath the

sidewall of a conventional tire as shown in Figure 5, where the stresses are at their greatest magnitude.

The forces incorporated in the models included a vertical load, corresponding to an average 30 psi (2.1 x 10^5 Pa) footprint pressure; a frictional force corresponding to a longitudinal shear stress of 6 psi (4.1 x 10^4 Pa) over the footprint area; and a transverse force, corresponding to a maximum cross shear stress of 20 psi (1.4 x 10^5 Pa) over the footprint area. The vertical load represented a portion of the vehicle weight and acted normal to the ice. Spatial variations of the vertical load lead to peak contact compressive stress values of 70 psi, for radial tires, near the edge of the footprint beneath the tire's sidewall. The frictional force, a function of the vertical load and the coefficient of friction between the ice and the rubber tire, acted as a shear force at the surface of the ice in a direction opposite to the direction of travel of the tire. The third force, a cross shear force, acted on the surface of the ice at a 90-degree angle to the frictional force. This transverse force results from the tire trying to expand into a larger footprint area.

Stress distributions in the ice layer beneath the tire were computed for a number of cases which included portland cement concrete and asphaltic concrete substrates. The substrate surface configurations investigated consisted of smooth surfaces and surfaces with specific contours such as square and sinusoidal waves of various amplitudes and wavelengths. The square contours were used to simulate pavement grooving conditions. The thickness of the ice layer considered in the numerical computations ranged from 1/8 in. (0.32 cm) to 3/8 in. (0.95 cm).

The resultant stress concentrations at the ice-pavement interface from the above combinations of loads and ice-pavement configurations were not of sufficient magnitude to promote favorable disbonding. The stress concentrations found at the edge of the footprint were an order of magnitude too small to initiate crack propagation.

More complex models were developed to represent rubber-modified asphalt pavement. Stress computations were made for cases considering discrete rubber particles at the ice-pavement interface and pavement grooves filled with strips of rubber. The FEA results of ice bonded to rubber-modified (aggregate) asphalt did indicate that cracks at the ice-pavement interface could be developed because of localized deformation of the rubber particles/strips at the interface. These encouraging results with rubber-modified asphalt served to focus attention on this type of passive pavement modification. Further FEA investigations of this type of pavement modification were halted in favor of an experimental evaluation of the material. The formulation and laboratory testing of rubber-modified (aggregate) asphalt are discussed in the next two sections.

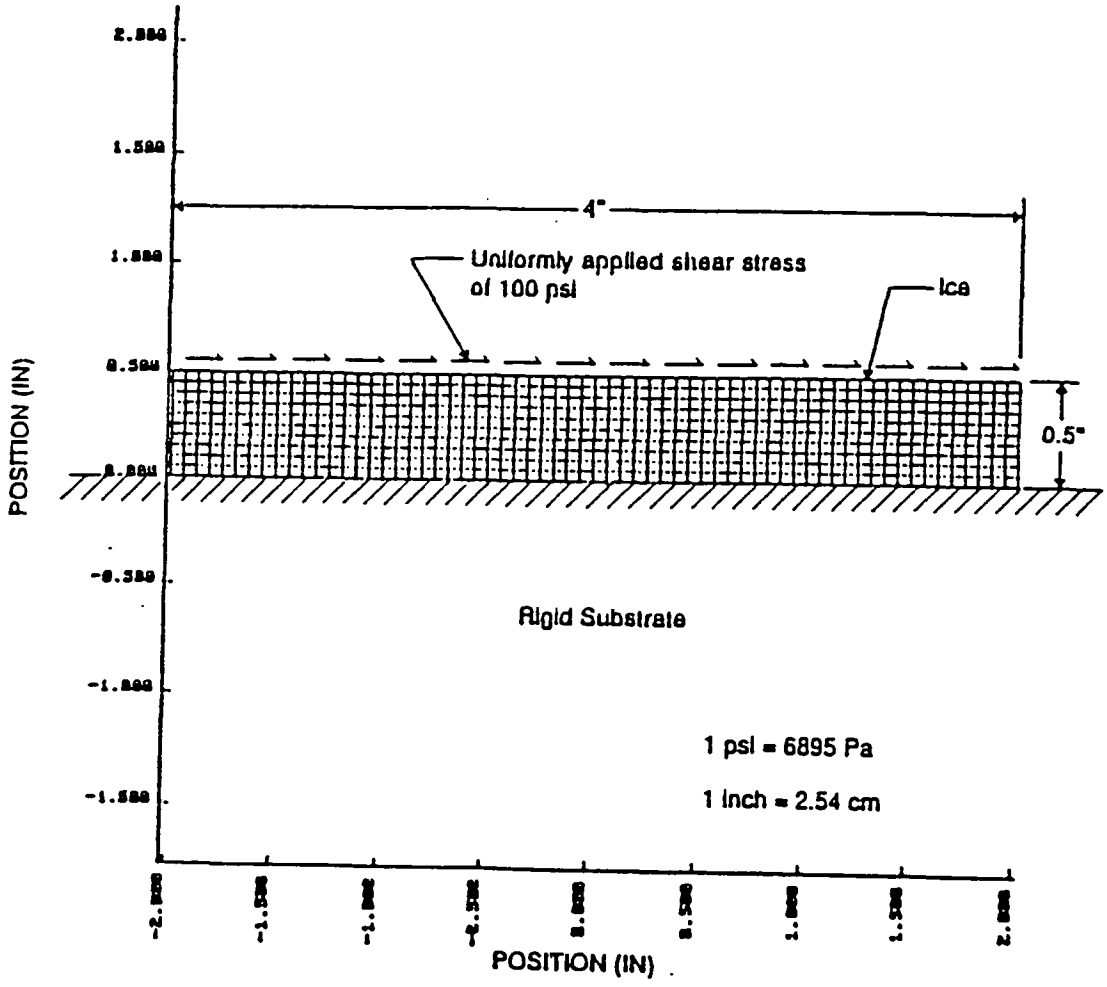

Figure 1. FEA simulation geometry for ice substrate shear tests with horizontal load applied to the free surface of the ice.

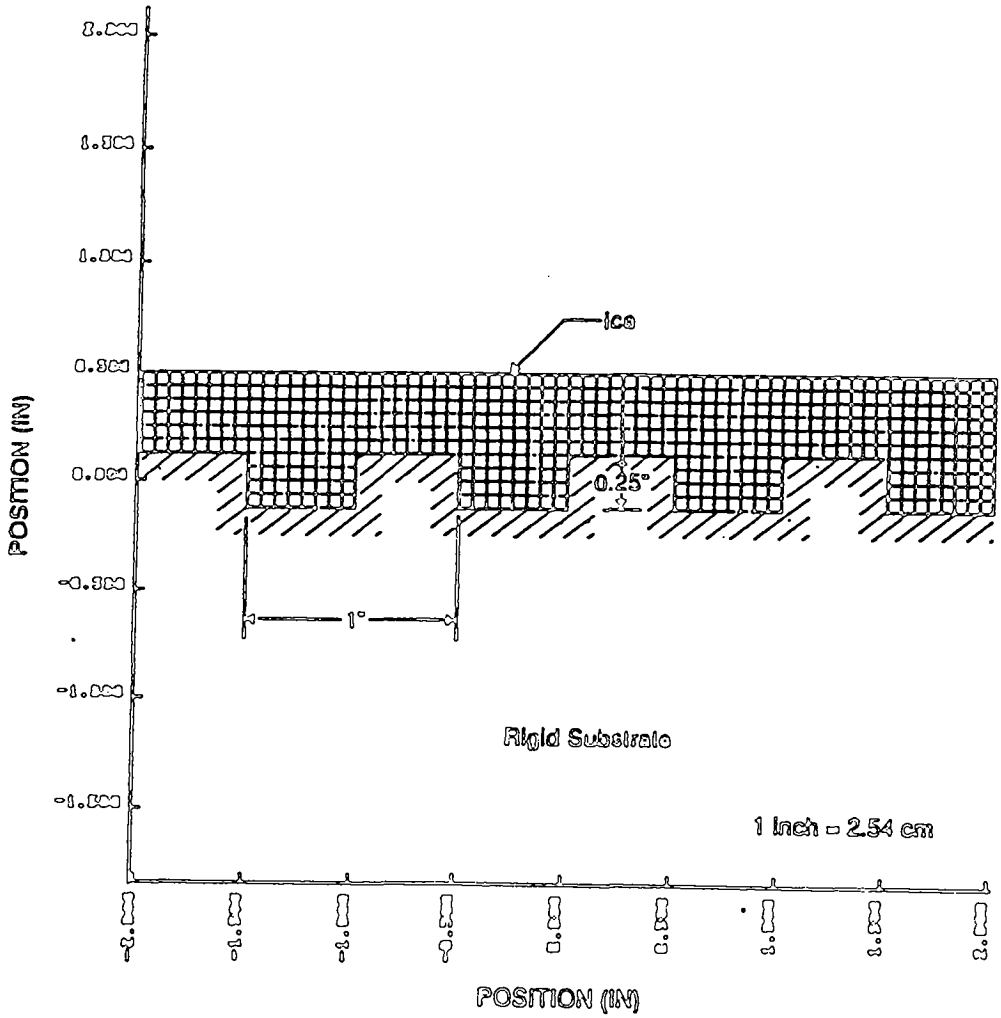

Figure 2. Profile of ice on a square wave substrate.

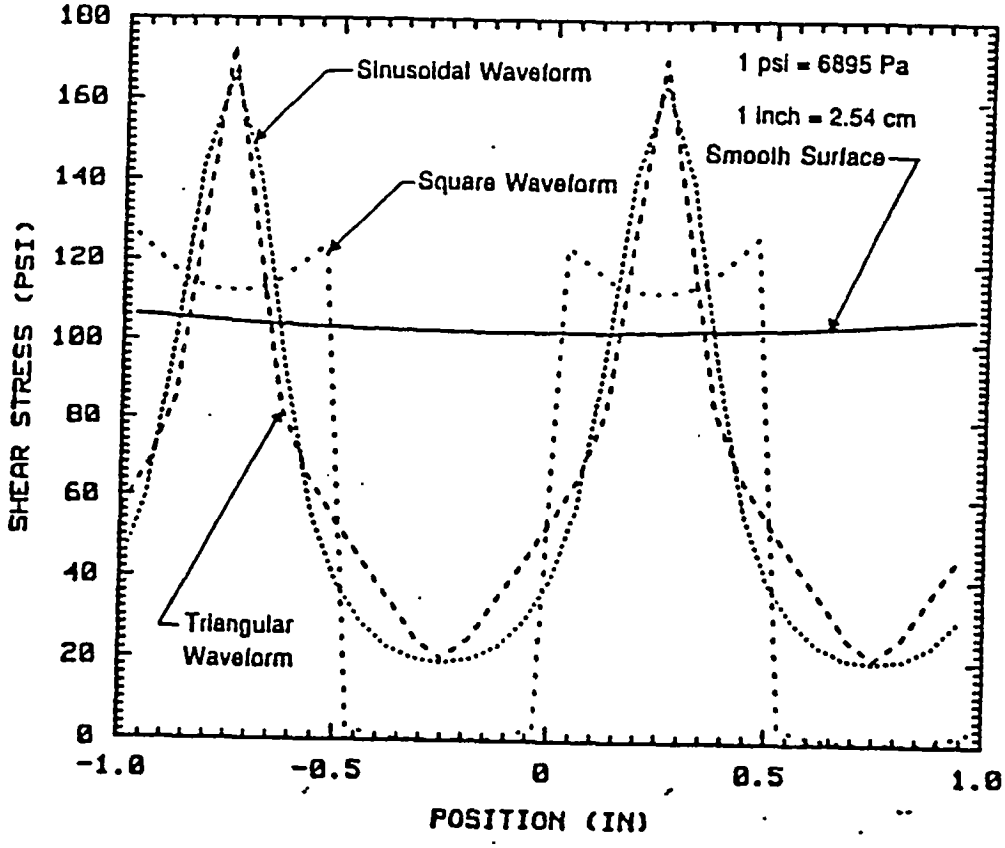

Figure 3. Effect of waveform on the ice-substrate interfacial shear stress from a uniformly applied shear stress on the top surface of the ice.

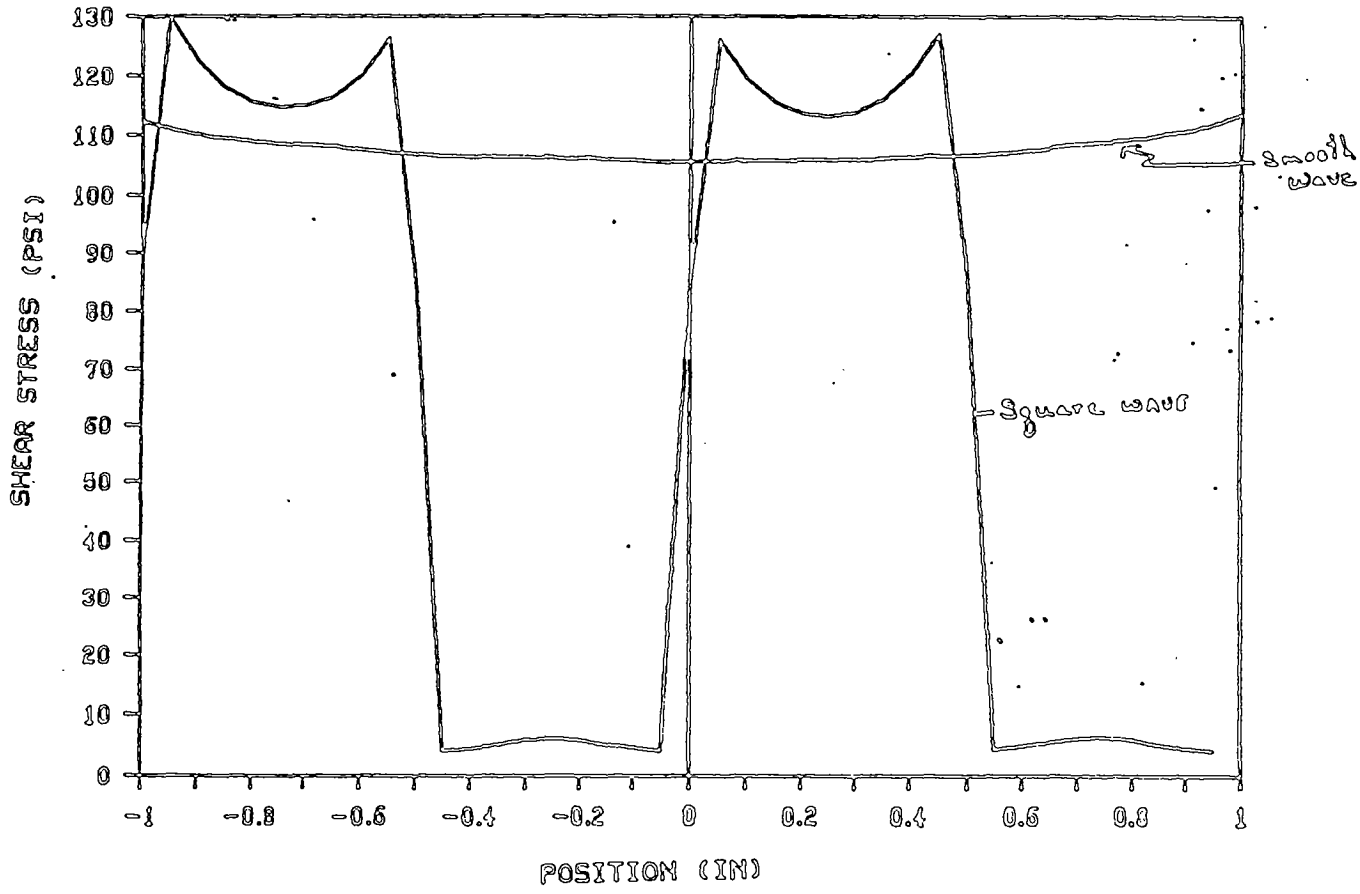

Figure 4. Effect of waveform on the ice-substrate interfacial shear stress from a uniformly applied shear stress on the top surface of the ice.

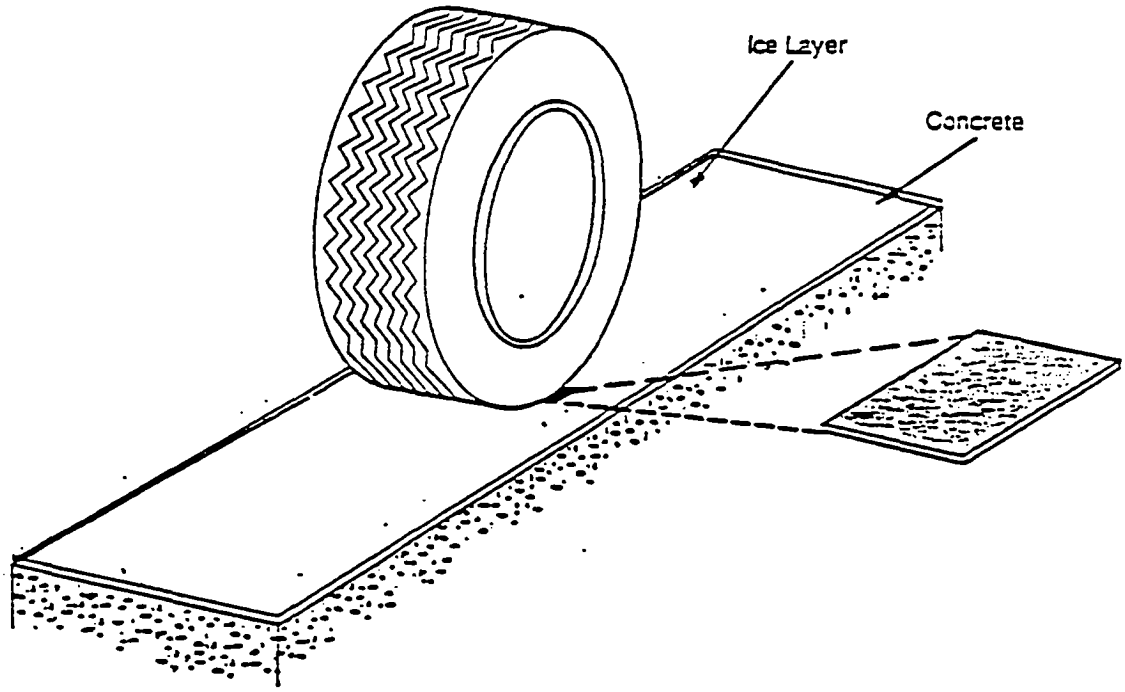

Figure 5. Tire-ice layer-pavement system showing footprint area investigated.

2. *Formulation of Rubber-Aggregate Asphalt Concrete*

Introduction

Passive pavement modifiers have been used in the past to either prevent ice from bonding to the roadway surface or to weaken the bond sufficiently so that the ice can be disbonded with wheel passages. These modifications have included the chemical additive Verglimit and various rubber additives derived from scrap rubber.

In the 1970s a deicer called Verglimit was developed by Chemische Fabrik Kalk in Cologne, West Germany, and tested in Europe as a means of improving ice control. Verglimit consists of particles (0.1 to 5 mm) of calcium chloride with a small amount of sodium hydroxide. This mixture is coated with a water-resistant layer of either linseed oil or polyvinyl acetate and is used as an integral part of the wearing course. The encapsulation keeps the material inactive until the particles break under the action of traffic. The additive then mixes with moisture in the air or on the pavement to form a salt solution on the pavement surface. The material has been used with mixed results in Europe, Japan, Canada, and in the United States. There have been unsubstantiated reports that the skid resistance of the pavement with Verglimit may be low in dry weather and that the life of the pavement may be reduced up to 50 percent (2). Because of these drawbacks and the general concern about chemical additives, it was decided the investigation of passive pavement modifications would focus on the use of rubber additives in asphaltic concrete. Consequently, no work was done with chemical additives to pavement materials.

Each year the United States disposes of about 200 million passenger tires and 40 million truck tires. This represents about 2.1 million tons of scrap passenger tires and roughly 1.9 million tons of scrap truck tires (3). One method of disposing of this huge amount of waste material is to recycle the ground rubber tires into the asphalt pavement.

In recent years, a growing number of state departments of transportation and municipalities have started to use scrap rubber to modify asphaltic pavements. Two different methods of incorporating scrap tire rubber into paving mixes have been developed. The first type of rubber modification uses finely ground rubber tire buffings that are mixed into the hot asphalt cement to create a rubberized asphalt binder. This binder is then added to a normal gradation of paving aggregate. This type of modification is called asphalt rubber concrete.

In the late 1960s, two Swedish companies, Skega AB and AB Vaegfoerbaettringar, developed the second type of rubber modification in a product named "Rubit." The Swedish design incorporated 3 to 4 percent rubber (by weight of a mixture) into an asphalt pavement surface mixture to increase skid resistance. The mixture provided a new form of ice control as well as reduced pavement/tire interaction noise (2). The overall mix consists of blending the larger rubber particles [1/16-in. (0.16-cm) up to

3/8-in. (0.95-cm) in size] into a gap graded aggregate mix, substituting the rubber particles for some stone aggregate. Thus, the rubber particles are relatively large compared to the particles used in the asphalt rubber concrete. In addition, the larger rubber particles are thought to act as elastic aggregates which flex on the pavement surface under traffic and contribute to ice disbondment.

In the United States, the trademark "PlusRide" is used to designate the Swedish formulation. PlusRide rubber is derived from granulating whole tires and tire buffings, and contains chopped cords. The recommended specifications for PlusRide paving mixtures for different levels of traffic are given in Table 1.

Many states and municipalities have placed, or are in the process of placing, test sections containing PlusRide derived from ground rubber tires. At least 18 states across the nation from Rhode Island to California, and even Alaska, have built test sections using PlusRide (2,3).

Because of the widespread interest in the PlusRide paving mixtures, it was decided to further concentrate the investigation of passive pavement modifications on the use of rubber aggregate. In particular, it was of interest to study the addition of higher concentrations of rubber to enhance the ice disbonding characteristics of this type of pavement modification.

Research Procedure

The initial investigation of rubber-modified asphalt concrete consisted of making some laboratory samples of the PlusRide mix with 3 percent by weight of a gradation of rubber particles substituted for the respective gradation of stone aggregate. Additional samples were then made by increasing the rubber content to 6 percent and 12 percent by weight (see Table 2).

The Marshall method of mix design was used to determine the optimum asphalt content according to ASTM D-1559. Five sets of samples were prepared for each mix design using varying percent asphalt contents. Three specimens were made for each level of percent of asphalt content, for a total of 15 samples for each mix design. The typical asphalt content range used for each mix design was 5 percent, 5 1/2 percent, 6 percent, 6 1/2 percent, and 7 percent of total aggregate weight. After testing, the data were plotted and the optimum asphalt content was determined by the curves generated. If the optimum asphalt content level could not be made from the first set of samples, more samples were made using more or less asphalt content until the optimum was determined. Guidelines and experience were then used in selecting the best mix from the materials considered. The final mix design for each rubber content selected was a balance of optimum asphalt content, air voids, stability, and flow.

Table 1. Recommended specifications for rubber-asphalt (PlusRide) paving mixtures for different levels of traffic.

Mix Designation	PlusRide 9	PlusRide 12	PlusRide 16
Average Daily Traffic	< 2500	2500-10,000	> 10,000
Thickness (in.) minimum	0.75	1.5	1.75
Aggregate % Passing			
Sieve Sizes:			
3/4 in.	-	-	100
5/8 in.	-	100	-
1/2 in.	-	-	65-80
3/8 in.	100	60-80	50-60
1/4 in.	60-80	30-42	30-42
No. 10	23-38	19-32	19-32
No. 30	15-27	13-25	12-23
No. 300	7-11	8-12	6-10
Preliminary Mix Design:			
Rubber, % of Total Mix			
by weight	3.0	3.0	3.0
by volume (approx.)	6.7	6.7	6.7
Asphalt, % of Total Mix			
by weight	7.5	7.5	7.5
by volume (approx.)	20.2	20.2	20.2
Maximum Voids (%)	2	2	2

Table 2. Mix designs for PlusRide

	Control 0 Percent Rubber 6 Percent A.C.		3 Percent Rubber 6 1/2 Percent A.C.				6 Percent Rubber 7 Percent A.C.				12 Percent Rubber 9 1/2 Percent A.C.			
			Rubber		Stone		Rubber		Stone		Rubber		Stone	
Sieve	% Passing	grams	%	grams	%	grams	%	grams	%	grams	%	grams	%	grams
1/2	100	0			100	0			100	0			100	0
3/8	80	240			70	300			69	285	80	21.6	71	229.6
No. 4	60	240			36	340			34	323	60	21.6	39	253.4
No.10	40	240	1	10	25	110	3	28.5	26	76	40	21.6	28	87.1
N0. 30	20	240	1	10	19	60	3	28.5	20	57	20	21.6	20	63.4
No. 200	10	120	1	10	10	90			11	85	0	21.6	10	79.2
PAN	10	120				100				95			10	79.2
Stone		1200				1000				921				792
Rubber		0				30				57				108
Asphalt		72				67				68.5				86

Test Materials

The stone aggregate used in the study was a Maryland gravel with the No. 4+ sieve size put through a crusher. The material was obtained from the SHRP aggregate storage facility in Texas.

The rubber aggregate used was obtained from Baker Rubber, Inc. It consisted of ground rubber produced from passenger and/or truck tires with a majority of the fabric removed. The maximum fabric content by weight was 0.5%.

The asphalt cement used was an Oklahoma Crude AC20. It was supplied in 5-gallon buckets and delivered cold.

Development of Rubber-Aggregate Asphalt Concrete Mix Design Based on the PlusRide Concept

The stone aggregate was sieved into the following sizes: 3/8, 1/4, No. 10, No. 30, No. 200, Pan. The 3/8 and 1/4 aggregate was then washed to remove fines. The material was weighed and combined in a metal pan and placed in an oven set at 350°F (177°C). The stone was placed in the oven in the afternoon and used the next morning. The asphalt was heated in a seamless tin with the cover on just prior to using. When the asphalt temperature reached 280°F (138°), the rubber aggregate was combined with the stone aggregate. The stone and rubber was then put in the oven for 5 to 10 min. The material was removed from the oven, placed on a balance, and tared. The asphalt

cement was added to the mix in the amount that depended upon percentage desired. The mixture was mixed until uniform and then compacted following the standard 50-blow Marshall procedure for a 4-in. (10.2-cm) diameter mold.

The samples were allowed to cool overnight and then extracted from the molds for testing.

The Marshall stability values were obtained for the four different rubber-aggregate asphalt mixes following ASTM D-1559. The average Marshall stability results are shown in Table 3. The optimum Marshall values for the four mix designs considering 0 percent, 3 percent, 6 percent, and 12 percent rubber content are presented in Table 4. The stability values for the 3 percent rubber-aggregate asphalt in Tables 3 and 4 are greater than the average value of 411 obtained from field test section results in Alaska with a 3 percent rubber-aggregate asphalt mix.

Table 3. Average Marshall stability results.

Asphalt Content	Rubber Content (by weight)			
(% by weight)	0 percent	3 percent	6 percent	12 percent
4	890			
5	1596		380	
5 1/2		530		
6	1888	540	398	
6 1/2		617		212
7	1478	583	407	
7 1/2		458		258
8			327	
8 1/2				297
9			298	
9 1/2				350
10				
10 1/2				277

The resilient modulus was also determined for the four different rubber-modified asphalt mixes following ASTM D-4123. This repeated-load indirect tension test method is conducted by applying compressive loads with a prescribed waveform and can be used to study effects of temperature, loading rate, and rest periods. Consequently, the values

of resilient modulus can be used to evaluate the relative quality of bituminous mixtures as well as to generate input for pavement design or pavement evaluation and analysis.

Table 4. Optimum Marshall values.

	Percent Rubber by Weight			
Percent Asphalt Content	0	3	6	12
6.0	1888			
6.5		616		
7.0			406	
9.5				350
Percent Air Voids	4.0	4.6	4.7	4.0

The resilient modulus was computed using the following expression:

$$M_R = \frac{P(\upsilon + 0.2734)}{tD}$$

where P = vertical load
υ = Poisson's ratio
t = specimen thickness
D = horizontal deformation

Mean values of M_R for the four mix designs are given in Table 5 as a function of temperature and pulse (load) time. The mean resilient modulus is also plotted in Figures 6 and 7 as a function of temperature. In Table 5, a 0.05-sec load time simulates 40 to 50 mph traffic conditions, and a 0.10-sec load time simulates a 15 to 25 mph traffic condition. A Poisson's ratio value of 0.35 was used in all the computations.

From Table 5 and Figures 6 and 7 it can be seen that the mean resilient modulus for the 3 percent rubber mix is roughly half of that for the mix with no rubber (0 percent). Likewise, the mean resilient modulus for the 12 percent rubber mix is roughly half of that for the mix with 6 percent rubber content. Basically, this trend remains the same as the load time is increased from 0.05 sec to 0.10 sec. The resilient modulus of the 0 percent rubber asphalt concrete shows the largest decrease in strength between the two loading times, especially at 40°F (4°C).

The resilient modulus increased with a decrease in temperature; also, as the load time increased, the resilient modulus decreased. Similar results were reported by Takallou et al. (3).

Table 5. Mean resilient modulus.

M_R (kg/cm² x 10^3)

	Pulse Time (sec)					
	40°F (4°C)		77°F (25°C)		100°F (38°C)	
Percent Rubber	0.05	0.10	0.05	0.10	0.05	0.10
0	12.142	7.251	1.647	1.319	0.277	0.214
3	6.030	4.717	0.665	0.526	0.113	0.089
6	3.544	3.592	0.476	0.384	0.077	0.061
12	2.096	1.742	0.250	0.194	0.048	0.035

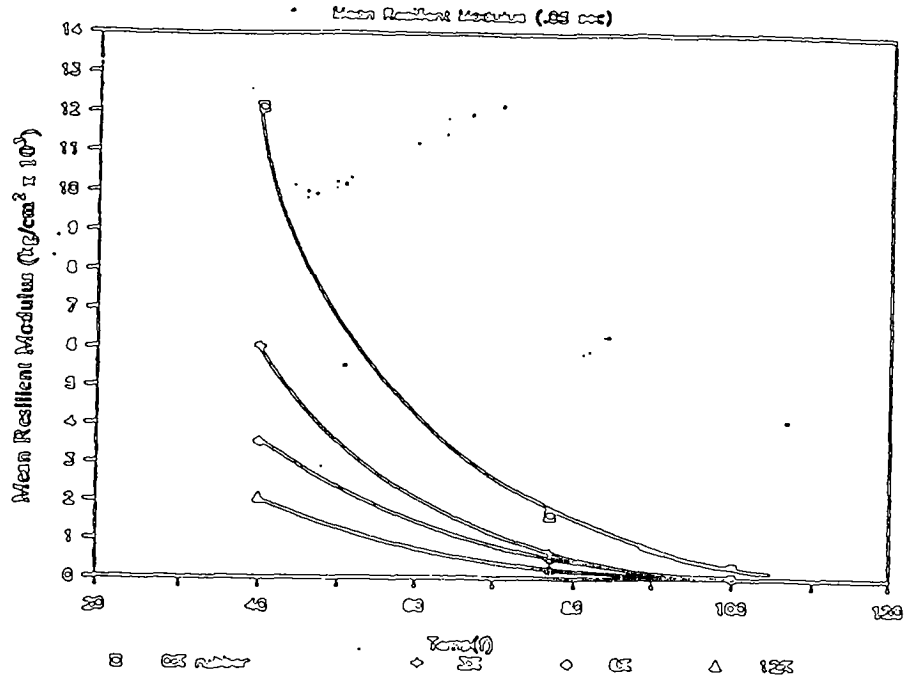

Figure 6. Mean resilient modulus for a 0.05-sec load time of four mix designs based on the PlusRide concept.

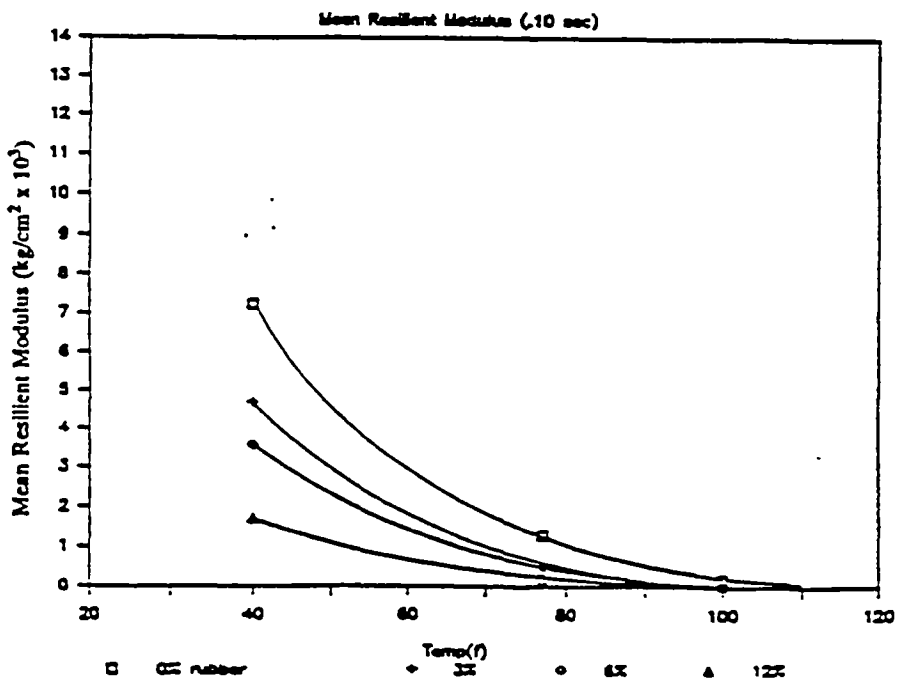

Figure 7. Mean resilient modulus for a 0.10-sec load time of four mix designs based on the PlusRide concept.

The creep modulus was also determined for the four mix designs. The creep modulus M_C is basically the same kind of measurement as M_R. The term is used as a convenience to indicate long loading times compared to the loading times used in the resilient modulus tests. For the creep test, 1000-sec load times (approximately 16 min) are used.

Table 6 and Figures 8 and 9 show the creep test results. Tests were not conducted at 40°F (4°C) as they were with the resilient modulus tests.

Table 6. Creep tests. 1000-sec second load time.

Load (kg)	Rubber (%)	Temperature (°C)	Total (cm x 10^{-4})	Mean Creep Modulus (kg/cm^2 x 10^3)
4.536	0	25	8.3	0.0508
		38	20.7	0.0204
	3	25	28.7	0.0157
		38	46.5	0.0097
	6	25	40.5	0.0114
		38	58.5	0.0079
	12	25	58.8	0.0076
		38	84.2	0.0053

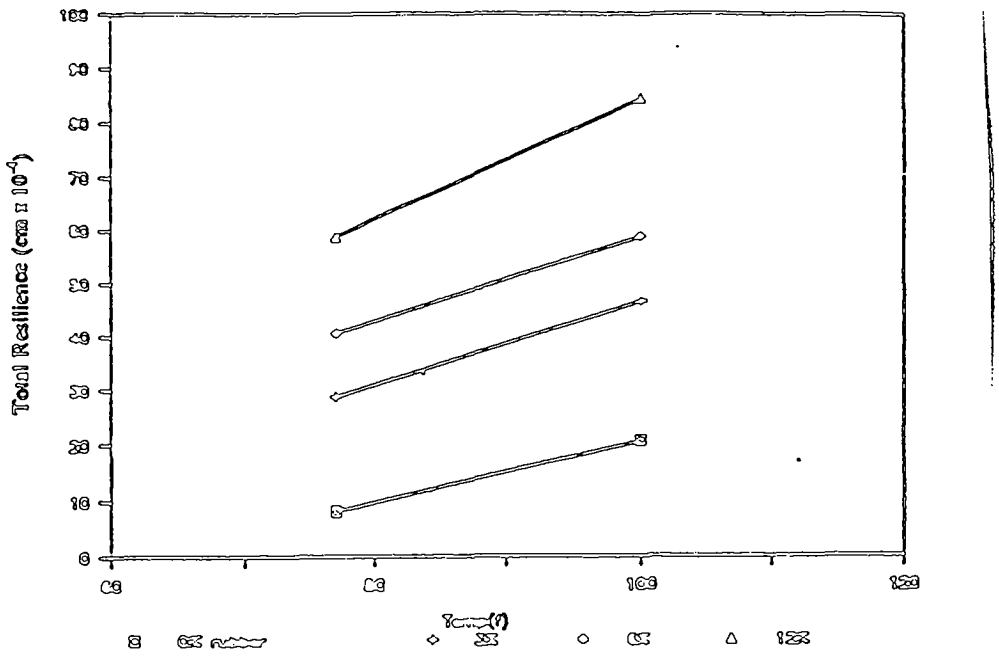

Figure 8. Total resilience of four mix designs based on the PlusRide Concept.

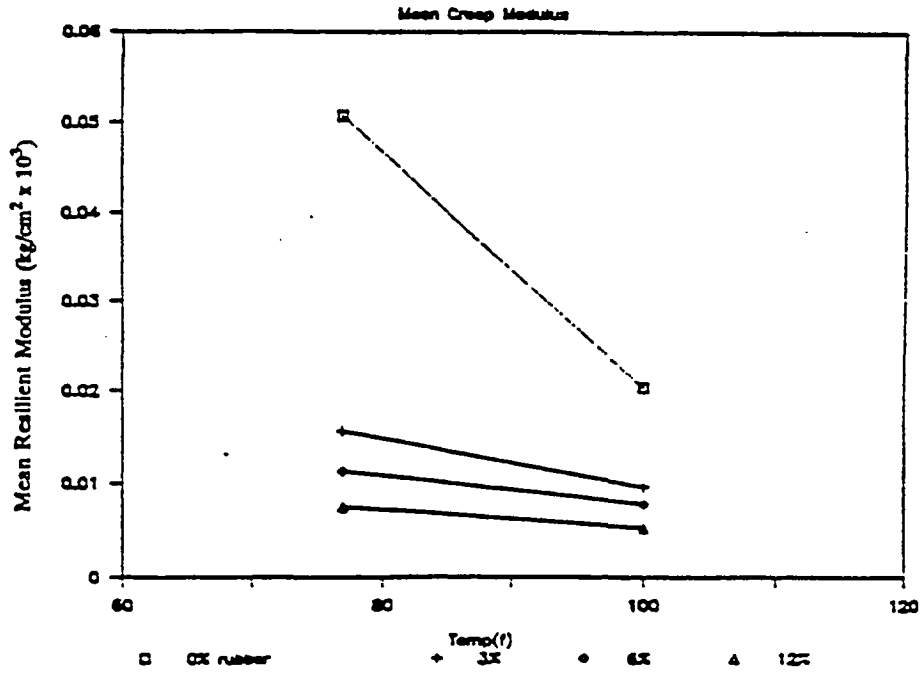

Figure 9. Mean resilient modulus of four mix designs based on the PlusRide concept.

Table 6 shows that the mean creep modulus is reduced, for a given temperature, by adding rubber to the mix. By adding just 3 percent rubber, the mean creep modulus is reduced by 1/3 from 0.05 to 0.016 at 77°F (25°C). The presence of rubber in the mix also stiffens the mix at higher temperatures, or reduces the rate of creep, as shown by the flatter slopes in Figure 9 of the rubber mixes versus the 0 percent mix.

The total creep, however, as shown in Figure 8, is higher for the rubber mixes, pointing out the benefits of their performance at lower temperatures, that is, greater elasticity.

Simulated traffic (wheel passage) tests of ice grown on the PlusRide rubber-aggregate asphalt samples were somewhat encouraging (see next section). The test results did not show significant ice disbonding but did suggest a way the mix design could be altered to improve the ice disbonding performance under traffic conditions. It was decided to increase the size of rubber aggregate to increase the potential for ice disbonding under wheel loadings. Consequently, further testing of the PlusRide mix concept was halted in favor of testing larger rubber aggregate mix designs.

Revised Chunk Rubber Asphalt Concrete (CRAC) Mix Design

A conclusion of the first part of the study was that the maximum size of rubber aggregate should be increased to promote more of an area-wide flexure of the ice/substrate interface under traffic loadings.

A new rubber-modified asphalt concrete mix design was developed, and various maximum sizes of rubber aggregate were tested. Based upon laboratory results and simulated traffic testing, the new mix design was defined (see Table 7).

The Chunk Rubber Asphalt Concrete (CRAC) mix design is denser than the original PlusRide mix designs first tested; however, the rubber aggregate is larger. Based upon current rutting problems and prior research results (4), it was decided to design for a minimum 3 percent air voids.

This finer mix may solve some of the surface aggregate loss experienced by the California Department of Transportation (CALTRANS) on their Route 395 test sections south of Ravendale (5,6,7). The higher air voids may also solve bleeding problems experienced by the Alaska Department of Transportation (7,8).

Table 8 presents the CRAC Marshall stability results and shows that the 3 percent, 6 percent, and 12 percent rubber mixes are more than twice as strong as the original mixes. Table 9 shows the final CRAC mix designs for 0 percent, 3 percent, 6 percent, 12 percent, 25 percent, 57 percent, and 100 percent rubber content.

Table 7. Chunk rubber asphalt concrete mix design.
Control--no rubber.

Sieve	Desired Percent Passing	Range
1/2	100	100
3/8	85	80-90
N0. 4	60	55-65
No. 10	40	35-45
No. 30	20	15-25
No. 200	5	0-10
(% by wt)		
Asphalt Cement	6	5.5-6.5

Table 8. Average Marshall stability results.

Asphalt Content	Rubber Content (by weight)			
(% by weight)	0%	3%	6%	12%
5.5	1600 (5.6)[a]			
6.0	1755 (4.6	950 (5.8)		
6.5	[b] 2025 (3.0)	1120 (4.9)	530 (6.3)	
7.0	2270 (2.2)	[b] 1310 (3.5)	605 (5.9)	
7.5	1885 (1.5)	1130 (3.0)	[b] 850 (4.1)	
8.0		1125 (0.6)	825 (3.3)	470 (5.3)
8.5			800 (2.7)	670 (4.2)
9.0				[b] 690 (3.1)
9.5				650 (2.8)
10.0				640 (1.8)

[a]Air voids - percent total mix.
[b]Optimum.

Table 9. Chunk rubber asphalt concrete mix designs.

% Rubber:	0	3			6			12		
	Stone Passing	Rubber Retained		Stone Passing	Rubber Retained		Stone Passing	Rubber Retained		Stone Passing
Sieve	(%)	(%)	(g)	(%)	(%)	(g)	(%)	(%)	(g)	(%)
1/2	100	0	0	100	0	0	100	0	0	100
3/8	85	2	21.6	87	3	31.1	89	6	57.4	93
No. 4	60	1	10.8	65	3	31.1	69	6	57.4	80
No. 10	40			40			40			40
No. 30	20			20			20			20
No. 200	5			5			5			5
Asphalt Cement (% total weight of aggregate)	6.0	6.5			7.5			9.5		
Rubber (% total weight of aggregate)	0	3			6			12		
Air Voids	3.0	3.5			4.1			3.1		

(continued)

Table 9 (continued)

% Rubber:	25[a]			57[a]			100[a]		
	Rubber Retained		Stone Passing	Rubber Retained		Stone Passing	Rubber Retained		Stone Passing
Sieve	(%)	(g)	(%)	(%)	(g)	(%)	(%)	(g)	(%)
1/2	0	0	100	0	0		0	0	100
3/8	3	24.0	100	10	61.7		85	68.8	100
No. 4	9	78.9	100	20	123.5		60	114.7	100
No. 10	13	102.9	73	20	123.5		40	91.7	100
No. 30			20	6.7	41.4	36	20	91.7	100
No. 200			5			9	5	68.8	0.1 0.59[b]
							Pan	22.9	0
Asphalt Cement (% total weight of aggregate)		12		16				20	
Rubber (% total weight of aggregate)		25		57				100	
Air Voids		8.7[c]		Did not measure			Could not measure		

NOTE: All figures are for standard 4-in. 0 Marshall pucks.

[a]No marshall Mix Design done for these three mixes.

[b]No stone added.

[c]Average of three samples.

Table 10 shows that the control (0 percent rubber content) CRAC mix design is more dense-graded than the corresponding PlusRide mix.

Table 10. Control Mix Design.

Rubber (%): Sieve (% passing by weight	PlusRide Mix 12	Control	Chunk	Rubber	Asphalt	Concrete
	0	0	0	3	6	12
5/8 in.	100	100	100	100	100	100
1/2 in.	-	95-100	-	-	-	-
3/8 in.	60-80	85-95	85	87(2)	89(3)	93(6)
1/4 in.	30-42	60-75	60	65(1)	69(3)	80(6)
No. 10	19-32	38-50	40	40	40	40
No. 30	13-25	19-27	20	20	20	20
No. 200	8-12	2-6	5	5	5	5
Asphalt (% total mix by weight)		7.5	6.4	6.5	7.0	9.5

Table 11. Mean resilient modulus for chunk rubber asphalt concrete (CRAC).

	40°F (4°C) Pulse (sec)	77°F (25°C) Pulse (sec)	100°F(38°C) Pulse	Time	Pulse	Time
% Rubber	0.05	0.10	0.05	0.05	0.05	0.10
0%	16.978	10.799	2.353	1.920	0.520	0.401
3%	8.321	6.462	0.705	0.533	0.244	0.193
6%	4.997	3.698	0.591	0.465	0.198	0.147
12%	2.934	2.352	0.300	0.228	0.094	0.069

The Mean Resilient Modulus results shown in Table 11 and in Figures 10 and 11 show that the CRAC mixes have higher resilient moduli at all temperatures and at both loading times. This is due to the finer, denser mix. The stronger mix will support higher loads, resist rutting better, and provide a stronger matrix from which the rubber particles will project above for better ice disbonding performance. The results of the ice disbonding tests under wheel passage conditions are discussed later in this section.

Rolling Resistance on Rubber-Aggregate Asphalt Pavements

A thorough review of the literature was undertaken concerning the addition of rubber particles to asphalt pavement mixes, with a particular emphasis on the potential increase in rolling resistance on rubber-aggregate asphalt surfaces.

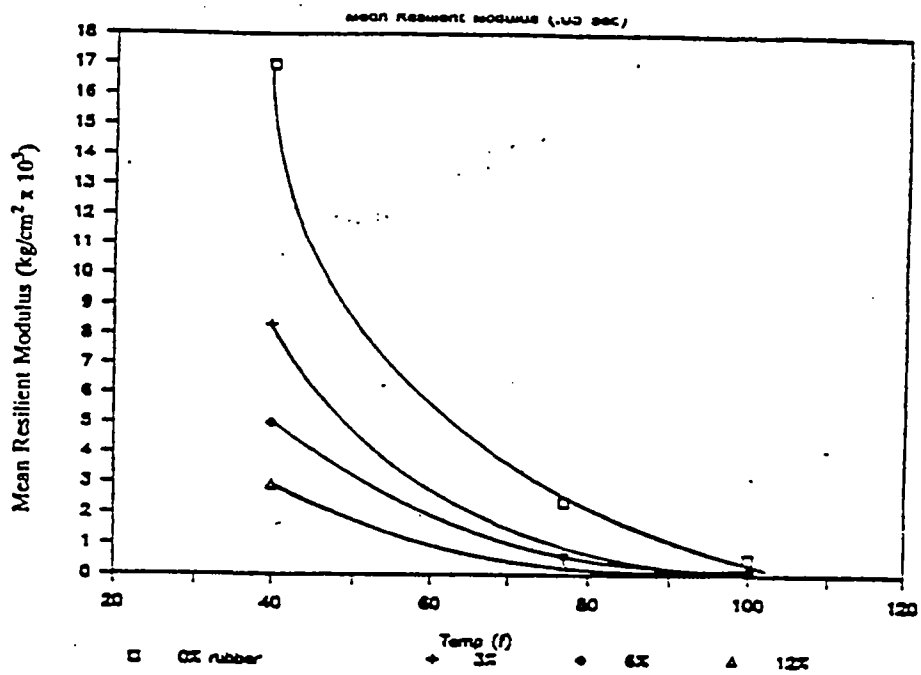

Figure 10. Mean resilient modulus for a 0.05-sec load time of various CRAC mix designs.

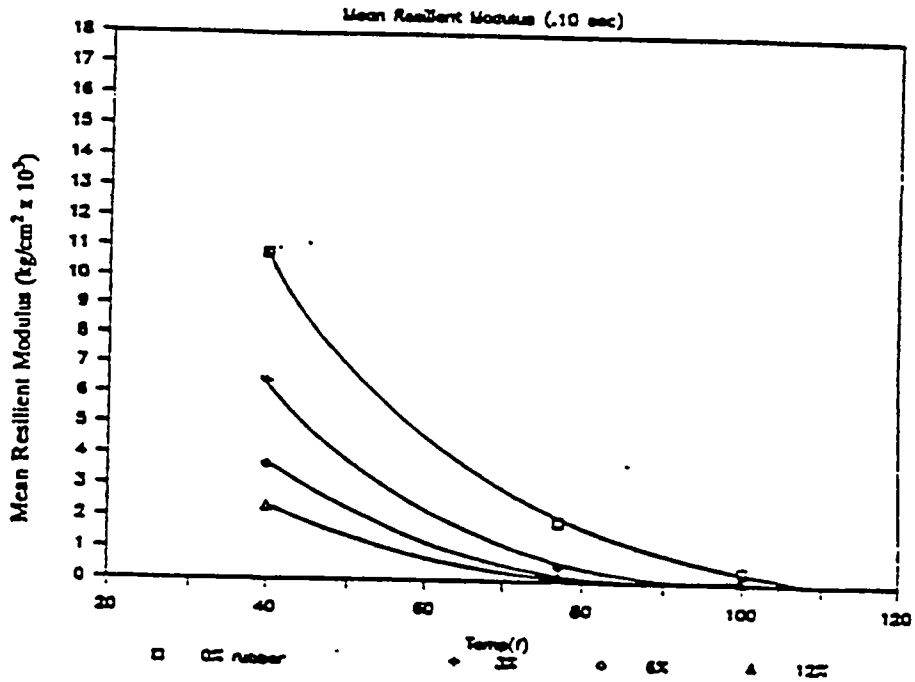

Figure 11. Mean resilient modulus for a 0.10-sec load time of various CRAC mix designs.

Rubber-modified asphalt surfaces have been constructed for evaluation purposes in at least 18 states, including Alaska, California, Kansas, Massachusetts, Minnesota, Missouri, Montana, Nevada, New Jersey, New Mexico, New York, Oklahoma, Rhode Island, South Dakota, Tennessee, Texas, Utah, and Washington (2,9-13). An extensive evaluation program of rubber-aggregate asphalt surfaces with rubber content from 1 to 3 percent rubber by weight is currently being conducted by the California Department of Transportation (Caltrans). The surfaces constructed by Caltrans with a rubber content of 3 percent were made with the PlusRide material (9,10).

No data were found in the literature that directly evaluated the rolling resistance of a rubber-aggregate asphalt surface. Laboratory data on the properties of a PlusRide mixture, including the modulus of resiliency, were found in a recent evaluation by the Federal Highway Administration (FHWA) (2). Table 12 and Figure 12 show the resilient modulus of a PlusRide pavement specimen (3 percent rubber content by weight), as a function of temperature and sample age, in comparison to a conventional asphalt pavement specimen. However, no relationships between the modulus of resiliency and the rolling resistance of a pavement surface were found in the literature.

Table 12. Effect of aging: resilient modulus test results (2).

Resilient Modulus (ksi)										
Temperature	Control Days					PlusRide Days				
(°F)	2	7	14	28	90	2	7	14	28	90
41	2140	2100	1970	2110	2130	904	909	1110	1160	1030
77	248	283	239	255	301	222	165	212	177	125
104	40.0	44.0	43.0	58.1	53.8	40.5	35.5	29.5	45.7	17.8

CRREL has estimated that the rolling resistance of a rubber-aggregate asphalt pavement surface may be 2 to 3 percent higher than a conventional asphalt surface. This estimate, while based on engineering judgment, seems reasonable given the available data on rolling resistance. Table 13 compares the rolling resistance of passenger cars on smooth pavements and various surfaces of lower quality. These values are based on the work of Claffey, who measured the increased fuel consumption for vehicle operation on lower quality surfaces (14,15,16). The table shows that, at a vehicle speed of 20 mph (32 kph), rolling resistance is increased by 16 percent on a badly broken and patched asphalt pavement, in comparison to a smooth asphalt pavement. This increase in rolling resistance is 38 percent for a vehicle speed of 40 mph (64 kph), and 65 percent for a vehicle speed of 50 mph (80 kph). However, the increased rolling resistance caused by small increases in deformation for a rubber-aggregate asphalt pavement would be expected to be much smaller than the increase in rolling resistance for a broken and patched pavement.

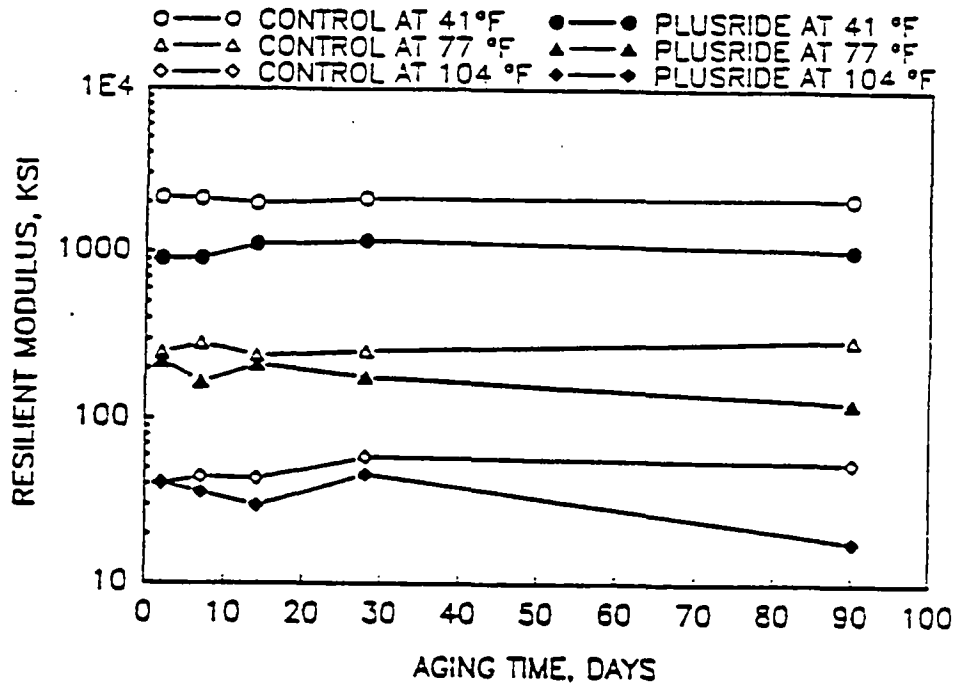

Figure 12. PlusRide: Resilient modulus vs. aging time and test temperature (2).

Table 13. Rolling resistances of passenger cars (14,15)

Vehicle Speed (mph)	Rolling Resistance (lb/ton of vehicle weight) Smooth Pavement	Badly Broken and Patched Asphalt	Dry, Well-Packed Gravel	Loose Sand
20	25	29	31	35
30	27	34	35	40
40	29	40	50	57
50	31	51	62	76
60	34	-	-	-

There does not appear to be any method short of full-scale testing to reliably quantify the effect of rubber-aggregate asphalt on vehicle rolling resistance. The literature is also

devoid of evaluations on the effect of the rubber content on the strength, serviceability, and rolling resistance of an asphalt pavement surface. While most U.S. evaluations have focused on pavements with rubber contents of 3 percent or less, the Texas Department of State Highways and Public Transportation reports using asphalt containing up to 25 percent crumb rubber (12). The increased rubber content would be expected to improve the deicing characteristics of the pavement surface.

3. Laboratory Testing of Pavement Modifications

Introduction

Laboratory experiments were conducted to investigate the effectiveness of various passive pavement modifications that might be used in combination with passages of wheeled vehicles to break the ice-pavement bond. The investigation was divided into four areas: development of testing equipment, test specimen preparations, initial static loading tests, and wheel passage tests. Each of these areas is discussed below.

Development of Testing Equipment

A brief search of the literature was made to determine if any test apparatus had been previously developed to test the effects of wheel passages on ice-pavement bond disbonding in the laboratory. The literature search did not identify any test machine which met the requirements of the proposed experiments. Therefore, a machine was designed and built to simulate wheel passages on pavement surfaces. This machine was a modification of the standard circular track polishing machine (ASTM E660) used in pavement surface wear research.

The wheel passage machine was designed with four rubber-tired wheels following a circular track around a central axis with a radius of 1.5 ft (45.7 cm). The surface of the track could accommodate up to 12 cylindrical pavement specimens, whose wearing surface was flush with the surface of the track. The design of the machine was such that each test surface could be up to 6 inches in diameter, with a maximum thickness of 2 in. When the machine is rotating at 31.8 rpm around its central axis, the wheels are traveling over the test pavement surfaces at an equivalent speed of 3.4 mph (5.5 kph). The wheels are loaded via calibrated compression springs which can be adjusted to apply a specified normal load.

The experiments were conducted using non treaded tires to eliminate ambiguous effects which the presence of tire treads could impose. Therefore, smooth pneumatic cart tires (4.10/3.50-5) with a width of 3.5 in. were initially used on the apparatus. Typical loadings for non treaded tires were found in the literature.

Preliminary runs indicated that the cart tires were not behaving in the same manner as conventional automobile tires, however. The cart tires were carrying the majority of

the normal load in the center of the tire's footprint rather than at the sidewalls. Further, heat buildup at the tire-ice interface due to the rubbing action of the untreaded tire turning in a tight radius caused ablation of the ice. The ablation of the ice and the heat buildup were substantially reduced by modifying the wheel assemblies to allow more independent movement. However, after several additional test runs, the wide pneumatic tires were replaced by narrow hard rubber wheels with a diameter of 9.875 in. (25.1 cm) and width of 1.625 in. (4.13 cm). The forces imposed on the ice under the narrow tires were equivalent to the forces imposed on the ice under the sidewall of a conventionally loaded automobile tire. The narrow tires also eliminated, to a great extent, the ice ablation due to tire rubbing.

Preparation of Pavement Surface Specimens

The pavement surface specimens used for testing were core samples taken from various parts of the country and laboratory-produced test specimens developed by CRREL using the Marshall method. The pavement surface specimens were provided by the highway or transportation departments of California, Connecticut, and New York and included several types of portland cement concrete, conventional asphalt and rubber-modified asphalt surfaces. The portland cement concrete specimens included both conventional smooth-finished surfaces and surfaces with 1/4-in. grooves. The conventional asphalt specimens included both dense-graded and open-graded mixes. The laboratory-produced specimens were rubber-modified asphalt samples in the form of 4- and 6-in. circular pavement specimens with varying percentages of rubber added.

Several preliminary 4 in. (10.2 cm) diameter rubber-modified asphalt specimens were produced in the laboratory by CRREL. The asphalt content of these specimens ranged from 6 percent to 9.5 percent by weight (see Table 4) and the maximum rubber particle size was 1/2 in. (1.3 cm). CRREL found that increased asphalt percentages were required as the amount of fine rubber particles used in the mix was increased. Based on the evaluation of the samples, it was hypothesized that the fine rubber particles contribute only to the elasticity of the material. A concern was expressed that a pavement surface constructed of a material with the necessary elasticity to cause destruction of the ice-pavement bond might increase tire-pavement rolling resistance and reduce pavement durability. It was further hypothesized that destruction of the ice-pavement bond could be achieved in a less elastic pavement if localized ice deflections at sites of rubber particles could induce crack propagation. Therefore, it was decided that CRREL should develop additional mix designs for rubber-modified asphalt mixes by increasing the percentage of large rubber particles and reducing the percentage of fine rubber particles to as small a level as possible. The maximum rubber particle size selected was 3/8 in. (0.95 cm) rather than the 1/2-in. (1.3 cm) size used in the earlier specimens.

The revised mix design (CRAC) was used by CRREL to produce the next set of rubber-modified asphalt specimens. These specimens were 4 in. (10.2 cm) and 6 in.

(15.2 cm) in diameter and 2.5 in. thick. Pavement specimens were made with the following rubber content: 0, 3, 6, 12, 25, 57, and 100 percent (by weight).

The coarse aggregate and rubber particles at the surfaces of the specimens, as received from CRREL, were covered with a thin coating of asphalt, a condition not typical of roadway surfaces that are open to traffic. Various techniques were used in an attempt to remove the asphalt coating from the surface of the aggregate and rubber particles located at the specimen surface. Hand sanding with coarse sandpaper, sandblasting, wire brushing by hand and machine, and cutting the sample with a diamond saw to expose a new surface all produced unsatisfactory results. The initial attempts at sandblasting the surface of the pavement specimen to remove the asphalt coating failed because the sandblasting left particles of sand embedded in the soft asphalt. However, these initial attempts were performed at room temperature. It was found that if the sample were frozen, the sand particles did not become embedded in the asphalt. Therefore, this method of freezing the specimens and then sandblasting them was used to remove the asphalt coating from the surface.

The surface of each specimen was cleaned using a procedure developed under SHRP Contract H-203. This cleaning procedure involved first rinsing each specimen with ethyl alcohol, scrubbing it with a stiff brush, rinsing it three more times with ethyl alcohol, drying it in a vacuum chamber for 1 hr, rinsing it again three times with deionized water, and letting it air dry. Ice was then grown on the cleaned surfaces in a bottom-up mode, again using the procedures developed under SHRP Contract H-203.

Preliminary Loading Experiments

Initial deflection and single event load tests were performed on saw cut rubber-modified (CRAC) asphalt surfaces with a thin ice layer [1/16 in. (0.16 cm) thickness] to gain an understanding of the force required to cause ice fracture on the specimens. An Instron tensile/compression machine was used in these tests. The Instron machine was equipped with an environmental chamber which encompassed the loading base and tup. The loading tup, which induced the forces onto the specimens, was constructed of a 2 in. (5.1 cm) diameter rubber stopper with approximately the same durometer reading as that of a conventional tire. This tup was attached with epoxy to a steel ram of the same diameter. The tests were conducted at a temperature of approximately 15°F (-9°C).

Pressure loadings ranging up to 150 psi (1.03×10^6 Pa) were imposed with the rubber tup on ice-covered rubber-modified asphalt surfaces containing 12 percent and 25 percent rubber. Cracks in the ice were not detected on any of these specimens. The thickness of the ice layer was then reduced from 1/16 in. thickness (0.16 cm) to a very thin layer. Again, the 150 psi (1.03×10^6 Pa) pressure loadings were applied, but only one small crack developed (on the specimen with the 25 percent rubber content). This crack seemed to heal itself in a short amount of time. From these facts, it was evident

that conventional ice fracturing on rubber-modified asphalt surfaces would have to be generated through repeated loadings and fatigue, not through the application of single loads. Consequently, it was decided to postpone further Instron testing.

Wheel Passage Tests

Initial runs with the wheel passage device were made with the various portland cement concrete, conventional asphalt specimens, and a rubber-modified (PlusRide) asphalt specimen acquired from California. The portland cement concrete specimens included smooth and grooved surfaces. The asphalt specimens included both dense-graded and open-graded asphalt types. The rubber content in the California specimens was unknown, but from observation of the specimens it was estimated to be less than 3 percent.

The initial tests were conducted at a temperature of 25°F (-4°C) and with an ice thickness of about 1/4 in. (0.64 cm). Each specimen was subjected to 400 wheel passages. No significant cracks were detected in the ice layers, and the ice-pavement bond remained intact and undamaged. The tests were terminated after the tires wore the ice down to the substrates with no visible cracking having taken place on most of the specimens. A few very small cracks were thought to occur around some of the exposed rubber particles of the PlusRide asphalt specimens. This ended the testing with the conventional portland cement concrete and asphalt specimens. Attention was then directed towards testing rubber-modified asphalt surfaces.

Wheel passage tests of rubber-modified asphalt surfaces were designed to investigate four factors that may contribute to crack initiation and propagation at the ice-pavement interface. These factors were: (1) the percentage of rubber content; (2) the ambient temperature; (3) the ice thickness; and (4) the number of wheel passages over the specimen surface. These additional wheel passage tests were conducted with ice layers grown on 6 in. (15.2 cm) diameter specimens made according to the chunk rubber asphalt concrete (CRAC) mix designs given in Table 2-9. The rubber content of these CRAC test specimens varied from zero to 100 percent. Tests were performed at two temperatures [15°F (-9°C) and 25°F (-4°C)] and two ice thicknesses [1/16 in. (0.16 cm) and 1/8 in. (0.32 cm)]. The number of wheel passes ranged from 1 to over 6000. Multiple tests of selected combinations of percent rubber content, temperature, and ice thickness were run to verify ice cracking and disbonding characteristics.

Specimens with zero percent rubber did not develop cracks in the ice layer or undergo any obvious deterioration of the ice-pavement bond. These results were the same for each temperature-ice thickness combination.

CRAC specimens with 3 percent rubber content developed occasional cracks in the ice at the locations of rubber particles on the surface of the specimen, but with no

regularity or consistency. One specimen developed a crack near its center, while another specimen developed a crack near its edge. Both of these cracks were in the wheel path and both were at the site of a rubber particle in the pavement surface. Neither temperature nor ice thickness appeared to make a significant difference in results.

For the CRAC specimens with 6 percent rubber content, ice cracking in the wheel path was observed to be more consistent and extensive than for the 3 percent specimens. The portion of the ice surfaces at the edges of the specimens, where the wheel passages began and ended, showed consistent cracking where the rubber particles were present. The cracking was observed at all temperatures and ice thicknesses. At 25°F (-4°C), however, the degree of cracking in the wheel path increased as the number of wheel passes increased much more markedly than it did for the same number of wheel passes at 15°F (-9°C).

For the CRAC specimens with 12 percent rubber content, a much greater occurrence of cracks was observed at both temperatures and ice thicknesses. Cracking developed around the rubber particles at the edges of the specimens in the wheel path after only a very few wheel passages. As the number of wheel passages increased, further cracking occurred at the sites of the rubber particles throughout the wheel path. During these tests, it appeared that the ice became fatigued and the disbonding at the ice-specimen interface began to take place. Deterioration of the ice-pavement bond continued to the point that the ice became fully disbonded from the pavement surface, leaving the specimen surface exposed.

Ice grown on the CRAC surfaces with 25 percent and 57 percent rubber content experienced cracking with as few as 10 wheel passes. After 6000 passes on the surface with 25 percent rubber content, as much as 50 percent of the wheel path area was cleared of all ice, while the remaining ice in the wheel path showed signs of severe deterioration of the ice-pavement bond. All CRAC specimens with rubber contents higher than 25 percent showed signs of severe cracking and ice-pavement bond deterioration after only a few wheel passes. The specimen with 100 percent rubber content experienced 50 percent ice removal in the wheel path after only 400 wheel passages and total ice removal after only 1000 wheel passages.

It was concluded from the wheel passage tests that the occurrence and frequency of cracking is directly related to the quantity of rubber at the surface of the specimen. The extent of the ice cracking on the specimens varied with rubber content and number of wheel passages from no cracking to total disbondment. The results clearly indicate that increased rubber content (i.e., an increased presence of larger rubber particles on the pavement surface) increased the incidence of cracking. Surface characteristics other than the presence of rubber particles did not appear to affect cracking.

The size and origin of the cracks for CRAC surfaces with lower rubber contents indicate that cracking of these surfaces relies on localized deflection around the rubber

particles to induce cracking, while asphalt surfaces with rubber content over 12 percent experienced disbondment through area deflection.

The location of the rubber particles in the asphalt surfaces with lower rubber contents (12 percent or less) was found to make a substantial difference in crack propagation. Testing indicated that cracks tended to develop at particles of rubber located on the pavement surface. Further, it was found that increasing the rubber content within the range of rubber content below 12 percent does not necessarily ensure a proportionate increase in crack propagation. For example, one surface with a 6 percent rubber content actually had more exposed rubber particles than a similar surface with 12 percent rubber content. Under the same loading, the 6-percent specimen developed more cracks in fewer wheel passes than the 12-percent specimen. Furthermore, it should be understood that the cracks which developed in the wheel path at the edges of the specimens cannot be attributed exclusively to edge effects. Even at these locations, cracks developed only at locations where rubber particles were present.

The area deflection experienced on CRAC surfaces with higher rubber contents results from the increasing elasticity of the surface and decreased ability of ice formed on that surface to support the wheel loads. As the amount of support provided to the ice decreases, due to the increased presence of elastic rubber particles, the ability to support the loading diminishes and the wheel load must increasingly be supported by the ice layer. Thicker ice layers have much greater strength and bridging ability, but the ice layers of 1/16 and 1/8 in. (0.16 and 0.32 cm) in thickness cannot support the loading imposed by a typical automobile tire on CRAC surfaces with high rubber content. Consequently, these thin ice layers begin to crack and fatigue after repeated loading and are eventually disbonded and separated from the asphalt surface.

Active Pavement Modification

Objective and Scope of Work

The objective of the work dealing with active pavement modifications was to investigate the use of a pavement surface treatment or impregnation which could be activated by some external energy source to facilitate the disbonding of ice from pavement materials. The energy source to be considered in the disbonding process was to be something other than wheeled vehicle loadings. Both asphaltic and portland cement concrete surfaces were to be considered in the investigation. The restrictions governing the pavement surface modifications were the same as those identified for the work with passive pavement modifications.

A proof-of-principle study was conducted on the concept of utilizing a microencapsulated deicing agent to modify pavement surfaces and enhance ice removal. Both economic and technical feasibility aspects of the approach were studied. Ethylene glycol was the deicing agent selected for encapsulation.

The basic concept of the active pavement modification approach is discussed first. This is followed by an estimate of deicer material requirements. The experimental efforts undertaken to develop a microencapsulation process are then discussed.

The Basic Concept

The approach taken in this part of the investigation was to determine if microencapsulated deicing materials distributed on the surfaces of highways prior to a storm event--specifically one which generates a layer of ice--could be activated on demand by an appropriate energy source. The activation process envisioned consisted basically of rupture of the walls of the microcapsules by incident radiation, so that the encapsulated ice-melting agent would be released to melt and undercut ice directly at the ice/pavement interface. The processes following release of the deicing materials would serve to weaken or completely destroy the ice/pavement interface. The ice overburden could then be mechanically removed by a plow blade or broken into pieces by vehicle wheel passages.

A brief literature search was conducted relative to the use of surface materials incorporating deicing additives which could be activated by an external energy source such as electromagnetic radiation. The portion of the electromagnetic spectrum considered was from the ultraviolet down to the microwave frequency range.

No research articles were found that specifically addressed the proposed approach. However, a few articles of indirect use were found and reviewed.

The concept of activating a pavement surface treatment or impregnation is based on the high transmission rate of ice to ultraviolet light, visible light, and possibly selected microwave frequencies. Ice is quite opaque to infrared radiation, which would only cause heating of the bulk ice with only a small amount of energy reaching the ice/pavement interface. Findings are given below relative to the activation of a pavement surface treatment or impregnation by the ultraviolet and visible light and microwave frequencies.

Ultraviolet and Visible Light Energy Source Range

The sun produces visible and near ultraviolet (UV) light in rather large amounts. This frequency range is not totally satisfactory for use because it would activate the surface treatment or impregnation at times when not needed (dry pavement conditions), as well as times when needed (ice-covered pavement conditions). The shorter wave segment of the UV spectrum does, however, have some potential, but also some drawbacks. An example of a shortwave UV source is a mercury vapor arc lamp. This shortwave UV is somewhat dangerous to animal life and thus must be well shielded. The presence of a snow cover over the ice will greatly reduce the shortwave UV light

penetration by reflection. This situation could limit the overall usefulness of this part of the electromagnetic spectrum.

The activation of chemical reactions by UV light is currently used in many chemical industries. It is possible that a UV-initiated decomposition of a suitable gas generator (such as an azide with a suitable energy transfer agent) dissolved in a microencapsulated glycol could be used to rupture the microcapsule wall and release the glycol. The glycol could then produce ice melt at the coated pavement interface.

It would be necessary to apply the microcapsules with a water-soluble binder as a dispersion prior to freezing weather. The microcapsule could thus be held in the voids in the pavement surface where they would not be quickly destroyed by traffic. Selection of a cross-linking, water-soluble binder will allow retention of the microcapsules on the pavement surface even under wet conditions for sufficient time to make the process feasible.

Use of Microwave Radiation to Rupture Microcapsules Containing Glycol

Electromagnetic radiation in the gigahertz ($n \times 10^9$ hertz where $50 > n > 1$) range can produce heating in lossy materials, for example, the heating of water by X-band frequencies (microwave ovens). The proper choice of lossy material (e.g., ferritic powders, magnetic iron oxide, etc.) and microwave frequency can produce relatively high absorption of incident radiation. The purpose of this preliminary examination was to determine the feasibility of using incident microwave electromagnetic radiation to trigger the release of a gas to rupture microcapsules containing glycol deicer.

The microcapsules would be applied to the road surface as a slurry in a water-based adhesive solution. The slurry would wash into the voids of the highway surface and would be bonded to the walls of the voids. On setting, the water-soluble adhesive would be cross-linked to produce a water-insoluble binder. The microcapsules should thus be protected for a reasonable time from rupture by traffic action.

Dispersion of a lossy, powdered microwave-absorbing substance (ferrites, iron oxides, carbon particles, and/or mixtures of these materials) in the glycol prior to its encapsulation could provide a means for selectively heating the capsules to cause rupture by thermal expansion. An alternative, and perhaps better approach would be coating the lossy powders with a nitrogen gas generator such as 4,4′-oxybis(benzenesulfonyl hydrazide), Celogen®, in a glycol-insoluble binder. This coating would thus be directly exposed to heat generated in the lossy powder particle on microwave irradiation.

The efficiency of coupling the microwave energy into these particles must be high to generate the 300°F (149°C) temperature required to decompose the Celogen® to yield 125 cc of gas per gram. This energy coupling is a very complex process.

Ranking of Potential Surface Treatments or Impregnation Materials

Selection of segments of the electromagnetic spectrum that could be used to remotely activate a preapplied surface treatment to produce melting of the ice-pavement interface was the first work performed. It was found that only the microwave and hard (far) ultraviolet frequency ranges are usable because the infrared, visible, and soft (near) ultraviolet output of the sun would be sufficient to cause untimely activation of the treatment system.

In order to obtain the desired interfacial melting, it is necessary that the melting agent be held in some kind of small, rupturable container. Fluids are readily encapsulated, while sharp-cornered particulates (salts) are very difficult to coat uniformly. These considerations led to the selection of ethylene glycol as the melting agent of choice. It is relatively inexpensive, noncorrosive, of limited toxicity, and is biodegradable. Liquid aqueous salt solutions, due to their high ionic strengths, are very hard to emulsify in an oil, which is a prerequisite to the operation of microencapsulation processes.

The use of hard ultraviolet radiation to produce chemical decomposition of a gas-releasing compound is based on the transparency of ice to this wavelength radiation. The presence of snow either free or partially compacted on the ice surface will produce scattering and reflection of incident UV radiation, thus compromising its effectiveness. Thus this process was the second choice of the two considered, with microwave radiation being the first choice.

Ice is relatively transparent to microwave radiation below 2 GHz, where the absorption coefficients are relatively low. Electromagnetic radiation in this frequency range can be highly absorbed by lossy ferrites with consequent heat production. The presence of snow cover on ice will not greatly perturb this larger wavelength radiation. The question whether adequate heating of the ferrite particles could be obtained to produce rupture of the microcapsules needed to be answered. However, this process appeared to be the one of choice.

The technical feasibility of the microencapsulation concept was felt to depend, to a large extent, on three key issues:

1. The success of producing suitable microcapsules.

2. The degree of success achieved in providing radiation-absorbing and radiation-sensitive materials which enable incident radiation to promote capsule-fracturing mechanisms.

3. The degree of success achieved in coupling energy sources with the microcapsules.

Experimental attempts to produce suitable microcapsules on a small scale are described later in this section after the discussion of the estimates of deicer material requirements.

Estimates of Deicer Material Requirements

As a first approximation, it is entirely reasonable to expect that a deicing chemical placed on a pavement surface before ice formation will be considerably more effective than one spread over the surface of the ice. An under-the-ice agent will expend its capabilities where the greatest and most effective impact will occur, namely at the ice/pavement interface, by weakening or destroying the bond. Thus the degree of control achieved by poststorm application of 400 lb/lane mile of rock salt should be realized from the application of a smaller quantity prior to a storm event.

Ethylene glycol is proposed as the deicing agent to be microencapsulated. The theoretical and actual ice melting capacities of ethylene glycol are somewhat less than the capacities of calcium chloride and sodium chloride. However, ethylene glycol shares with calcium chloride the capability to expend its ice-melting capacity in 1 hr or less, even at 0°F. Undercutting data available for ethylene glycol exist only for a system in which the glycol is placed in a conical cavity in ice, 3/8 in. in diameter at the ice/pavement interface.

The majority of the undercutting data for calcium chloride has been obtained with pellets placed on the surface of a 1/8-in. thick layer of ice. Neither test configuration yields data which are directly applicable to a deicer released at the ice/pavement interface. The following exercise and calculations have been performed in order to estimate the extent and rate of ice undercutting expected with ethylene glycol released at the ice/pavement interface.

First, the fraction of calcium chloride required to create a cavity in ice 3.175 mm in depth and 5 mm in diameter has been calculated at various temperatures.

Second, the quantity of calcium chloride expended in melting the cavity has been allocated exclusively to undercutting, and existing undercutting data, in square centimeters per gram of deicer, adjusted to the appropriate higher values.

Third, undercutting data for ethylene glycol have been developed by multiplying calcium chloride data by the ratios of the melting capacities of ethylene glycol and calcium chloride. The data for ethylene glycol obtained by this approach are presented in Table 14.

Table 15 presents the quantities of ethylene glycol required to completely undercut 1 lane-mile (63,360 ft^2) of firmly and uniformly bonded ice; data for 50% undercutting

are also presented. The application rates in Table 15 are higher than those typically used in general snow and ice control where complete undercutting is not a requirement.

The cost of ethylene glycol is about $0.50/lb in bulk. It is clearly evident from the data in Table 15 that materials costs for ethylene glycol will be prohibitively expensive for firmly bonded ice. The economic feasibility of the proposed concept will accordingly be determined by two factors: (1) the magnitude of the difference between field-generated ice and laboratory ice; and (2) the percentage of the total ice/pavement interface which needs to be undercut or weakened to effectively eliminate the safety hazard associated with ice.

A substantial inventory of data is available which quantitatively describes the extent and rates of disbonding from pavement by chemical deicer undercutting processes. These quantitative data have, however, been obtained with ice which is very firmly and uniformly bonded to the pavement substrate. Experience with the deicer undercutting phenomenon also includes an inventory of semiquantitative, that is, largely qualitative, information. These data on the undercutting process which occurs at the ice/pavement interface are less ideal from the standpoint of usefulness in comparing deicing materials and determining temperature effects. In brief, undercutting with the nonideal ice/substrate systems tends to be much more rapid and extensive. The ice/substrate interfaces encountered under field conditions can be expected to generally be closer to the nonideal conditions than to the artificially formed ice/substrate interfaces developed and used in laboratory tests of undercutting.

It is reasonable to expect that a substantial increase in undercutting capacity could be found for "nonideal" ice where catastrophic undercutting is possible. If one further assumes that weakening/undercutting 50% of the ice/pavement interface will suffice, the application rates presented in Table 15 may be lowered by a factor of 20. Application rates estimated from factors of 10 and 20 are presented in Table 16. The rates presented in Table 16 would appear to be reasonable and credible by comparison with rates employed for poststorm application of rock salt. The rates are clearly much more attractive, from a cost standpoint, than the very unattractive costs associated with rates presented in Table 15.

It is quite evident, however, that the overall economic attractiveness of the proposed approach would become evident only after the several key assumptions are addressed in studies involving field condition ice/pavement interfaces.

Experimental Attempts to Develop a Microencapsulation Process

Several experimental attempts were made to develop a satisfactory microencapsulation of ethylene glycol. If positive results were obtained (i.e., prediction of stable glycol-containing microcapsules in the 20 to 100-micron size range), capsules containing either a hard ultraviolet decomposable gas-generating agent and/or a lossy

Table 14. Ethylene glycol undercutting capabilities. Melting action confined to ice/substrate interface. Ice/substrate condition: firmly and uniformly bonded. Time: 1 hr or less

Temperature (°F)	cm^2 undercut/g	ft^2 undercut/lb
25	87	43
20	71	35
15	59	29
10	52	26
5	45	22
0	40	20

Table 15. Ethylene glycol quantities required for undercutting one lane-mile of uniformly and firmly bonded ice.

Temperature (°F)	100% UC lb/lane-mile	50% UC lb/lane-mile
25	1470	735
20	1800	900
15	2180	1090
10	2476	1235
5	2850	1425
0	3200	1600

Table 16. Ethylene glycol adjusted rates (lb/lane-mile).

Temperature (°F)	Factor of 10	Factor of 20
25	150	75
20	180	90
15	220	110
10	250	125
5	285	145
0	320	160

ferritic material that would be heated by microwave radiation to produce gas generation were to be prepared. The purpose of gas generation is to produce capsule rupture and release of the ethylene glycol on exposure to the selected electromagnetic radiation.

A brief hand search of the literature cited in *Chemical Abstracts* from 1970 to the present did not show any examples of encapsulation of ethylene glycol. Several examples of microencapsulation of glycerol, a chemically very similar compound, were reported, however. All of the examples reported made use of modified interfacial polymerization encapsulation techniques. The following two general encapsulation methods were selected for further investigation.

1. Formation of a Polyester Shell

Reaction of an aromatic diacid chloride with the glycol to form an aromatic polyester shell was the first method examined. The reaction chemistry was:

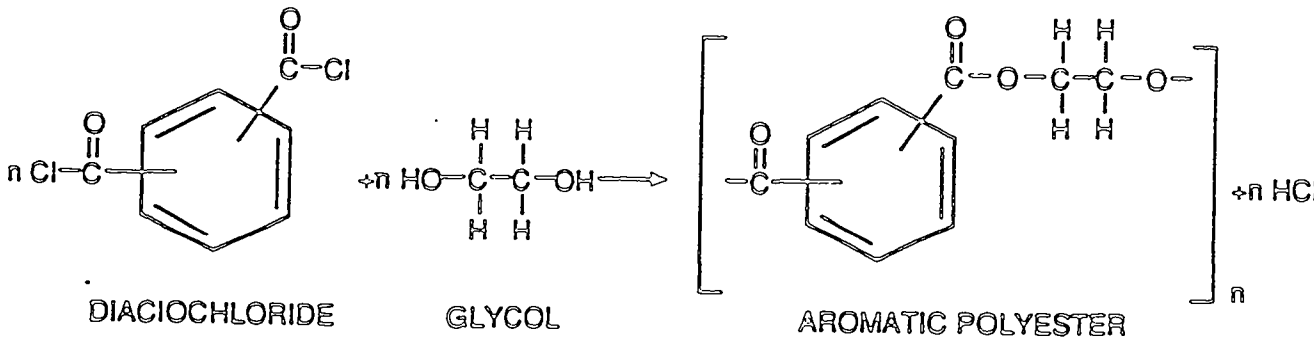

The HCl formed must be neutralized by a base (scavenger) in order for the reaction to produce good polymer yields. Two acid chlorides were used in these trials, isophthaloyl chloride and terephthaloyl chloride. Triethylamine was added to the ethylene glycol at a 5 wt % level to serve as the acid scavenger. The acid chloride was added to anhydrous methylene chloride (CH_2Cl_2) at a 10 wt % level. The acid chloride solutions were kept in airtight containers until used because the solutions rapidly react with atmospheric moisture. Methylene chloride was chosen as the reaction medium because the acid chlorides are readily soluble and the glycol is quite insoluble.

The polymerization (encapsulation) trials were performed on a small scale (approximately 5 mL total reaction volume) in Reacti-Vials™ containing a wedge-shaped Teflon®-coated magnetic stirrer. All reactions were performed at room temperature [75°F (24°C) to 80°F (27°C)]. The diacid chloride solution, ~ 3 mL, was changed into a clean, dry vial, and stirring was initiated. About 0.25 mL of the ethylene glycol/ triethylamine solution was then added dropwise to the stirred solution over a period of about 30 sec. The resultant stirred mass took on a cloudy appearance almost immediately after addition of the ethylene glycol. Stirring was allowed to continue for 5 additional minutes, after which the stirring was stopped. A drop of the reaction fluid was then placed on a microscope slide and observed under 0 to 80X power using an American Optical Binocular Microscope.

Approximately 20 such runs were made using both magnetic stirring and hand shaking without the production of whole, sound microcapsules. It was necessary to provide motion to produce suspension of the glycol in the methylene chloride solvent. This motion appeared to cause rupture of the capsules as they were forming. Pieces of spherically shaped cell walls could be observed under the microscope. The interfacial polymerization did proceed as desired, but the walls formed were either too thin to resist the stirring reaction, or formed at too slow a rate. On several occasions, complete, spherical particles were temporarily observed in the reaction fluid, but on standing, they were observed to rupture as the highly soluble methylene chloride evaporated. The polyester resin method was then abandoned in favor of the second, or polyamid resin shell, approach.

2. Formation of a Polyamid Shell

The reaction rate during the interfacial polymerization of a diacid chloride and an aliphatic diamine is substantially faster than that for the polyester reaction; thus this method was examined next. The reaction chemistry employed was:

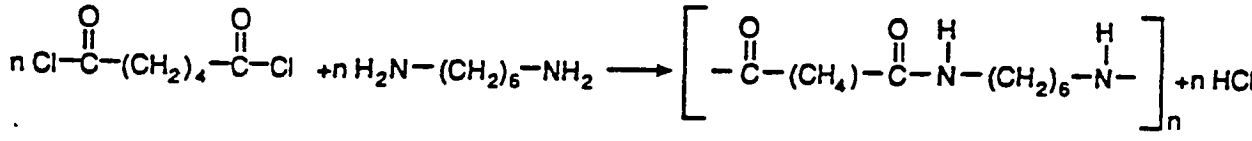

ADIPOYL CHLORIDE 1,6–HEXANEDIAMINE A POLYAMID (NYLON 6,6)

The aliphatic diacid chloride and the aliphatic diamine react to form a well known polymer, nylon 6,6. This reaction is quite fast and the polymer is very tough. In these trials the diamine and an acid scavenger (triethylamine) were dissolved in the ethylene glycol and the acid chloride in the chlorinated solvent.

The same mixing procedures described for the polyester shell were initially used in evaluating the polyamid shell, with the exception that the acid chloride content in the methylene chloride was increased to 10 wt %. Experimental results using the Reacti-Vial™ mixing chambers were somewhat more promising because a much larger number of coated spheres in the 10- to 20-micron diameter range were produced. Again, however, it was noted that these spheres collapsed on drying, indicting a weak shell formation. A series of tests was made using different stirring speeds and mixing orders, such as initially suspending the treated ethylene glycol in pure methylene chloride followed by addition of a concentrated (20 wt %) solution of the acid chloride in methylene chloride. In an attempt to reduce the stirring necessary to suspend the ethylene glycol, a mixture of n-hexane (31.8 vol %) and methylene chloride (68.2 vol %) was prepared which had the same density as the ethylene glycol (1.11 g/cc). The treated ethylene glycol was suspended in this mix under stirring. The pure fluid acid chloride was then added to this suspension while low-speed stirring was being maintained. No great improvement in the formation of microcapsules was observed.

At this point in the work it was felt that a demonstration of the ability of the system to form capsules under any condition was required. A method described in U.S. Patent 3,270,100 and utilizing two different density fluids was chosen. Fifty milliliters of a 5 wt % solution of an adipolychloride in trichloroethylene was prepared along with 50 mL of a 5 wt % solution in toluene. The trichloroethylene solution was poured into a 200-mL beaker over which the less dense toluene solution was carefully floated. This produced a two-layer solution with a rather sharp interface. One drop of the amine-containing ethylene glycol was then dropped into the toluene layer from a syringe with a 22-gauge needle. This drop, being denser than the toluene layer, sank to the interface with the trichloroethylene layer, where it slowly came to rest. The drop maintained a spherical shape, and the formation of a skin was observed almost instantaneously as the drop fell through the toluene layer. After 2 min, the encapsulated drop could be lifted from the solutions with the aid of a spoon-shaped piece of fine (100-mesh) screen. The sphere was nearly 2 mm in diameter, withstood washing with acetone and water, but ruptured with application of a little pressure. The skin was less than 0.5 mil in thickness. This experiment was repeated several times with essentially identical results. The experiment shows that, in the absence of shear forces, macrocapsules can be formed in a relatively short time.

A final set of experiments was conducted to determine if smaller diameter microcapsules could be produced using the lowest possible mixing forces. These experiments used a larger scale mix size (50 mL) and a 1 3/4-in. diameter three-bladed propeller at the lowest rotation rate that would maintain a dispersion of the ethylene glycol in methylene chloride. Two milliliters of the ethylene glycol/amine mixture were charged dropwise into 50 mL of methylene chloride in a 150-mL beaker containing the subject stirrer rotary of 600 rpm. Once the glycol was suspended, the stirrer speed was reduced to 300 rpm, at which point any further reduction in speed causes loss of suspension stability by particle agglomeration. Four milliliters of a 10 wt % solution of

the acid chloride was then added as fast as possible to the stirred mix. Mixing was continued for 5 min and the mix examined under the microscope. It was found that only a stringy gelatinous mass of polymer was produced under these and similar conditions. Apparently both the amine and the glycol reacted with the acid chloride, producing an unstable mixed polymer system that had little physical strength.

At this point in the work it was not apparent why these methods had failed so completely. The results do suggest that reaction with diacid chloride to form a polymer skin on ethylene glycol is not usable for microencapsulation.

One alternate interfacial polymerization reaction was examined late in the study: the reaction between the ethylene glycol and a diisocyanate to form a polyurethane.

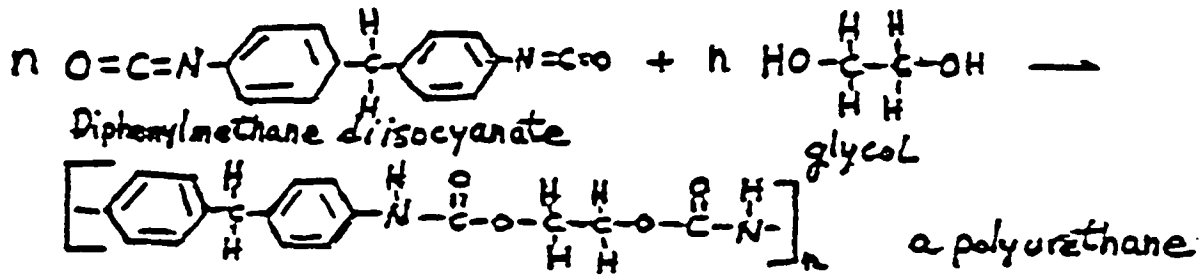

The reaction between the isocyanate and the hydroxyl group of the glycol can be made quite rapid by the use of selected amine and tin ester catalysts. The reaction was examined, as were the polyester and polyamid encapsulating reactions. This reaction is singular in nature as there is no third reactant present to complicate the polymerization.

The isocyanate used in this study was obtained from a local source and was typical of the diphenylmethane diisocyanates used in polyurethane foam production. This compound has an average of 2.3 isocyanate groups per molecule. The increased functionality is desirable for this application because it will produce cross-linking in the capsule wall, making it stronger. The isocyanate was not completely soluble in methylene chloride but was readily soluble in trichloroethylene ($Cl_2C=CHCl$). Dibutyltindilaurate was added to the ethylene glycol at a 0.5 wt % level to speed up the isocyanate-alcohol reaction.

A 2-mL portion of the catalyzed ethylene glycol was suspended in 50 mL of trichloroethylene using the three-bladed propeller as described previously. Propeller speed was reduced to 300 rpm from the initial 600 rpm while still maintaining suspension of the glycol droplets. A 5-mL portion of a 10 wt % solution of the isocyanate in trichloroethylene was rapidly added to the suspension, with stirring at 300 rpm being continued for 5 min. Examination of the resulting suspension under the microscope showed only

agglomerates of gel-like particles. Repeated trials at decreasing levels of reactants (glycol and isocyanate) in the 50-mL solvent batch failed to yield the desired microcapsules.

As a result of the failure of several attempts to produce the desired microcapsules, further work toward deicing by this method was abandoned.

Conclusions and Recommendations

This section of the final report presents conclusions and recommendations that the authors have developed after considering all the information obtained during the investigation of the role of passive and active pavement modifications on disbonding ice from pavement surfaces.

Conclusions

1. Finite element analysis (FEA) approaches can be used effectively to investigate the ice disbonding potential of selected pavement surface profiles when subjected to wheel passage conditions.

2. FEA simulation results indicated that resultant stress concentrations at the ice-pavement interface from conventional tire passages are not of sufficient magnitude to promote favorable ice disbonding from portland cement concrete or asphalt concrete even when exaggerated pavement surface profiles are considered.

3. Laboratory results show it is not possible to disbond ice from conventional portland cement concrete and asphalt concrete surfaces with passages of wheeled vehicles.

4. A new rubber-modified asphalt concrete mix design was developed that has characteristics superior to existing rubber-modified asphalt mix designs. The new design, called chunk rubber asphalt concrete (CRAC), can use chunk rubber derived from waste tires.

5. Ice can be disbonded readily from CRAC surfaces with passages of wheeled vehicles.

6. The concept of utilizing a microencapsulated deicing agent to modify pavement surfaces for the enhancement of ice removal remains unresolved. The experimental efforts undertaken to develop a microencapsulation process for ethylene glycol were unsuccessful.

Recommendations

- Test sections of CRAC pavements with varying percentages of rubber content should be constructed outdoors for full-scale tests.

- Controlled field tests should be conducted with CRAC surfaces and actual vehicles to determine the extent of ice-pavement bond destruction under a variety of temperature and tire loading conditions.

- Field tests of CRAC pavements should include rolling resistance measurements.

References

1. R.R. Blackburn, A.D. St. John and P.J. Heenan. Physical Alternatives to Chemicals for Highway Deicing. Final Report of MRI to FHWA. U.S. Department of Transportation, December 1978.

2. K.D. Stuart and W.S. Mogawer. Laboratory Evaluation of Verglimit and PlusRide. Draft Version of Report No. FHWA-RD-88-173. Federal Highway Administration, November 1988.

3. H.B. Takallou, J. McQuillen, Jr., and R.G. Hicks. Effect of Mix Ingredients on Performance of Rubber Modified Asphalt Mixtures. FHWA-AK-RD-86-05. Federal Highway Administration, May 1985.

4. C.R. Foster. The Strength of Asphalt Pavements. Paper submitted to Association of Asphalt Pavement Technologists Symposium on Asphalt Mix Design. February 1985.

5. J.L. VonKirk. CALTRANS Experience with Asphalt-Rubber Concrete--An Overview and Future Direction. Paper presented at the National Seminar on Asphalt-Rubber, Kansas City, Missouri, October 30-31, 1989.

6. R.N. Doty. Flexible Pavement Rehabilitation, Using Asphalt-Rubber Combinations--A Progress Report. *Transportation Research Record 1196.*

7. Personal discussions with Jack VanKirk, Robert Doty, and Bob Page, CALTRANS, Sacramento, California.

8. Personal discussions with David Esch, Alaska Department of Transportation, Fairbanks, Alaska.

9. A. France. Asphalt Rubber Tested in Caltrans I-80 Project. *Roads and Bridges*, March 1989.

10. R.N. Doty. Flexible Pavement Rehabilitation Using Asphalt-Rubber Combinations--A Progress Report. California Department of Transportation, Presented at the 67th Annual Meeting of the Transportation Research Board, January 1988.

11. D.C. Esch. Construction and Benefits of Rubber-Modified Asphalt Pavements. *Transportation Research Record 860*, 1982.

12. Old Tires Bounce Back. News Briefs, *Civil Engineering*, June 1990.

13. J.A. Dvorak. Old Tires Cover the Road. *Kansas City Star*, August 18, 1990.

14. A.D. St. John and D.R. Kobett. Grade Effects on Traffic Flow Stability and Capacity. *NCHRP Report 185*. Transportation Research Board, 1978.

15. Institute of Transportation Engineers. *Transportation and Traffic Engineering Handbook*. Second Edition, Prentice-Hall, 1982.

16. P. Claffey. Running Costs of Motor Vehicles as Affected by Road Design and Traffic. *NCHRP Report 111*. Transportation Research Board, 1971.

Non-Contact Methods

Electro Magnetic Radiation (Microwaves)

Introduction

Research Associates of Syracuse, Inc. (R.A.S.) has been tasked under Michigan Technological University (MTU) Subcontract No. MTU-41995 for the purpose of investigating the usefulness of microwave power to disbond ice from road surfaces (non-contact method). The ice is nearly transparent to the microwaves. This transparency allows the microwaves to penetrate to the road surface and heat up the road surface causing the ice to melt at the road interface and disbond the ice.

Unfortunately, road materials such as portland cement concrete (PCC) and asphalt have a relatively large skin depth at microwave frequencies causing the microwave energy to penetrate deep into the road material. Consequently, according to the results presented on previous efforts, the absorption of the microwaves at or near the surface (i.e., 1 cm) only amounts to about 4 to 5 percent.

After initial test results indicated that standard road materials would result in ice disbonding at speeds too low to be practical, RAS has concentrated on finding materials that would result in a road surface overlay that would result in far more efficiency. Two major problems exist with the microwave technique in order to demonstrate its practicability. First, an overlay surface of special energy absorbant material must be developed which will result in high efficiency heat transfer causing ice disbondment. Second, once this better material is developed, tests with rapid disbondment (i.e., Less than 1 second) must be accomplished in order to achieve the desired vehicle speeds. It was suggested that RAS conduct a literature search for appropriate absorbant materials and to determine which of the FCC approved operating frequency bands would be best suited for the microwave disbonding. It was also suggested that RAS spend more time on analysis that could reduce the amount of experimentation time required and more efficiently search for the appropriate material characteristics and parameters resulting in high energy absorption. A sensitivity analysis would indicate which material parameters are critical and which are not. These suggestions have been carried out and the results are reported here.

Literature Search

A literature search has been conducted to accomplish several things. First, materials of high microwave energy absorption were sought to enhance the ice disbonding process by using this material as an overlay on the normal pavement surface. Also, the frequency sensitivity of these materials were investigated to determine if there is an optimum frequency band of operation within any of the FCC approved frequency

bands. The dielectric properties of these materials were sought so that they could be used in the mathematical model generated for further analysis of their microwave energy absorption characteristics.

Materials of High Microwave Energy Absorption

A paper was located in the library that was quite useful. It is entitled "Applications of Microwave Energy in Extractive Metallurgy"[1] by S.L. McGill and J.W. Walkiewicz. The authors have taken many materials and measured the heat rise in them when they were exposed to microwave radiation. Table 17 was taken from this paper and it shows that carbon is one of the most energy absorbing materials. Coal is a natural form of carbon and not too expensive. Some of it was obtained for the purpose of running experiments. Ferrite material has previously been shown to be microwave absorbing by virtue of a patent applied for[2] by an individual making a microwave browning device for hamburgers, etc. Ferrites and carbon are the two materials that we have concentrated on in our analysis and our experimentation.

Frequency Dependence of the Dielectric Properties of Coal

A paper was found[3] in which the authors measured the dielectric properties of various types of coal found around the United States. The dielectric properties of coal were measured over the frequency range of 1 MHz to 12 GHz. These properties were reported for run-of-mine (ROM) samples, for five different sources and for light and dense fractions from some of those samples. Carbon appears to be one of the most microwave energy absorbing materials.

This paper shows that the dielectric properties of coal varies considerably over the 1 MHz to 12 GHz frequency range. However, the FCC approved range of frequency for industrial heating purposes does not vary nearly as wide. There are four frequencies between 0.9 and 22 GHz.

FCC Approved Industrial Heating Frequencies

The federal communications commission has four frequencies set aside for industrial heating purposes. These are 0.915, 2.45, 5.85 and 22.125 GHz. RAS was asked to determine whether one frequency or another might be more optimum for purposes of microwave energy absorption by a special material overlay. It appears that for coal, over this relatively narrow frequency range, that absorption is not favored significantly at any one frequency. Since it is still much easier and cheaper to obtain high microwave power at 2.45 GHz (the frequency most commonly used by home and industrial microwave units), it is assumed that future testing done at this frequency will be applicable.

Table 17. Microwave Absorption Data on Various Materials

Table 1. Effect of microwave heating on the temperature of reagent grade elements and compounds*.

Chemical	Temp. C	Time min.	Chemical	Temp. C	Time min.
Al	577	6	Mo	660	4
$AlCl_3$	41	4	MoS_3	1,105	7
C	1,283	1	NaCl	83	7
$CaCl_2$	32	1.75	Nb	358	6
Co	697	3	NH_4Cl	31	3.5
Co_2O_3	1,290	3	Ni	384	1
CoS	158	7	$NiCl_2$	51	2.75
Cu	228	7	NiO	1,305	6.25
CuCl	619	13	NiS	251	7
$CuCl_2 \cdot 2H_2O$	171	2.75	Pb	277	7
CuO	1,012	6.25	$PbCl_2$	51	2
CuS	440	4.75	S	163	6
Fe	768	7	Sb	390	1
$FeCl_2$	33	1.5	$SbCl_3$	224	1.75
$FeCl_3$	41	4	Sn	297	6
$FeCl_3 \cdot 6H_2O$	220	4.5	$SnCl_2$	476	2
Fe_2O_3	134	7	$SnCl_4$	49	8
$Fe_2(SO_4)_3 \cdot 9H_2O$	154	6	Ta	177	7
Hg	40	6	$TiCl_4$	31	4
$HgCl_2$	112	7	V	557	1
HgS	105	7	YCl_3	40	1.75
KCl	31	1	W	690	6.25
Mg	120	7	WO_3	1,270	6
$MgCl_2 \cdot 6H_2O$	254	4	Zn	581	3
$MnCl_2$	53	1.75	$ZnCl_2$	609	7
MnO_2	1,287	6	Zr	462	6
$MnSO_4 \cdot H_2O$	47	5			

*Maximum temperature obtained in the indicated time interval.

Table 18. Effect of microwave heating on the temperature of natural minerals[a,b].

Mineral	Chemical Compostion	Temp. °C	Time min.
Albite	$NaAlSi_3O_8$	82	7
Arizonit	$Fe_2O_3 \cdot 3TiO_2$	290	10
Chalcocite	Cu_2S	746	7
Chalcopyrite	$CuFeS_2$	920	1
Chromite	$FeCr_2O_4$	155	7
Cinnabar	HgS	144	8
Galena	PbS	956	7
Hematite	Fe_2O_3	182	7
Magnetite	Fe_2O_4	1,258	2.75
Marble	$CaCO_3$	74	4.25
Molybdenite	MoS_2	192	7
Orpiment	As_2S_3	92	4.5
Orthoclase	$KAlSi_3O_6$	67	7
Pyrite	FeS_2	1,019	6.75
Pyrrhotite	$Fe_{1-0.8}S$	886	1.75
Quartz	SiO_2	79	7
Sphalerite	ZnS	87	7
Tetrahedrite	$Cu_{12}Sb_4S_{13}$	151	7
Zircon	$ZrSiO_4$	52	7

[a]Maximum temperature obtained in the indicated time interval.
[b]High purity as identified by X-ray diffraction.

Dielectric Properties of Ferrites

Dielectric properties of ferrites have been looked at but up until this time, the data at the anticipated operating frequency has not been found. However, data at lower frequencies has been found in The Electronic Designers Handbook[4]. Table 18 is included here which shows some ferrite dielectric characteristics. As can be seen, dielectric characteristics vary widely with the specific material. If a particular lossy ferrite material can be found, the math model shows that this would make a good microwave absorptive material.

Math Model for Ice Disbonding

A mathematical model of microwave energy penetrating an energy absorbing material at the ice/pavement interface has been generated to better understand the efficiency one can attain using certain materials. This model has been completed and has been exercised to some degree. The work is reported in Appendix 2 of this document.

This effort indicates that with the dielectric parameters selected from lossy ferrite material, a layer as thin as 3 mm can result in 95% of the energy being absorbed. This is the kind of material we have been looking for but now a search for a specific material must be launched. A great deal of the ferrite material used in electronics has lower loss than that used in the model. Dielectric properties of ferrites are shown in Appendix 3 taken from reference No. 4.

Unfortunately, the dielectric properties taken from coal reported in reference 3 does not give acceptable absorption rates. However, recent microwave tests with coal samples show a high degree of absorption, the best from any material we have seen to date. These results are reported in Section 4 of this document. Since dielectric properties of coal vary widely, the data used in the model may not be accurate. All that is known of the coal sample is that it is authricite (hard coal), most likely from Pennsylvania and stored in an indoor coal bin for at least 30 years. It would be desirable to have the dielectric characteristics of this coal measured.

Laboratory Test Results

Several tests have been run in the laboratory to ascertain the properties of the coal and ferrite material being used in the experimentation. Some reflection and absorption tests have been conducted which are reported here.

Network Analyzer Tests (Return Loss Measurements)

A Hewlett Packard 8700 series network analyzer was used to make a return loss measurement of several samples of material to get an idea of the level of reflected power from these test samples. This data has been included in Appendix 4. Tests were run

between 1.69 and 2.65 GHz. Eccosorb 2.5 has 11.4 dB which means that more than 90% of the incident energy is absorbed in the material. It is suspected that ferrite is in this material but the company manufacturing it will not reveal its content. Asphalt using a carbon aggregate of coal (~ 1/4" thick) has a return loss of 3.5 dB which means that about 45% of the power is reflected. Similar measurements at 9 GHz were taken on the same samples and the return loss was between 8 and 12 dB. This data is included in the next section of this report.

Power Meter Tests (9 GHz)

Tests were run in the laboratory at 9 GHz to determine the return loss and the percent of microwave energy absorption with various material samples.

Measured Characteristics of Asphalt and Coal Samples

Case 1

Return Loss

Test Setup (Tests conducted at 9 GHz)

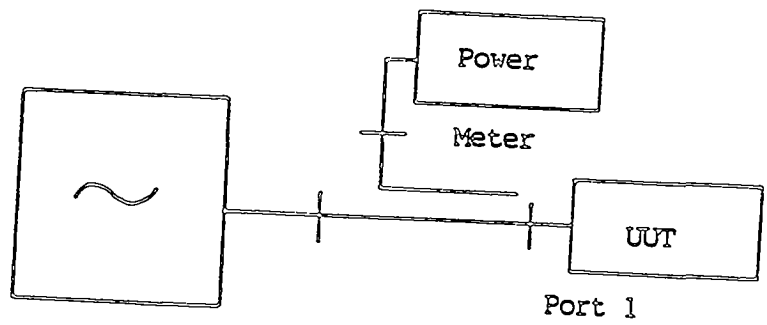

Amplitude of return loss relative to a short at port 1 is measured.

Coal with asphalt	Return loss
No back on sample	12.3 dB
Conductive plate on back of sample	11.2 dB

Coal and sand with asphalt

No back on sample	8.2 dB
Conductive plate on back of sample	7.5 dB

Case 2

Insertion loss

Test setup (tests conducted at 9 GHz)

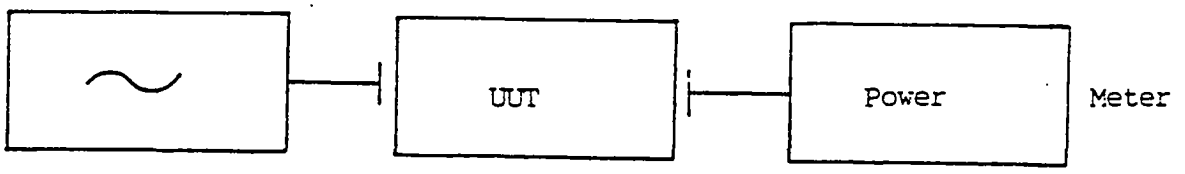

Amplitude of signal relative to amplitude with an air gap

Coal with asphalt	-9 dB
Coal and sand with asphalt	-8 dB

The measurements noted above indicate that more than 80% of the incident energy is absorbed in the test medium whether or not a metallic backing is used. The characteristics of the test medium from reference 3 indicate that the characteristics of this material are broad band enough that these results measured at X-band (9 GHz) can be interpolated to S-band (2.45 GHz) where the ice removal system will operate. When the measured data on absorption and reflection is compared to the rate of rise for the temp of a given sample subjected to microwaves at 2.45 GHz, we can conduct that 80% to 90% the incident energy is absorbed in the test medium. This assessment is supported by a calculated rate of rise of 30° per second at the power density of the experimental 20 kw unit.

Microwave Heating Tests

Several samples of absorbing material have been tested in the laboratory microwave unit as a measure of the length of time to give rise to temperatures causing the material to flash and burn. The coal sample has the shortest time to burn and coal asphalt is nearly the same. The data is presented in Table 18.

Material	Power Density in watts/gram	Set Fire (Burned) in seconds
Eccosorb 2.5	60	22
Iron Filings	75	27
Coal	60	8
Coal Asphalt	25	10
$Fe_3 O_4$	100	25

This information shows that coal absorbs energy more readily than any of the other materials tested.

Conclusions

At this point in time, there appears to be two materials that have high microwave energy absorbing characteristics although all of the data gathered does not correlate the way we would desire. A temperature probe is on order that would yield some rate of rise information on the various material samples. The math model generated indicates ferrites as being extremely energy absorbant although RAS has not obtained test samples that have these dielectric loss factors used in the model. The computer runs indicate that 3 mm of material can absorb 95% of the incident power.

The math model has used dielectric characteristics for coal taken from reference 3 which does not show favorable results for energy absorption. However, actual microwave tests with coal and coal asphalt indicate significant microwave energy absorption. Some laboratory tests at 9 GHz indicate at least 80 to 90 percent energy absorption. Additional time will be needed to ascertain why some of these differences exist but it does appear that high energy absorption may be possible to improve the efficiency of the microwave ice disbonding approach.

Microwave De-icing Project Synopsis

Future Projections of Microwave Ice Removal

The microwave de-icing project was terminated by SHRP due to the fact that a rather immediate payoff was not in sight and that more development would be required to make this approach economically and technically feasible. In an attempt to synthesize the project results and to incorporate data that would suggest future research efforts and projected equipment costs, the following pages have been included for project completeness.

Microwave De-Icing Project

The use of microwaves for the purpose of releasing ice from pavement surfaces is an interesting approach because there is virtually no environmental impact and no damage to the road surfaces or the microwave equipment when designed properly. The FCC has assigned a frequency for industrial use which can be applicable for road maintenance. Current efforts have shown that ice can be released from pavement surfaces with microwaves although the dielectric characteristics of normal highway materials, such as portland cement concrete (PCC) and asphalt, are not correct to achieve the desired efficiency and vehicle speeds.

The efforts within the past several months have concentrated a search for materials that have high microwave energy absorption at the frequency of operation while using thin layers. This search has led to carbon (coal) and ferrites as two possible candidate materials to be used in a pavement overlay. Experiments with coal aggregate asphalt have cut the ice disbonding time by approximately a factor of 10 compared to current pavement materials. More recently, a British firm has been located that claims greater than 95% energy absorption with a material the thickness of a coat of paint. These materials will need to be obtained and tests run to verify this level of performance.

Once efficient, low cost materials can be tested and verified, rapid ice disbonding tests with a moving microwave source will be required to determine the ultimate vehicle speed that can be attained. Midwest Research Institute has generated a report stating that ice melting on the order of 2 to 10 microns is sufficient for disbonding. Calculations show that if 10 microns of ice melting is sufficient, a 60 KW microwave device could remove ice on an 8 foot lane width at nearly 20 mph if at least 90% of the microwave energy is used for melting.

Microwave Project Accomplishments

- Developed Analytical Model
    - Shows with appropriate materials, >90% energy absorption can be achieved with thicknesses in the millimeter range.

- Have not had time to obtain the materials and verify analytical model with test data.

- Analytical model shows great sensitivity to dielectric loss tangent. Analytical model can be used in search/verification of material characteristics/performance.

○ Literature Search

- Several papers located presenting data on microwave absorption characteristics of various materials, the best appearing to be carbon (coal) and ferrites.

- Company located in England that claims absorption >95% with a thickness on the order of a coat of paint.

- Specific microwave frequency of operation not critical.

○ Test Results

- Verified that coal absorption of microwave energy is extremely high.

- Ice disbonding time is 10 times faster when coal is used to replace the aggregate in asphalt.

Remaining Tasks on Microwave Project for this (Second) Year

○ Further materials search and laboratory tests to determine optimum pavement overlay materials.

○ Contact company in England, get samples, run tests on microwave absorbing material.

○ Perform cost analysis on materials (cost per mile of application).

○ Make dielectric measurements in laboratory on various overlay materials (special equipment required costing ~ $10K in addition to existing RAS test equipment). This data can be used in analytical model for further verification of materials involving absorption efficiency.

○ Analyze/test microwave absorbing materials for strength, friction and wear

characteristics.

- Design and fabricate a mechanism that will test the ice release point on pavement samples using the 20 KW microwave generator, and the amount of force required for release. This data will be obtained simultaneously with the application of microwave power.

- Some testing may be accomplished out of doors (this winter) with the 20 KW generator although test conditions will not be controllable.

- Approximately $50K required for this effort in addition to the test equipment.

Efforts Required on Microwave Project

THIRD YEAR

- Design and fabricate a partial scale model microwave de-icing machine including ice removal blade (will not have prime mover but will work on 1/4 lane width).

- Fabricate 10 foot sections of test pavement with special overlay material developed previously (in 2nd year).

- Reform tests at CRREL (or similar suitable facility) under climatically controlled conditions and vehicle speeds. Ice blade removal force will also be measured.

- Optimum ice removal blade design will be used from University of Iowa development effort.

- Obtain design data for an actual microwave de-icing machine including cost to own/maintain/operate in addition to road treatment cost/lane mile.

- Run tests to determine the amount of microwave energy leakage with microwave shield design around applicator to insure safety for operators and bystanders.

- Approximately $100K - $120K required for this effort.

FOURTH YEAR

- Refine design of scale model de-icing machine, including prime mover.

- Implement controls for handy operation by operator.

- Perform tests under actual outdoor conditions with varying temperature. Gather performance data and operator comments.

- No cost estimate.

Cost Projection of a Microwave De-Icing Machine

Capital Cost (est.)

Prime Mover (truck, hydraulic controls and ice removal blade)	$120K
120 KVA Generator	70K
60 KW Microwave Generator	100K
	$290K Total

Operating Costs	Cost/Year
Maintenance (scheduled)	
Prime Mover	$1000
120 KVA Generator	200
60 KW Microwave Generator	1000
Maintenance (unscheduled)	1000
Total Maintenance	$3200 Total

Fuel	Cost/Year
120 KVA Generator (300 hp) 15 gal/hr at $1.25 gal	$19.00
Prime Mover: 3 mi/gal at 20 mph at $1.25/gal	8.88
	$27.33 Total

Assume unit is used 8 hr/wk, 21 wks/yr or 168 hrs/season (168 hrs x 20 mi = 3360 mi/yr). System end of life is assumed to be 8 yrs.

	Cost/Year
Capital Expense (290K/8 yr)	$36,250
Maintenance	3,200
Fuel at $27.33/hr x 168 hr/season	4,600
	$44,050 Total
Cost per hr at 168 hr/yr	$ 262/hr
Cost per mi at 168 hr/yr x 20 mph = 3360 mi/yr	$ 13.11/mi

References

1. "Applications of Microwave Energy in Extractive Metallurgy", by S.L. McGill and J.W. Walkiewicz found in the Journal of Microwave Power, Vol. 22, No. 3, 1987.

2. Microwave Browning Utensil by Jorgensen, Patent No. 4,496,815, dated January 29, 1985.

3. "Frequency Dependence of the Dielectric Properties of Coal - Part II", by S.O. Nelson, S.R. Beck-Montgomery, G.E. Fauslow and D.D. Bluhm, found in the Journal of Microwave Power, 16, (3 & 4), 1981.

4. Electronic Designers Handbook, J.L. Giacoletto, 2nd Edition, McGraw-Hill, 1977, TK7825L3.

High-Pressure Abrasive Liquid Jets

Nomenclature

AFR = Abrasive flow rate
ALJ = Abrasive liquid jet
AWJ = Abrasive Waterjet
d_m = Mixing tube diameter
d_n = Orifice diameter
h = Depth of cut
H = Workpiece ice thickness
L = Jet stand-off distance
l_m = Mixing tube length
P = pressure
U = Jet traverse speed
W = Width of cut (cutting kerf)
ω = Rotational speed

Introduction

Previous Research. Use of high pressure waterjets as an ice-breaking aid has been attempted in the past. From the open literature, it appeared that waterjets were first proposed as supplementary cutters for mobile ice-breaking equipment in Russia in the mid to late 1960's. Our literature search, however, failed to identify any relevant reports on the results (if any). The only apparent source of information was a 1971 paper by Shvayshteyn (1971) in which general qualitative waterjet characteristics were summarized with virtually no mention of any definite findings with respect to ice cutting applications.

In the United States initial efforts appeared to have started in the mid 1960's and mainly by the U.S. Army Cold Regions Research and Engineering Laboratory (USACRREL). The main focus of the USACRREL efforts was directed towards excavation of frozen ground (Mellor, 1972). A study was initiated in 1972 at USACRREL which explored the possibilities of using waterjets as ice-braking aids on inland waters. However, during the course of experiments, the project faced many difficulties which caused uncertainties in the validity of the measured data. The overall conclusion (as reported by Mellor, 1972) was that "continuous ice cutting with high pressure waterjets was not a feasible method due to: (1) excessively high power requirement and (2) unreliable state of the art high-pressure waterjet pumping equipment".

In the mid 1970's a collaborative study on cutting ice with high-pressure waterjets was initiated by USACRREL and the National Research Council of Canada, as reported by Coveney (Coveney, 1981). The potential of small to medium size high-pressure

waterjets to cut slots in an ice sheet, primarily for possible use as an assist of ice braking, was investigated in this study. Tests were performed on both fresh water ice and simulated sea ice. Among other results, a maximum penetration depth of 71.1 cm (28.1 in) for a 0°C fresh water ice with traverse speed of 0.21 km/hr (0.13 mph) was obtained. The nozzle pressure under these operating conditions was about 11MPa (1600 psi). Using the data collected, an empirical relationship which correlated the jet penetration to the power in the jet, the jet traverse speed, the nozzle stand-off and the estimated ice temperature was developed. Overall, the report's conclusions did not include any definite recommendations with respect to use of high-pressure waterjets in the ice cutting/disbonding applications.

Previous research in studying physical properties of ice and its formation characteristics on surfaces suggest that the physical strength of ice is often less than its adhesive force to a surface (e.g. Stallabrass, 1962 and Raraty, 1958). This implies that an effective de-icing mechanism utilizes its main energy thrust at the interface of ice and the paved surface where disruption of a strong bond is needed. Perhaps this is the main reason for failure of many mechanical (direct contact) devices in de-icing applications. These techniques often are capable of fracturing the ice but fail to remove the thin layer bonded to the paved surface.

While use of plain high-pressure waterjets for cutting and cavitation experiments dates back to the early 19th century, introduction of high-pressure abrasive-waterjet cutting is a newly born innovation which has dramatically enhanced the capability and effectiveness of this technique for various industrial application. The technique was first commercialized in 1983 and has since then been incorporated in many industries including construction, aerospace, paper, and automotive. The technique is now successfully used in situations where a "controlled-depth" concept is needed. Two of such examples include stripping the paint off the relicensed commercial airplanes and cleaning of airport runways from rubber deposits due to the landing/take-off of aircrafts.

The Present Study. A series of basic experiments to address the feasibility of high-pressure liquid abrasive jets for highway de-icing applications will be reported here. Experiments were performed to investigate effect of various jet/system parameters on cutting effectiveness and disbonding characteristics of ice using simulated pavement substrates. The parameters sudied included: jet pressure, jet temperature, stand-off distance, orifice diameter, abrasive flow rate, strategy and rate of traverse, and concentration of the chemical additive which prevented refreezing of the ice during and after detachment process. Experiments with both linear and rotary jets were performed. Collective results of the study suggest that ice erosion characteristics compare closely with those of brittle type materials. With respect to the feasibility of the technique for de-icing applications, the results are very promising and of practical interest.

Experimental Apparatus and Procedure

Schematic presentation of the experimental set up is shown in Figure 13. The main component of the experimental apparatus was a triple-intensifier 150 hp pump which was connected to a PASER nozzle assembly. The system was a commercially available unit, manufactured by Flow International Inc., Kent WA., U.S.A. Under maximum operating conditions the pump could deliver up to 30.3 L/min (8.0 gpm) of flow. Garnet (mesh size ranging between 60 and 80) was used as the abrasive material. Entrainment of abrasives into the nozzle assembly and mixing with water was through combined gravity and jet pump-induced effects. The abrasive flow rate was controlled by a calibrated orifice plate mounted on an abrasive hopper. Clear plastic tubing was used to transport abrasives from the hopper to the nozzle assembly.

Simulated ice samples were prepared in a temperature controlled cold room environment. The ice was cast on a pre-cured concrete substrate in a specially designed mold that permitted casting of the ice at a desired thickness. Different sample thicknesses were needed for the various parametric studies in the present work. To monitor the ice temperature during the cutting process, two type E themocouples were embedded in the mold (at the ice-substrate interface) prior to the freezing process. For a given experimental run, several samples were prepared in the cold room under an equal freezing environment. Shortly before the experimental run was performed, the samples were transferred to the site of the experiments. The average ice temperature during the cutting process was recorded by a strip chart recorder. The depth and width of cut were measured manually with a finely gaged scale. The duration of the cut for a given sample was less than a minute. This was small enough to prevent a significant change in the mean sample temperature during the cut. Moreover, to perform experiments under equal equilibrium conditions, minimum elapsed time was allowed between cutting of two consecutive samples. Overall, the average deviation of sample temperature from each other during an experimental run was 0.50°C or less. Further details of the experimental apparatus and procedure can be found in Haase (1990).

Results and Discussion

Presentation of selected parametric study results, and feasibility evaluations will be given here. More comprehensive documentation of the results can be found in quarterly reports Nos. 3, 4, and 5 on this project (1989,1990, and 1990, respectively). Video-taped documentation of linear and rotary jet experiments is available at the Institute of Snow Research (ISR), Michigan Technological University.

Parametric Studies

Linear Jet Cutting Experiments.

Effect of jet pressure on depth of cut at four different traverse speeds is shown in

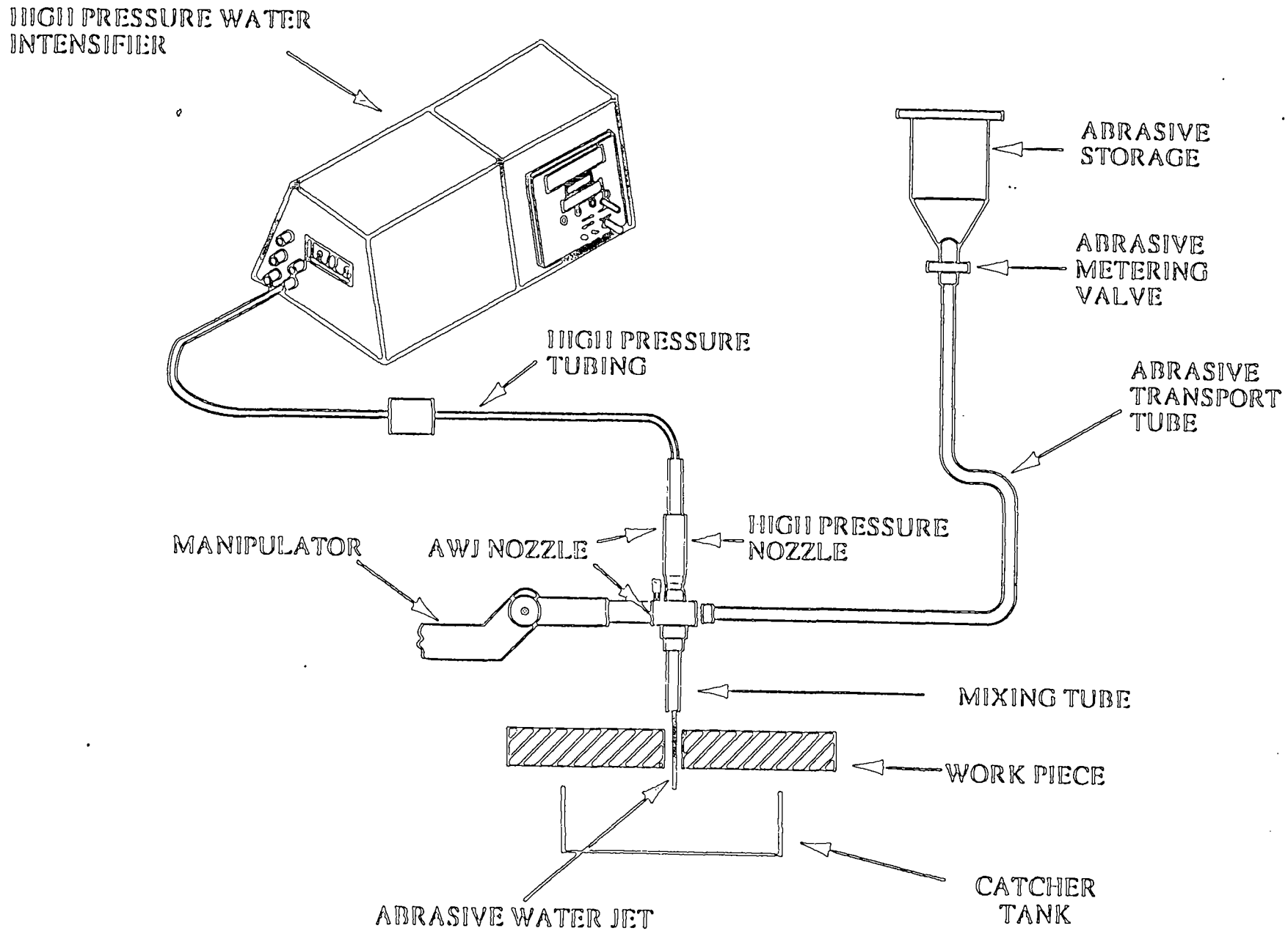
HIGH PRESSURE WATER INTENSIFIER
ABRASIVE STORAGE
ABRASIVE METERING VALVE
HIGH PRESSURE TUBING
ABRASIVE TRANSPORT TUBE
MANIPULATOR
AWJ NOZZLE
HIGH PRESSURE NOZZLE
MIXING TUBE
WORK PIECE
ABRASIVE WATER JET
CATCHER TANK

Figure 13

Figure 14. It is seen that the sensitivity of depth of cut to the jet pressure is more pronounced of lower traverse speeds. The orifice diameter is another important parmeter whose effect at various pressures is shown in Figure 15. As shown thre, a higher jet pressure and/or orifice diameter results in higher jet total momentum and, therefore, improved depth of cut. A similar effect on width of cut can be seen in Figure 16. However, beyond a certain pressure (here 12 ksi) additional increase in the jet pressure did not appear to have any pronouced effect on width of the cut. It is interesting to note that, however, the orifice diameter has a significant effect on width of cut at all of the jet pressures experimented.

Abrasive flow rate (Figure 17) appears to have an optimum value at which highest depth of cut can be obtained for a given set of parameters. At lower pressures abrasive enterainment process is inefficient which results in lower depth of cuts as indicated in Figure 17. Effect of jet beam angle on depth of cut is presented in Figure 18. From the results in Fig. 6 it is clear that maximum depth of cut occurs at approximately 75 to 80 degrees from the workpiece plane (horizontal in this case). This finding is consistent with studies by Finnie (1967) who showed that for a brittle material's maximum reveal rates that take place at sharp angles (close to 90 degrees in most cases).

Effect of external heating of the jet and the corresponding heating power requirements are shown in Figures 19 and 20, respectively. For the range of parameters studied, a jet temperature of approximately 80°C appears to be the optimum value. The corresponding heating power requirement is approximately 5 kw (Figure 20). In the light of significant improvement in depth of cut with reasonable power consumptions, incorporation of external for heating liquid jet de-icing applications appears to be a wise choice.

Comparison of three freezing point depressants with that of plain tap water is provided in Figure 21. In all cases the concentrations shown were large enough to prevent refreezing of the detached ice. Brine is the least expensive of the three alternatives considered, and when used in conjunction with an Abrasive Water Jet (AWJ), its accumulation on the road environment is negligible (compared to any of the conventional techniques currently in use). Therefore, it may be recommended as the preferred choice over ethylene glycol and CMA for the application at hand.

Rotary Jet Cutting Experiments. A plain (non-abrasive) rotary waterjet system was used to perform parametric and feasibility studies for de-icing applications. The system was capable of housing up to six jets, equally spaced on a six-inch diameter rotating leg. Flow distribution to these six jets was designed to be more or less equal once the system reached it operating conditions shortly after it was turned on. The design did not incorporate use of abrasive (in fact rotary jets with abrasives are still in the laboratory stage and not commercialized in the U.S. yet. Photocopies of the rotary system pictures,

DEPTH OF CUT VS. TRAVERSE SPEED

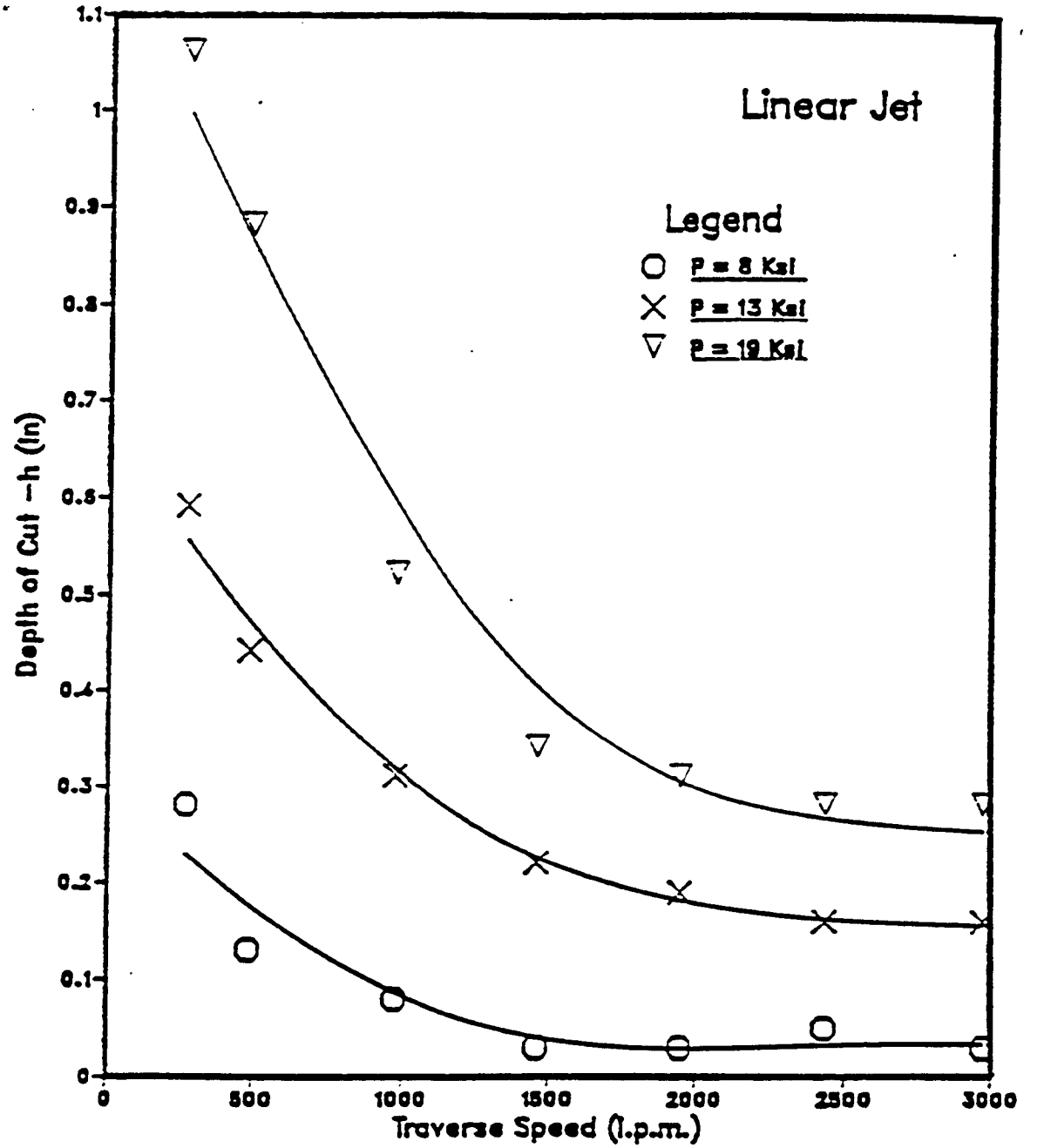

AFR = 0.54 lb/min, Mesh No. 80, L = 7.5 in

dn = 0.018 in, dm=0.075 in, lm = 3.0 in

Figure 14

EFFECTS OF ORIFICE DIAMETER ON DEPTH OF CUT

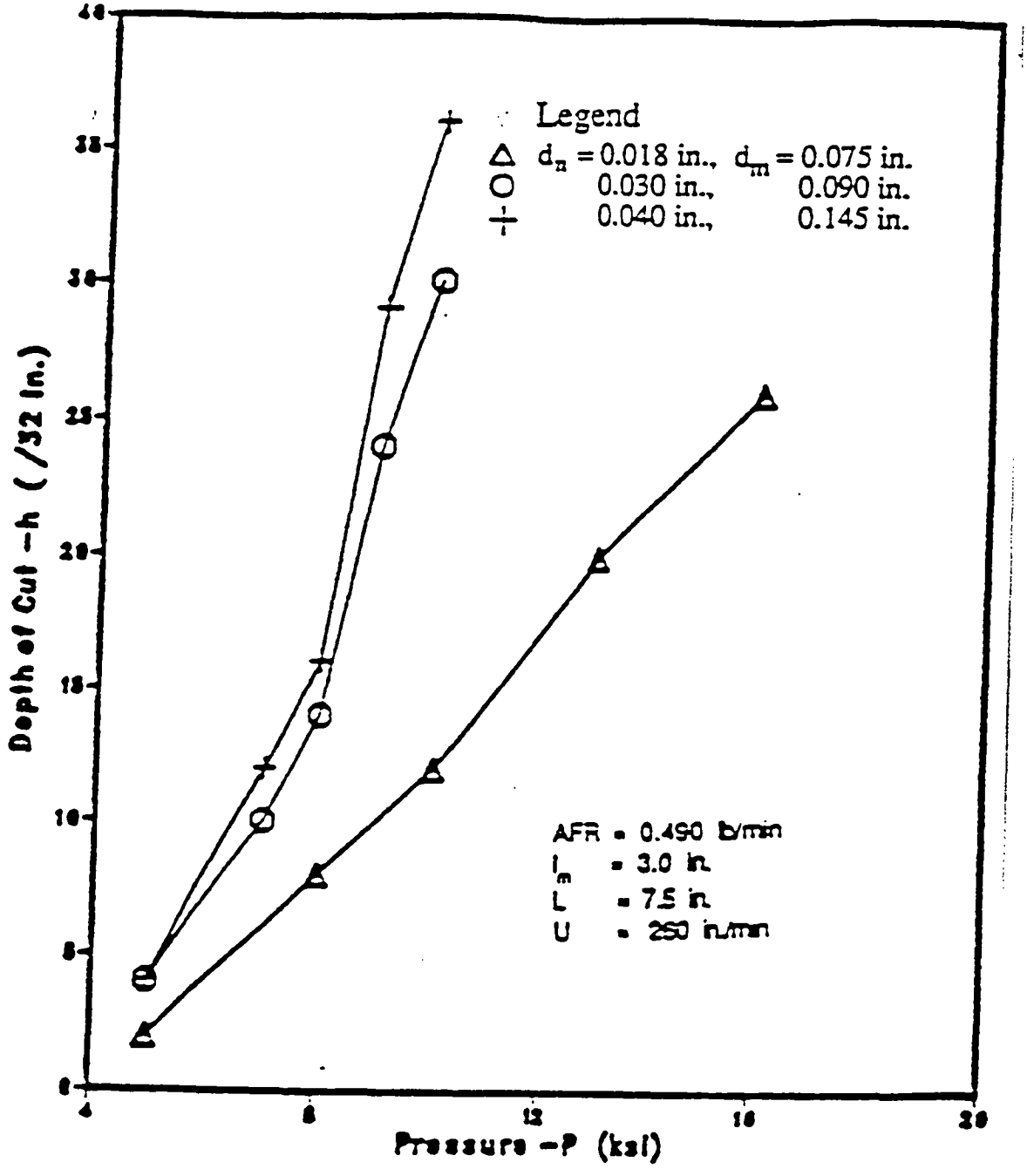

Figure 15

EFFECTS OF ORIFICE DIAMETER ON WIDTH OF CUT

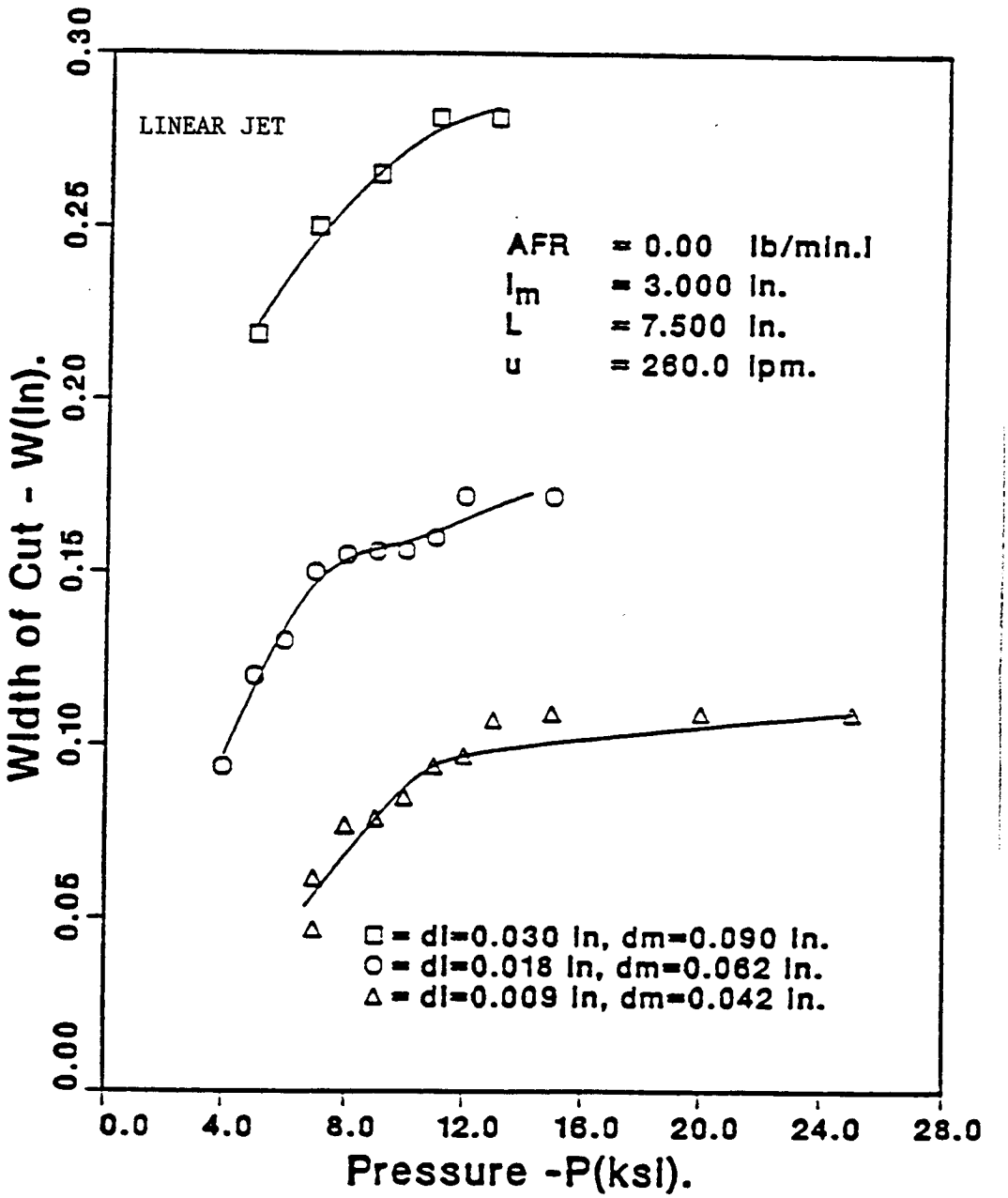

Figure 16

EFFECTS OF ABRASIVE FLOWRATE

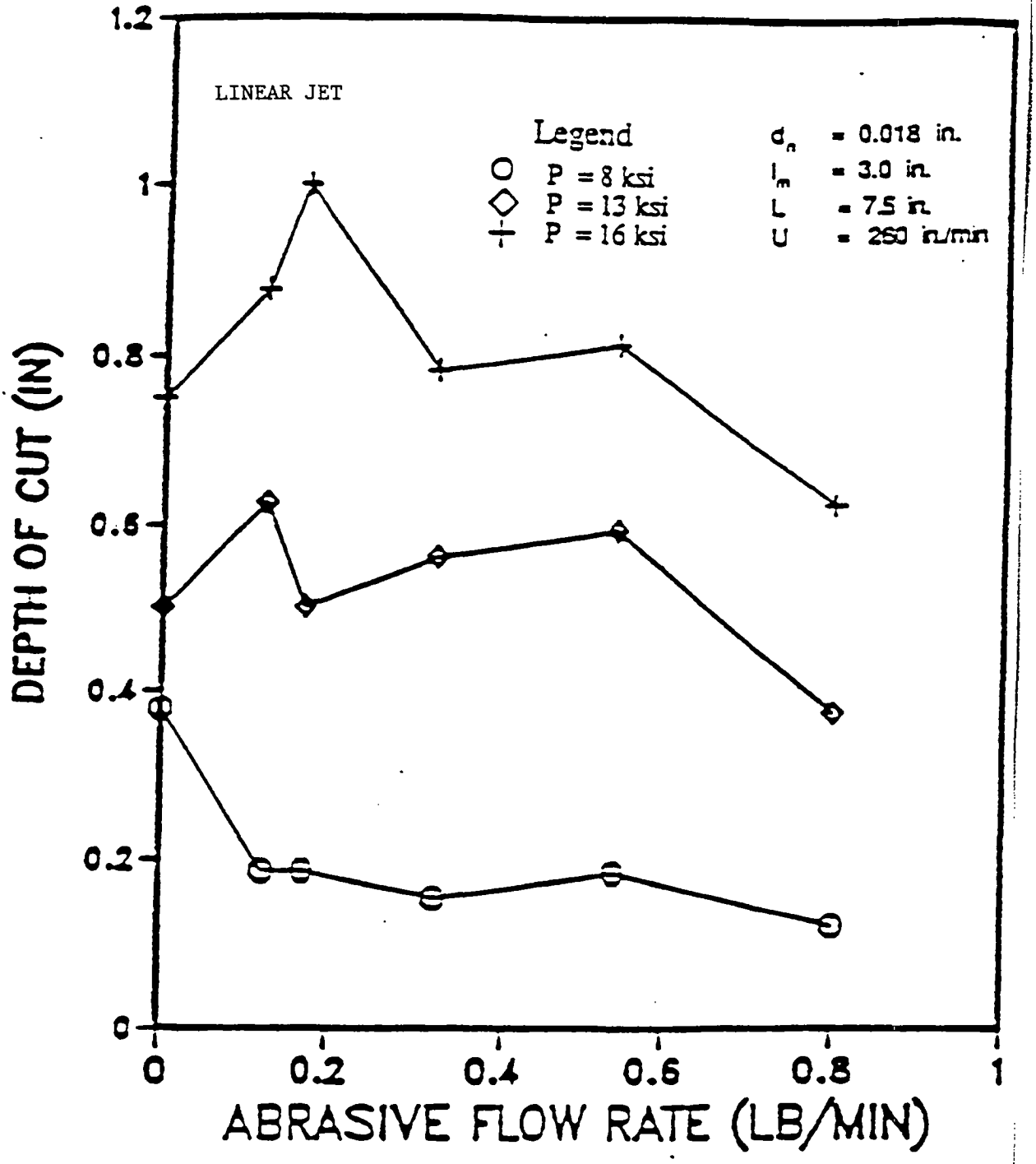

Figure 17

EFFECTS OF JET BEAM ANGLE ON DEPTH OF CUT

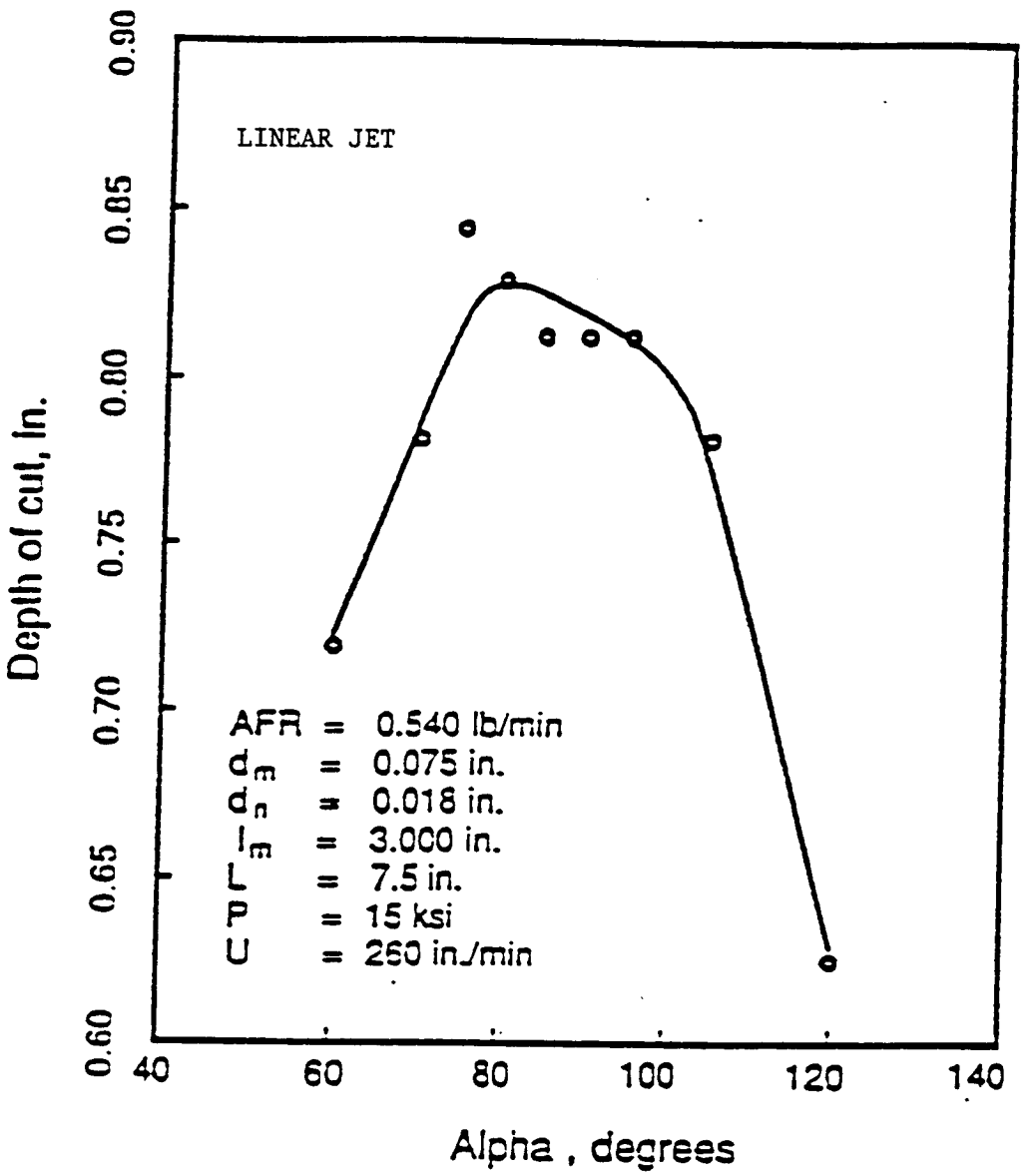

Figure 18

EFFECT OF TEMPERATURE ON DEPTH OF CUT

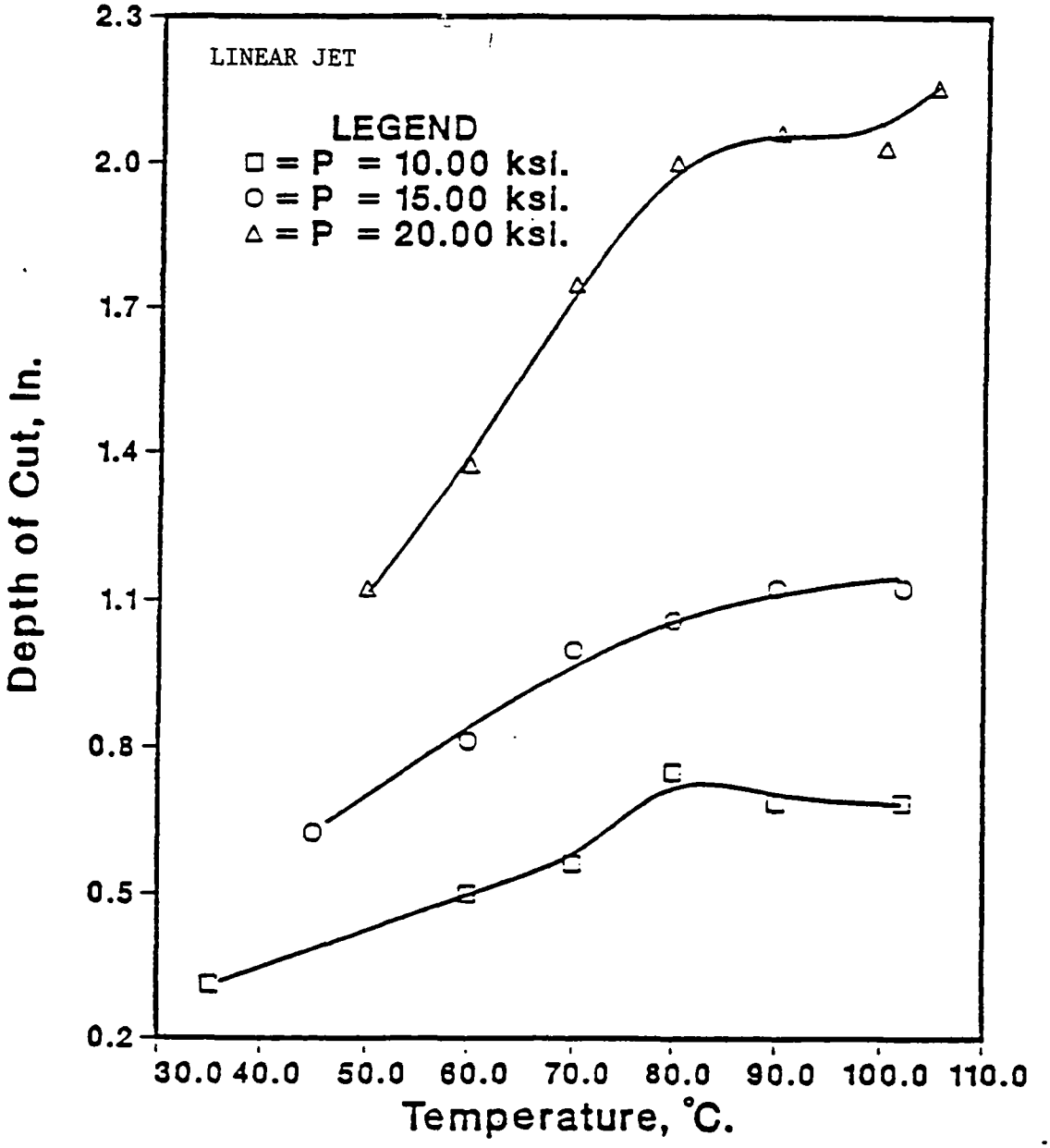

AFR = 0.540 lb/min, d_n = 0.018 in. L = 7.5 in.
d_m = 0.075 in. l_m = 3.0 in. P = 15.0 ksi.
Garnet Mesh NO. 80

Figure 19

POWER CONSUMPTION FOR HIGH TEMPERATURE AWJ

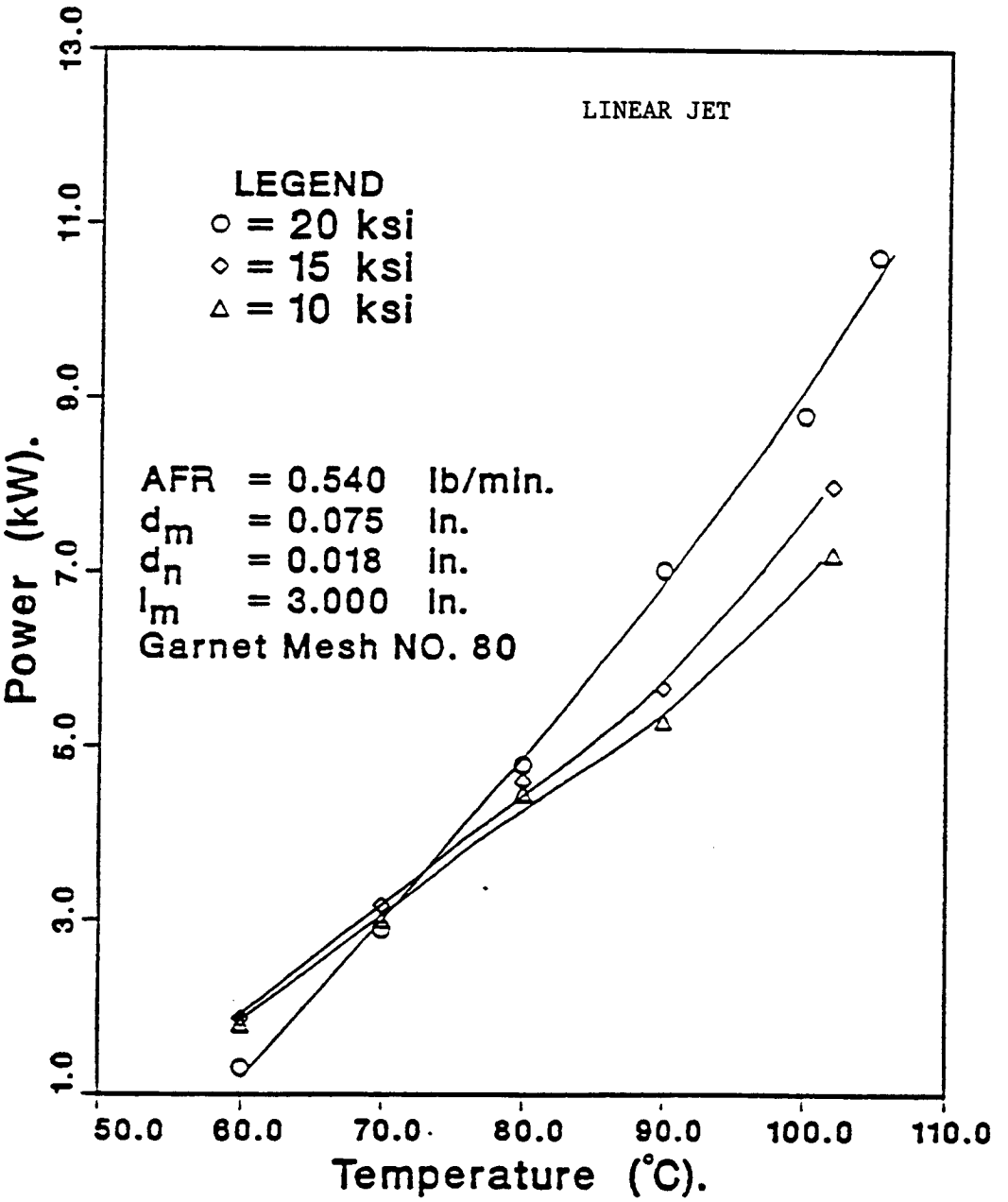

Figure 20

COMPARISON OF FREEZING POINT DEPRESSIVE SOLUTIONS WITH TAP WATER

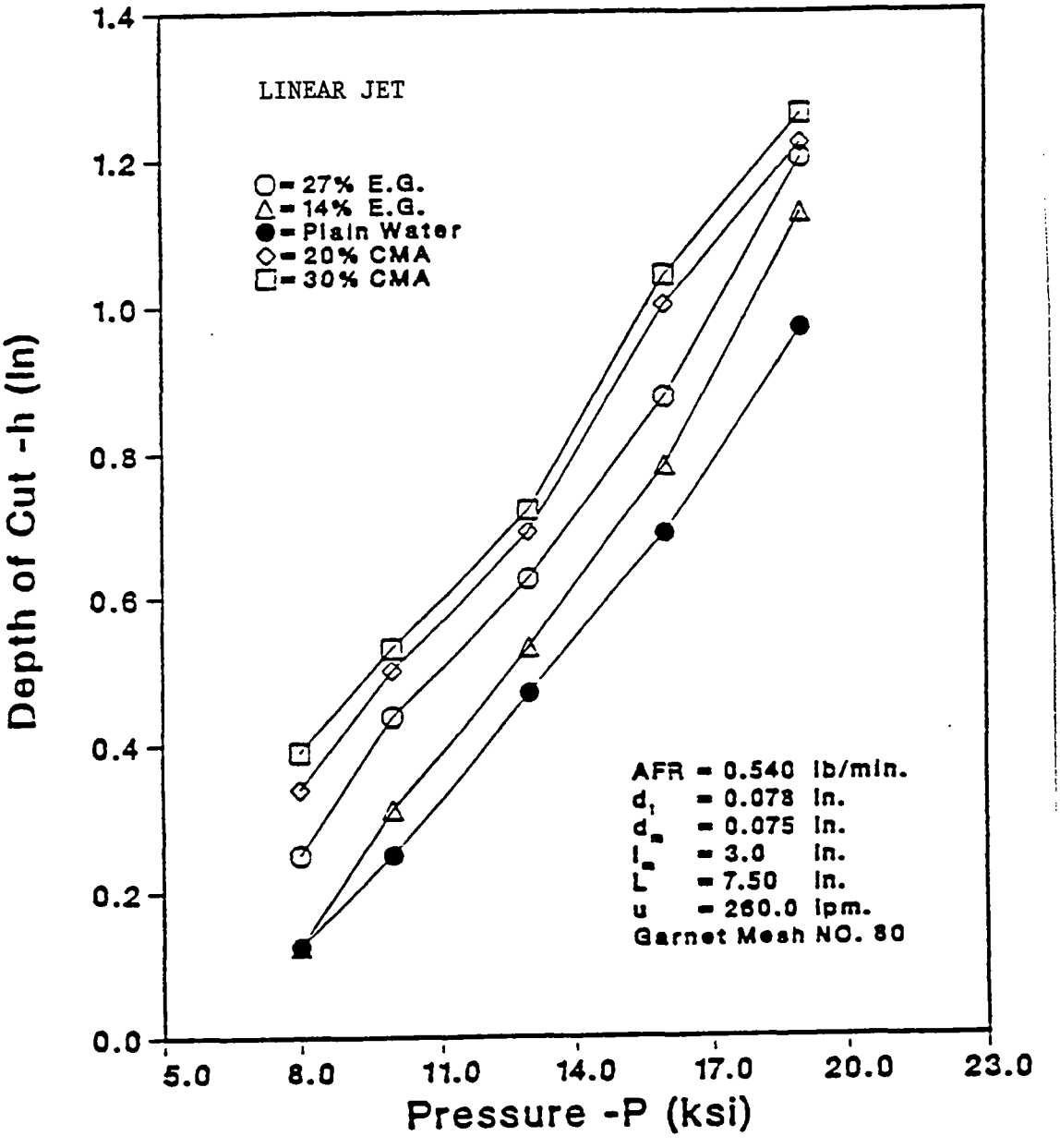

Figure 21

at pressures of 10 and 25 ksi at a rotational speed of 700 rpm, are shown in Figures 22 and 23, respectively. While it is difficult to identify detailed differences between those two figures, the 25 ksi jets have a higher coherency and impact momentum.

Similar to those of the linear jet cutting, a series of experiments were performed to investigate depth of cut as a function of jet pressure (Figure 24) rotational speed[1] (Figure 25), traverse speed[2] (Figure 26) and stand-off distance[3] (Figure 27). As seen in these figures, the corresponding trends are similar to those of the linear jets. That is, higher pressures result in an exponential increase in depth of cut while a higher traverse speed or stand-off distance causes an exponentially reduced depth of cut. The rotational speed (Figure 25) appears to have a moderate effect at lower rpms (here up to approximately 300 rpm). However, at higher rpms the effect becomes diminishingly negligible. A short video on the rotary jet experiments was prepared and is available at the Institute of Snow Research at MTU.

Although the rotary jets offer certain advantages (e.g., a wider and more uniform cutting groove), their use over the linear jets does not appear to the preferred choice at this stage. The technology is in infancy, and it lacks many design optimizations which over the years have been incorporated into the linear jet cutting systems. With the current design, for a given jet pressure and flow rate, the energy conversion efficiency in rotary jets may be considerably less than their corresponding linear jets. More importantly, currently no abrasive rotary heads are available in the market place, which may put the rotary jets at a significant disadvantage for the application at hand.

Mathematical Modeling. Mathematical modeling of the process was attempted by modifying an existing model to address the conditions in de-icing applications. Details of the model can be found in (Ohadi, et al., 1990). Comparison of the mathematical modeling results with those of the experimental measurements for three different traverse speeds are shown in Figure 28. The agreements between the two sets of data is reasonable, particularly at higher pressures where AWJs are used in most applications. Next, using the model , it was predicted that a pressure of 69 ksi is needed to de-ice a 1/4" thick ice layer at 20 mph traverse speed (Fig. 17). The model predicted results in Figure 29 compare closely with the corresponding experimental results in Figure 14. The estimated 69 ksi pressure is well within the operating range of modern high-pressure pumps which could deliver up to 100 ksi and currently are manufactured in West Germany and Japan.

---

[1]The rpm of the rotating jet assembly.

[2]The linear moving velocity of the jet orifice/nozzle assembly..the traversing speed.

[3]Distance between the end of the collimating tube and the workpiece

ROTARY JET CUTTING OF ICE

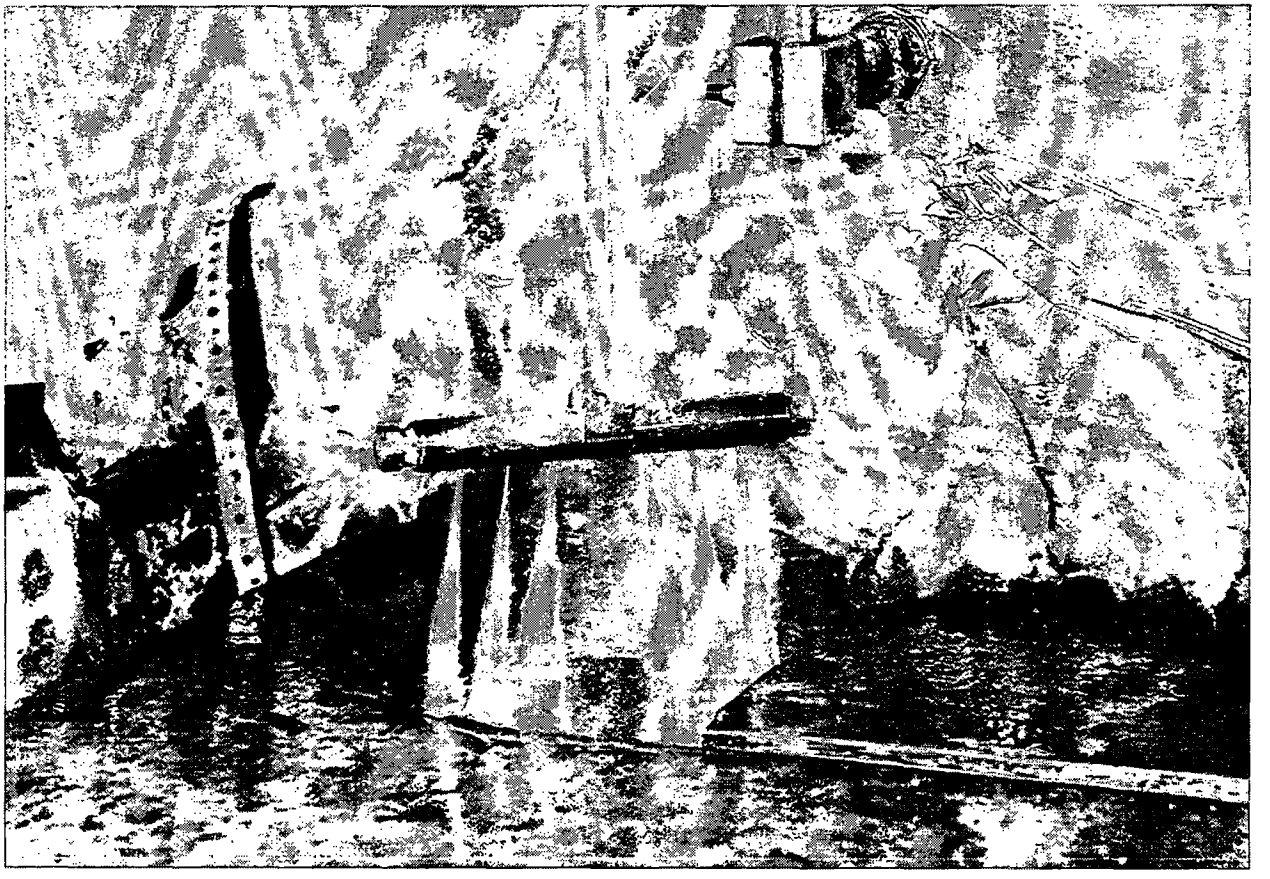

Pressure of 10 KSI Rotational Speed 700 rpm

Figure 22

ROTARY JET CUTTING OF ICE

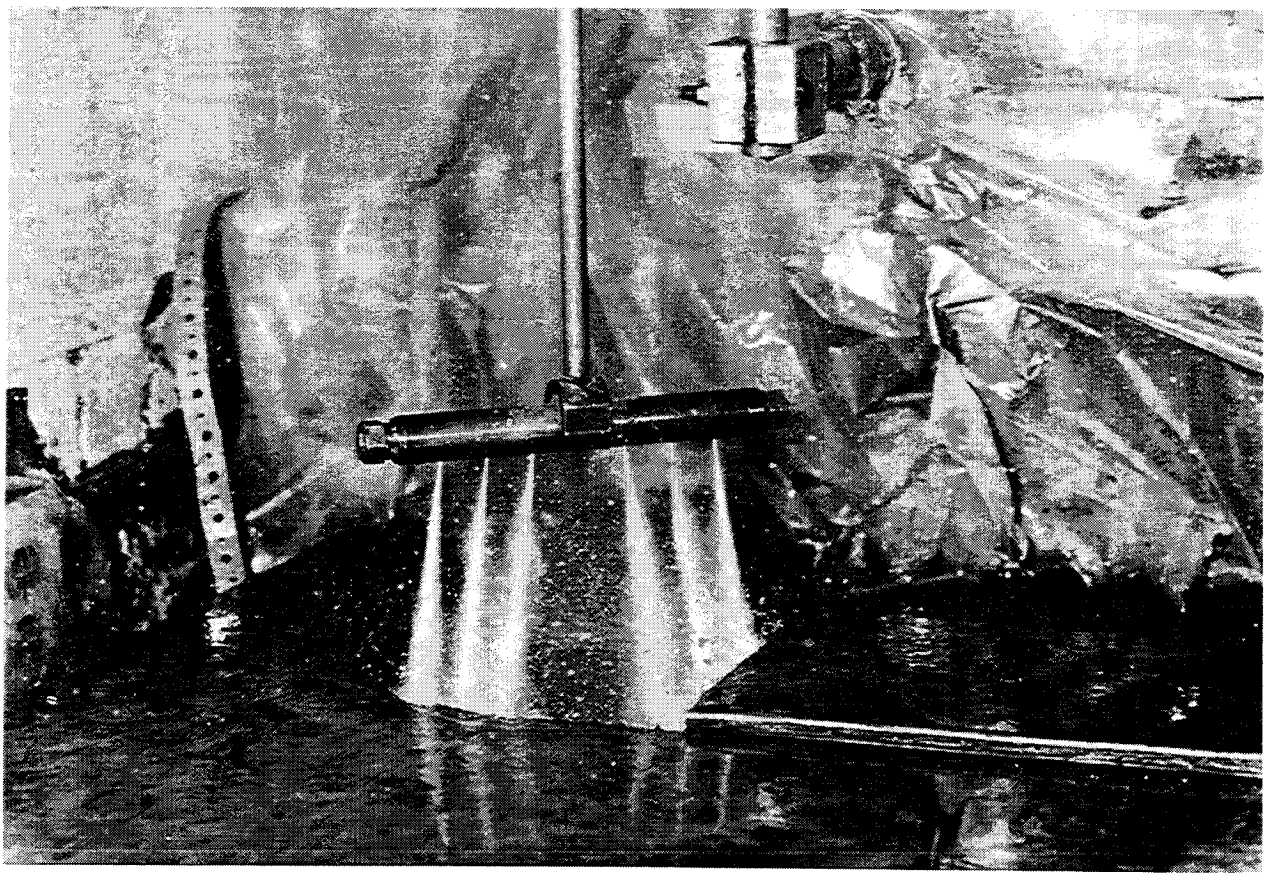

Pressure - 25 KSI Rotational Speed 700 rpm

Figure 23

DEPTH OF CUT VS. PRESSURE

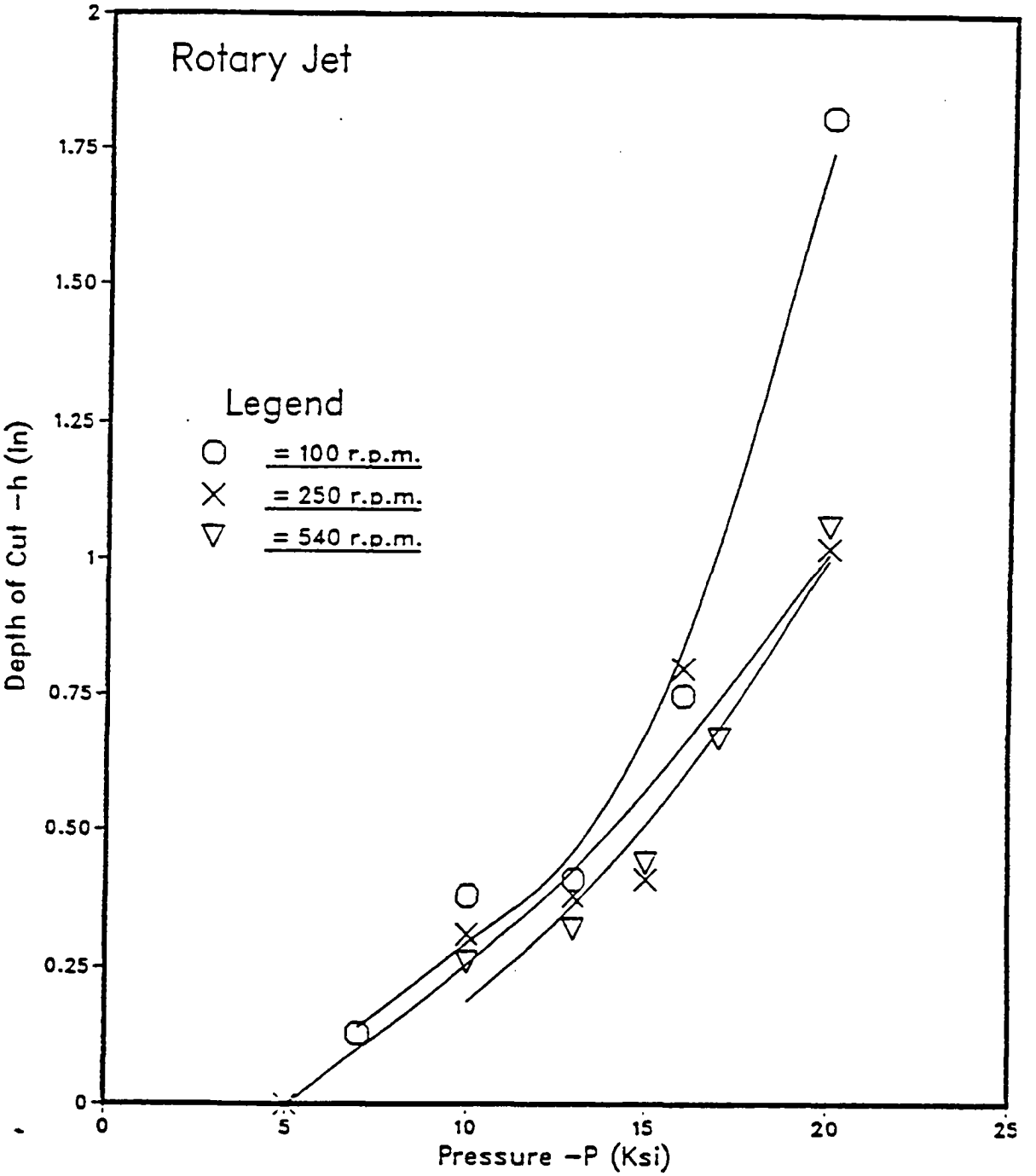

U = 260 in/min, dn = 4 at .018 in, L = 1.0 in

Figure 24

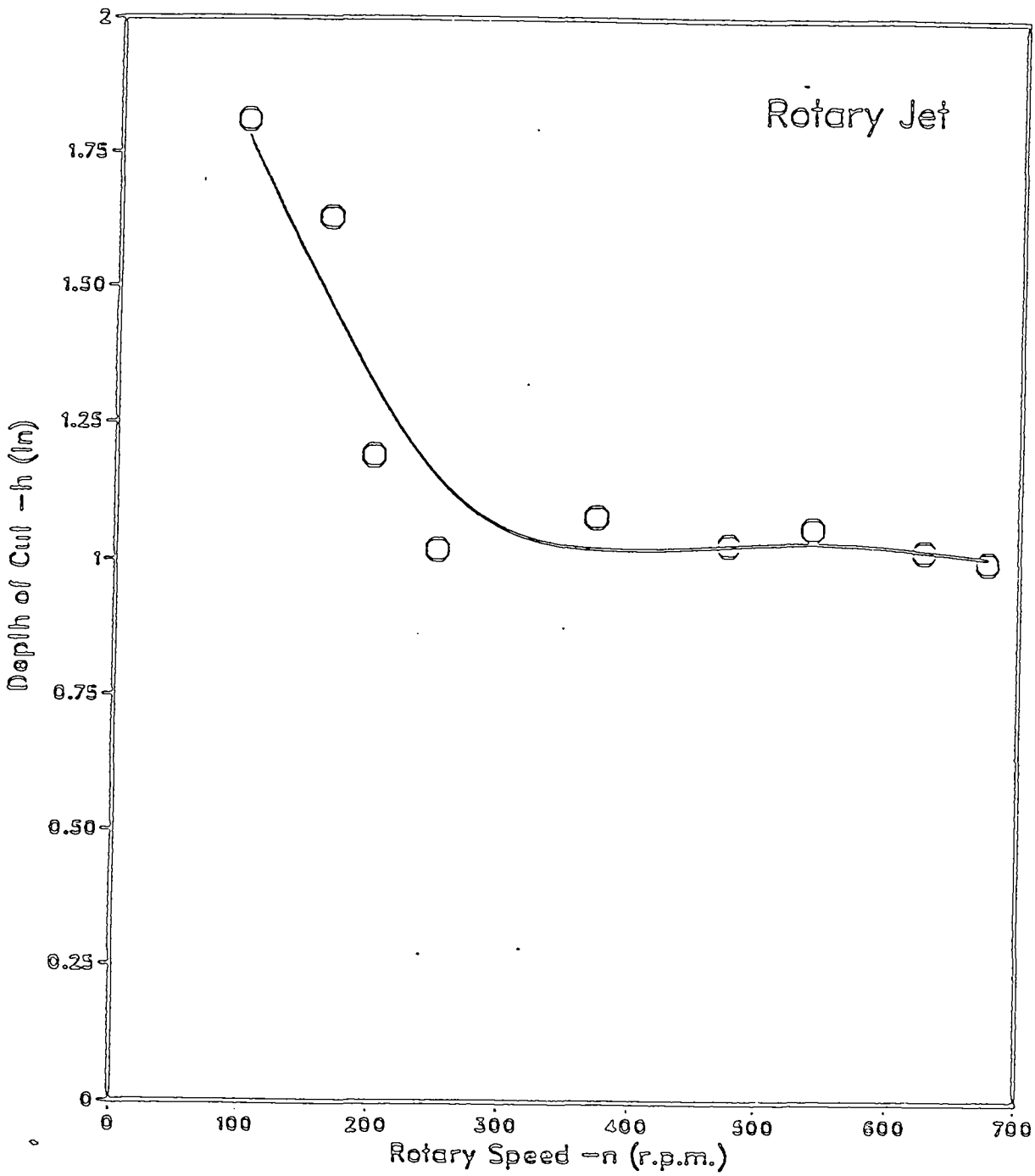

P = 20 Ksi, dn = 4 at .018 in, U = 270 ipm, L = 1.0 in

Figure 25

DEPTH OF CUT VS. TRAVERSE SPEED

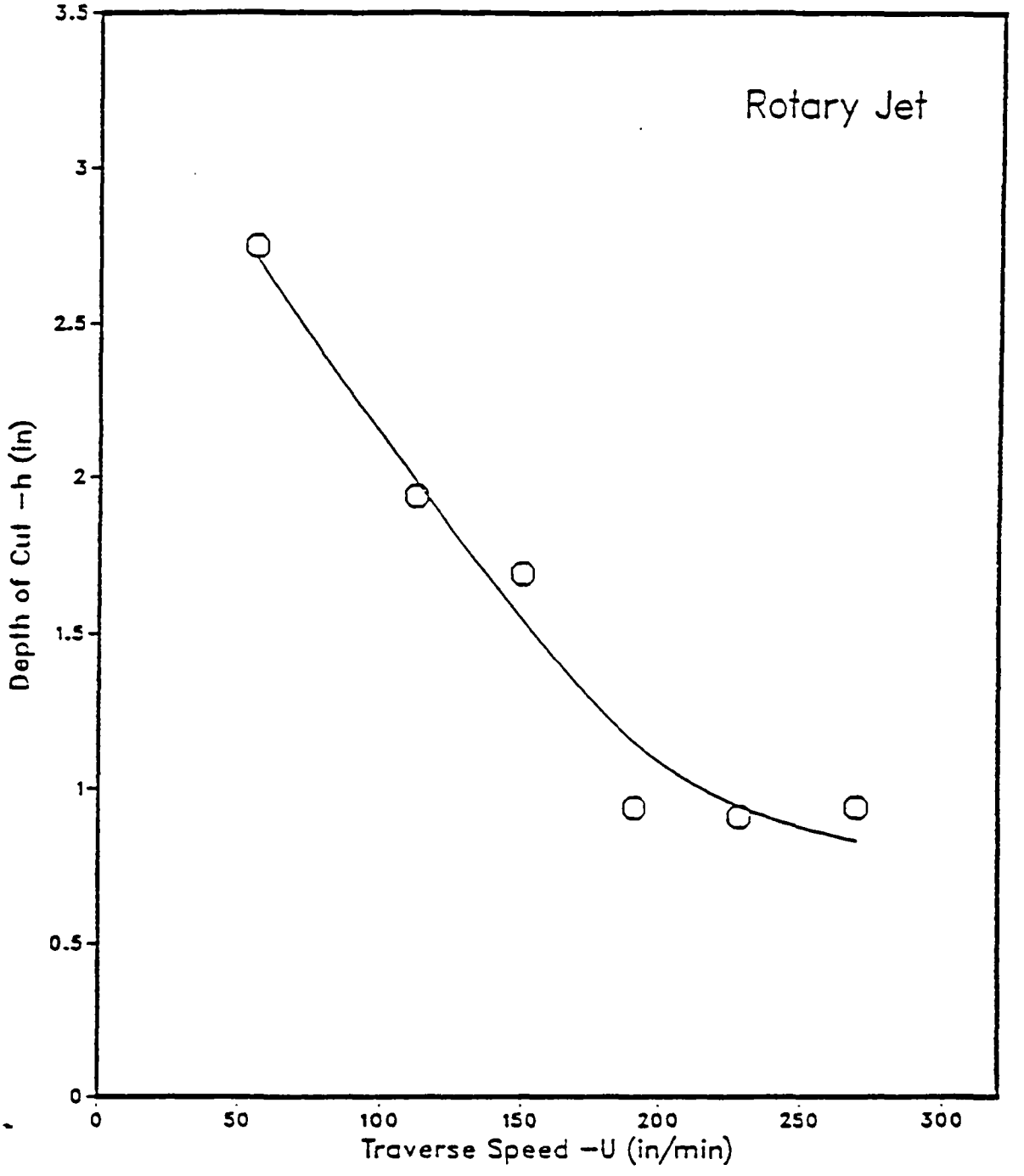

P = 20 Ksi, dn = 4 at .018 in, n = 540 rpm, L = 1.0 in

Figure 26

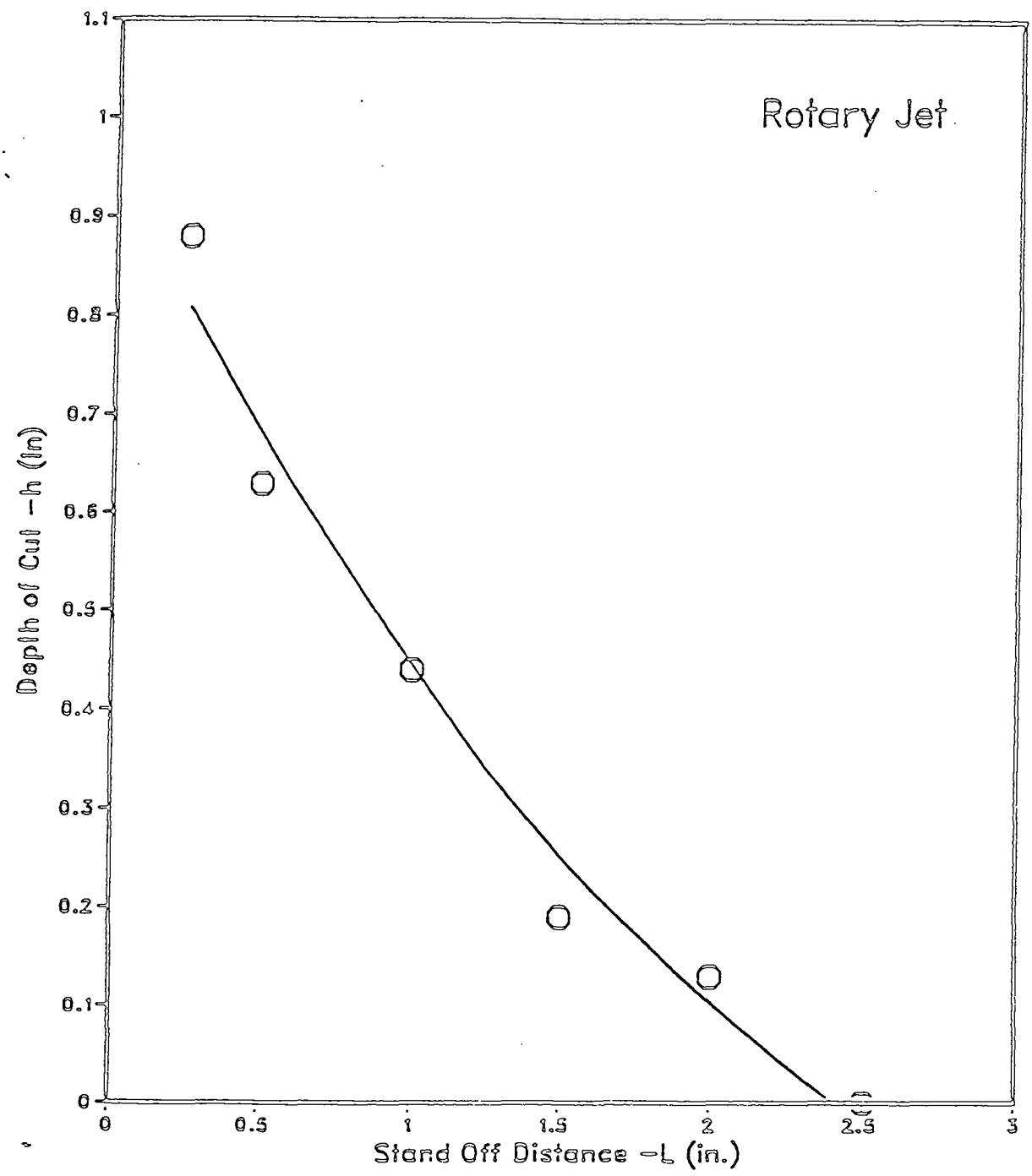
DEPTH OF CUT VS. STANDOFF DISTANCE
Rotary Jet
Depth of Cut - h (in)
Stand Off Distance - L (in.)
1.1
1
0.9
0.8
0.7
0.6
0.5
0.4
0.3
0.2
0.1
0
0
0.5
1
1.5
2
2.5
3
P = 15 Ksi, dn = 4 at 0.018in, n = 540 rpm

Figure 27

COMPARISON OF MATH MODEL WITH EXPERIMENTS

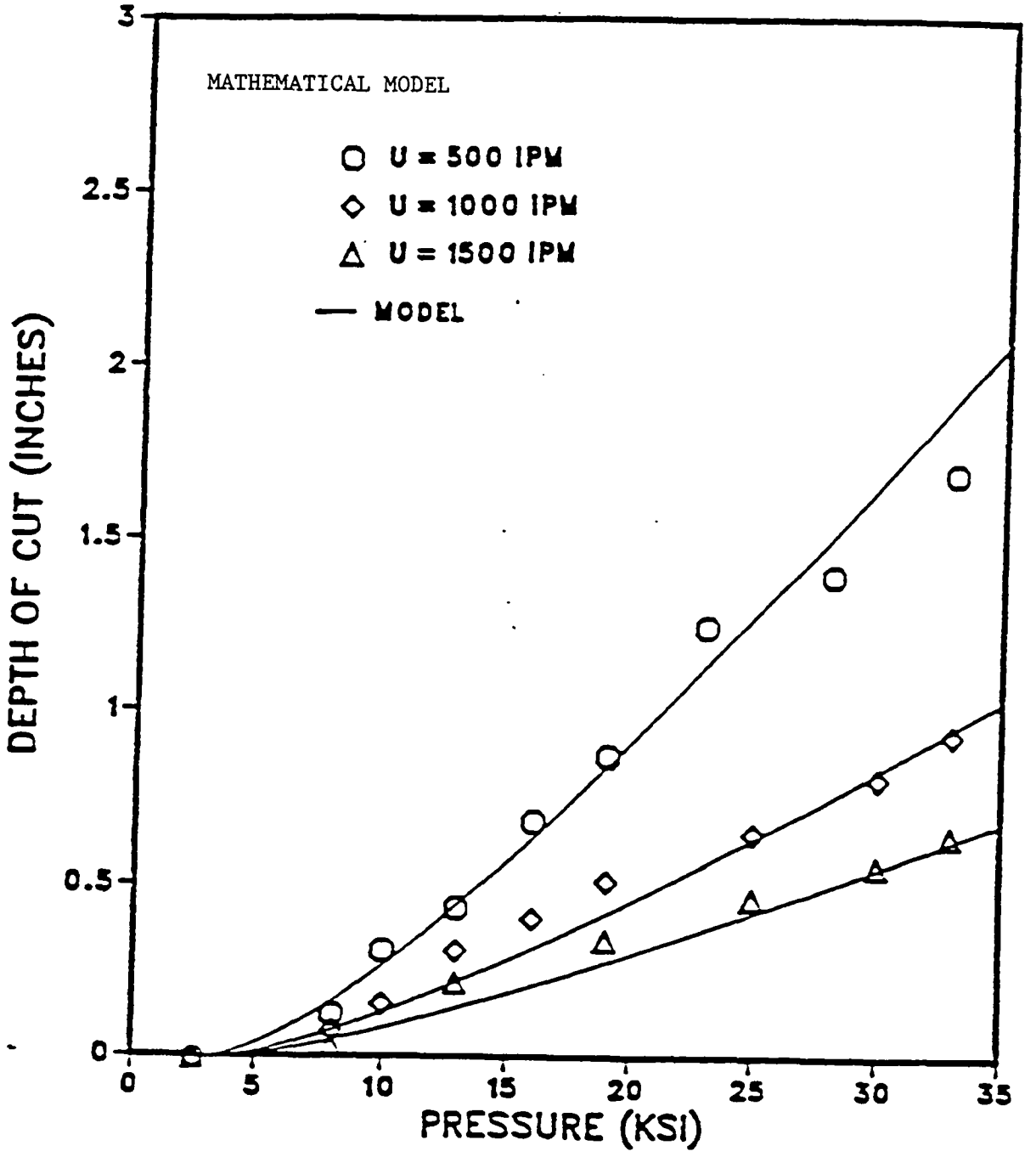

Figure 28

COMPARISON OF MATH MODEL WITH EXPERIMENTS

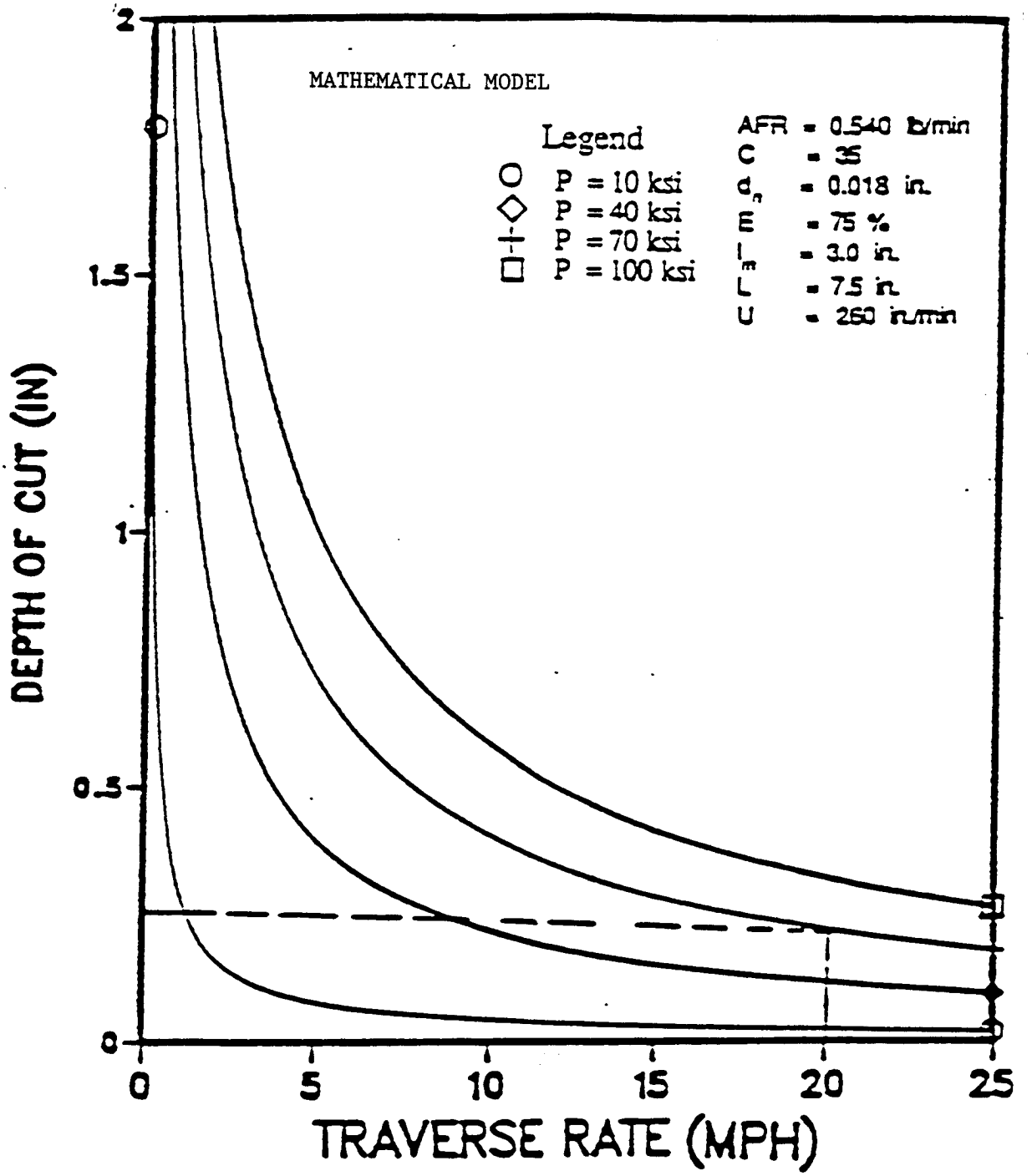

Figure 29

Linear Jet Cutting Contours. Figures 30(a) to 30(h) present cutting contours for a case in which a larger orifice (0.040 in vs. 0.018 in the earlier experiments) in conjunction with a higher jet traverse speed (Maximum of 3000 i.p.m. vs. 260 i.p.m. in the older cuts) was used. These figures represent top views and the depth of cut is indicated in each case. The experimental parameters are listed at the bottom of each figure. Note that the ice thickness is 1.250 in all cases. This thickness was deep enough to allow examining the maximum potential depth of cut or lifting of the ice over a wide range of operating parameters.

As the traverse speed is increased, an interesting pattern in the cutting contours of Figs. 30(a)-30(h) can be identified. At lower traverse speeds a groove-type cut can be observed. As U is increased, the cut width expands at a much faster rate. At velocities higher than 500 i.p.m., the groove-type cut changes into an area removal type. Thus, at higher jet traverse speeds, better utilization of the jet impact energy on the workpiece takes place. Note that in all cases, a time-lag between the start of the cut and where expansion into a larger cutting area takes place is present. All workpieces were 13"x13", and the jet traversed along the workpiece mid line to eliminate any edge effects. Based on the observations in Figs. 30(a) to 30(h), a stress propagation ratio of as much as 14 times the mixing tube diameter and 120 times the orifice diameter can be observed. Therefore, if extrapolation of the results holds true, a total of six jets, each with a 0.1875" (3/16") orifice diameter, may be sufficient to de-ice a twelve-foot wide lane under the listed operating parameters. An arrangement similar to that illustrated in Figure 31 can be used. Note that here the pressure is only 13 ksi, and other than the presence of abrasives, no other auxiliary effects (such as external heating of the jet or the optimum jet retardation angle, etc.) are present.

The results at high traverse speeds are very encouraging, and it is unfortunate that they were not available at the time of SHRP feasibility review meeting in August 1990. Due to the project's termination, we were unable to verify the above suggested estimated requirements. This may be a proper beginning point if this research is to be revisited in the future.

LINEAR JET TRAVERSE CUTTING PATTERN

U = 270 i.p.m

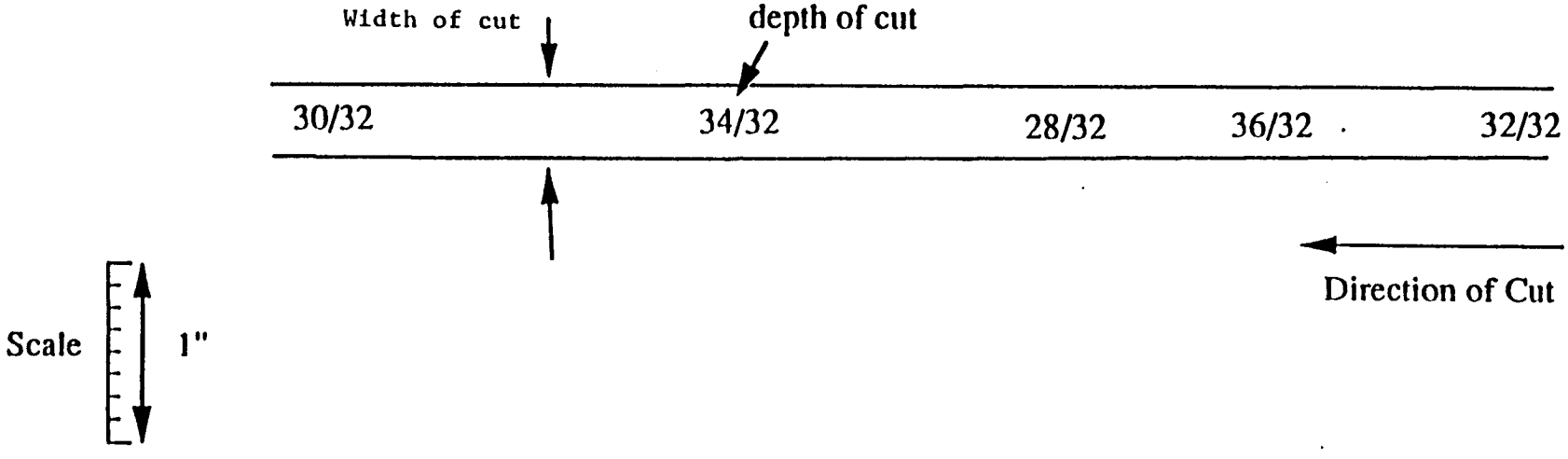

Experimental Parameters: AFR = 2 lb/min (Garnet mesh #80), P = 13 ksi, L = 7.5", d_n= 0.040", d_m= 0.145", ice thickness, H = 1.25", Square Sample, 13" x 13".

* All depth of cut dimensions in [in.]

Figure 30(a)

LINEAR JET TRAVERSE CUTTING PATTERN

U = 350 i.p.m

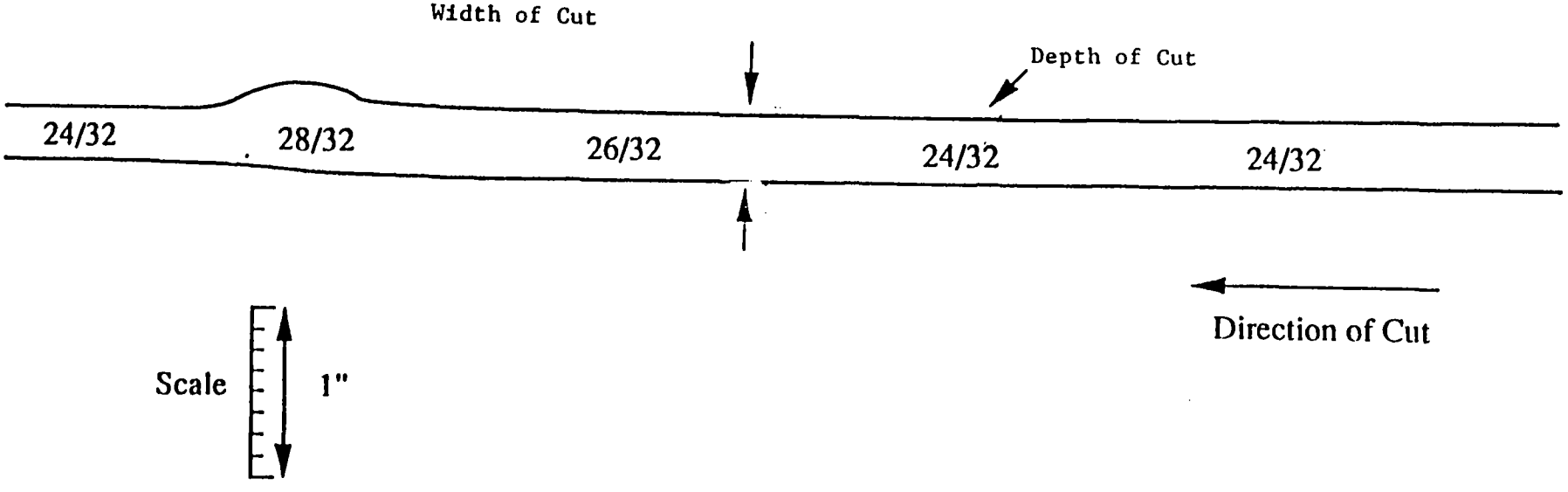

Experimental Parameters: AFR = 2 lb/min (Garnet mesh #80), P = 13 ksi, L = 7.5", d_n= 0.040", d_m= 0.145", ice thickness, H = 1.25", Square Sample, 13" x 13".

Figure 30(b)

LINEAR JET TRAVERSE CUTTING PATTERN

U = 400 i.p.m

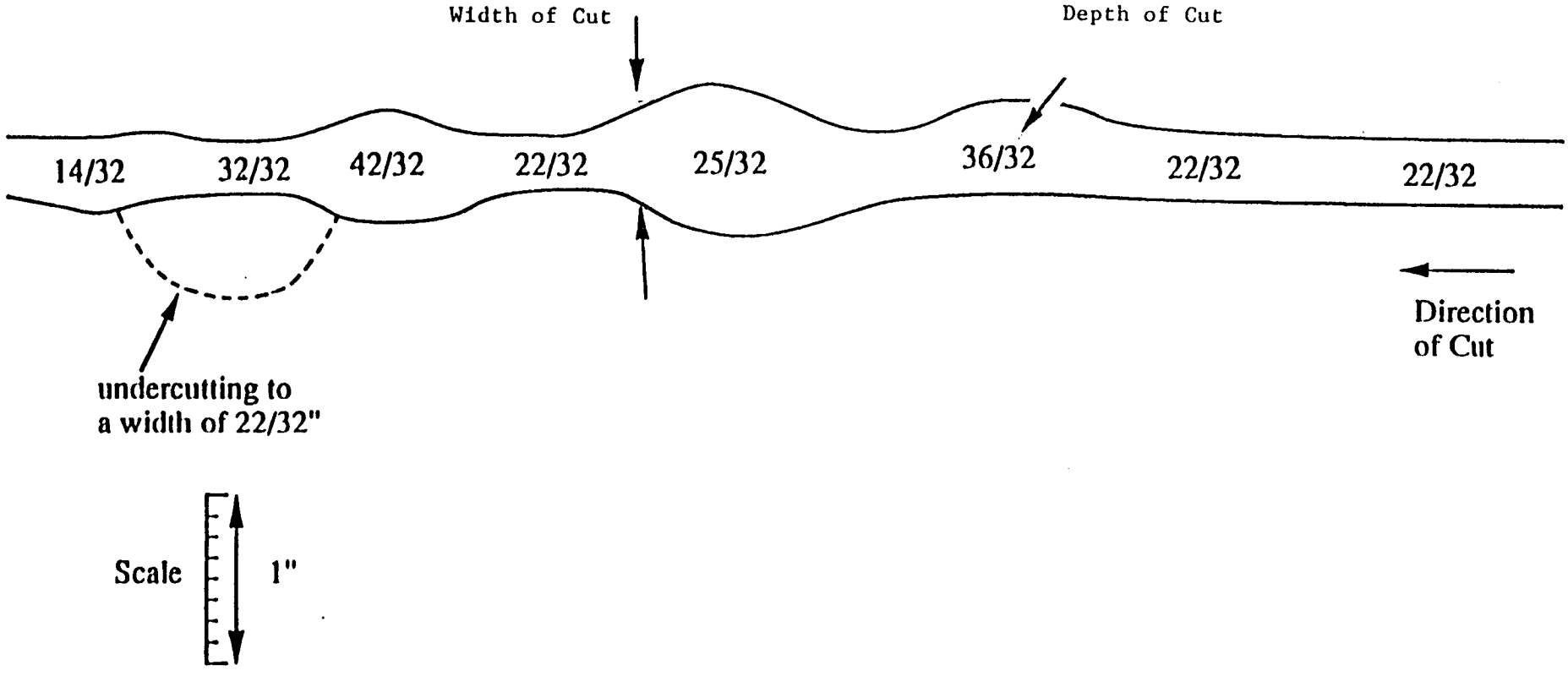

Experimental Parameters: AFR = 2 lb/min (Garnet mesh #80), P = 13 ksi, L = 7.5", d_n= 0.040", d_m= 0.145", ice thickness, H = 1.25", Square Sample, 13" x 13".

Figure 30(c)

LINEAR JET TRAVERSE CUTTING PATTERN

U = 450 i.p.m

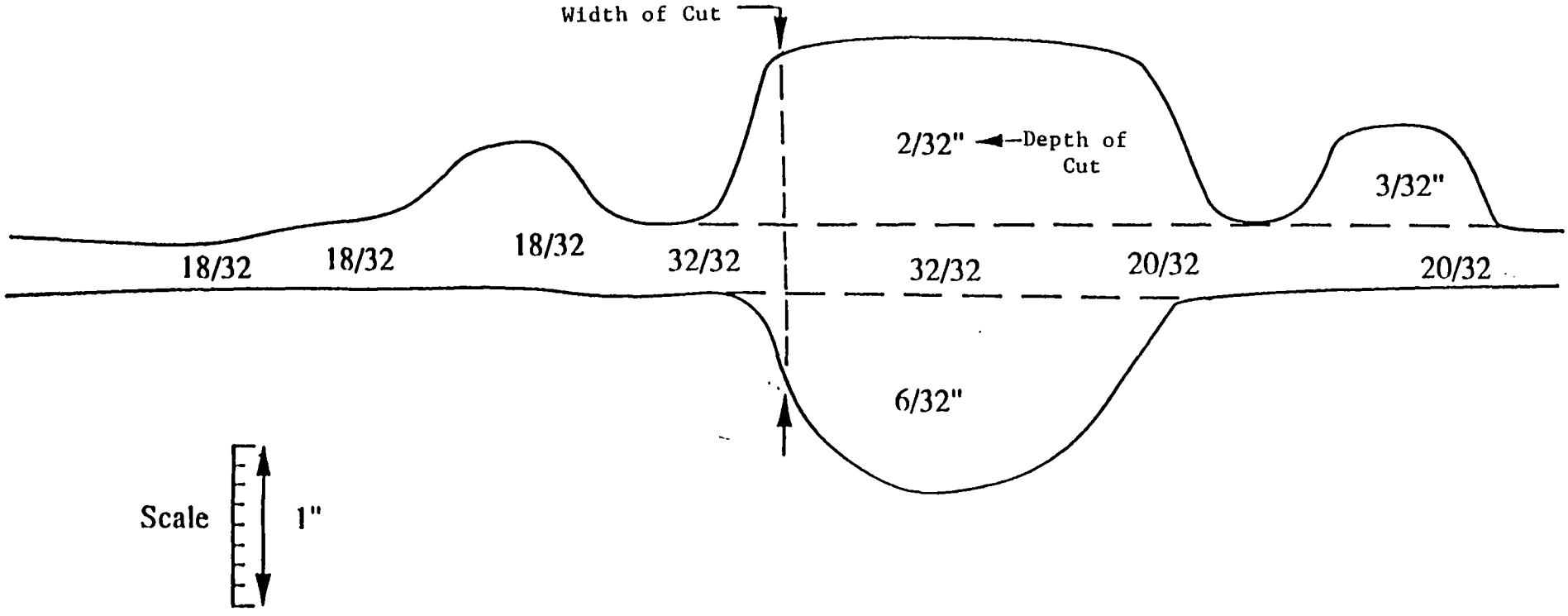

Experimental Parameters: AFR = 2 lb/min (Garnet mesh #80), P = 13 ksi, L = 7.5", d_n= 0.040", d_m= 0.145", ice thickness, H = 1.25", Square Sample, 13" x 13".

Figure 30(d)

LINEAR JET TRAVERSE CUTTING PATTERN

U = 500 i.p.m

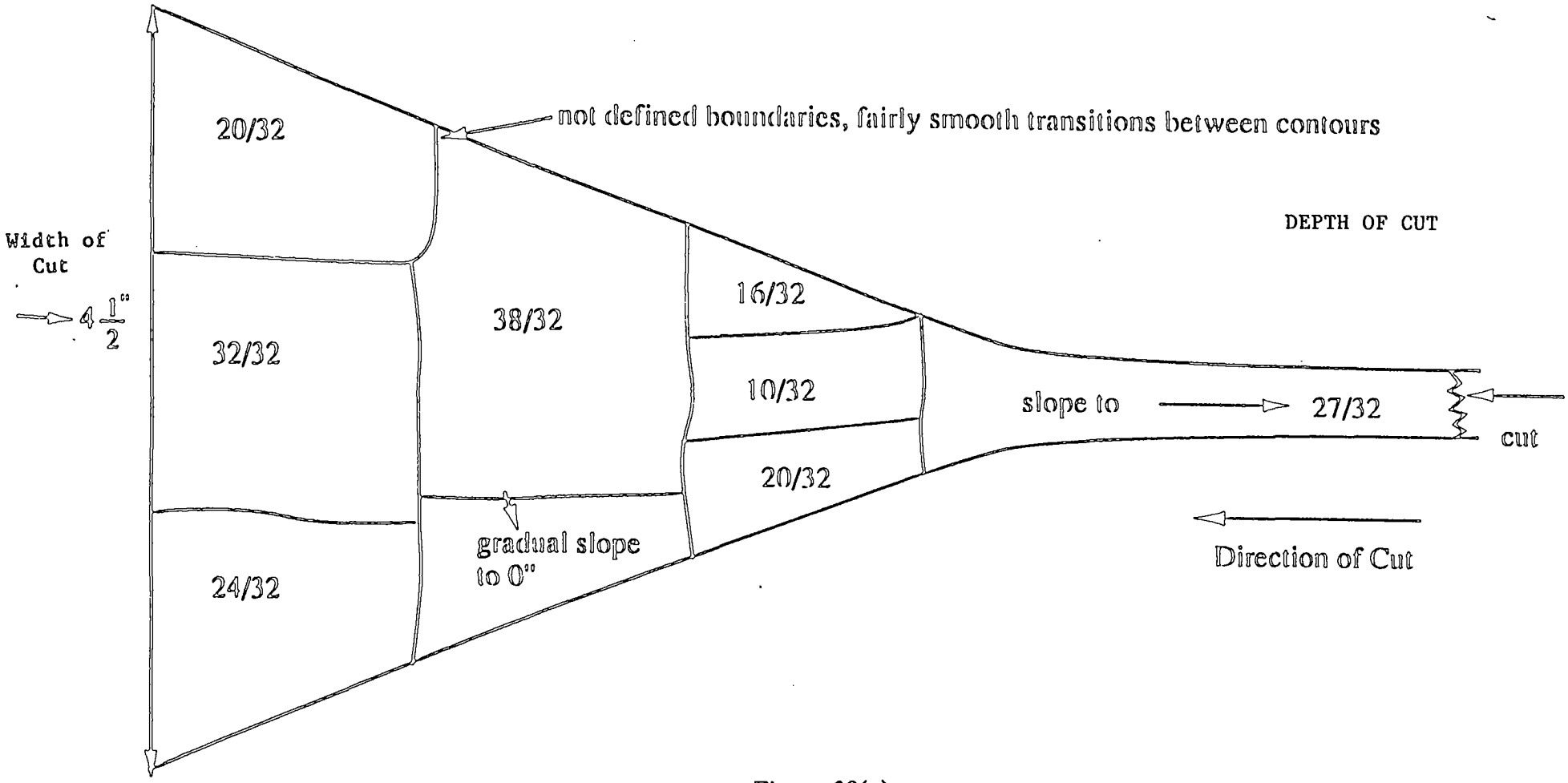

Figure 30(e)

# LINEAR JET TRAVERSE CUTTING PATTERN
U = 1000 i.p.m

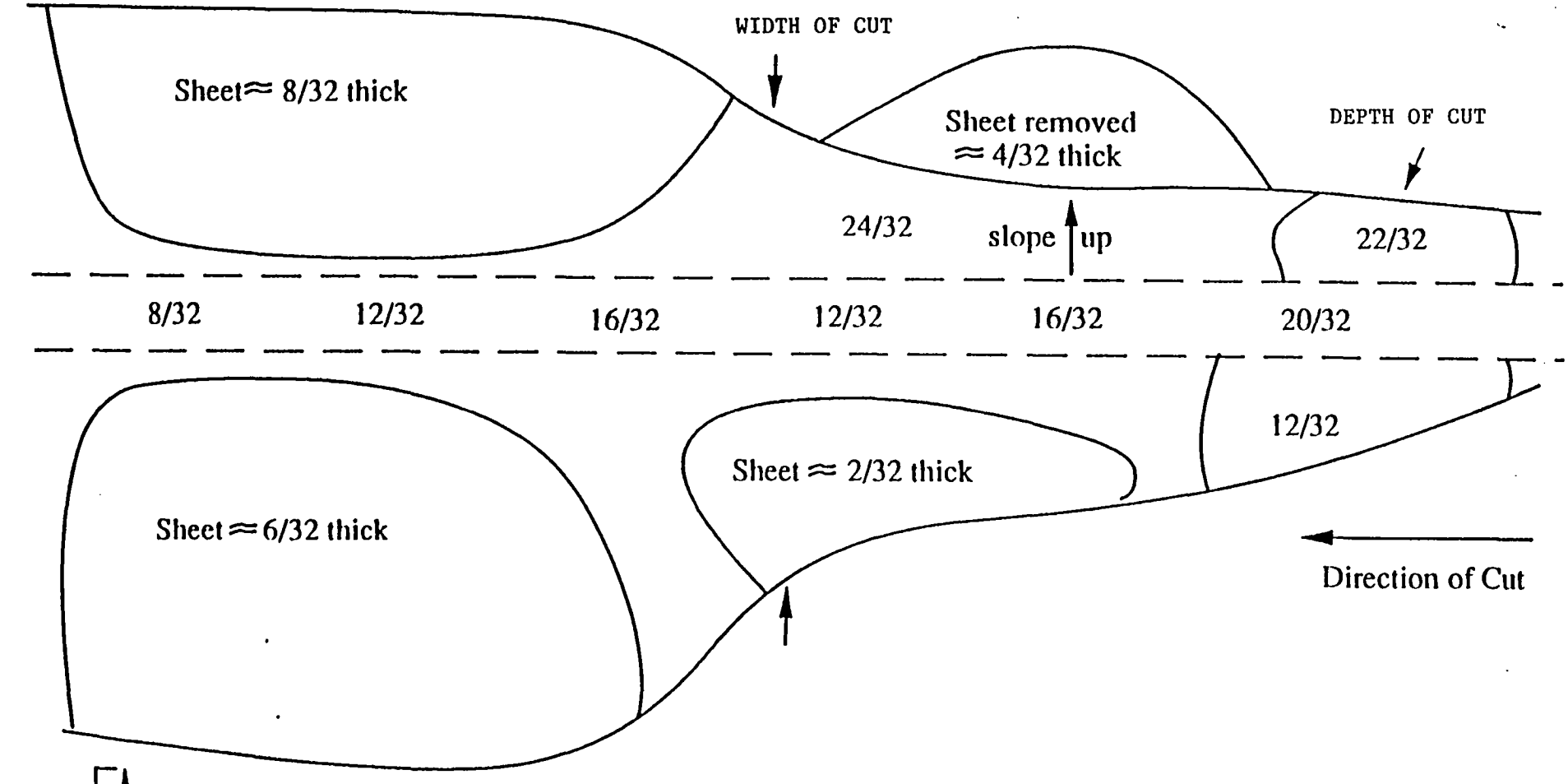

Scale 1"

Experimental Parameters: AFR = 2 lb/min (Garnet mesh #80), P = 13 ksi, L = 7.5", d_n= 0.040", d_{nf}= 0.145", ice thickness, H = 1.25", Square Sample, 13" x 13".

Figure 30(f)

LINEAR JET TRAVERSE CUTTING PATTERN
U = 2000 i.p.m

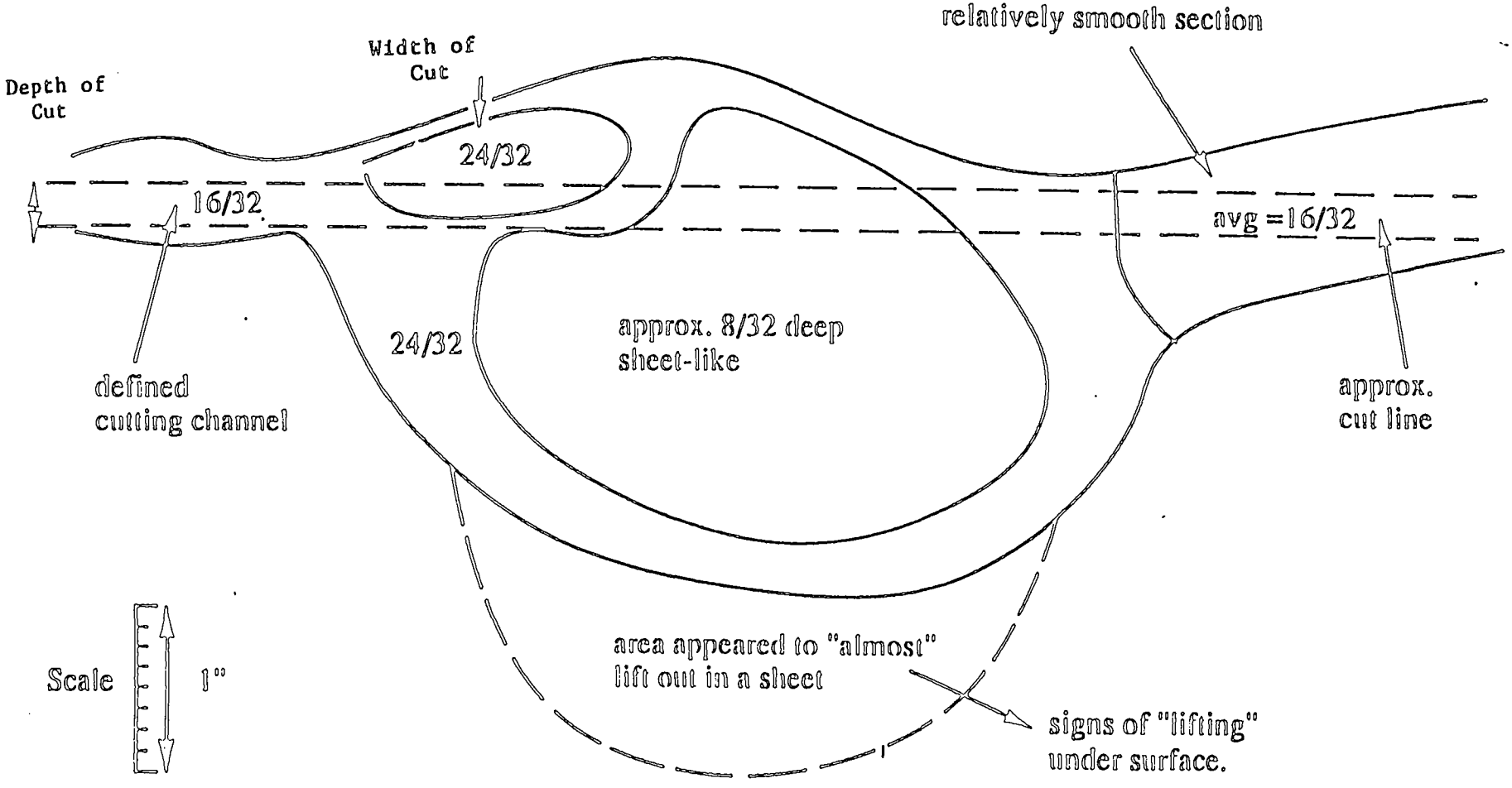

Experimental Parameters: AFR = 2 lb/min (Garnet mesh #80), P = 13 ksi, L = 7.5", d_n = 0.040", d_{nf} = 0.145", ice thickness, H = 1.25", Square Sample, 13" x 13".

Figure 30(g)

LINEAR JET TRAVERSE CUTTING PATTERN

U = 3000 i.p.m

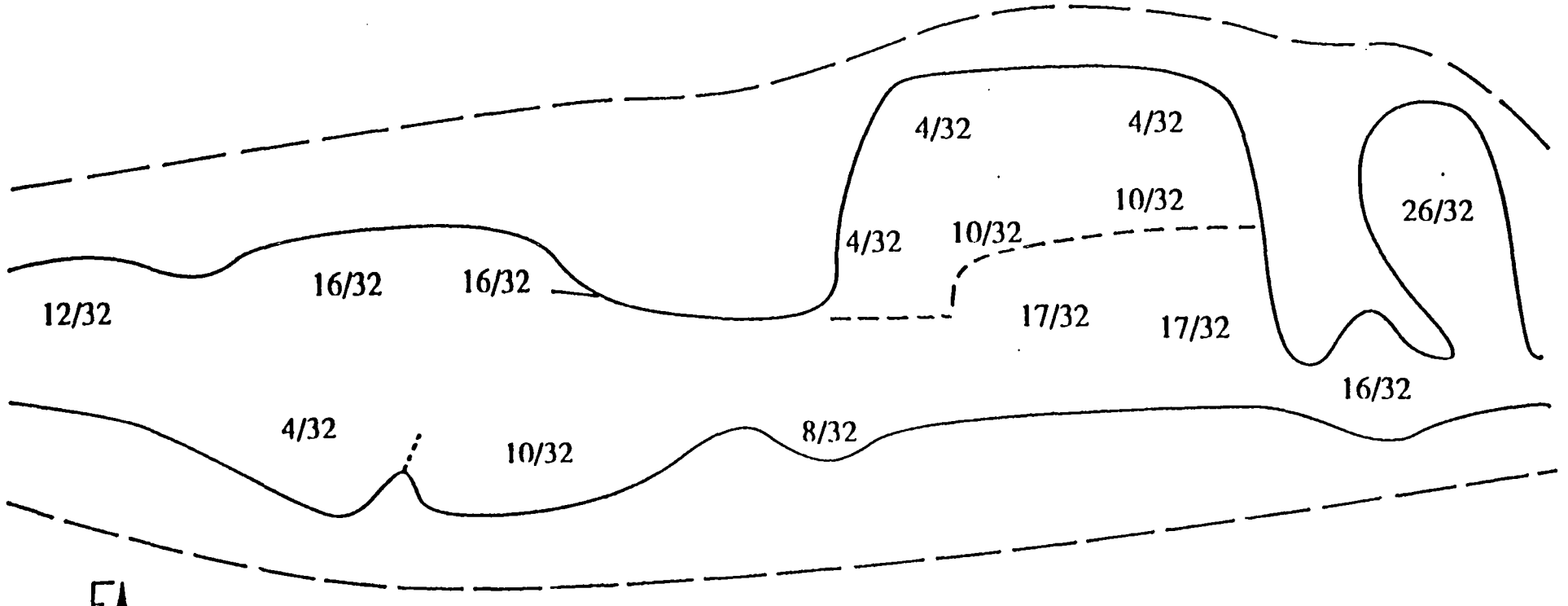

Actual cut line virtually invisible. Very erratic.

Experimental Parameters: AFR = 2 lb/min (Garnet mesh #80), P = 13 ksi, L = 7.5", d_n= 0.040", d_{nf}= 0.145", ice thickness, H = 1.25", Square Sample, 13" x 13".

Figure 30(h)

MULTIPLE LINEAR JET ARRANGEMENT

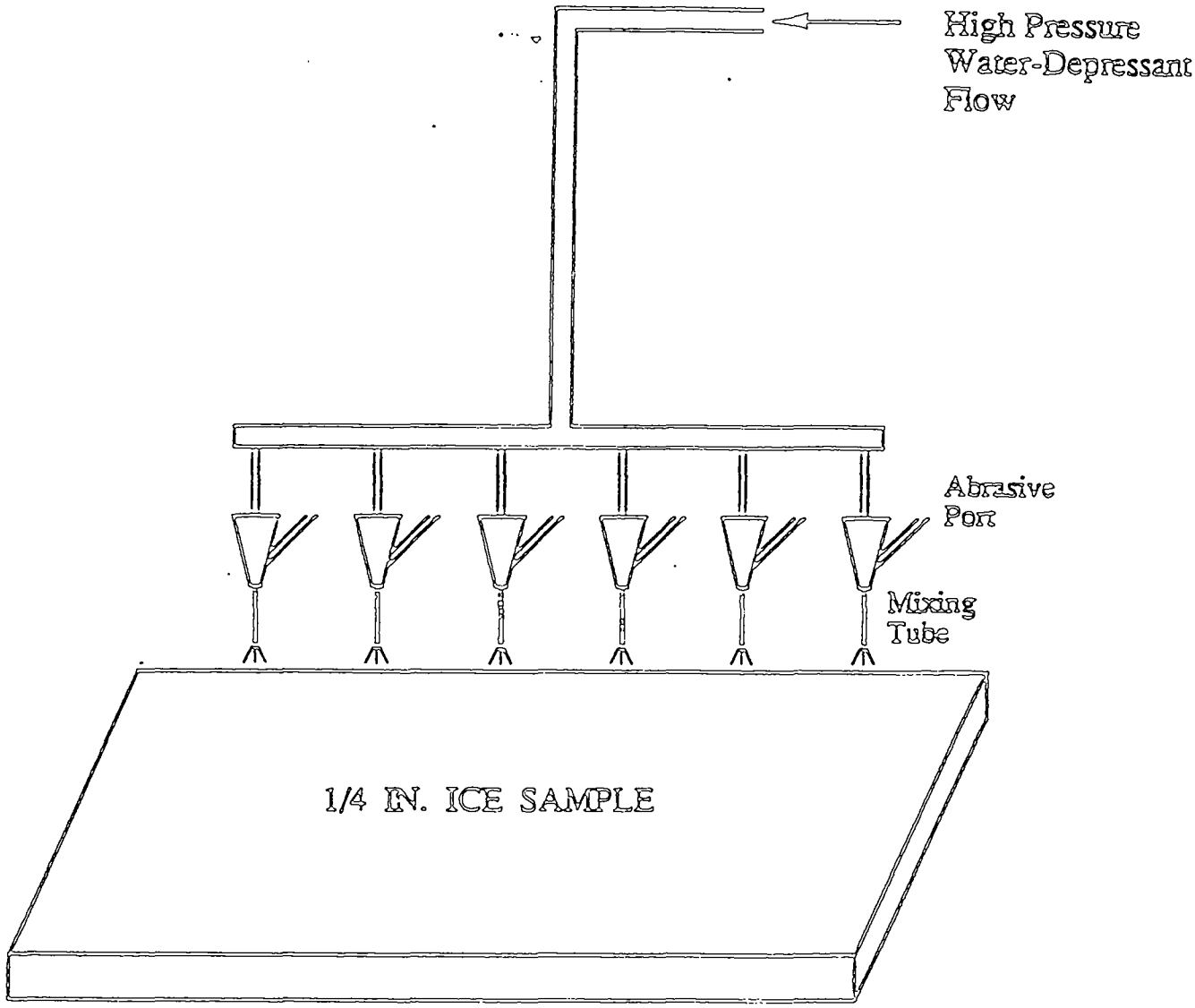

Figure 31

References

1. Shvayshteyn, Z.I. "Cutting Ice with a Continuous High-pressure Waterjets." Trudy Ankticheskogo I Antarkticheskogo Nauchne-Issledovatel'skage Institutu, 300, Leningrad, p. 168, 1971.

2. Mellor, M., "Jet Cutting in Frozen Ground," Proceedings of First International Symposium on Jet Cutting Technology, BHRA. Coventry.

3. Coveney, D.B., "Cutting Ice with 'High' Pressure Water Jets", National Research Council of Canada, Report No. MD-57, NRC No. 19643, 1981.

4. Stallabrass, J.R. and Price, R.D., "On the Adhesion of Ice to Various Materials", Aeronautical Report LR-350; National Research Council of Canada, M.R.C. No. 6980, 1962.

5. Raraty, L.E. and Tabor, D., "The Adhesion and Strength Properites of Ice," Proceedings, Roy. Soc., Vol. 245A, No. 1241, p. 184, 1958.

6. Haase, R.A., "Ice-Pavement Bond Disbonding via High-Pressure Liquid Abrasive Jets," M.S. Thesis, Michigan Technological University, 1990.

7. Finnie, L. and Wolak, J. and Kabil, F., "Erosion of Metal by Solid Particles," Journal of Materials, Vol. 2, No. 3, pp. 682-700, 1967.

8. Ohadi, M.M., Cheng, L.C., and Hashish, M., "Modeling of Depth of Cut in Abrasive - Waterjet Cutting," Proceedings of IASTED International Conference on Modeling and Controls, July 1990.

FIGURE CAPTIONS
(Task 2b)

FIG. 13 Schematic of the experimental setup

FIG. 14 Effect of pressure and transverse speed on depth of cut

FIG. 15 Effect of the pressure and orifice diameter on depth of cut

FIG. 16 Effect of the pressure and orifice diameter on the cutting kerf (width)

FIG. 17 Effect of the abrasive flow rate on depth of cut

FIG. 18 Effect of jet beam angle on depth of cut

FIG. 19 Effect of auxiliary heating of the jet on depth of cut

FIG. 20 Power consumption requirements for the high-temperature jet

FIG. 21 Comparison of various ice freezing point depressants

FIG. 22 Rotary jets at 10 ksi pressure and 700 rpm

FIG. 23 Rotary jets at 25 ksi pressure and 700 rpm

FIG. 24 Effect of pressure on depth of cut, rotary jet

FIG. 25 Effect of rotational speed, rotary jet

FIG. 26 Effect of transverse speed on the cut's depth, rotary jet

FIG. 27 Effect of stand-off distance on the cut's depth, rotary jet

FIG. 28 Comparison of experimental and mathematical model results

FIG. 29 Model-predicted results

FIG. 30(a)-30(h) Linear jet cutting patterns at various traverse speeds

FIG. 31 Multiple linear jet arrangement

Abrasive Air Jets

Introduction

An investigation was conducted to determine if abrasive air blasting could be a feasible method of removing ice and compacted snow from paved roads and runways. The focus of this study was to investigate and experiment with current off the shelf equipment that could be installed on a highway department truck. A literature search was first conducted to determine what was currently available on the market and what may be best to use to remove compacted snow and ice at a minimum speed of 20 mph (32 km/h). At the same time a laboratory fixture was designed and fabricated to carry out a number of parametric studies using a scaled down abrasive air blast system. The laboratory studies, which were conducted in a cold room, were performed to determine if the idea had potential for removing ice and compacted snow on a larger scale and to determine what parameters were the most effective in removing the material. The results of the laboratory study were verified and extrapolated using a mathematical flow model and finally a short field test was performed to demonstrate that the concept would actually remove ice at 20 mph (32 km/h).

Literature Search

The literature search revealed that several studies had been conducted with air pressure or air assisted displacement snowplows (1,2,3,4). But most studies, as in Posey (1), utilized low pressure (5 psi), high volume air through a slot and were unable to remove the strongly bonded compacted snow or ice. In most cases, the bond between the pavement and compacted snow or ice is much stronger than the intergrannular bonds of compacted snow or ice. These studies consisted of blasting air through a narrow slot located directly behind the plow blade in an attempt to break up the snow or ice on the road as the truck was plowing the road. Nobody had ever attempted to use high pressure, high volume air or an air abrasive mixture through a nozzle.

Shortly after the contract was awarded, a preliminary test was run using a small air compressor and sandblaster that was on hand at KRC. This was used to examine the potential of using air alone, with CMA as an abrasive and with a common abrasive for this purpose. This was done in a preliminary manner in the late spring. High pressure air did remove some compacted snow but not all of the snow nor any ice. The CMA removed more compacted snow than air alone but appeared to bounce off the ice or break up as it hit the ice. The other abrasive could remove the snow and also some of the ice. This led to the conclusion that air alone would not work, that CMA in its round pellet, lightweight form would not work, but the hard, coarse abrasive may have a chance of being successful.

A literature study was then conducted to gather information about current types of air compressors, abrasive air blasters, abrasives and nozzles available on the market. Most air compressors are typically used in the 80 to 150 psi (5.8 to 10.9 Kg/cm^2) range although they do provide as much as 6,000 psi (435.3 Kg/cm^2) in special models. Air flow rates also vary from 5 cfm (.14 m^3/min) up to 3,000 cfm (84.95 m^3/min.) and possibly higher. Most smaller compressors are operated by an electric motor while the high pressure or high flow rate models are powered by gasoline or diesel engines. Compressors can be stationary or mounted on a truck or trailer for portability. Most compressors for sandblasting applications are rated for 200 psi (14.5 Kg/cm^2) or less but use high volume flow rates, depending on the application. Very high pressure or flow rate air compressors may cost anywhere from $60,000 to $150,000. Air compressors generally have a ten year or longer operating life if they are well maintained.

Several sandblasting companies were contacted. Most sandblasters are used in the 60 to 120 psi (4.4 to 8.7 Kg/cm^2) range. Some have used pressures as high as 175 psi (12.7 Kg/cm^2)for removing paint from bridges. Most sandblasting tanks, the part that is pressurized, are rated for 200 psi (14.5 Kg/cm^2) per ASME code. This is a strict code due to the fact that as the pressures increase in a sandblasting system the wear rate of the tank and other components (i.e., hoses, valves, etc.) increase exponentially and may result in a dangerous situation for the operator or people near the sandblaster. Direct pressure sandblasting as compared to siphon or suction type sandblasting would be the most appropriate method for this application. Direct pressure pushes the abrasive air stream while suction types siphon the abrasive out of the nozzle. Higher pressures may result in higher sound levels and may cause noise pollution. If a sandblaster is used in a cold environment a water separator should be used to prevent ice from blocking orifices and hoses. When air is compressed, the temperature increases and when in a cold environment, moisture will condense out of the air and freeze. Compressed air is considerably more dangerous than high pressure liquids and therefore cannot be used at very high pressures as are liquids. If a large amount of wear occurs in a sandblasting tank an explosion could result whereas in a liquid system only a leak may be produced.

As a result of the above mentioned information one could surmise that the optimum system may be an operating pressure between 100 and 175 psi (7.3 to 12.7 Kg/cm^2) with a very high volumetric flowrate.

During the literature and phone search, information was also obtained for abrasives. It would be nice if a non-corrosive deicing or anti-icing type of material could be used, but as was discovered in the initial tests, CMA was too light and was not abrasive enough. There are numerous types of sandblasting abrasives on the market. Several are for very specific applications. Some of the abrasives considered for this project were: glass beads, aluminum oxide, silicon carbide, steel shot, steel grit, plastics, ice chips, silica sand, black beauty (a by-product of coke furnaces) and solid carbon dioxide. Most of the abrasives listed first are expensive. Ice chips and solid carbon dioxide would be desirable because they would disintegrate leaving no mess to clean up

but require special equipment to produce and a special system for introducing into the compressed air stream. It was decided to conduct the initial laboratory tests with three types of abrasives, steel grit, silica sand and ground up slag (Black Magnum). It was desired to use an abrasive that has a large mass and sharp edges. Each of these abrasives have advantages and disadvantages.

Steel grit has sharp edges and large mass but the cost may be prohibitive. Steel grit may also rust and bond to the road leaving an undesirable appearance. Silica sand is inexpensive but may cause silicosis. Black Magnum is also inexpensive but may be carcinogenic. If Black Magnum does work well, a flint rock abrasive may be used in its place as it has very similar characterisitics and costs about the same.

The size of the abrasive used depends in part on the size of the nozzle orifice used. If an abrasive is too large in size, then the nozzle may become obstructed causing downtime. Ideally, a large coarse abrasive would be the most effective for removing large surface areas of snow and ice but it will be limited by the nozzle size and the nozzle size will be limited by the volume of air available. The volume of air available will be limited by the cost of the system.

In most body shops or where small scale sandblasting is done, ceramic converging type nozzles are used. Air velocities through a converging type nozzle may approach mach 1 speeds. For projects requiring large areas to be blasted and heavy materials to be removed, a converging-diverging or DeLaval nozzle is used. When enough volume flow rate is available, the DeLaval nozzle will develop air and particle velocities up to mach 3 which would assist removal of the compacted snow and ice. The DeLaval nozzles are sometimes called venturi nozzles and the ones that are made of Tungsten Carbide cost $135 each and last approximately 300 hours, depending on the abrasive. For the laboratory tests, a venturi nozzle could not be used because there was not enough air flow available with the compressor used. Thus, a simple converging type ceramic nozzle was used in the laboratory experiments. Figure 32 shows both a converging and venturi nozzle.

Laboratory Test Setup

During the first year a series of laboratory tests were conducted in the cold room to determine optimum parameters for removing ice and compacted snow from paved roads.

A test fixture was first fabricated such that a sandblasting nozzle could be fixed above a table at various heights and angles. The nozzle would remain in a fixed position while below it a road surface could be moved at various speeds simulating the effect of a nozzle, mounted on a vehicle, moving over an ice covered road. Four, one by two foot (.305 by .610 meter) road surfaces were made following ASTM specifications, two for concrete and two for asphalt. An aluminum cake pan type frame was made to freeze

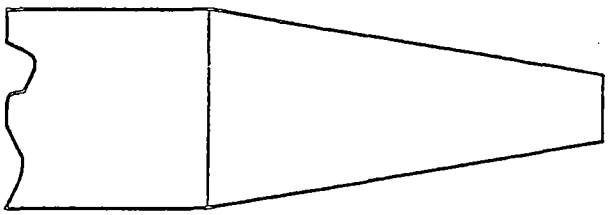

Converging Nozzle

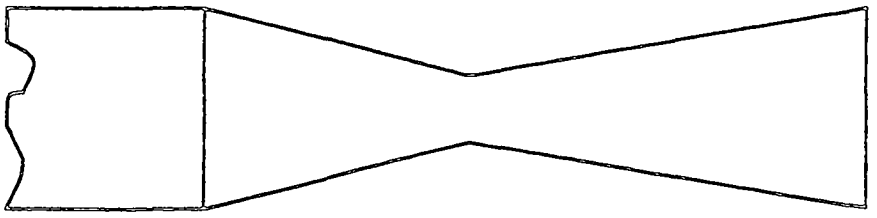

Venturi Type Nozzle

Figure 32. Drawing of a converging and venturi type nozzle.

water on top of the simulated road surfaces and form ice layers at desired thicknesses. The table was designed such that the road surface could be moved at a constant speed underneath the nozzle. Speed could be varied anywhere from 0 to 1.2 mph (0 to 1.9 km/h). Ice was used for most of the tests since it was understood to be the most difficult to remove. Some tests were run using compacted snow but only to determine how much deeper the cut would be versus that of ice. The tests were run with a small compressor and sandblaster that was available since there were not enough funds in the project to allow purchase of a larger unit. The pressure was generally 145 psi (10.5 Kg/cm^2) at the compressor and the volume flow rate was 10 cfm (.28 m^3/min.) or less. There was sufficient volume flow for these short tests but a venturi nozzle could not be used. The ceramic converging nozzle had a .25 inch (.63 cm) orifice. Figure 33 is a photograph of the laboratory test fixture.

Laboratory Test Results

Tests were conducted to determine optimum: air pressure, nozzle height, abrasive type, traverse speed and nozzle angle versus depth of cut into the ice.

During the first series of tests, the substrate was damaged. A one quarter to one half inch (.63 to 1.26 cm) layer of ice was formed on some of the early pads and at slower speeds the abrasives went through the ice and exposed some aggregate. This occurred equally for both the concrete and asphalt road surfaces. The abrasive air jets tend to wear the ice away rather than disbonding the ice from the road surface. This leads to the conclusion that ice samples up to two inches (5 cm) thick could be used because only the depth of cut into the ice was important.

Initial tests with the nozzle in the vertical position (90 degrees from the horizontal) and in the 60 degree from the horizontal position showed that the cuts were deeper in the vertical position. Keeping in mind that these first tests were at very low traverse rates, from 0.05 to 0.23 mph (.080 to .368 km/h), one can see that at low speeds the nozzles should be fixed vertically. At traverse rates up to 20 mph (32 km/h) the nozzle may work better at a slight angle but this was never proven because full scale tests were never conducted at 20 mph (32 km/h).

The laboratory system was initially set up to run at speeds up to .23 mph (.368 km/h). Later in the study the system was modified to run up to speeds of 1.2 mph (1.9 km/h). Some of the results below were run at the lower speed range only. In some cases it was not necessary to conduct the tests in the higher speed range.

Air pressure versus depth of cut into the ice tests were run with silica sand as the abrasive. Tests were all run at a 3 inch (7.62 cm) nozzle height and at .23 mph (.368 km/h). The data is presented in Table 19 and shows that as the pressure increases the

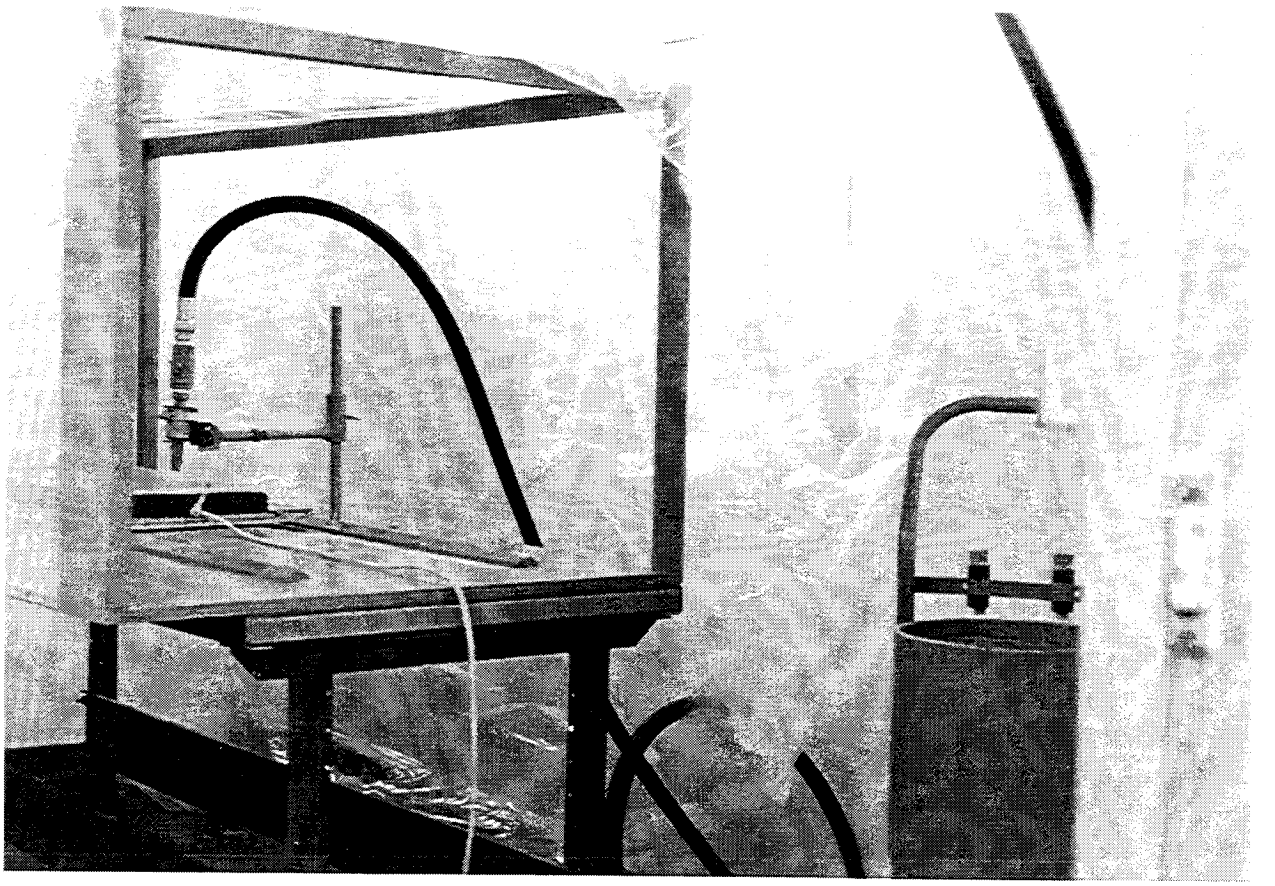

Figure 33. Photograph of the laboratory test fixture.

depth of cut increases but at a decreasing rate. Thus, increasing the air pressure to more than 145 psi (10.5 Kg/cm^2) would not result in a significantly deeper cut for the converging nozzle.

Table 19 Air Pressure vs Depth of Cut on Ice
Silica Sand, 3 inch Height, .23 mph
(7.62 cm Height, .368 km/h)

Air Pressure (psi)	Depth of Cut (in.)
100	0.25
120	0.50
145	0.55

in.x2.54 = cm
psi x 0.073 - Kg/cm^2

Tests were conducted for nozzle height versus depth of cut for all three types of abrasives. This provided an answer as to which abrasive was the best and how nozzle height affected depth and width of cut. As it turned out, Black Magnum (a ground up slag) was the most abrasive and it had the best results at a 3 inch (7.62 cm) height above the ice surface. Although the steel grit was more dense the Black Magnum was slightly larger in size, and therefore appeared to have a more errosive effect. These data are presented in Table 20 and Figure 34 is an example of the abrasive cut into the ice surface.

Toward the end of the laboratory tests, when the higher speed tests were run, tests were run at 3 and 1 inch (7.62 and 2.54 cm) nozzle heights with Black Magnum at 145 psi, (10.5 kg/cm^2) 1.2 mph (1.9 km/h) and there was no difference in the depth of cut, but width of cut was reduced using the 1 inch (2.54 cm) nozzle height. Therefore, for these conditions, the 3 inch (7.62 cm) nozzle height was the most effective height.

Another set of tests were made using compacted snow on simulated road surfaces. These were run at both the 90 and 60 degree nozzle angles at the four highest rates of speed. Black Magnum was used as the abrasive at 145 psi (10.5 Kg/cm^2) and a 3 inch (7.62 cm) nozzle height. The results are presented in Table 21. Again, even at relatively higher speeds, the 90 degree position proved to be the most effective. Figure 35 shows the abrasive air jets effect on compacted snow. Some undercutting was observed due to the particles bouncing off of the hard subsurface.

The final data generated during the laboratory testing was traverse speed vs depth and width of ice cut. These were carried out using Black Magnum, and 145 psi air pressure at a 3 inch (7.62 cm) nozzle height. Data generated from these tests is

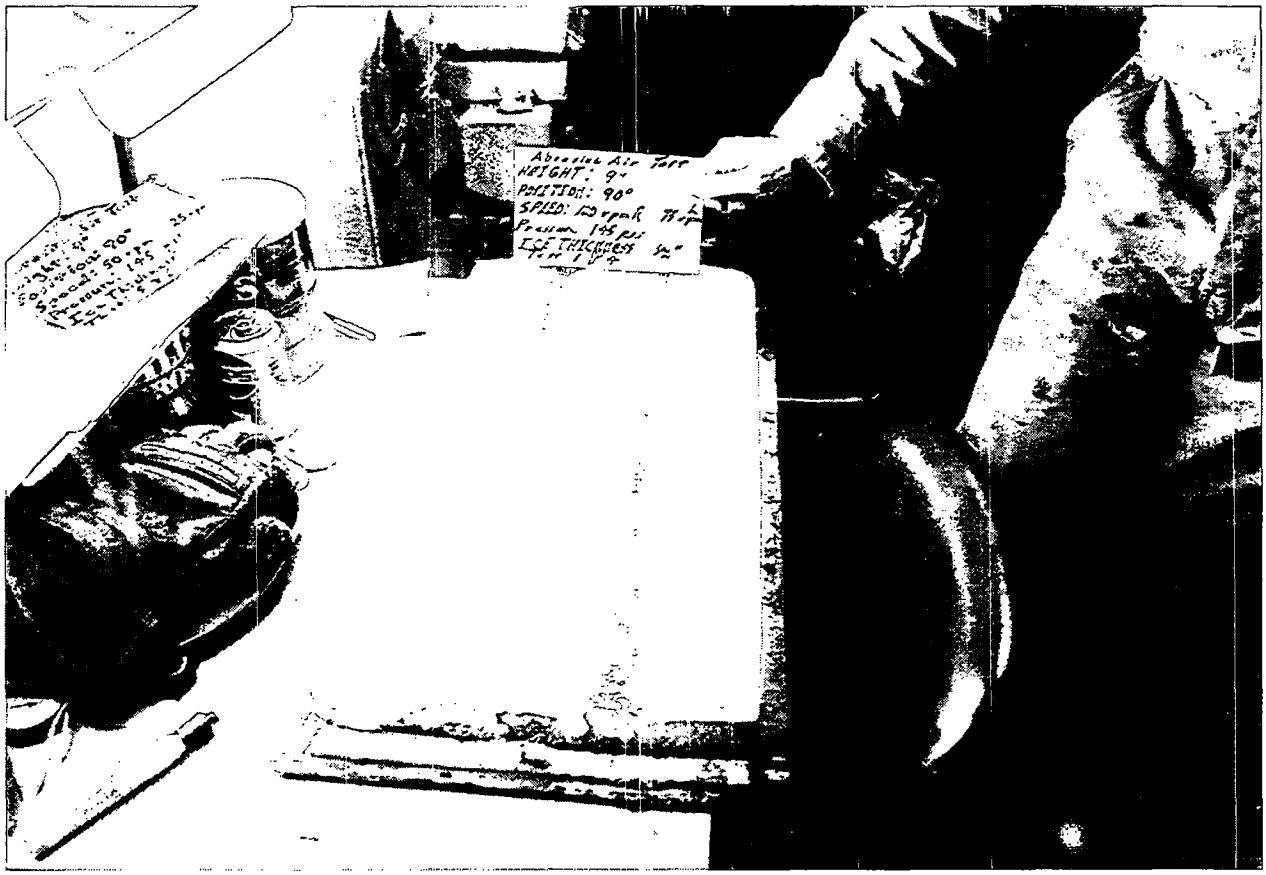

Figure 34. Photograph showing the abrasive cut into the ice.

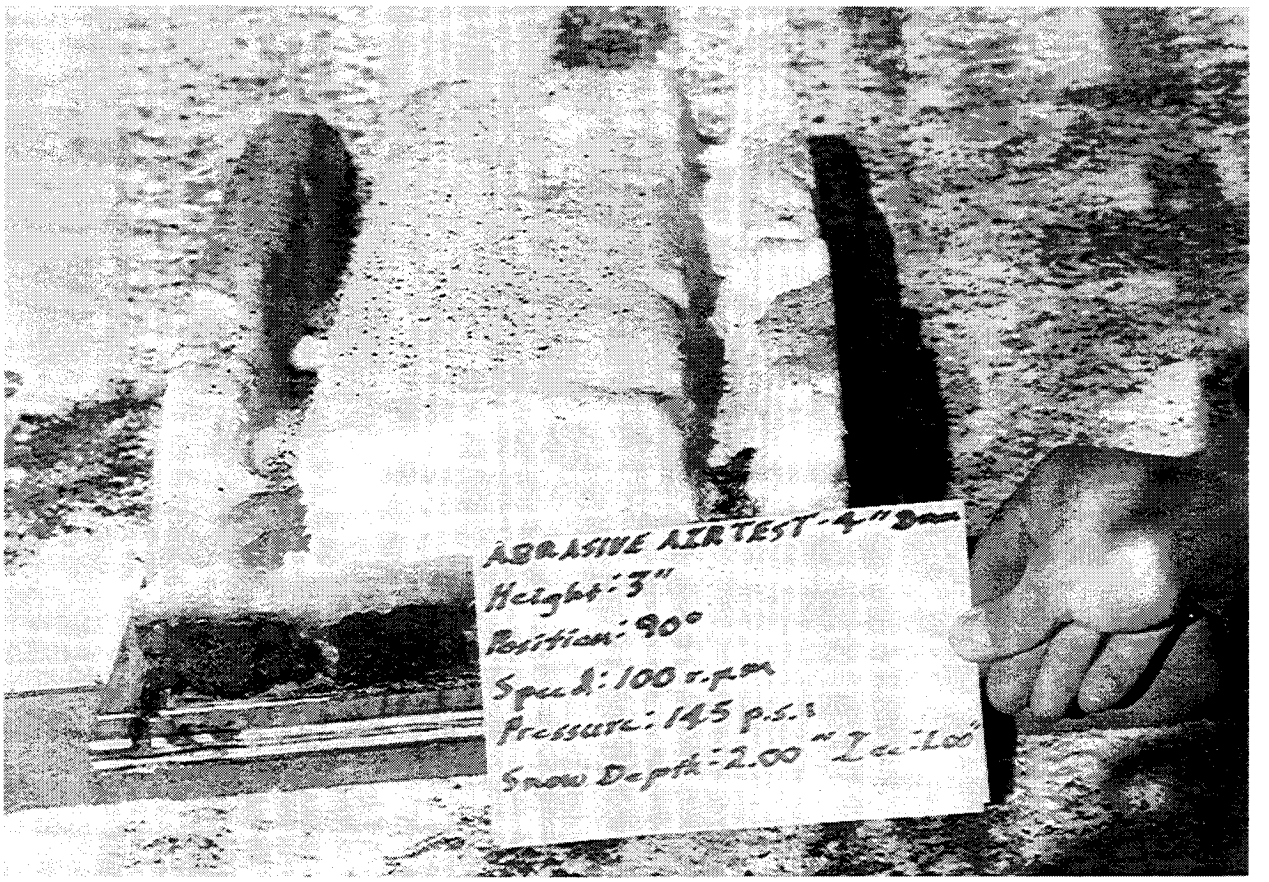

Figure 35. Photograph showing the abrasive cut into compacted snow.

Table 20 Nozzle Height vs Depth and Width of Cut
145 psi, 0.23 mph on ice
(10.51 Kg/cm², .368 Km/h)

Silica Sand	Nozzle Height (in.)	Depth (in.)	Width (in.)
	3	0.75	1.00
	6	0.63	1.25
	9	0.50	2.00

Steel Grit	Nozzle Height (in.)	Depth (in.)	Width (in.)
	3	0.813	1.00
	6	0.688	1.25
	9	0.625	2.00

Black Mag	Nozzle Height (inc.)	Depth (in.)	Width (in.)
	3	0.875	1.00
	6	0.813	1.88
	9	0.750	2.63

in x 2.54 = cm

Table 21 Black Mag Abrasive - Compacted Snow Surface
Traverse or Longitudinal to 60°
Speed vs Depth and Width of Cut
145 psi, 3 inch height, 90 and 60 degrees in direction of travel
(10.5 Kg/cm², 7.62 cm height)

Speed (mph)	90° Depth/Width (in.)	60° Depth/Width (in.
0.3	3.50/1.50	3.00/1.50
0.6	2.00/1.50	1.13/1.50
0.9	1.25/1.25	1.00/1.25
1.2	1.13/1.25	0.94/1.00

mph x 1.6 = km/h
in. x 2.54 ≅ cm
psi x 0.073 ≅ Kg/cm²

presented in Table 22 and shown graphically in Figure 36. This data shows that as traverse speed increases the depth of cut decreases. This experimental data was then

used along with a mathematical flow model, which is described in the following section, to predict depth of cut at speeds up to 20 mph (32 km/h).

Table 22. Traverse Speed vs Depth and Width of Ice Cut
145 psi, Black Magnum, 3 inch nozzle height
90 degree nozzle angle
(10.5 Kg/cm^2, 7.62 cm nozzle height)

Speed (mph)	Depth of Cut (in.	Width of Cut (in.)
0.05	1.25	2.00
0.09	1.00	1.00
0.16	0.75	0.88
0.23	0.55	0.75
0.60	0.38	1.00
0.90	0.31	1.25
1.20	0.25	1.00

mph x 1.6 = km/h
in. x 2.54 = cm
psi x 0.073 = Kg/cm^2

In summary of the laboratory tests, it was found that the most effective results for the conditions tested occur when Black Magnum is used as the abrasive at a 3 inch (7.62 cm) nozzle height in the vertical position at an air pressure of 145 psi (10.5 Kg/cm^2). These results then led into the analytical model which was first modified to fit the experimental data and then extended to predict the depth of cut at 20 mph (32 km/h). The model work is discussed in the next section.

Mathematical Flow Model Correlation

A mathematical flow model originally developed for water/abrasive jets, by Hashish (5) was modified for the air abrasive jet study. The model is fairly complex and considers the following parameters for input into the model:

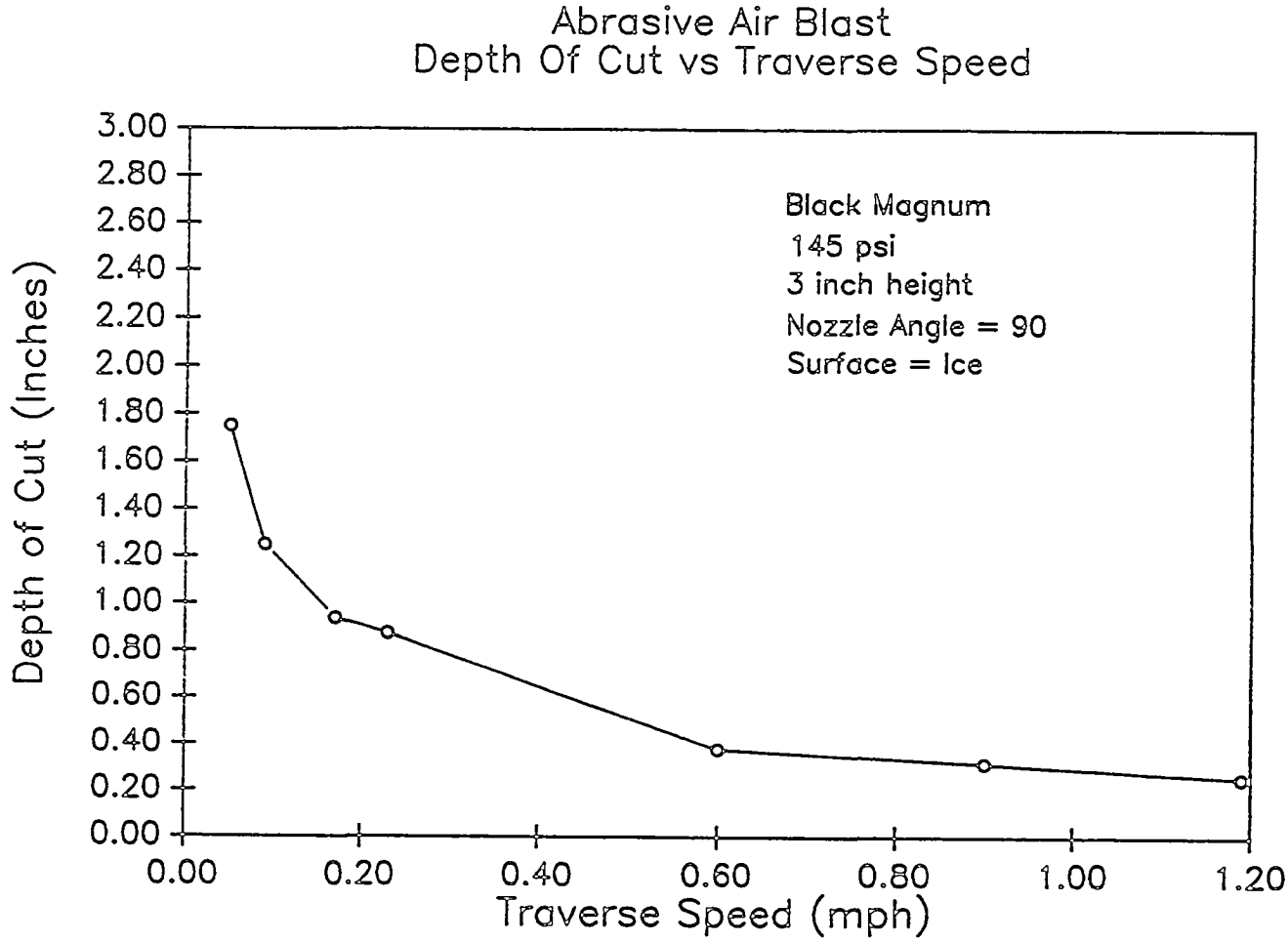

Figure 36. Plot of experimental depth of cut versus traverse speed.

For the abrasive:

- particle radius
- particle mass
- Young's modulus
- Poisson's ratio
- particle density
- abrasive mass flow rate
- initial particle velocity
- moment of inertia
- particle roundness

For the ice:

- flow stress
- coefficient of friction
- yield strength
- Poisson's ratio
- Young's modulus
- flow stress coefficient

For the cutting system and air:

- traverse rate
- jet diameter
- air jet velocity at nozzle exit
- loading ratio
- air density
- air pressure
- air flow rate
- particle velocity
- mixing efficiency

Some of the parameters were estimated and some were converted from water to air since the model was originally developed for water. First the model was fit to correlate the model data to the experimental data shown in Table 22 for speeds up to 1.2 mph (1.9 km/h). Figure 37 shows the model and experimental data for depth of cut versus traverse rate. The data appears to correlate well as most often one can not expect experimental data to correlate exactly with computer model data. After developing the model to correlate at speeds up to 1.2 mph (1.9 km/h), the model was extrapolated to predict the depth of cut into the ice at a traverse rate of 20 mph (32 km/h). This is shown in Figure 38 and indicates that at 145 psi (10.51) approximately one sixteenth inch of ice could be removed at a speed of 20 mph (32 km/h). Also notice

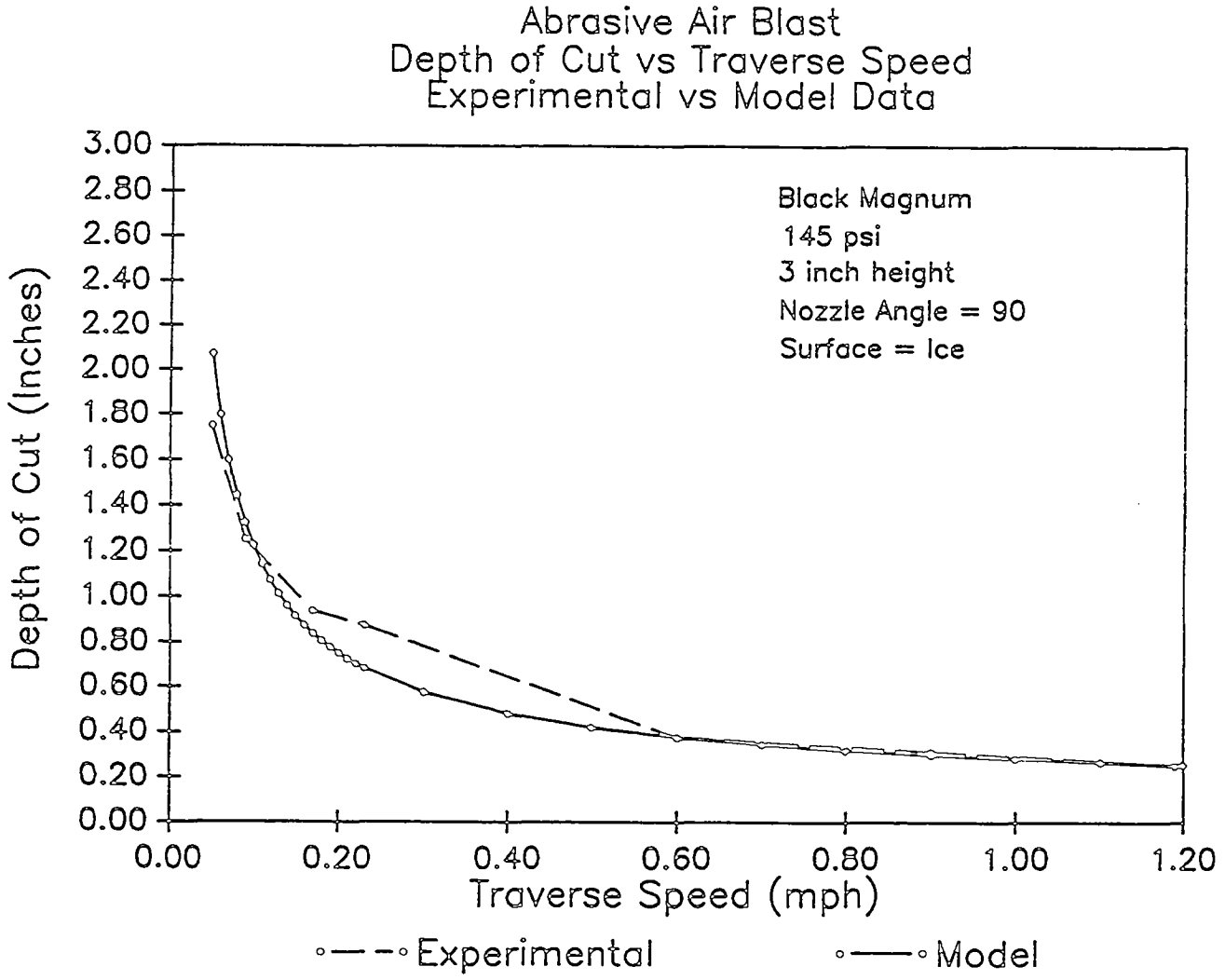

Figure 37. Plot of model and experimental versus traverse speed up to 1.2 mph (1.9Kmh).

how the curve levels out or becomes asymptotic at speeds above 5 mph (8 km/h). This is important for using abrasive air jets at speeds greater than 20 mph (32 km/h).

Since the mathematical model indicates that theoretically ice can be removed at 20 mph (32 km/h), experimental verification was justified.

Initial Field Studies

In an attempt to verify removal of ice at 20 mph (32 km/h), a large portable air compressor, 375 cfm at 100 psi (10.6 m^3/min. at 7.3 kg/cm^2) and a 600 lb. (272 kg) pot sandblaster were leased from a local sandblasting company. This also included a 3/8 inch (.953 cm) venturi type nozzle. Blace magnum in the 12-40 grit size was used as the abrasive. For this test, ice was formed on large wooden sheets which were carried outside for testing. Tests were carried out at speeds of 5, 10, 15 and 20 mph (8, 16, 24 and 32 km/h). The sandblaster was placed in the back of a pickup truck and the air compressor was towed behind the truck. At 5 mph (8 km/h), a 1/4 inch (.63 cm) layer of ice was removed. At 10, 15 and 20 mph (16, 24 and 32 km/h) a 1/16 to 1/8 inch (.16 to .32 cm) layer of ice was removed. As the model predicted, there was not much difference in the depth of cut between 10, 15, and 20 mph (16, 24 and 32 km/h). These tests were conducted at 100 psi (7.3 Kg/cm^2) and if a system was built, the 145 psi (10.5 Kg/cm^2) pressure as demonstrated in the laboratory, would be used to enhance the ice removal process. Also in this test, the compressor was pulled behind a pickup and 25 foot (7.6 meter) air supply lines and sandblasting lines were used. In a field unit the compressor and sandblaster would be mounted in the back of the truck where shorter supply lines and hoses could be used. This would result in more efficient use of the air being supplied by the compressor as the line losses can be significant, especially in a multinozzle system. Figure 39 shows the final depth of cut vs traverse speed plot with both the experimental and computer model data up to 20 mph (32 km/h). This brief field test proved that an abrasive air jet system can be used to remove ice at 20 mph (32 km/h).

Other Considerations

Although it has been shown that an abrasive air blast system can remove ice at traverse rates of 20 mph (32 km/h), more research should be conducted. A field unit should be developed with multiple nozzles for removal of wide sections of roadway. Tests need to be conducted to determine optimum nozzle size, abrasive type and size as well as nozzle control. Tests need to be carried out on actual roadways with ice and compacted snow. Operator or automatic control systems need to be developed for the nozzles and air compressor to obtain maximum removal without pavement damage under all types of road conditions.

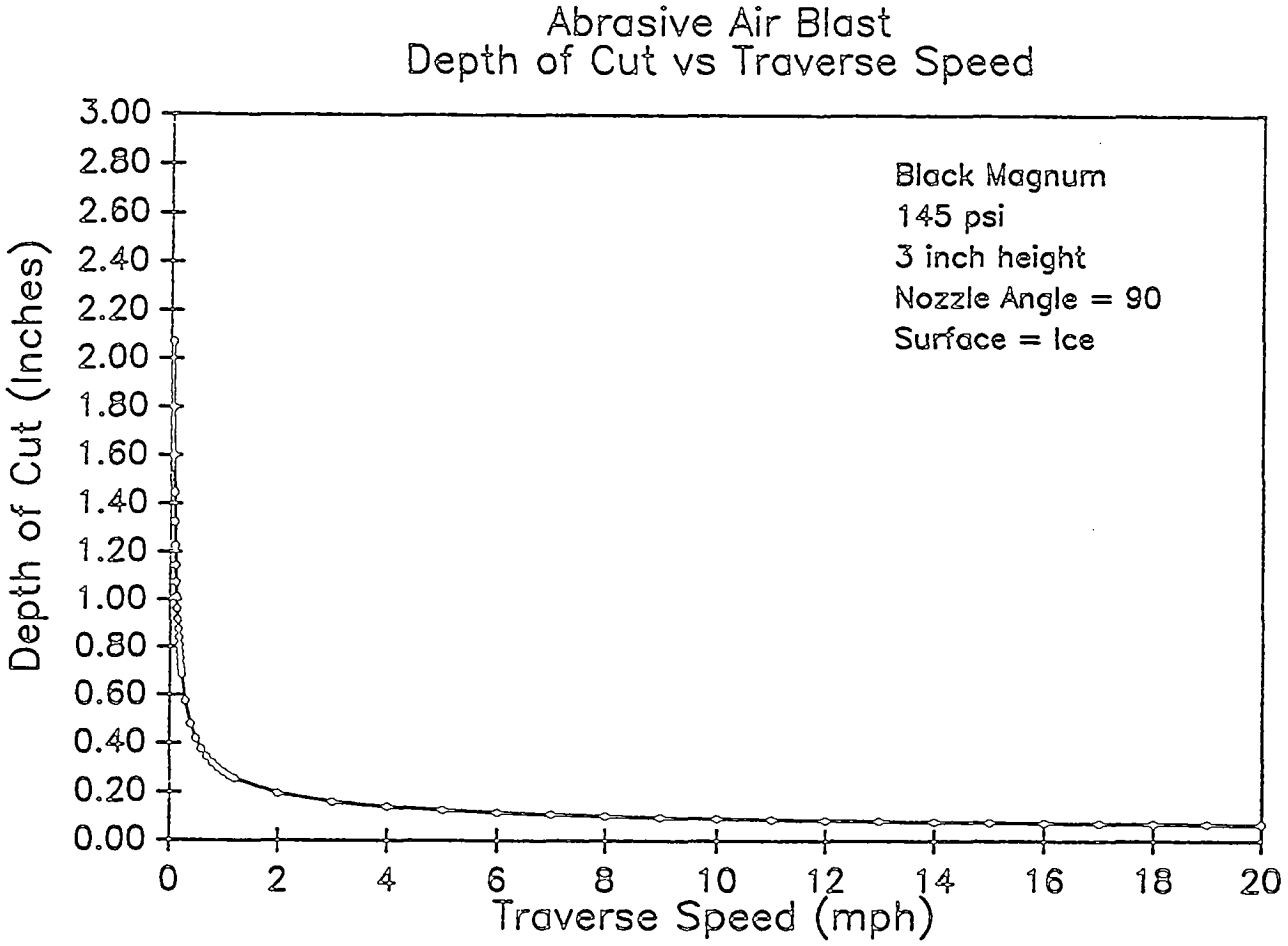

Figure 38. Plot of Abrasive Air Blast computer model data.

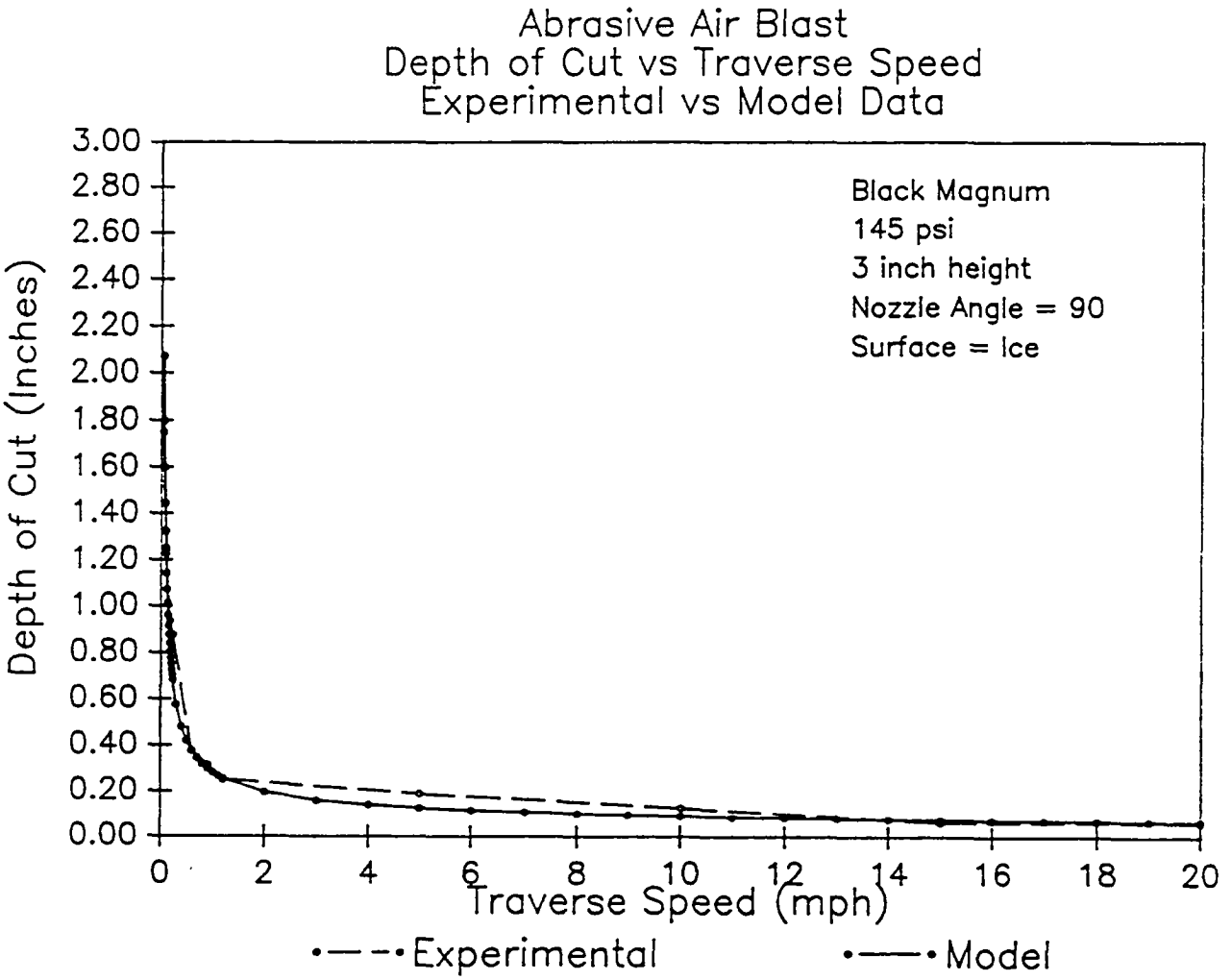

Figure 39. Plot showing both model and experimental depth of cut versus traverse speed up to 20 mph (32 Kmh).

During this study, several other issues have been considered. For example, during initial laboratory studies when traverse rates were low and ice layers were thin the abrasives cut into pavements. Although the damage was limited to exposing aggregate particles, this situation needs to be considered as repeated use of an abrasive air jet system may cause substantial damage to the road surface. The amount of abrasive used during a typical winter season or on a per lane mile basis has been calculated to determine if the costs are exceedingly high or, if too much is used, how it can be removed in the spring. The costs of initially purchasing a system and maintaining the system, either overall or on a per lane mile basis was considered. One problem area is in cold weather a compressed air system produces water in the air lines and this may freeze, eventually plugging air lines. These issues are discussed in the following paragraphs.

Pavement Damage Considerations

Pavement damage has already been considered. It may appear to be a problem but when tests were conducted at KRC at 5, 10, 15 and 20 mph (8, 16, 24 and 32 km/h), some of the abrasives were blasted at the asphalt pavement in the parking lot with no apparent damage. The problems will most likely occur when the vehicle slows down or stops.

There are two ways to effectively control snow and ice removal, one is to raise or lower the nozzles and the other is to control nozzle output through a shutoff valve at the nozzle. There are essentially two areas of concern for controlling system performance without pavement damage. One is the method of sensing snow/ice thickness or the absence of snow/ice and the other is controlling nozzle height and operation.

Snow/ice thickness on bare pavement sensing will probably be the most difficult part of the control system. The best method, at this time, appears to be the use of two wheel fixtures, one mounted near the front of the vehicle and one mounted behind the blasting nozzles. The wheel fixtures will have two functions, one will be to measure slip (coefficient of friction) and the other will be to measure vertical displacement. Vertical displacement measurements will verify snow/ice thickness that would be ahead of the nozzles. For example, if the thickness would decrease, nozzle height would be higher. The wheels at each location would be set with some type of brake so that they would roll on higher friction pavement and slide on low friction snow/ice. If, for example, some but not all ice is removed, the coefficient of friction measurement would tell a microprocessor controller to lower nozzle height.

Timing of events would be controlled by a signal sent from a transducer measuring vehicle wheel speed. All sensors would continuously send signals to a microprocessor controller which would then send a control signal to either the nozzle height adjustment or nozzle control valves. Experimental data obtained from the research conducted during the SHRP program would be used to help the microprocessor make decisions, such as nozzle height corresponding to a certain snow/ice thickness.

Amounts of Abrasives

Simple calculations were made to determine the amount of abrasives used per lane mile. Sandblasting data for a 1/4 inch (.63 cm) venturi nozzle shows that 494 lbs. (224.5 kg) of abrasive would be used each hour. For a vehicle traveling at 20 mph (32 km/h), this would be 24.7 lbs. per nozzle - mile (7 Kg per nozzle km). If 16 nozzles were used to cut an 8 foot (2.44 m) wide path, the total amount of abrasive used per lane mile would be about 395.2 lbs (179.6 kg). Discussions with the Michigan State Highway personnel (Unpublished Data) showed that current sand spreading techniques for increasing road friction use approximately 400 lbs. (181.8 kg) per lane mile. Therefore, about the same amount of sand or abrasive would be used as is currently used. Current cost estimates show that the abrasives cost about $0.04 per pound in the 100 lb. (45.4 kg) bags. Large bulk purchases may reduce this cost and it should be realized that the abrasives cost is no more than what is currently used for the sand because no more abrasive is required than what is currently used.

Estimated Costs of Operation and Maintenance

A rough estimate of the cost to purchase, operate and maintain a complete full scale abrasive air blast system was calculated based on earlier information from sandblasting and air compressor companies, abrasive costs, fuel costs and usage, etc. This estimate was for a 16 nozzle system and included the cost of the prime mover. A ten year life expectancy was used in the estimate and it was assumed that the system might be used approximately four months per year, or 13,860 miles (22,176 Km) per year at 20 mph (32 km/h). The costs provided below are on a per lane mile (km) basis and may actually be lower than shown if abrasives are purchased in bulk quantities.

Description	Cost/Mile	(Cost/Km/h)
Prime Mover, (Ini. & Maint.)	$ 0.93	$ 0.58
Abrasive	$15.81	$ 9.88
Fuel	$ 0.58	$ 0.36
Nozzles	$ 0.36	$ 0.23
Maint. (Blasting Sys.)	$ 0.07	$ 0.04
Air Compressor (Ini. Cost)	$ 1.08	$ 0.68
Blaster (Ini. Cost)	$ 0.07	$ 0.04
Total	$18.90	$11.81

This is only a rough estimate based on current anticipated costs. But once again it should be noted that the abrasive is roughly 80 percent of the cost but this is a cost that is also currently in the system now, so the real additional cost above which is currently being spent is about $3.00 per lane mile (1.875 per lane km).

Water Condensation Problems

The final major problem that was considered before project funding was cut is the condensation of moisture out of the compressed air. When air is compressed and then cooled water condenses out of the air mixture. In a winter environment this may be a problem as temperatures below freezing could cause ice formation in the air supply and abrasive air lines. Reduced air line size usually results in inefficient operation. A good filtration/separation system will have to be incorporated into the system and this will be one of the most important maintenance functions of the operator in his daily routine. Another method that may reduce this problem would be to heat and insulate the lines, perhaps even enclose the air compressor leaving the sandblaster exposed for easier loading of abrasive through a hopper.

Summary

Through laboratory testing, information gathering, mathematical modelling and preliminary field testing, an abrasive air jet system has been proven to be an effective, practical means of removing strongly bonded compacted snow and ice from roads and runways. There is still a great deal of research and testing required to refine and optimize the system, but as a whole, the abrasive air blast system may be one effective method of making highways safe for the public motorist.

References

1. C. J. Posey, "Snow Removal and Ice Control Research, Plow Without Scraping", HRB Special Report 115, Pages 251-256, 1970.

2. M. M. Kasinskas, "Development of the Air Jet Snowplow, Final Report", State of Connecticut Department of Transportation, State Research Project 175-225, Joint Highway Project 70-4, July 1972.

3. T. Townsend and P. Green, "Transport Canada Pneumatic Sweeper", Field Evaluation Final Report To Transport Canada, AK-71-09-216, August 1986.

4. J. L. Andersen, "Test Report on Engineering Test Instruction No. 71033-T002 Airblast Assisted Snowplow", Land Engineering Test Establishment, Report Number 11/75, February 1975.

5. M. Hashish, "Prediction of Depth of Cut in Abrasive Waterjet (AWJ) Machining", ASME Conference On Modeling Of Materials Processing, Vol. 3, Pages 65-82, 1987.

This approach focused on the fundamental considerations for introducing acoustic energy into ice bonded to pavement for the purpose of destroying that bond.

Acoustic disbonding requires that sufficient energy be introduced into the ice to cause fracturing or failure of the bond. Physical constraints on the problem include: contact between the acoustic source and the ice is to be avoided and, in general, there will be an air interface between the ice and the source; also, pavement damage is very undesirable. Other desirable features include: no noise pollution; high energy efficiency; and the method should be robust over a variety of ice/snow conditions.

Three acoustic energy sources were considered:

1) Electro-Mechanical (loudspeaker) This is an easily controlled source which can be tuned over a range of frequencies. Only limited amount of power is available and the efficiencies are rather low.

2) Explosive Mixtures (air/propane) This source has a high energy capability, offers good efficiency and uses a widely available fuel. It is difficult to direct the energy from such a device; the heat generated may or may not be an asset to such a source.

3) Sonic Gas Jet (compressed air) Such a source is easily directed and is capable of producing high energy levels. If combustible mixtures are used, additional energy can be obtained.

All of the above sources will operate under the constraints of the fundamental physics of sound propagation which govern the use of any source. Among these is acoustic wave type. While solids can support a variety of waves, including compressional waves, shear waves, and boundary waves such as Rayleigh waves, fluids can support only compressional waves. Thus, air, which is present in the coupling of a non-contact acoustic source, restricts the ability to introduce energy into the bonded ice.

(Air impedance - Ice impedance)/(Air impedance + Ice impedance)

The impedance mismatch (approximately a factor of 1000 between ice and air) produces a reflection coefficient very close to one. The result is that very little acoustic energy will be coupled from the air into the ice because of the air interface. These considerations apply to linear conditions and it is thus likely that nonlinear conditions must be established to couple significant amounts of energy through the air and into the ice.

A recent study of ice-pavement disbonding (Midwest Research Institute Quarterly

Progress Report, July, 1989) reported on simulating planar shock waves in the ice in order to achieve disbonding. An impactor was simulated to introduce the shock waves and, thus, the problem of the air interface was removed. It was concluded that ice could be disbonded without crushing the ice and that the results were appropriate to any type of concrete. A fundamental problem with the results is the fact that planer waves were assumed to be introduced into the ice layer. In the case of irregular pavement surfaces and irregular coverage of ice on the pavement, it is unlikely that one would be able to introduce the required waves across the entire face of the ice to be disbonded. Also, no effort was made to identify the possible long term deleterious effect of "banging away" at the pavement surface with a nylon faced hammer throughout several winters. The approach, that of circumventing the intervening air layer, is attractive even though a set of problems is introduced.

A much earlier report (T. W. Mouat and R. L. Sanders, British Columbia Research Council) on ice disbonding discussed vibration/ultrasonic techniques. This practical work found that jackhammers were ineffective and that although ultrasonic transducers properly coupled to ice caused some surface fracturing there was no disruptive effect at the ice/pavement interface.

The conclusion of these analyses is that inefficient energy coupling and the difficulty of focusing the vibrational energy at the ice/pavement interface severely limit the potential successes that might be attained with acoustic/vibrational methods. We, therefore, do not recommend that acoustic techniques be considered further for ice disbonding.

Plunger Application of Deicer

The usual way of delivering a freezing point depressant from the ice surface to the ice-pavement interface is by spreading the anti-freeze on the ice surface. Such a method is time consuming and the anti-freeze is diluted when it reaches the interface. If the anti-freeze could be applied directly to the interface, delivery of anti-freeze would be more rapid and efficient. This approach considered using a plunger having a nozzle on the tip pressed to the ice surface to create crack as shown in Figure 39. When the crack is produced, high pressure solution could be sent from the nozzle to the surface through the channel made by the crack. Eventually, the anti-freeze solution will spread on the interface between ice and pavement. If the ice is loaded by sand grains, particles may cause clogging of the nozzle. A modified version of the plunger as shown in Figure 40 was designed to clean the nozzle by a smaller plunger at each anti-freeze delivery that would lessen this problem. The smaller plunger would also act to generate high pressure fluid. In the field operation, a set of plungers could be mounted ahead of the plow blade as shown in Figure 41. This method may not be effective on soft snow.

A simple single plunger was constructed and tested under various conditions in the laboratory to study the range and limit of application and fluid penetration. The basic

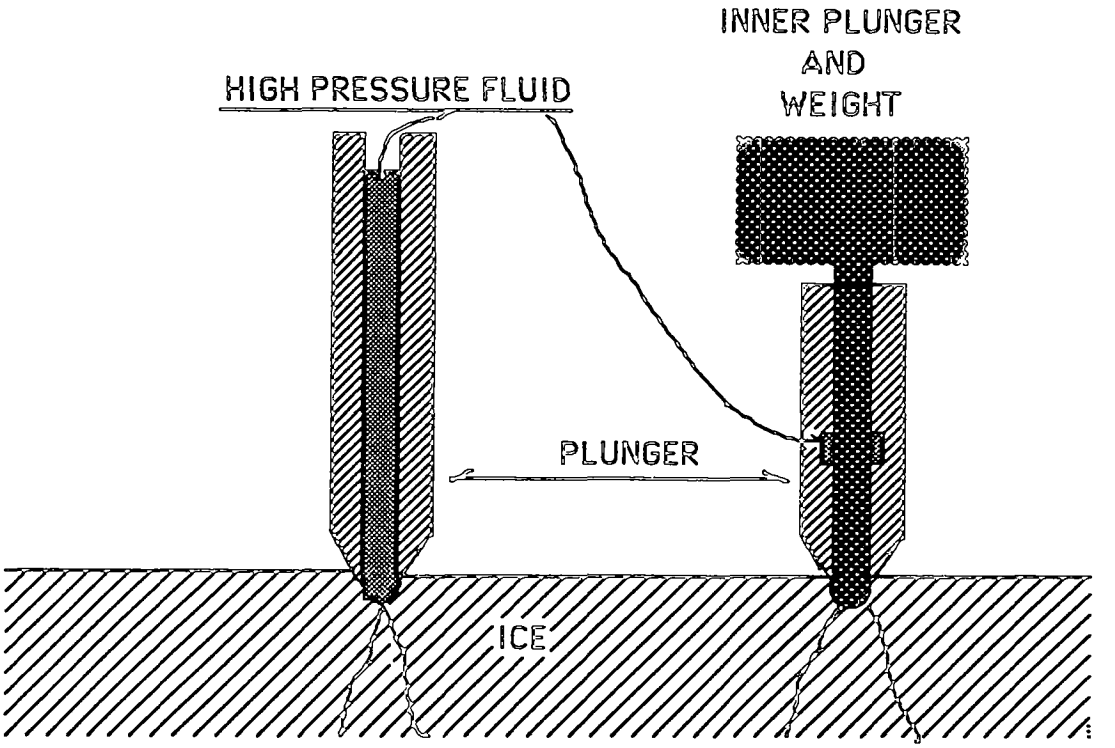

FIG. 39

FIG. 40

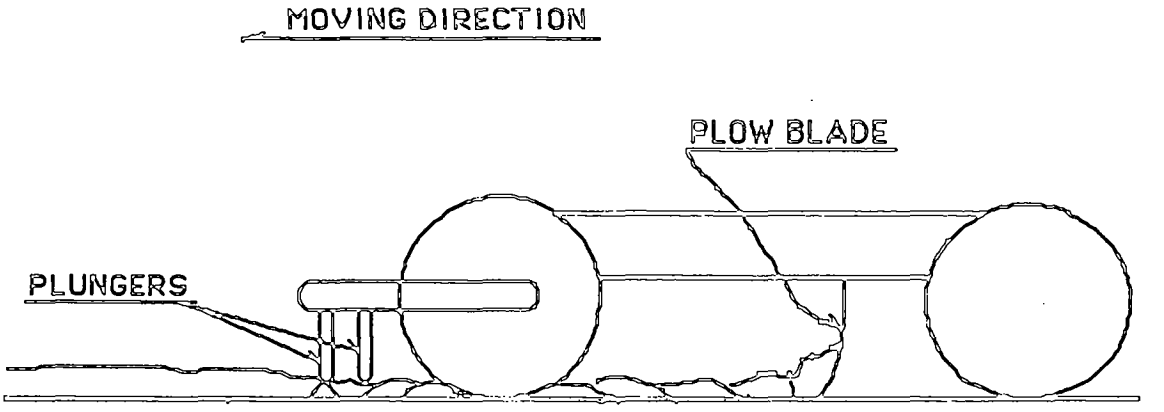

FIG. 41

concept of the plunger system was to start a crack by concentrated mechanical force, then to spread the crack by high pressure anti-freeze solution and deliver the anti-freeze through the crack to the ice-road interface.

Mechanical initiation of crack was achieved by piercing the ice with conical or pyramidal point. Delivery of high pressure anti-freeze was made through a channel in a hollow cone or pyramid. Generation of high pressure anti-freeze can be also done by a small size plunger sliding in the bore. The small plunger can also clear the channel clogged by dirt.

The design of the plunger system is as follows:

Generation of both mechanical force and plunger is made by two 1/2" pneumatic cylinders. Control of air pressure was done by a simple pressure regulator and valve for the pneumatic cylinder.

A preliminary test made on ice frozen onto a 1/4" (6.4 mm) thick rusty steel plate. 420 lb(1,850 N) force produced by 85 psi (590,000 Pa) air pressure was insufficient to penetrate through the 1/2" (12.5 mm) thick ice by a 90° cone indenter, but 1/4" (6.4mm) thick ice could be removed easily. Video image and visual inspection after the test indicated that the crack reached to the interface and spread concentrically from under the plunger. If the plunger location was close (about 3 cm) from the edge of the ice, a perpendicular crack started at the plunger and combined with an interface crack eventually resulted in removal of a triangular piece of ice.

Taking into account such factors, the success rate appeared to be reasonably good. If the pavement surface was contaminated and polished by traffic, the success rate would increase considerably. Also, this was the first trial and the system was not optimized. Success rates can be improved extensively by an optimized system on real contaminated pavement surfaces.

The major drawback was the complexity of the system for field usage. Plumbing for the multi-plunger system could be difficult. A straight-edge plunger system (suggested by Mr. Wuori) could reduce the problem considerably. Damage to the pavement could then be controlled well.

Some spreading of the anti-freeze between the ice and road interface of asphalt or concrete surface was observed. The fluids used in the tests were mixed with dye (Fluorescein) in the anti-freeze. Since Fluoresceins luminesce, a minute amount of solution penetration could be detected. Observations indicated the spreading was limited near the plunger indentation only.

The original anti-freeze solution was a 30% solution of PEG 400 which has the consistency of syrup. Spreading of anti-freeze through thin cracks seemed slow. Lower

viscosity anti-freeze (alcohol) tests were made. Leaks around the plunger tip were found to be excessive under present configuration.

Tests using fluid having intermediate viscosity between alcohol and PEG 400 was planned. Candidate fluid included lower molecular weight PEG (PEG 50-100 range). Instead, tests were made with a CMA solution according to recommendation by Mr. Wuori for less slipperiness and lower corrosiveness. Thirty percent solution of CMA has a consistency similar to water. With the 60° plunger, it worked generally fine although leakage seemed a little high. For the pyramidal plunger, excessive leakage prevented sufficient fluid pressure build-up. Apparently, the flat tip of the pyramidal head prevented good sealing.

Tests using three types of plunger head were made. They are blunt angle (90°) and sharper angle (60°) conical-tip plungers and a pyramidal plunger. Tests showed the blunt angle (90°) plunger was not able to penetrate 1/2" (12.8 mm) ice using 85 psi (590,000 Pa) air pressure which produced 420 lbf (1,850 N) of force.

The pyramidal plunger was expected to start the crack at the corners so that there would be more control on cracking. However, the pyramidal plunger was not effective due to its flat tip. The plunger was unable to penetrate ice and fluid leaked from the tip. Modifications were made to remove the flat part so that sufficient stress could be applied to penetrate ice but no tests were made.

As a preliminary study for a multiple plunger system, interaction of cracks produced by the plunger were observed by testing the plunger in a triangular pattern. When the tip was placed on the crack generated by the previous indentation, frequent successful ice removal was observed. When the crack spread in a fixed pattern by the interaction of two or more plungers, ice removal was much easier.

Frequently, it was noticed that the ice-road interface is slightly melted in the sunny early spring afternoon. Ice on the road can be easily cracked and lifted up under such conditions. When lifting takes place, plowing of ice is much easier. In conjunction with this observation, surface temperature measurement were made at the interface when irradiated by IR radiation.

Thermo-couples were cemented on one of each of asphalt concrete and Portland cement concrete sample surfaces. The temperature rise by IR irradiation was recorded by a strip chart recorder. The sample was placed 19 cm from a 150 W flood lamp. Average temperature rise rate for asphalt concrete was 2.3°C/min. and Portland cement concrete was 1.4°C/min. Darker asphalt concrete would be expected to absorb IR radiation faster than the lighter Portland cement concrete.

Plunger tests made at a surface temperature of -1°C after the irradiation resulted in little difference than the tests without irradiation. There were up to 30% cases of ice

lift-up without warming the interface. The surface may have to be brought to the melting point for easy ice removal.

Observed Results

Several possible cases under the various conditions was predicted and most of the predictions were found to be reasonably correct.

Case a. If the ice is very thick (more than 2 in.) and hard, the crack would penetrate to certain depth and stop. Anti-freeze may widen the crack and stay there. This prediction was found to be valid except that the high pressure anti-freeze tended to create concentric cracks around the plunger tip.

Case b. When the ice and the road surface is very cold as frequently observed in early cold mornings, anti-freeze reaches to the road surface and then spreads along to some extent but does not effectively lift the ice. Anti-freeze will spread through to the interface, gradually acting as a pre-treatment. This prediction was generally correct but the amount of anti-freeze with the present design plunger seemed insufficient for pre-treatment. In order to increase anti-freeze delivery, a larger volume pump or multiple delivery may be needed.

Case c. It was frequently observed during sunny early spring afternoons that the ice pavement interface is slightly melted. Ice can be easily lifted from the pavement under this condition. This was not tested but the ice/pavement interface was heated by IR radiation up to - 1°C. The results were negative indicating that the process would require real melting conditions.

Case d. When ice is mixed with sands, initiation and propagation of crack may be difficult. The tip of the plunger may suffer damage. Selection of proper material becomes important.

Case e. If the ice thickness is thin (less than 1/4"), the area of cracked ice is limited around the plunger so that effectiveness will be limited.

It was concluded that the concept of initiating a crack mechanically and spreading it by hydraulic force was effective in removing ice from the pavement surface. However, the channel produced by the extended crack seemed insufficient to deliver enough anti-freeze to the ice/pavement interface. This system may be too complicated for wide usage but may find applications in certain problems. A single hand-held plunger could be used to crack localized ice in place of an ice chizzle.

Contact Methods

Cutting Edge Profiles Design Analysis

The work in this area was initiated to investigate the possibility of developing a curved, "optimized", cutting edge profile. The purpose of such a profile is to remove a bonded ice layer from highway pavements by promoting fracture at the interface between the ice and the pavement. Initially, the literature was reviewed and it was found that the mechanics of layer removal had been studied by two independent researchers. Each author considered the removal of an elastic layer from a rigid substrate. Chronologically, Hellan [1,2] was the first to consider this problem. In Hellan's analysis the mechanics associated with debonding an elastic layer under the action of a prescribed axial force (A), shearing force (V), and bending moment (M), was considered in Figure 42b. In this initial analysis, inertial effects within the layer were included and layer debonding addressed. The next researcher to address the problem of layer removal was Huang [3-6]. Following Hellan's work, Huang studied the removal of an elastic layer by the use of a wedge shaped scraper. In addition to considering debonding of the layer, Huang also considered buckling and crushing of the layer as possible failure modes.

Both Helland and Huang assumed that the interfacial crack would continue to grow along the interface. This assumption relies on the presence of an interface which requires less energy to initiate and propagate a crack then either the layer or substrate. In the case of many interfaces, especially the one between a roadway and ice or compacted snow, the bonding at the interface may be stronger and the fracture energy higher at the interface. In this situation, cracks initiated at the interface may turn and propagate toward the surface of the layer or into the substrate. Here, the shape of "cutting edge" profiles were explored which would promote continued interfacial crack propagation. To accomplish this, first the finite element method was used to determine the functional relationship between the length of the interfacial crack and the loading required for continued interfacial fracture. Next and energy approach, similar to Huang's, was used to generate profiles which would deliver this loading to the layer.

Finite Element Modeling

Since the purpose of the finite element modeling was to predict the loading which must be transmitted to the surface layer for interfacial fracture, a criterion was required which could predict the direction of crack propagation. Initially, it was thought that a suitable criterion would involve the maximization of $\sigma_{\theta\theta}$ (see Figure 43). This criterion, the maximum normal stress criterion, was initially proposed by Erdogan and Sih [7]. It has been used extensively for predicting the direction of propagation in homogeneous materials. Erdogan and Sih's version of the criterion involved the use of only the singular term in the Williams [8] eigenfunction expansion for the near tip stress field. Other researchers have also included nonsingular terms when using the criterion and were thus

LIFTING OF A SURFACE LAYER WITH A WEDGE SHAPED SCRAPER

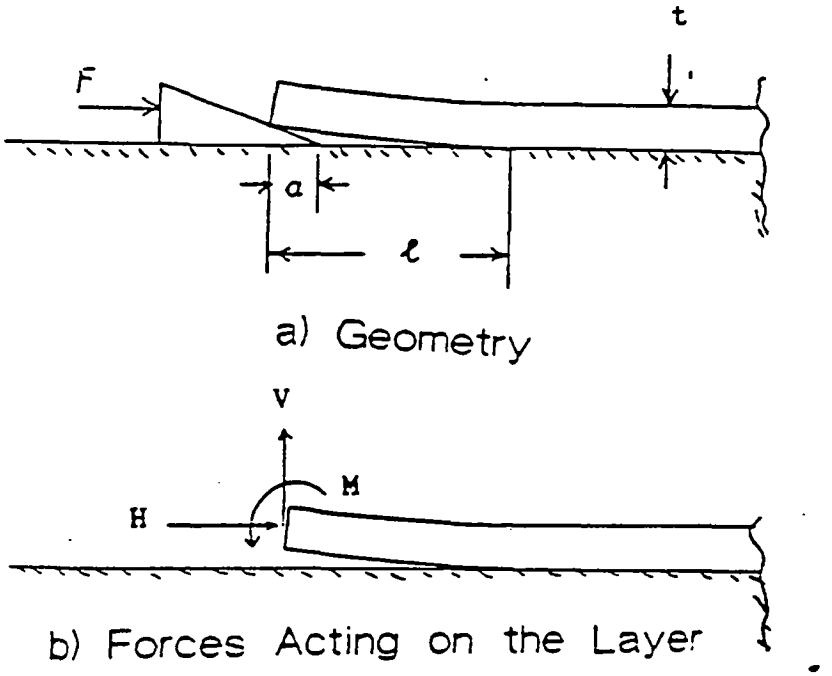

Figure 42

CRACK TIP POLAR COORDINATE SYSTEM

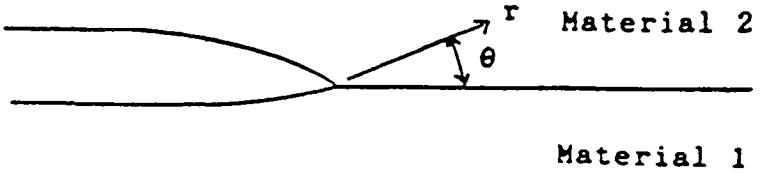

Figure 43

forced to choose a reference radius when evaluating $\sigma_{\theta\theta}$ criterion). All versions of the normal stress criterion have yielded reasonable results when cracks in homogeneous materials were studied. When interfacial cracks between dissimilar materials are considered the approach becomes questionable. The singular term in the England [10] expansion of $\sigma_{\theta\theta}$ for interfacial cracks takes the form

$$\sigma_{\theta\theta}=\bar{K}r^{(-1/2+i\epsilon)}[f^{I}_{re}(\theta)+if^{I}_{im}(\theta)+Kr^{(-1/2-i\epsilon)}[f^{II}_{re}(\theta)+if^{II}_{im}(\theta)] \tag{1}$$

where

$$K=K_I+iK_{II}$$

$$\epsilon=(1/2\pi)\ln\left[\frac{\mu_1+\mu_2\chi_1}{\mu_2+\mu_1\chi_2}\right]$$

$$\chi_\alpha=3-4\nu_\alpha,\ \alpha=1,2 \tag{2}$$

$$r^{(-1/2+i\epsilon)}=r^{(-1/2)}[\cos(\epsilon\ln(r))+i\sin(\epsilon\ln(r))]$$

Here K represents the complex conjugate of K, μ_α the shear modulus, and ν_α Poisson's ratio (see Smelser [11]). From equations 1 and 2 the oscillatory behavior of $\sigma_{\theta\theta}$ is evident. For small values of r $\sigma_{\theta\theta}$ oscillates rapidly as r varies. Therefore, the choice of a reference radius for evaluation of $\sigma_{\theta\theta}$ is required. Because of these rapid oscillations near the crack tip, small changes in the choice of the reference radius could greatly change the predicted propagation direction. Thus, the maximum normal stress criterion was found unsuitable.

The second criterion considered predicts crack propagation in the direction of the maximum energy release rate. This criterion has been previously used with the finite element method by Barr et. al. [12]. In order to apply this criterion using finite elements, the geometry is discretized with a near tip mesh similar to that shown in Figure 44. After application of the required loading, the strain energy of the cracked body (U_A) is calculated with the crack located in a reference position (Terminating at A). The crack is then allowed to advance to B. Holding the displacements of the loads equal to those

NEAR TIP FINITE ELEMENT MESH

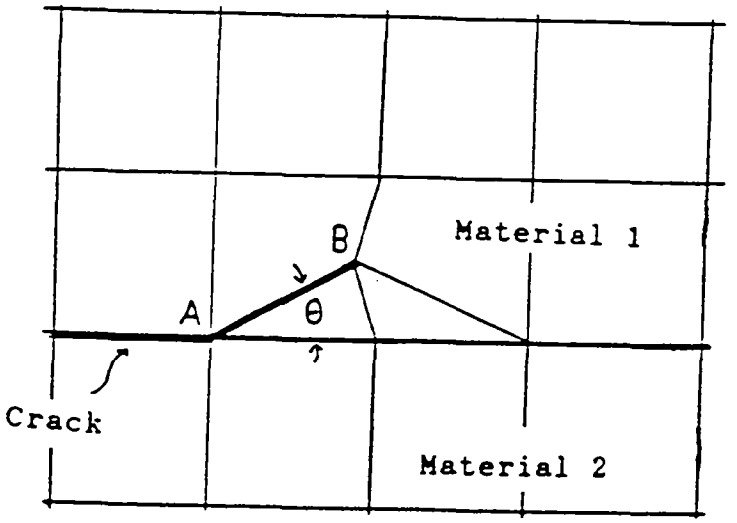

Figure 44

calculated with the crack in its reference position, the strain energy is once again evaluated (U_B). The average energy release rate for the crack extension from A to B can then be calculated as

$$\frac{dU}{da} = \frac{U_A - U_B}{L_{AB}}$$

where L_{AB} is the length of the allowed extension. By allowing θ to vary while holding L_{AB} constant, the direction of crack propagation which will maximize the energy release rate can be determined. This approach eliminates the use of the England expansion and thus, the direct involvement of the oscillatory stress field. The approach has been shown to yield good results even when very dissimilar materials are considered and relatively large values of L_{AB} are used [13]. In the present calculations L_{AB} was held constant. Therefore, the quantity (U_A - ^ U_B) was maximized when determining the preferred propagation direction.

In order to address the accuracy of the maximum energy release rate approach, and to determine the mesh refinement necessary for calculations of this type, the problem shown in Figure 45 was analyzed. This problem had been previously considered by Erdogan and Gupta [14]. Erdogan and Gupta used an integral equation approach to evaluate stress intensity factors and the maximum normal stress criterion to determine the direction of propagation for cracks lying at $h_1/h = 0.1 \rightarrow 0.5$. Since interfacial fracture was the ultimate concern of this work $h_1/h = 0.1$ was chosen for comparison. Various mesh refinements were tried until convergence was obtained. The mesh finally used

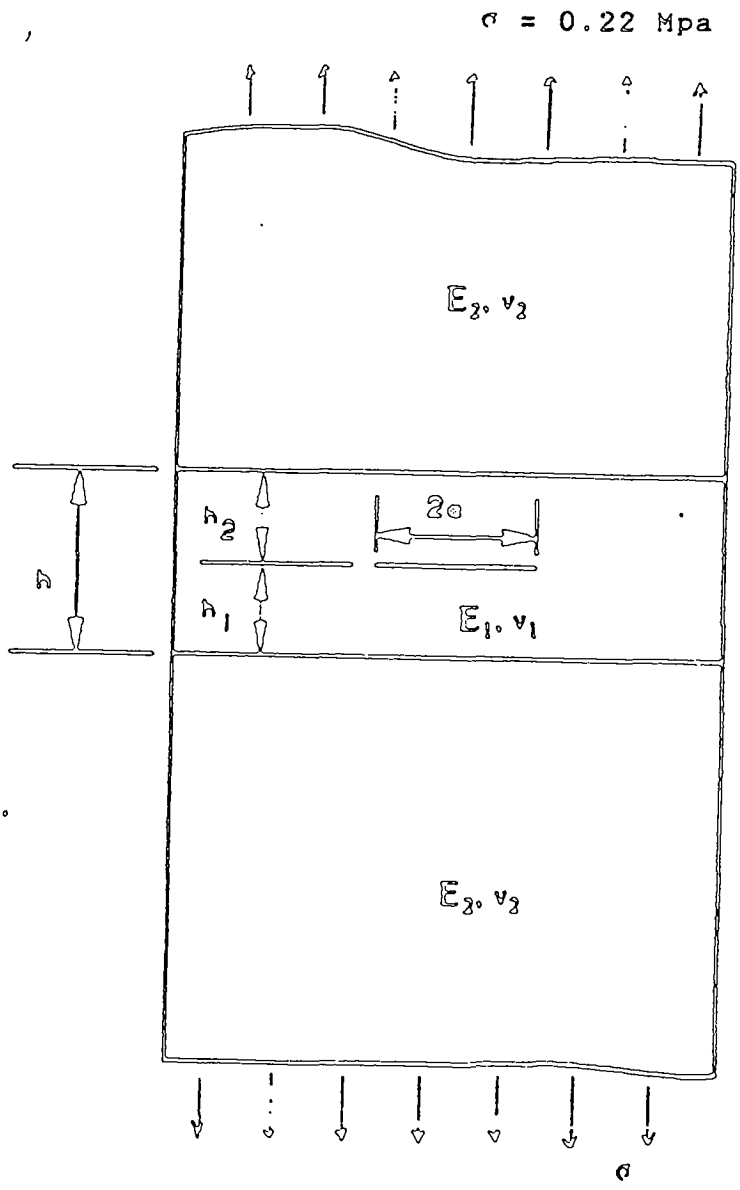

h = 25.4 mm

h/2a = 1

E_1 = 3.1 GPa ν_1 = 0.3

E_1 = 69.1 GPA ν_2 = 0.3

Figure 45
Geometry Addressed
by
Erdogan and Gupta

consisted of quadratic isoparametric elements with edges 0.1 in long near the crack tip. The midside nodes of all element sides terminating at the crack tip were moved from the midpoint to the quarterpoint to provide the correct singularity [15]. The results shown in Table 23 contrast the results generated using the finite element method to Erdogan and Gupta's results.

Table 23. FEM Comparisons with Erdogan and Gupta

Parameter	Finite Element Result	Erdogan & Gupta Result
K_I	22.51	22.46
K_{II}	-2.98	-2.96
θ_o	15°	15.08°

In determining the stress intensity factors K_I and K_{II} with the finite element method displacement extrapolation was utilized, in calculating the direction of preferred propagation θ_o the previously described maximum energy release rate criterion was employed with the value of θ_o finally obtained from Figure 46.

Using the information gained from the comparisons with Erdogan and Gupta's results, interfacial fracture was attacked. The geometry modeled is shown in Figure 47 and both 12.7 mm. and 6.3 mm. thick layers were considered. Since the problem is linear in nature, only the ratio between the horizontal (H) and the vertical (V) loads applied to the layer is unique, the finite element study focused on the determination of this ratio. With the final interest lying in the removal of ice and compacted snow layers from highway pavements, the layer width will always be much greater than the layer thickness. Thus, the plane strain idealization was chosen for the analysis. The applied loads (H & V) were moved to various nodes along the discretization of the debonded portion of the layer to simulate different debond (interfacial crack) lengths.

Calculating the H/V ratio required for continued interfacial crack propagation ($\theta_o = 0$) using the finite element method is a multi-step procedure. While initially one may think that the ratio of the loads, H/V, applied to the layer could be adjusted until the energy released by an increment of continued interfacial crack growth was greater than that required for equivalent increments of crack growth at $\pm\theta$. Since elements with large aspect ratios (θ small) perform poorly, this approach could only provide an uncertain value of the H/V ratio necessary for continued interfacial fracture. The approach used here to predict H/V for interfacial propagation is based on an extrapolation from the H/V ratios determined to produce non-zero values of θ_o. Plots such as Figure 48 were generated for interfacial crack lengths of 7.6, 12.7, 25.4, and 48.3 mm. Extrapolation

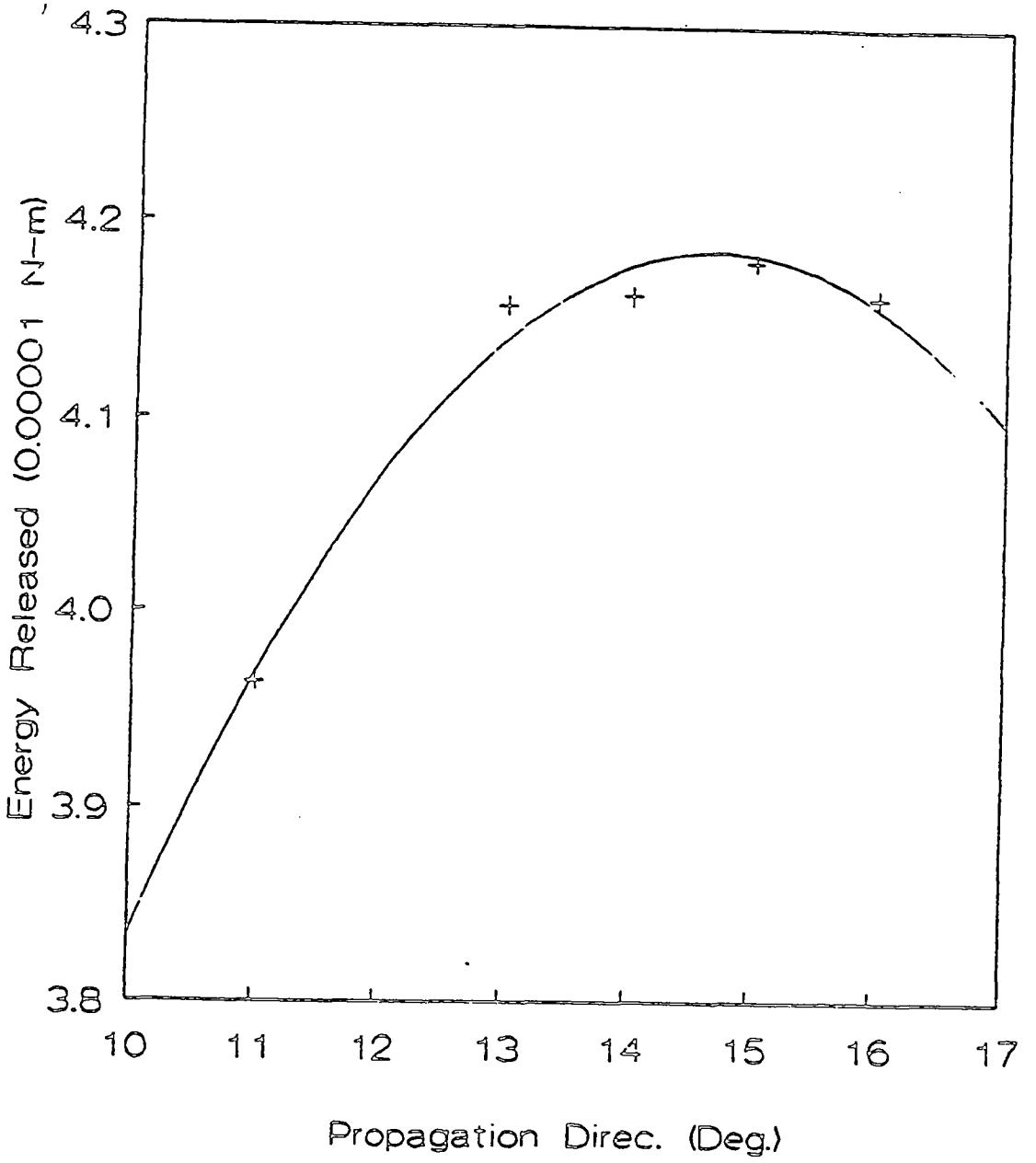

Figure 46
Preferred Propagation Direction
(Erdogan & Gupta)

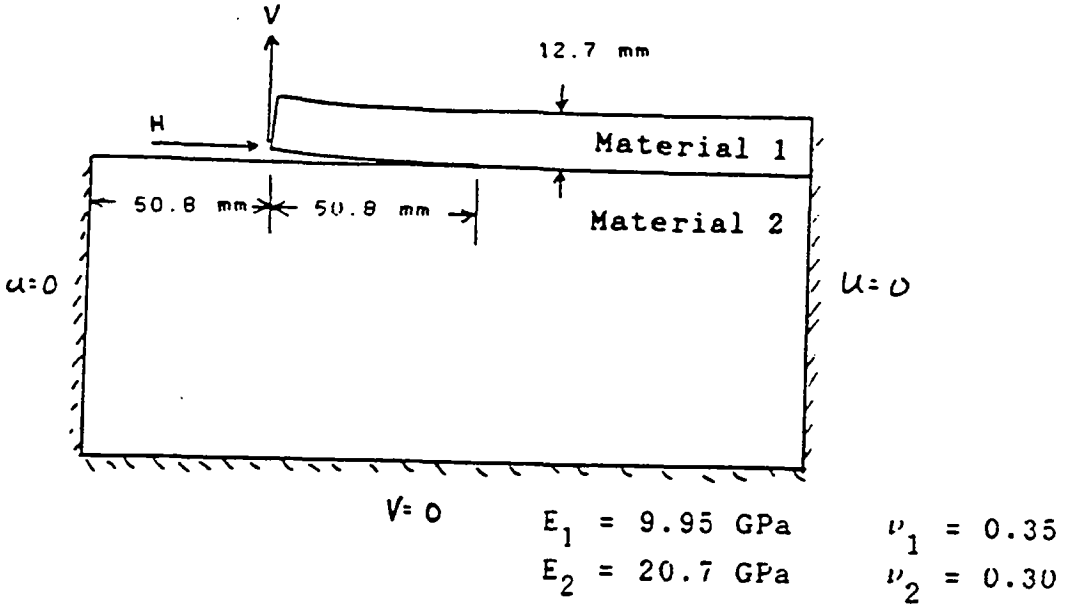

Figure 47
Layer Geometry
and
Boundary Conditions

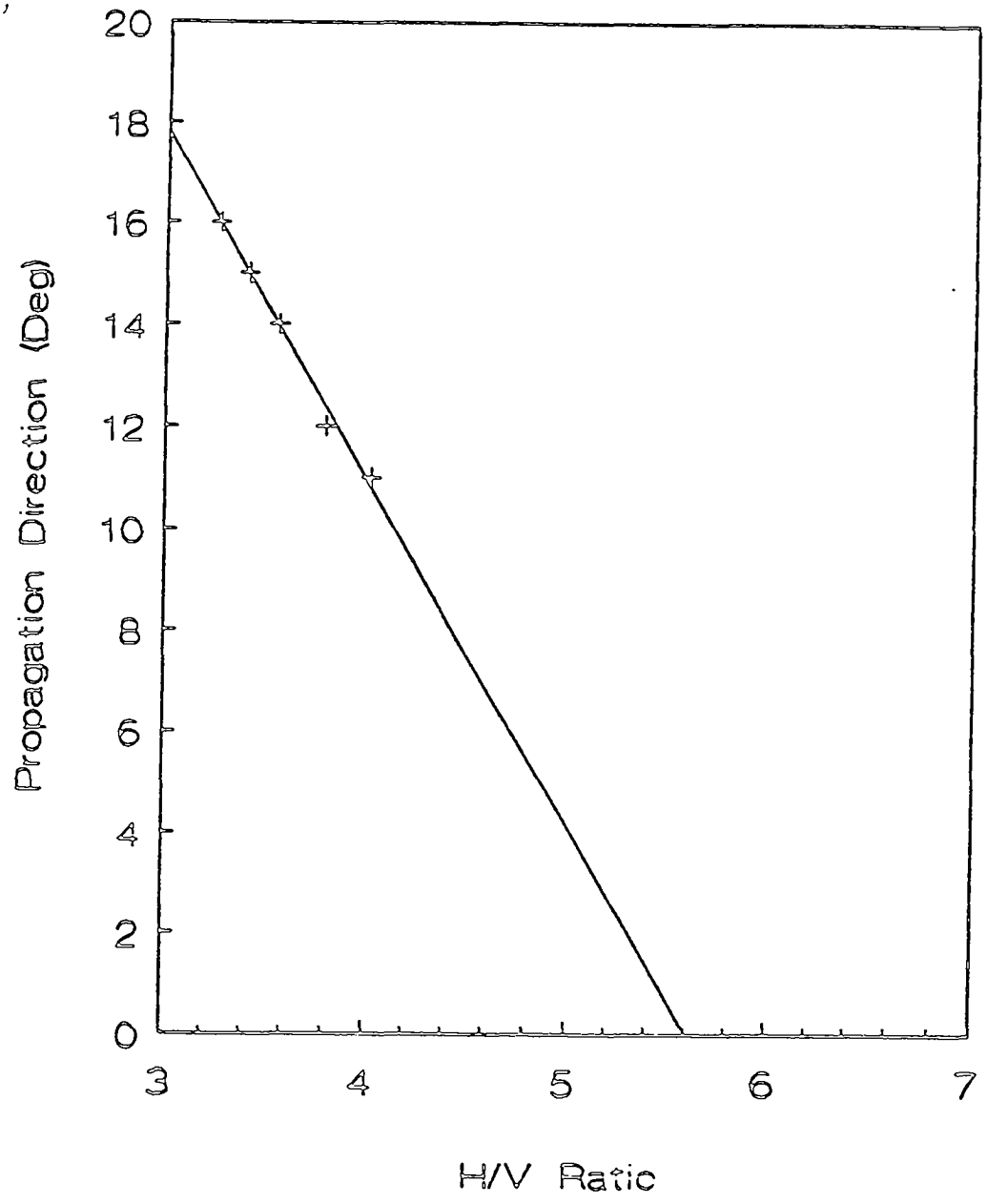

Figure 48
H/V Determination
for
Interfacial Fracture
$t = 12.7$ mm. $\ell = 48.3$ mm.

from these plots allowed the required value of H/V for interfacial propagation to be determined for each crack length. Figure 49 shows these results for both 6.3 mm. and 12.7 mm. thick ice layers lying on concrete.

The value of the Mode II stress intensity factor (K_{II}) was calculated at the H/V ratios necessary to provide continued interfacial propagation. In all cases $K_{II} = 0.0$ at the values of H/V. Thus, when an ice-pavement interface is present, loading which forces $K_{II} = 0.0$ will promote interfacial propagation. This criterion can be used to determine the H/V ratios of Figure 49 and it is much more computationally efficient.

Scraper Shapes

With the relationship between the loads which must be transmitted to the layer (H/V) determined, a method to develop the scraper profile necessary to supply these loads was necessary. Huang's work [3] on the lifting of surface layers by wedges is the kernel of the method developed. Since the ratio, H/V, can be translated directly into the slope of the surface which must contact the layer's edge, Huang's results were adjusted and incrementally applied to generate a curved scraper face.

In Huang's work differential equations were developed using both a displacement and an energy approach. Once these equations were generated, an eigenvalue problem resulted which allowed the calculation of the force necessarily applied to the impinging wedge to initiate fracture. The following represents an abbreviated summary of Huang's work adjusted to include compressive effects. Timoshenko beam theory is utilized.

Assuming no friction between the wedge and the layer, the forces transmitted from the wedge to the layer can be replaced by equivalent loads acting at the layer's neutral axis (Figure 42b). Equilibrium of the wedge, allows the following relationships between these equivalent loads and the force, F, driving the wedge to be calculated

$$H=\frac{FS}{(S+\mu)}, V=\frac{F}{(S+\mu)}, M=\frac{H(t)S}{2(S+\mu)} \tag{3}$$

Here, μ is the coefficient of friction between the scraper and the substrate, S is the slope of the scraper front, and t is the layer thickness. In terms of these loads, the vertical displacement of the loading point, v, can be expressed as

$$v=\frac{1}{EI}\left[\frac{Vt^3}{3}-\frac{\rho bt^4}{8}-\frac{Mt^2}{2}\right]+\frac{6}{5GA}\left[vt-\frac{\rho bt^2}{2}\right] \tag{4}$$

where E is Young's modulus, G the shear modulus, I the area moment of inertia, A the cross-sectional area, b the layer width, and ρ the weight density of the surface layer. The

differential form of this equation becomes

$$\delta v=\left[\frac{1}{EI}\left[\frac{F\ell^2}{(S+\mu)}-\frac{\rho b t\ell^3}{2}-\frac{St\ell F}{2(S+\mu)}\right]+\frac{6}{5GA}\left[\frac{F}{(S+\mu)}-\rho b t\ell\right]\right]\delta\ell + \left[\frac{1}{EI}\left[\frac{\ell^3}{3(S+\mu)}-\frac{S\ell^2}{4(S+\mu)}\right]+\frac{6\ell}{5GA(S+\mu)}\right]\delta F \tag{5}$$

When the compression of the surface layer due to the horizontal load is considered, the displacement v can also be written as

$$v=S(x-\frac{H\ell}{AE}) \tag{6}$$

or differentially

$$\delta v=S\delta x-\frac{S\ \ \delta F}{AE(S+\mu)}-\frac{FS\ \ \delta\ell}{A(S+\mu)E} \tag{7}$$

The inclusion of compressive effects also alters the relationship between the displacement of the wedge x and the wedges insertion under the surface layer a. This relationship becomes

$$a=x-\frac{H\ell}{AE} \tag{8}$$

The differential equation which is derived from energy considerations follows from the energy balance proposed by Griffith [16]. Griffith postulated the onset of fracture when the energy available equaled the energy necessary for crack propagation. Neglecting the kinetic effects of the scraping process, the differential form of this energy balance becomes

$$-F\left[\frac{S}{(S+\mu)}\right]\delta x=\left[\frac{1}{EI}\left[\frac{\rho^2b^2\gamma^2\ell^4}{8}-\frac{F^2\ell^2}{2(S+\mu)^2}+\frac{F^2S\ell}{4(S+\mu)^2}\right]+\frac{6}{5GA}\left[\frac{\rho^2b^2\gamma^2\ell^2}{2}-\frac{F^2}{2(S+\mu)^2}\right]\right] \tag{9}$$

$$\left[-\frac{F^2S^2}{2(S+\mu)^2AE}-\gamma b\right]\delta\ell+\left[\frac{I}{EI}\left[\frac{-F\ell^3}{3(S+\mu)^2}+\frac{FS\ell^2}{4(S+\mu)^2}\right]-\frac{6F\ell}{5GA(S+\mu)^2}-\frac{FS^2\ell}{AE(S+\mu)^2}\right]\delta F$$

where γ is the energy required to produce a unit area of crack extension.

When equations (5) and (7) are combined to eliminate δv and organized so that only the S δx term remains on the left hand side, the combination of the resulting equation with equation (9) yields the following eigenvalue problem.

$$[AF^2+BF+C]\delta\iota=0$$

$$A=\frac{1}{(S+\mu)^2}\left[\frac{1}{EI}\left[\frac{\iota^2}{2}-\frac{S\iota t}{4}\right]+\frac{3}{5GA}+\frac{S^2}{AE}\right]$$

$$B=\frac{-\rho bt\iota}{(S+\mu)}\left[\frac{\iota^2}{2EI}+\frac{6}{5GA}\right] \qquad (10)$$

$$c=\frac{\rho^2b^2t^2\iota^2}{2}\left[\frac{\iota^2}{4EI}+\frac{6}{5GA}\right]-\gamma b$$

The roots for the quadratic in (10) predict the amount of force, F, which must be applied to a wedge shaped scraper with a slope of S in order to initiate interfacial fracture of a crack with length ι. Once this value of F is known, the lifted height of layer's end (v) can be calculated from (3) and (4), and the wedge insertion from (6) and (8).

At this point the theory necessary to develop a scraper profile which can transmit the necessary loading is in place. It must be remembered, however, that this theory was developed for wedge shaped scrapers. Wedge shaped scrapers have constant slopes which can only apply a constant value of H/V. Since the H/V ratio required to remove the strongly bonded layers considered here varies with the crack length, scrapers with curved fronts are required. In order to generate a curved profile with the developed theory, incremental application is necessary. The scraper profiles generated will thus consist of many straight segments. Since the analyst defines the number of segments, a curved front can be approximated well by choosing a large number of increments.

Development of a scraper profile proceeded as follows. Initially, a short interfacial crack was assumed to exist. From that assumption, the H/V ratio required to

reinitiate interfacial fracture of this crack could be obtained from Figure 49. This H/V ratio was set equal to the slope $(S)_1$ of the first segment of the scraper profile. The required F, v, and a, were then calculated from equations 4, 6, 8, and 10. The first segment was now defined, it had a slope $(S)_1$ and a length $(a)_1$. Next, the crack length was incremented, and new values of F, v, and a calculated. Since the theory assumes the presence of a wedge with constant slope, the incremental insertion, Δa, needed to be calculated in the following way (See Figure 50). For any increment, increment i, the initial insertion of an updated wedge (one with the slope S_i required to promote continued interfacial fracture of the incremented crack) a_o was calculated using the lift v_{i-1} of the previous increment $(v,F)_{i-1}$ from equations 6 and 8. The final value of lift and force for increment i, $(v,F)_i$, and the final insertion of the updated wedge α_f was calculated from equations 4, 6, 8, and 10. The increment of insertion for the scraper thus became $\Delta a = a_f - a_o$. The final shape of the scraper was generated by continually incrementing the crack, determining the required slope, S, and the incremental insertion of each segment $\Delta\alpha$.

When this approach was used to generate a profile which would remove a 12.7 mm. ice layer from concrete, the results were somewhat surprising. After the interfacial crack grew to a length were the slope required of the scraper exceeded 1.3, the calculated $\Delta\alpha$ became equal to zero. If the procedure was continued $\Delta\alpha$ became negative in subsequent increments. The question of how to proceed was raised. If the slope of the scraper was not increased, the crack would propagate toward the surface. If the slope of the front was increased, the layer would no longer climb the front as the crack grew. As the crack grew, even larger slopes would be required to keep the crack at the interface but the layer would still not climb the front. Thus, in order to keep a growing crack at the interface, the remaining portion of the scraper front needed to be made vertical. The vertical portion of the profile would attempt to force the crack into the substrate. In the case of a roadway, it was assumed that this was impossible. A sketch of this shape is shown in Figure 51. In order to arrive at this profile, the values input were E_{ice} = 9.95 GPa, μ = 0.01, ρ = 9030.0 Kg/m^3, γ = 1.53 x 10^{-4} N/m. While the value of μ is very low, it only effects the force necessary to push the scraper not the scraper's shape. The shape developed for a 6.3 mm. thick layer also lying on concrete is very similar to that shown in Figure 10, with even a shorter curved region.

Effects of Interfacial Bond Strength

Since the cutting edge profiles necessary to promote ice removal by interfacial fracture are unfeasible when the interface is as strong as the ice layer, the effect of lowering the interfacial fracture energy was studied. In order to perform this study, the finite element method was once again utilized and the mesh used for determining the H/V ratios of Figure 49 used. For each crack length, the maximum energy release rate

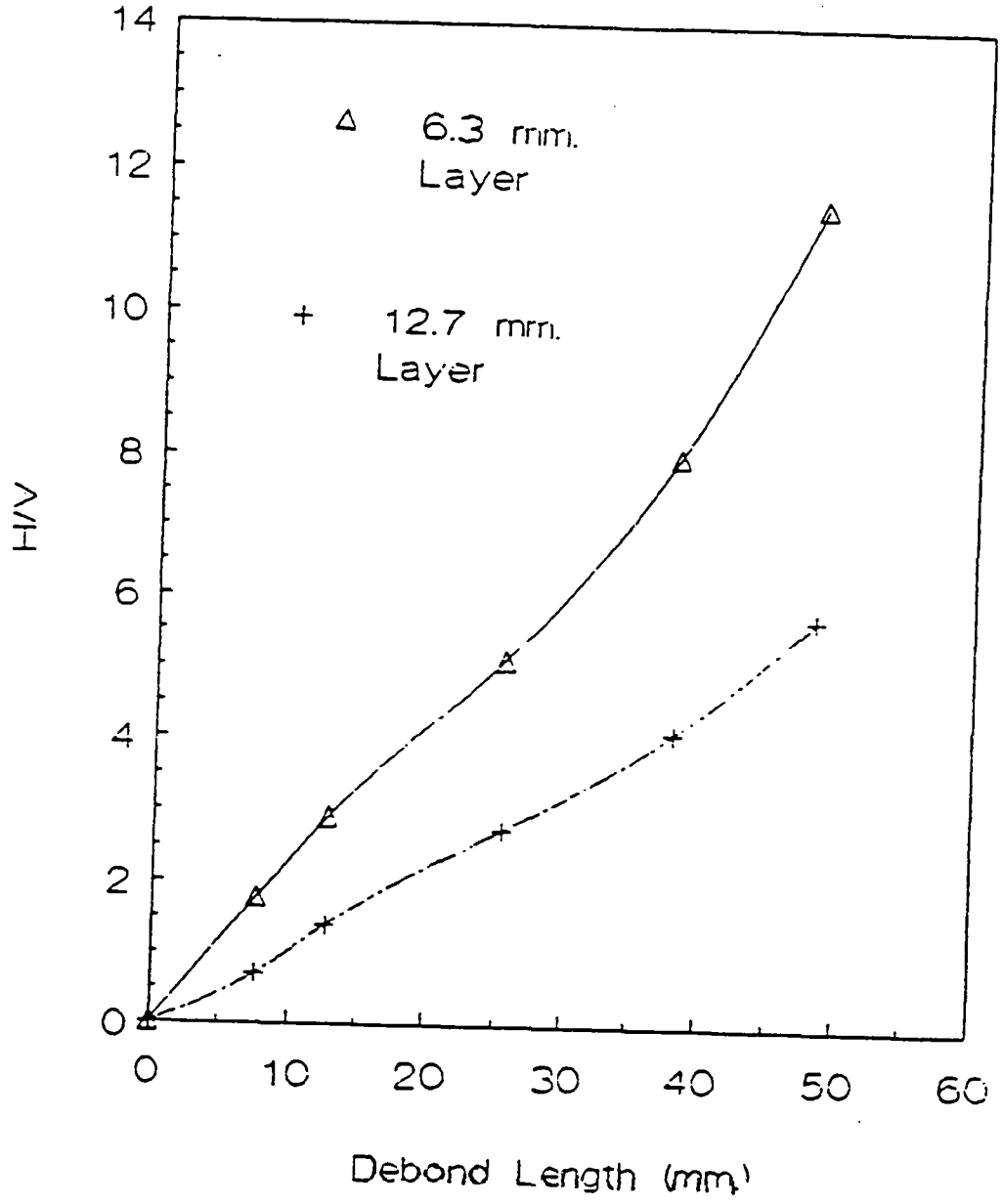

Figure 49
H/V Required
for
6.3 mm. & 12.7 mm. Thick
Ice Layers

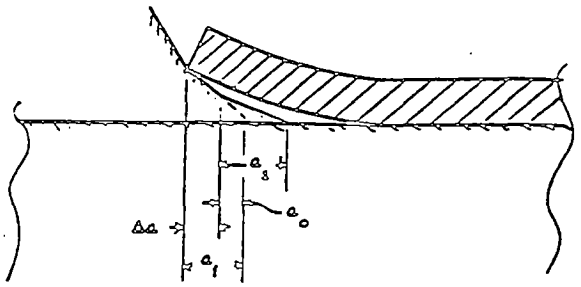

Figure 50
Incremental Insertion

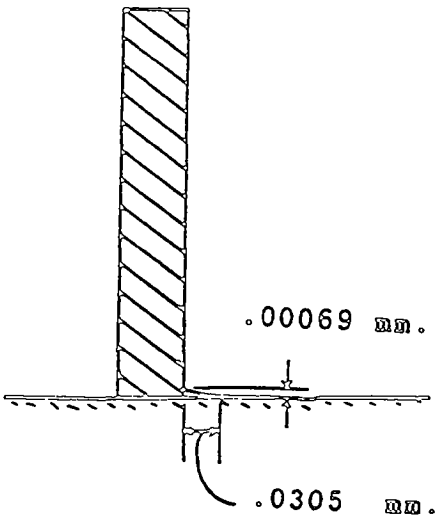

Figure 51
Scraper Profile
for
Interfacial Fracture

was calculated for various H/V ratios. These energy release rates were then compared to the energy release rate for continued interfacial crack propagation at identical crack lengths and H/V ratios. Assuming that a Griffith type energy balance holds at fracture initiation, the percentage drop in the interfacial energy necessary to allow continued interfacial disbonding could be calculated. In order to illuminate this approach, consider the following. Suppose that for a H/V = 3 and ι = 20 mm. the maximum energy release rate occurs at 50° from the interface and is equal to 5 N. Also, suppose that the energy release rate along the interface for identical H/V and ι is 3 N. In this hypothetical case 60% of the required energy in the layer, propagation would occur along the interface. Using this reasoning, and assuming that initially the interfacial energy requirements are equal at the interface and within the layer, Figure 53 can be developed.

Without interfacial energy reduction, the previous analysis indicated that a vertical cutting edge developed. Figure 53 indicates that this vertical face can be avoided or at least postponed if there is a means to reduce the interfacial fracture energy requirement. Suppose that a 45° angle of attack is desired. Figure 53 then shows that a 15% reduction in the interfacial fracture energy would allow interfacial cracks to propagate the 20 mm. in length, a 35% reduction would allow interfacial cracks 33 mm. long to develop, and a reduction of 42% will allow interfacial cracks to reach a length of 46 mm.

In conclusion, this work indicates that the removal of an ice layer from pavement by fracture, along the interface, is unfeasible unless the interface can be weakened. If an auxiliary device could be employed in conjunction with the cutting edge. If such a device could be developed, Figure 12 indicates that a cutting edge can remove an ice layer by chipping of relatively large pieces. In this case, the cutting edge would supply the energy required for ice removal while the auxiliary device focuses its energy just on the interface. Possibly this tandem usage would be the most efficient employment of each device.

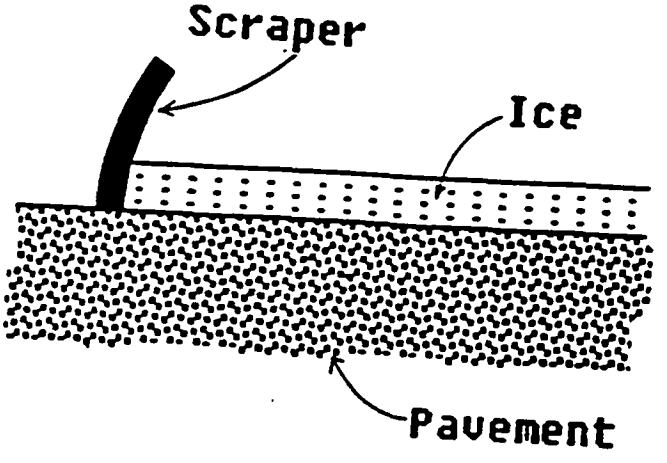

Figure 52. Inverted Grader Blade Attacking an Ice Layer

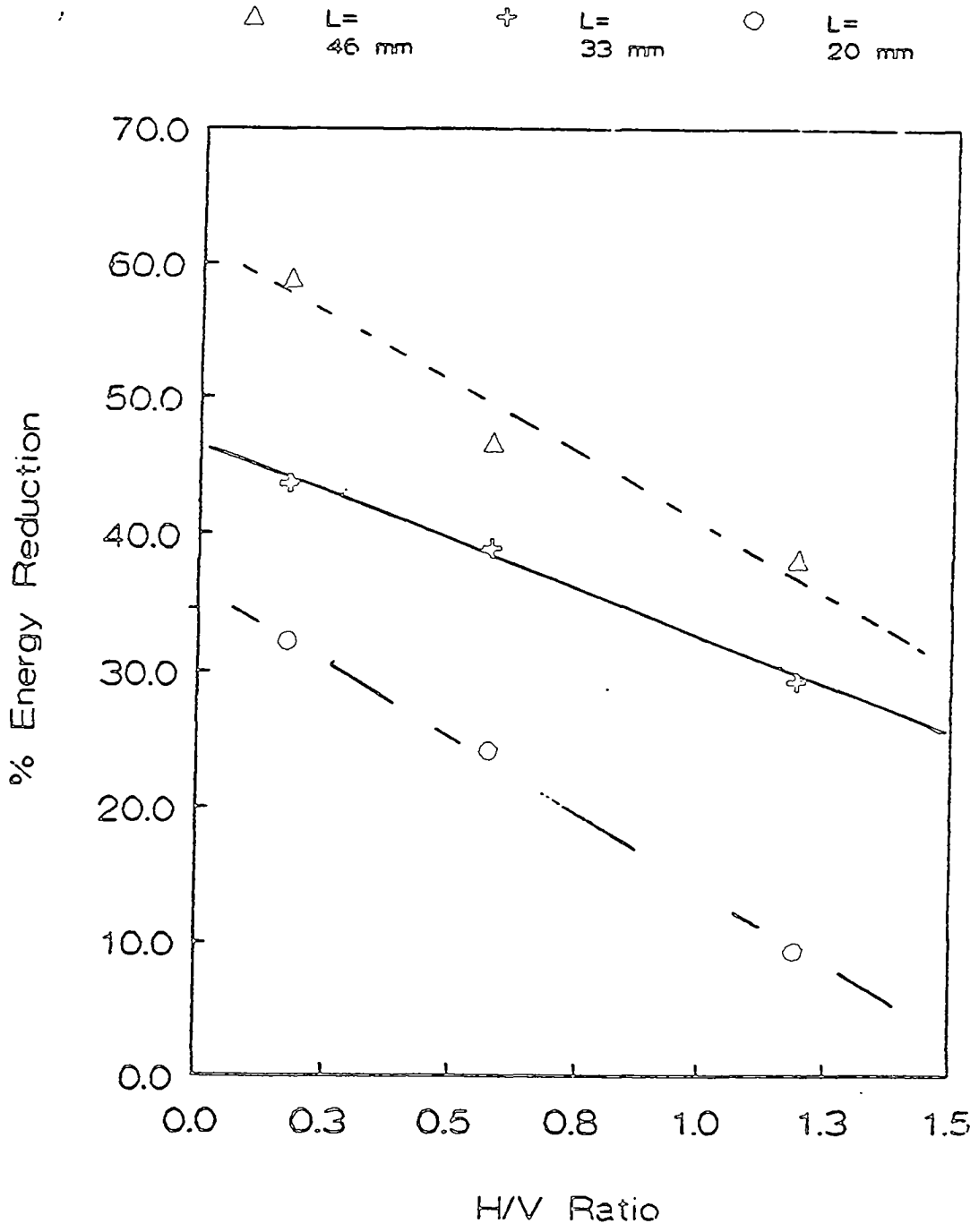

Figure 53
Energy Reduction
Necessary for
Continued Interfacial Fracture

References

1. Hellan, K., "Debond Dynamics of an Elastic Strip, I: Timoshenko-Beam Properties and Steady Motion," Int. J. Vol. 14, No. 1, 1978, pp. 91-100.

2. Hellan, K., "Debond Dynamics of an Elastic Strip, II: Simple Transient Motion," Int. J. Frac., Vol. 14, No. 2, 1978, pp. 173-184.

3. Huang, N.C., "Mechanics of Ice-Lifting from a Flat Road Surface Through Penetration with a Sharp Blade," J. App. Mech., Vol. 48, 1981, pp. 936-942.

4. Huang, N.C., "Dynamic Instability in Ice-Lifting from a Flat Road Surface Through Penetration with a Sharp Blade," J. App. Mech., Vol. 49, 1982, pp. 187-190.

5. Huang, N.C., "Interfacial Crack Propagation Induced by Scraper Action on Ice," Eng. Frac. Mech., Vol. 21, No. 6, 1985, pp. 1083-1095.

6. Huang, N. C., "Crack Propatation Due to Indentation with Constant Speed," Int. J. Frac., Vol. 28, 1985, pp. 143-155.

7. Erdogan, E. and Sih, G. C., "On the Crack Extension in Plates under Plane Loading and Transverse Shear," ASME J. Basic Engng., Vol. 85, 1963, pp. 519-525.

8. Williams, M. L., "On the Stress Distribution at the Base of a Stationary Crack," Trans. ASME, J. Appl. Mech., Vol. 24, 1957, pp. 109-114.

9. Chang, K. J., "Further Studies on the Maximum Stress Criterion on the Angled Crack Problem," Eng. Frac. Mech., Vol. 14, 1981, pp. 125-142.

10. England, A. H., "On Stress Singularities in Linear Elasticity," Int. J. Engng. Sci., Vol. 9, 1971, pp. 571-585.

11. Smelser, R. E., "Evaluation of Stress Intensity Factors for Bimaterial Bodies using Numerical Crack Flank Data," Int. J. Frac., Vol. 15, No. 2, 1979, pp. 135-143.

12. Barr, B.I.G., Evans, W.T., Watkins, J., and Rouhi, M.R., "Fracture Path Prediction using Numerical and Experimental Techniques," Proceedings of the First International Conference on Numerical Methods in Fracture Mechanics, Swansea, UK, 1978, pp. 193-206.

13. Vilmann, C. R., Miskioglu, I., Pawloski, J. S., and Pariseau, D., "Directed Bi-Material Crack Propagation using Photoelasticity," to be published in the Proceedings of the 1990 Society for Experimental Mechanics Spring Conference, Albuquerque, NM, June 4-6, 1990.

14. Erdogan, F. and Gupta, G., "The Stress Analysis of Multilayered Composites with a Flaw," Int. J. Solids Struc., Vol. 7, 1971, pp. 39-61.

15. Barsoum, R. S., "On the Use of Isoparametric Finite Elements in Linear Fracture Mechanics," Int. J. Num. Meth. Engng., Vol. 10, No. 1, 1976, pp. 25-37.

16. Griffith, A. A., Phil. Trans. R. Soc., Vol. A221, 1920, pp. 163.

Cutting Edge Experimental Program

The aim of task 3 b has been to provide two cutting edges which can be attached to the snow plow blade being developed by the University of Wyoming under project H-206. These two cutting edges will be selected on the basis of laboratory testing, which will show that they are better at removing ice and compacted snow than the equipment which is currently used for those tasks. Once delivered to the University of Wyoming, the cutting edges will be used for a winter field test, and their behavior will be evaluated from those tests. In addition to producing the two cutting edges, task 3b has also been charged with developing other physical means of improving current ice removal technique. At this stage of the project, final work on task 3b has not been completed. Accordingly, the present plan is that task 3b will be continued after the rest of H-204 is terminated, so that the two cutting edges can be provided to the University of Wyoming. Additional testing to develop other physical techniques for ice removal will also be developed.

Currently, the established practice for removing ice from roads is to turn the cutting edge so that it makes an angle of 90 degrees with the road surface. For the given geometry of plow blade cutting edges, this makes sense, since they are designed with a flat bottom (the part in contact with the road) and to tilt back the plow blade would simply cause the cutting edge to rise up onto the ice (see Figure 54.) However, the mechanics of the "square on" approach mean that the ice is crushed away from the pavement, which is a very energy intensive process, requiring as it does the creation of many small cracks within the ice. A better solution would be to introduce cracks which run through the ice for long distances, so that larger pieces of ice can be "flaked off" without crushing. It is not practically feasible to propagate a crack along the ice road interface, first because this interface is so strong (apparently stronger than the ice) and secondly because this interface is so irregular, especially in field situations. What is then required is a blade which can flake off significant parts of the ice, and crush as much of the remnant ice as is possible. Experiments have concentrated on developing such a blade.

Experimental Technique

The experimental rig is shown schematically in Figure 55 and in a photograph in Figure 56. Cylindrical pavement samples were used, of both asphaltic and portland cement concrete type. The asphaltic pavement samples were obtained by taking small (4" diameter) cores from larger pavement cores supplied to the Iowa Institute of Hydraulic Research (IIHR) by SHRP. Some samples were also supplied by Michigan Technological University. Concrete samples were cast to size at IIHR. All experiments were conducted in the IIHR cold rooms. Details of the individual samples are given in Nixon and DeJong, 1990.

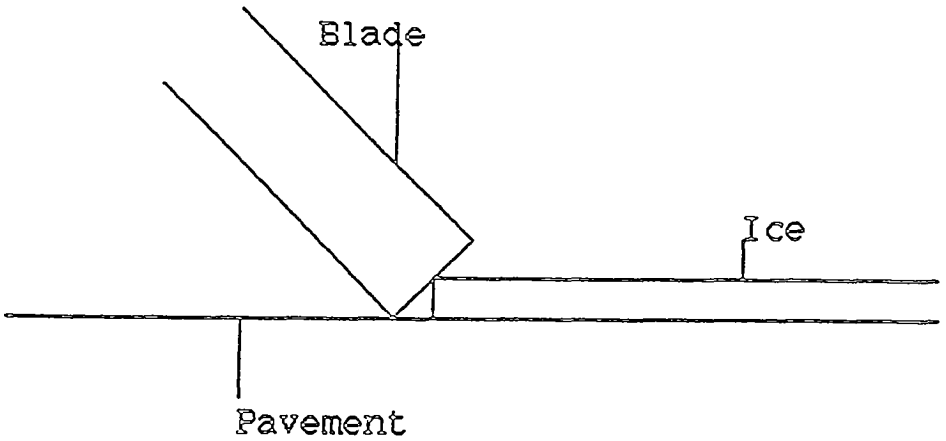

Flat bottomed cutting edge at a lay-back angle

Figure 54.

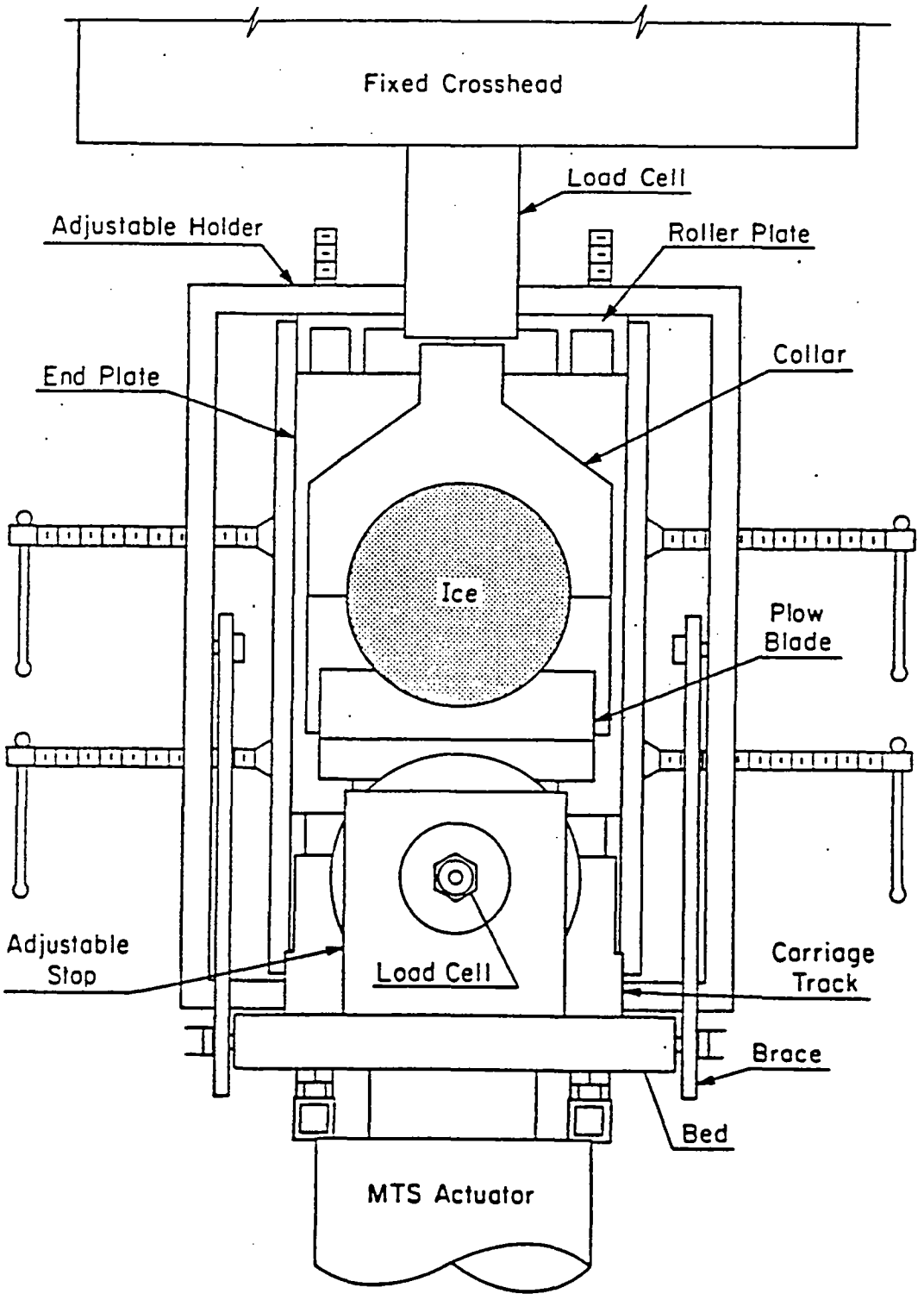
Fixed Crosshead
Load Cell
Adjustable Holder
Roller Plate
End Plate
Collar
Ice
Plow
Blade
Adjustable
Stop
Load Cell
Carriage
Track
Brace
Bed
MTS Actuator

Figure 55.

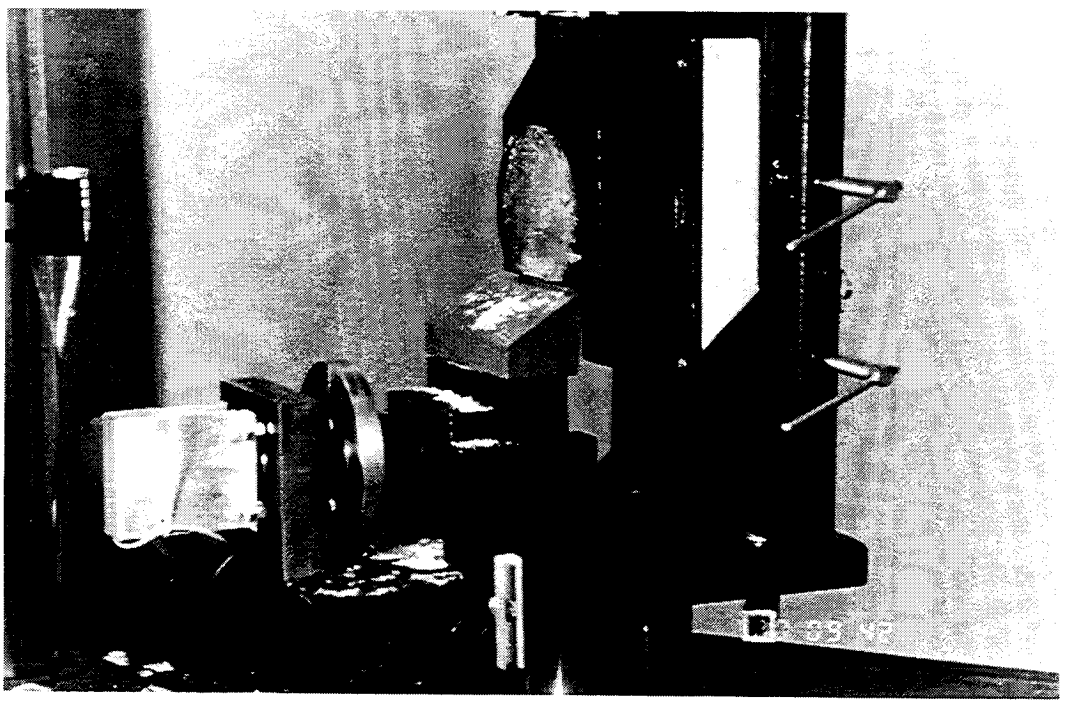

Figure 56. Hydraulic testing machine with experimental cutting edge scraping ice specimen.

One quarter inch thick layers of ice were frozen onto the pavement samples in a standard method, used for all tests and illustrated schematically in Figure 57. The samples were placed in a tube, which was sealed so as to avoid leakage, and water at 0°C was poured onto the pavement. The samples were pre-chilled to -5°C, which was the temperature of the room in which the samples were frozen. After the water was poured, the samples were left for twenty four hours while the water froze and became isothermal. The samples were then prepared for testing by removing them from the molds, and cutting a small amount of ice away from the sample surface so that the blade on the test rig was in contact with the ice along the whole of its length. The cutting edge was then given a down force against the pavement surface by means of a spring, which was instrumented with a load cell, so that variation of the downforce could be recorded. The test rig was mounted in an MTS materials testing machine, with a testframe capacity of 110,000 lbs, using a 5,000 lb load cell. The test machine has an electronically controlled servo hydraulic actuator, which was programmed by the electronic control center to provide a constant sliding rate for the cutting edge over the pavement surface.

As the blade moved forward over the testpiece, a greater length of blade would come into contact with the ice, until the center of the test piece was reached, after which a shorter length would be contacting. Data from tests was always presented with load per unit blade width in contact with the ice as a variable (units of lbs/in) as opposed to simply load. Figure 58 shows a typical load/unit width vs. distance travelled trace from a test. A number of points common to all test results can be made. There is an initial high spike, which is caused by the high load needed to propagate the first crack within the ice. However, once this first crack has formed, the load per unit width drops to a nearly constant level, suggesting a steady state type of behavior that is in general representative of the ice removal process. Towards the end of the test the load drops off to zero as the end of the sample surface is reached. This reduction in load is due to edge effects. Thus, the load most representative of the ice removal process is that obtained during the middle portion of the test (i.e. when the load per unit width is approximately constant). However, the initial peak load is also of importance, because when encountering ice that is previously unloaded, a plow blade would experience a similar sort of peak.

Results

Once the test method had been developed and reliable and repeatable results obtained, a number of test series were performed, to determine the behavior of the cutting edge under a variety of conditions. The following variables were considered: Rake angle of the blade (see Figure 59); Rate of scraping; Download on the pavement surface; and Amplitude of the pre-load. Figures 60 through 63 show the general trends observed. A minimum of four tests were performed for each condition. The data from the tests is presented in an appendix to this report.

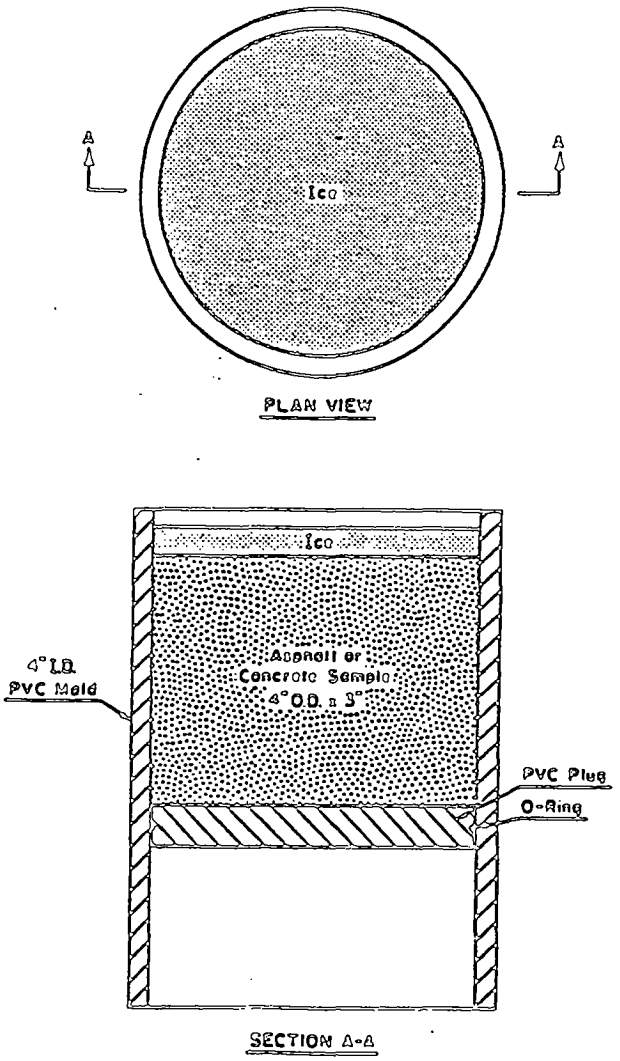
A
A
Ice
PLAN VIEW
Ice
4"LD
PVC Mold
Asphalt or
Concrete Sample
4"OD x 3"
PVC Plug
O-Ring
SECTION A-A

Figure 57.

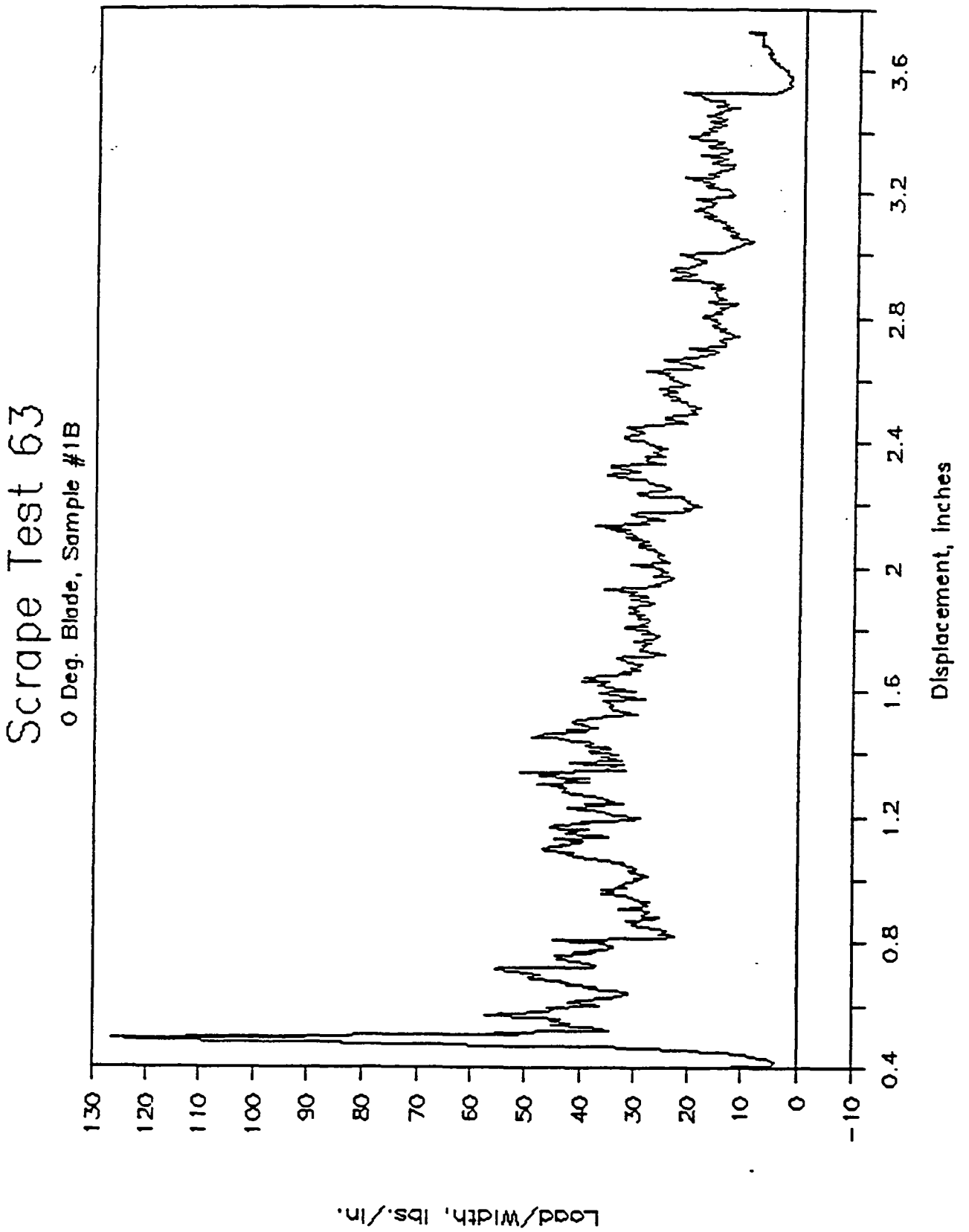
Scrape Test 63
0 Deg. Blade, Sample #1B
Load/Width, lbs./in.
130
120
110
100
90
80
70
60
50
40
30
20
10
0
-10
0.4
0.8
1.2
1.6
2
2.4
2.8
3.2
3.6
Displacement, inches

Figure 58.

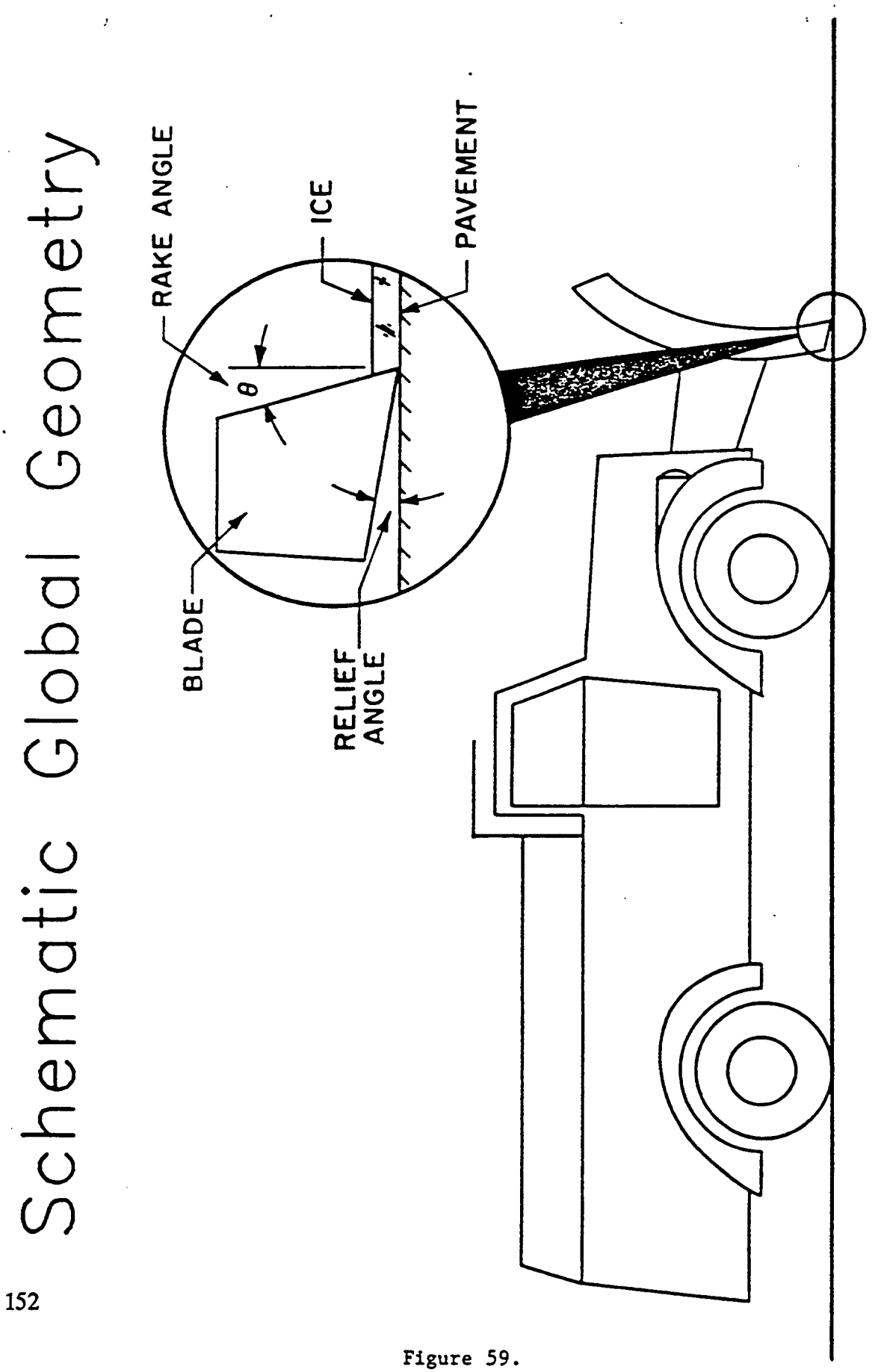
Schematic Global Geometry
RAKE ANGLE
ICE
PAVEMENT
θ
BLADE
RELIEF ANGLE

Figure 59.

VARIATION OF PEAK FORCE PER UNIT WIDTH WITH RAKE ANGLE

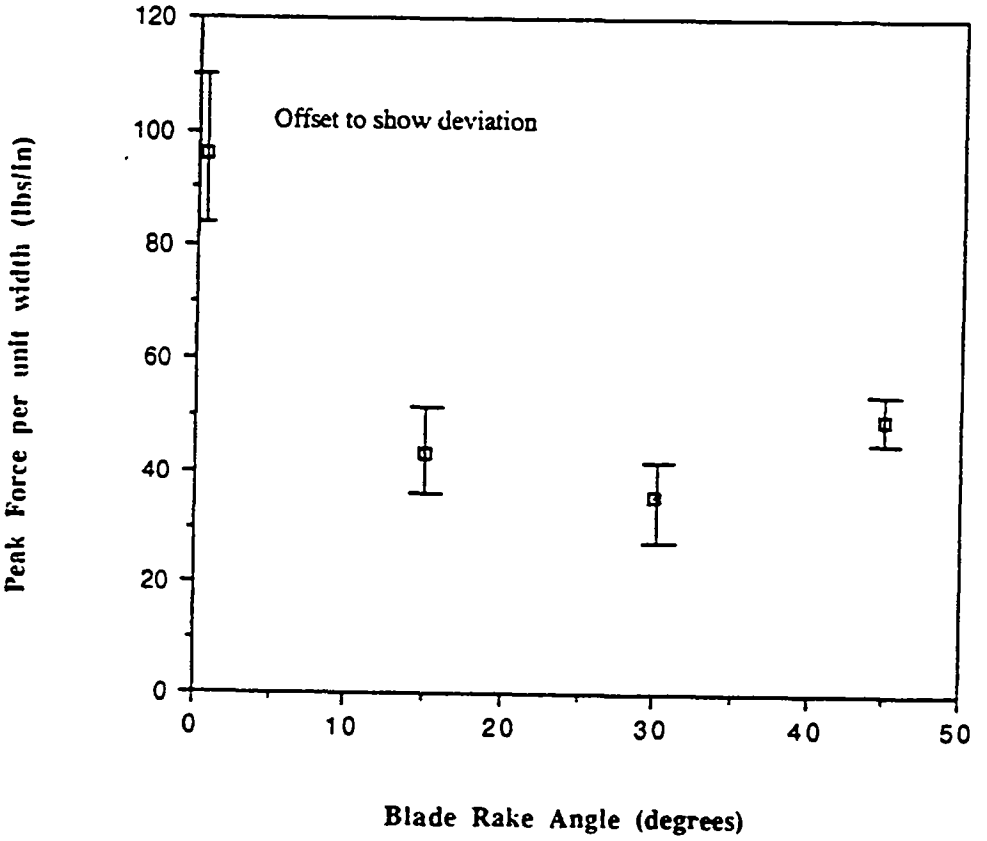

Figure 60.

EFFECT OF SCRAPING RATE

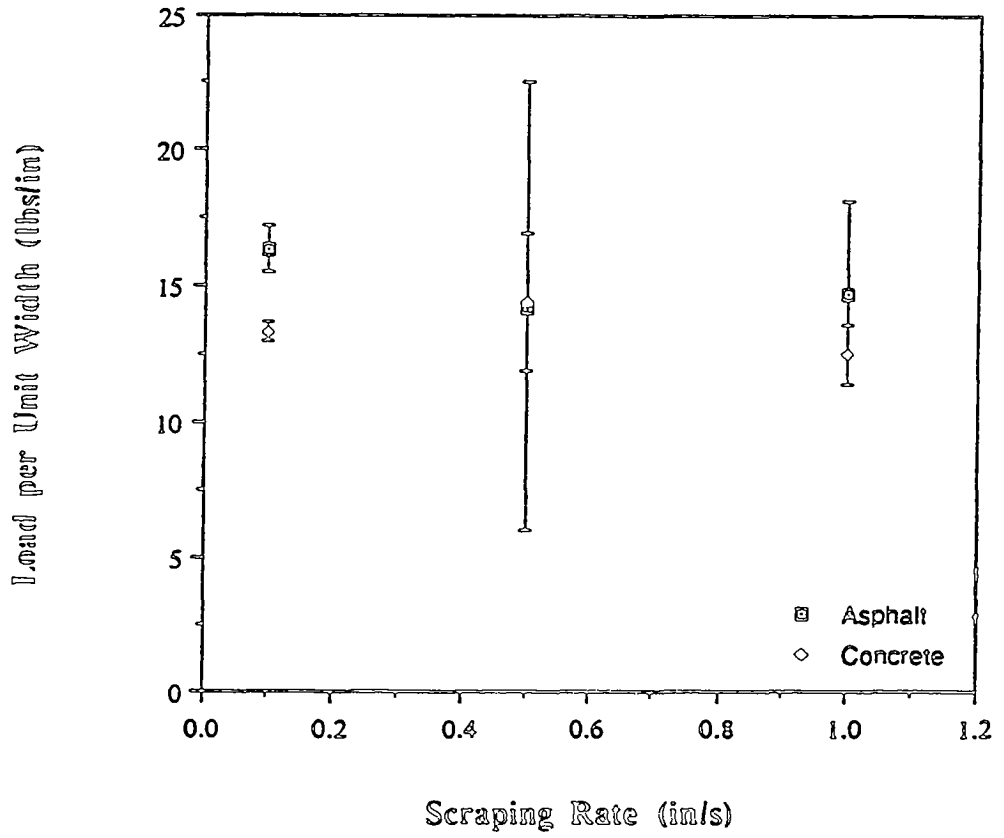

Figure 61.

EFFECT OF VERTICAL DOWN-LOAD

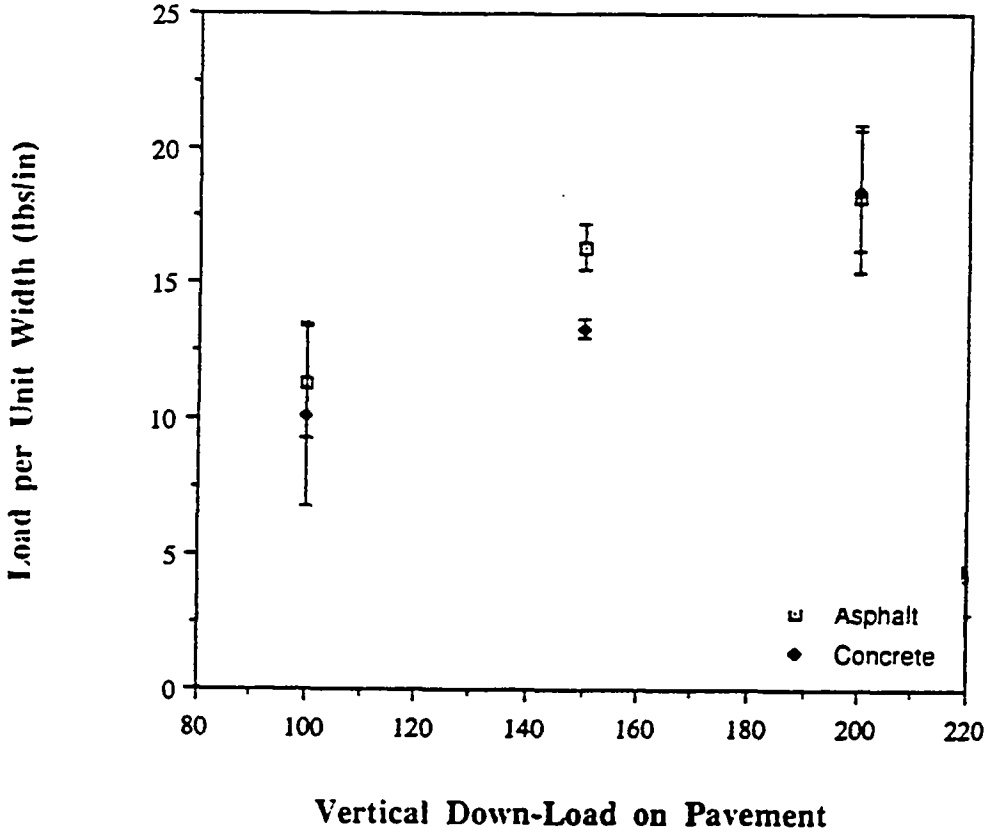

Figure 62.

EFFECT OF COMPRESSIVE PRE-LOAD

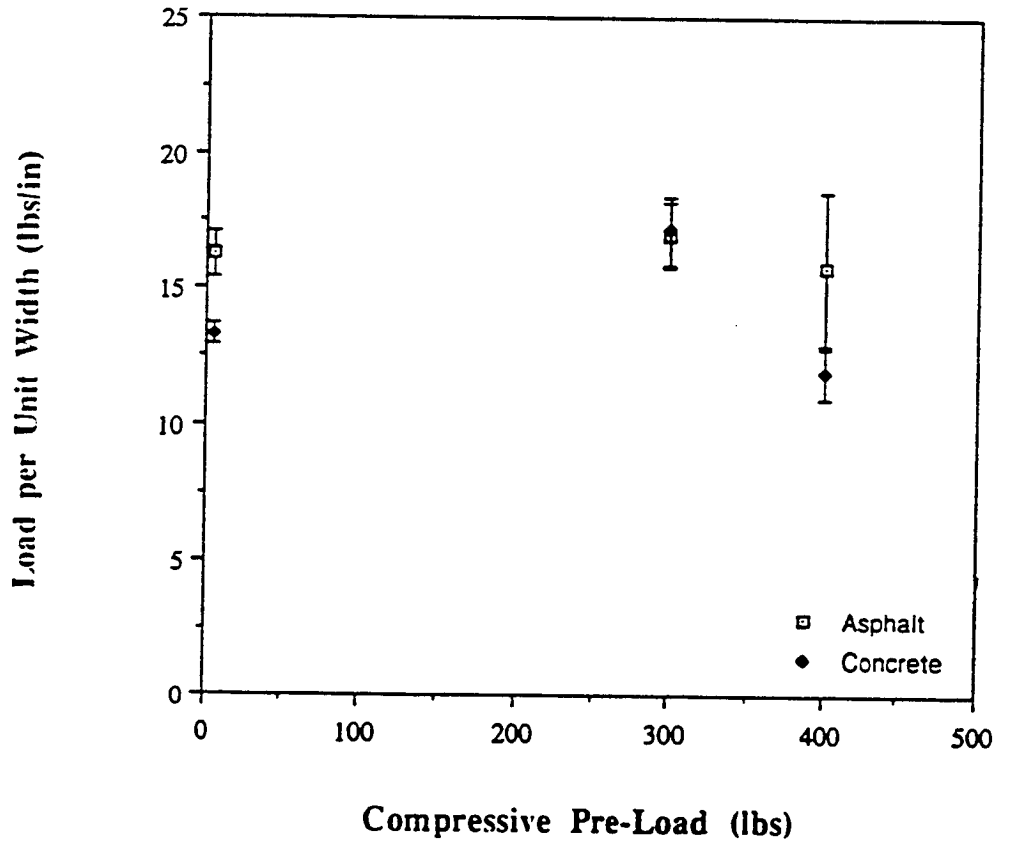

Figure 63.

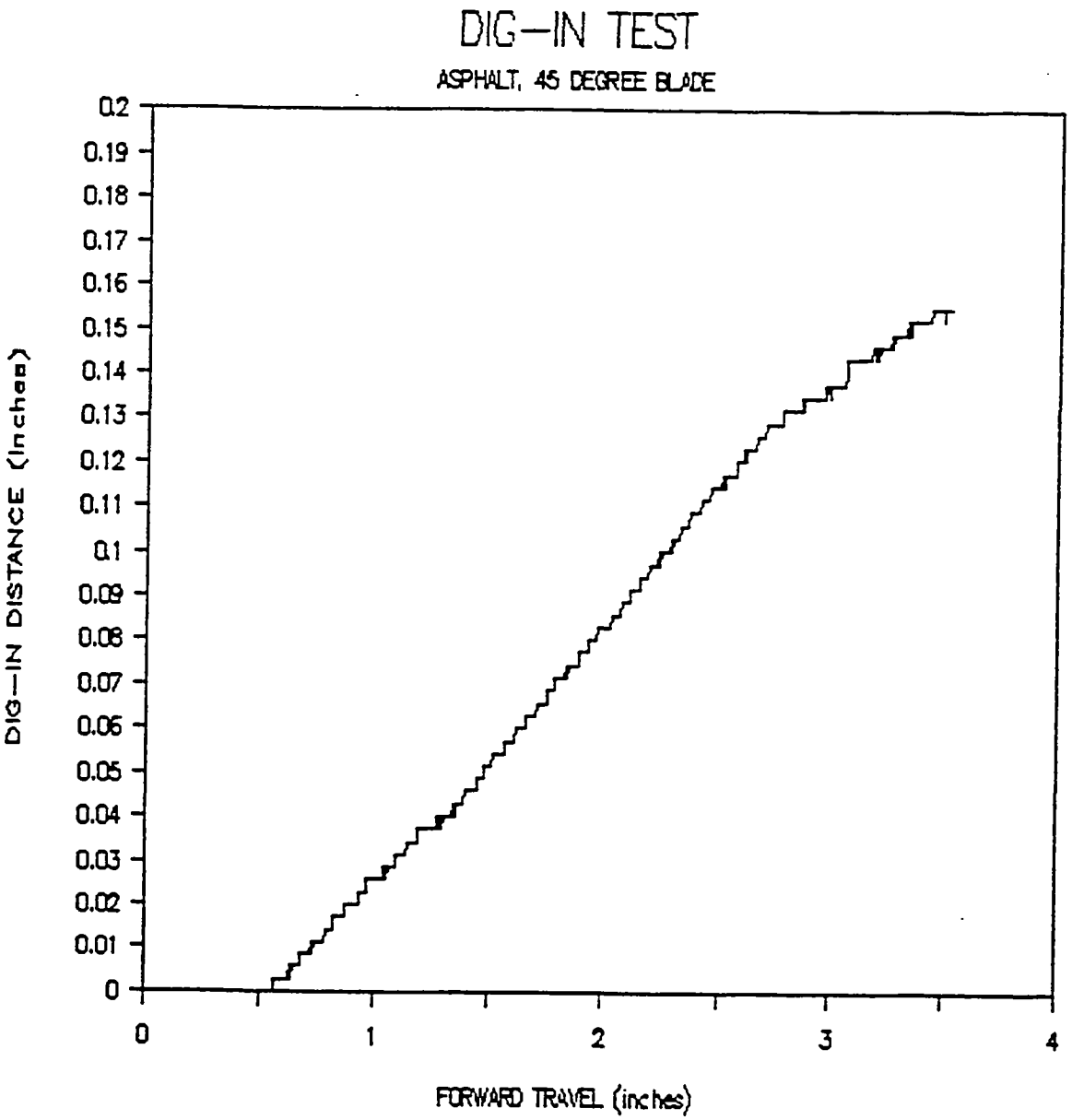
DIG—IN TEST
ASPHALT, 45 DEGREE BLADE
DIG—IN DISTANCE (inches)
0.2
0.19
0.18
0.17
0.16
0.15
0.14
0.13
0.12
0.11
0.1
0.09
0.08
0.07
0.06
0.05
0.04
0.03
0.02
0.01
0
0
1
2
3
4
FORWARD TRAVEL (inches)

Figure 64.

A series of tests was also performed to determine the "dig-in" characteristics of the blade. The rationale behind these tests was that a blade would often begin or at some stage during the scrape process be found, resting on top of the ice cover. If the blade cannot dig into the ice to start scraping it away, then it has little or no value as an ice removal tool. Figure 64 shows the vertical load on a blade as it progressed forward over the ice.

Discussion

The results clearly show that there is an optimum blade angle at which scraping should be performed to minimize the forces on the blade. This optimum angle is somewhere between 15 and 40 degrees of rake angle, as can clearly be seen from Figure 60. It remains to be seen whether such a blade is an appropriate choice for field operations,, and whether or not it can survive typical pavement features, such as joints, and manhole covers.

The effect of scraping rate on the loads necessary to remove ice from the pavement is shown in Figure 61. As can be seen, the loads appear to decrease as the scraping rate increases. This is not inconsistent with current understanding of the mechanical behavior of ice. Nixon and Schulson (1987) showed that the fracture toughness of ice decreases with increasing loading rate until some plateau value is attained and work by Cannon (1985) and Lee (1985) indicate that both compressive and tensile strength of ice respectively exhibit similar behavior. Accordingly, given the brittle nature of the ice removal process as observed in the tests to date, it is felt that data obtained at 0.1"/s loading rates will be in all likelihood somewhat higher than loads experienced under similar conditions at field removal speeds. Unfortunately, limitations of testing apparatus, and lack of time and funding to create a more field type environment prevent this hypothesis from being completely tested at this time. This question is of considerable importance because results conducted at higher loading rates under project H-203 indicated that the energy required to remove ice increased as loading rate increased. In the continuation of the cutting edge work this question will be examined in more detail.

The effect of download on the scraping load is very interesting. As can be seen in Figure 62, as the download increased, the scraping load also increased. This is perhaps not surprising in hindsight, since a greater download will result in a greater friction force on the pavement surface opposing scraping. Whilst there had been the possibility that a greater down force might cause more easy fracturing of the ice, it is apparent that this is not the case. In practical terms, this suggest that operators should use the minimum down pressure on the blade consistent with maintaining good contact with the road, and also maintaining good vehicle safety.

In order to try and fracture the ice prior to scraping, tests were performed in which the ice was pre-loaded prior to scraping. The purpose of this was to introduce

cracks into the ice layer, which would thus reduce the force needed to scrape away the ice. However, although loads were applied (by means of a heavily knurled indenter) to the ice and cracks introduced into the ice layer, no statistically significant reduction in scraping load was observed. In the next phase of the project, loads will be introduced by means of a flail, with nylon braids. Nylon has been selected because of results obtained from H-203 which indicated a material of the stiffness of nylon would be optimum for removing ice from pavement surfaces. Further, a nylon flail is less likely to cause pavement damage than, for example, a steel flail.

It is of vital importance to determine whether or not a blade can dig into an ice layer when it has been riding along the top of such a layer. In the field, it would be impossible to cut a starter notch, as has often been used in testing. Two points are of particular concern here. First, what download (i.e. load perpendicular to the pavement) is needed to achieve ice cutting, and second, would such a download cause the blade to dig into the pavement. Tests have shown conclusively that at reasonable levels of downloading (300 lbs or less on the blade) significant dig in can be achieved. It is important to note in this regard how downloading is achieved in the test apparatus. The blade is preloaded onto the ice by means of a spring. Thus, as the blade digs into the ice, the download decreases. Figure 64 shows the download during one such test. As can be seen, the download decreases in a very linear manner by about 50 lbs during the test. This corresponds to a dig-in depth of 1/8". The angle at which the blade dug into the ice was $\approx 4°$. This is very close to the blade clearance angle which is nominally 5°. It can be stated that for the current blade geometry, even if the blade begins on the ice surface, it will dig into the ice and be effective in ice removal. This is a crucial point for field operations.

Conclusions

A series of test have been conducted at low rates of scraping which indicate the following trends:

1. There is an optimum cutting edge rake angle for ice removal, somewhere between 15 and 30 degrees.

2. At the rates tested herein there was no obvious rate effect.

3. As the download on the ice was increased, the scraping load also increased.

4. Pre-loading the ice layer to introduce cracks into the ice produced no statistically significant reduction in ice scraping load.

5. The blade geometry used in these tests has demonstrated an ability to "dig-in" to the ice layer, when it starts a test on top of the ice layer.

References

1. Cannon, N. P., M.S. Thesis, Thayer School of Engineering, Dartmouth College, Hanover, NH, 1985.

2. Lee, R. W., M. S. Thesis, Thayer School of Engineering, Dartmouth College, Hanover, NH, 1985.

3. Nixon, W. A. and DeJong, D. T., "Scrape Rig Development and Pavement Sample Classification,", IIHR internal report, 1990.

4. Nixon, W. A. and Schulson, E. M., "A Micromechanical View of the Fracture Toughness of Ice," J. de Physique, Colloque C1, Tome No. 48, 313-319, 1987.

APPENDIX 1

APPLICATION OF MICROWAVE ENERGY FOR DISBONDING ICE FROM PAVEMENT

by

R.N. Lothes

Background

There are serious objections to chemical (i.e., salting) methods of clearing ice from pavements. Straightforward melting by application of heat is economically infeasible. The energy cost of melting 1/4 inch of ice from a highway is 4.4 million BTU per lane mile, even if 100% efficiency could be achieved [1]. If a method could be found for disbonding the ice from the pavement, the ice might be plowed away at an acceptable cost.

Microwave heating has been proposed as a method of disbonding ice. Perhaps only a few microns of ice at the pavement surface need be melted to loosen the bond. If, for instance, only 5 microns melt depth suffices to disbond the ice, the energy cost drops to 0.08 percent of the figure quoted for total melting of a 1/4 inch layer.

Microwave Disbonding

If microwave methods are to succeed, the disbonding operation must be quickly followed by mechanical removal of the ice before refreezing can occur. An operational system would consist of an applicator wide enough to cover a lane, with a plow blade immediately behind the applicator. Before any judgement can be made as to the feasibility of the microwave disbonding approach, the following three aspects of the problem must be understood.

1. Microwave propagation; the injection of microwave energy into the ice/pavement/earth strata under the applicator.

2. Transient heat flow; the conductive flow of injected heat energy, producing a time varying temperature distribution in the strata, and possible melting at the ice/pavement interface.

3. Microwave properties of materials; the properties of the various strata determine the quantities and locations of heat injected. In order to place a significant fraction of the heat at the ice/pavement boundary to cause melting, the top layer of pavement will have to be modified by addition of a material that is, an effective absorber of microwave energy. The thermal properties of this modified layer will then impact the transient heat flow problem. The problem to be solved is the following: given the vertical distribution of deposited heat, how rapidly is this heat conducted up to the ice/pavement boundary to contribute to melting? Part of the heat, of course,

---

[1] Lane width assumed to be 8 ft. The 4.4 million BTU is only for melting. Additional energy is required to bring the ice up to the melting point if it is initially below 0°C (4.4 million BTU is equivalent to about 37 gallons of fuel oil).

is conducted downward. From the standpoint of microwave absorption, the thicker the layer, the greater will be the amount of energy absorbed. From the heat conduction standpoint, the thinner the layer, the quicker the heat reaches the surface to cause melting.

The Microwave Propagation Problem

Figure 1 illustrates the five strata (air, ice, absorber, pavement and earth) in which microwave propagation occurs. Microwave energy is launched vertically downward. It can be assumed that this is a plane wave propagation process with the wavefront parallel to the boundary planes between the strata; that is, propagation occurs at normal incidence. At each interface, part of the incident energy is transmitted and part is reflected. This, of course, results in multiple reflections of downward and upward propagating waves within a given stratum. The duration of the applied microwave "pulse" is of the order of a second (the time required for the moving applicator to pass over a given point)[2]. The transit time of a given wave component through a stratum is of the order of nanoseconds or fractions of a nanosecond. This amounts to a continuous wave (CW) situation, in that the various components of transmitted and reflected waves overlap in time.

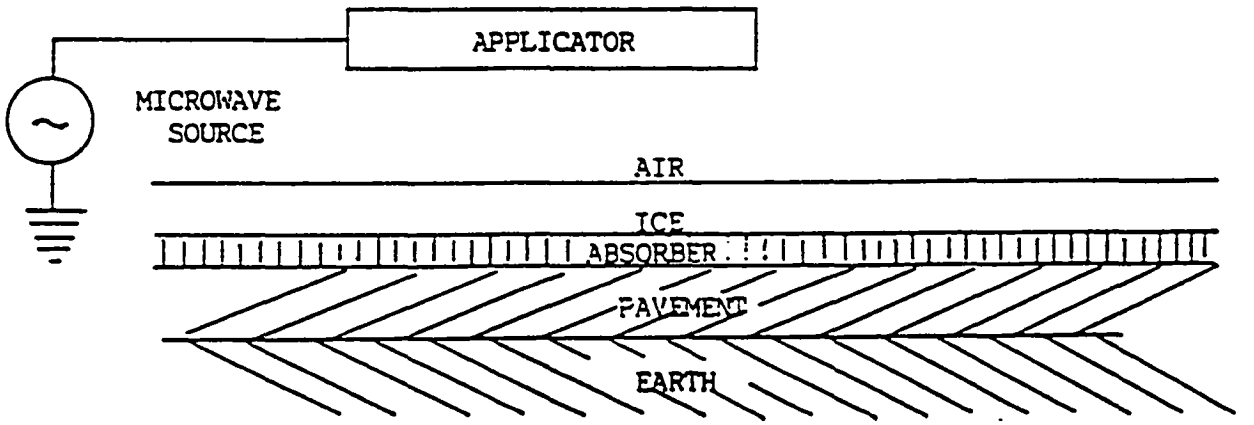

Figure 1. Application of Microwave Energy

Thus, the multiple reflections produce standing wave patterns within the various strata.

[2] At a rate of travel of 20 ft/s, an applicator that is 2 ft long will pass over a given point in a tenth of a second.

This plane wave propagation situation has an analog in electrical transmission line theory. That is, the wave equation in terms of electric field (E) and magnetic field (H) are identical in form to transmission line equations in terms of line voltage (V) and current (I). This analogy reduces the wave propagation problem to a transmission line problem that is more familiar to engineers. Figure 2 is the transmission line analog of the wave propagation problem of Figure 1. The line consists of five segments of lengths, l_a, l_i, l_m, l_p and an infinitely long segment. These correspond respectively to the thicknesses of the air path, the ice path, the absorber path, the pavement path, and an effectively infinite earth path. The corresponding characteristic impedances are Z_a, Z_i, Z_m, Z_p, Z_n, and Z_e. We are mainly concerned with what happens to this absorbing layer whose analog is shown in Figure 3[3]. In Figure 3(a) the absorbing layer is represented as a transmission line segment of length l_m and characteristic impedance Z_m. In Figure 3(b) the transmission line segments are replaced by their electrical equivalents as four-terminal networks. We are especially concerned with, P_m, the power dissipated in the absorbing layer. This is the difference between the power, P_1, flowing in, and P_2, the power flowing out. The values of P_1 and P_2 can be expressed in terms of the phasor voltages and currents as,

$$P_1 = \mathrm{Re}\,[V_1 I_1^*]$$

$$P_2 = \mathrm{Re}\,[V_2 I_2^*]$$

where I*1 and I*2 are, respectively, the complex conjugates of I_1 and I_2. Therefore, P_m, the power dissipated in the microwave absorbing layer is

$$P_M = P_1 - P_2 = \mathrm{Re}\,[V_1 I^*1 - V_2 I^*2]$$

The values of V_1, I_1, V_2 and I_2 can be determined provided that the sending end parameters (the microwave applicator equivalent circuit), the far end parameter (infinite earth characteristic impedance) and the four-terminal parameters of each of the strata equivalent circuits are known.

We can approximate the microwave source as a voltage source in series with an impedance equal to the wave impedance, Z_{FS} of free space,

[3] Of course, when melting begins we have an additional very thin layer to account for. Also if the pavement contains a grid of steel reinforcing rods this too will modify the model. We shall omit these effects for the present.

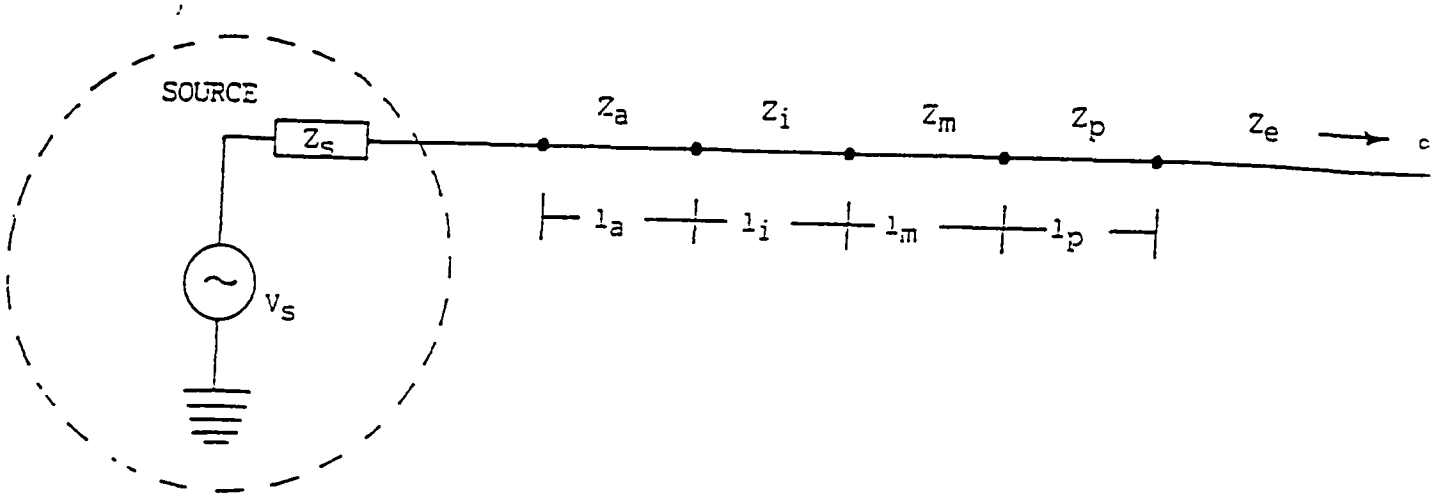

Figure 2. Transmission Line Analog

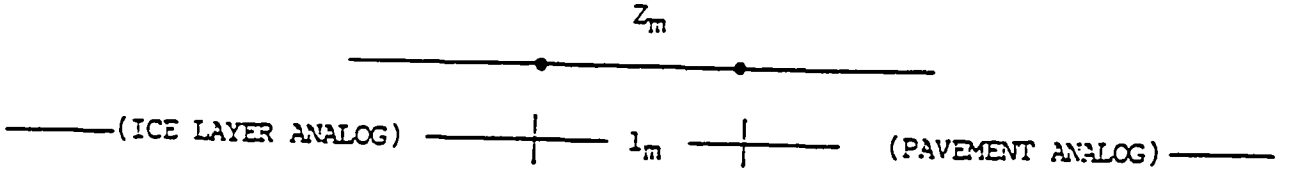

(a) Transmission Line Analog

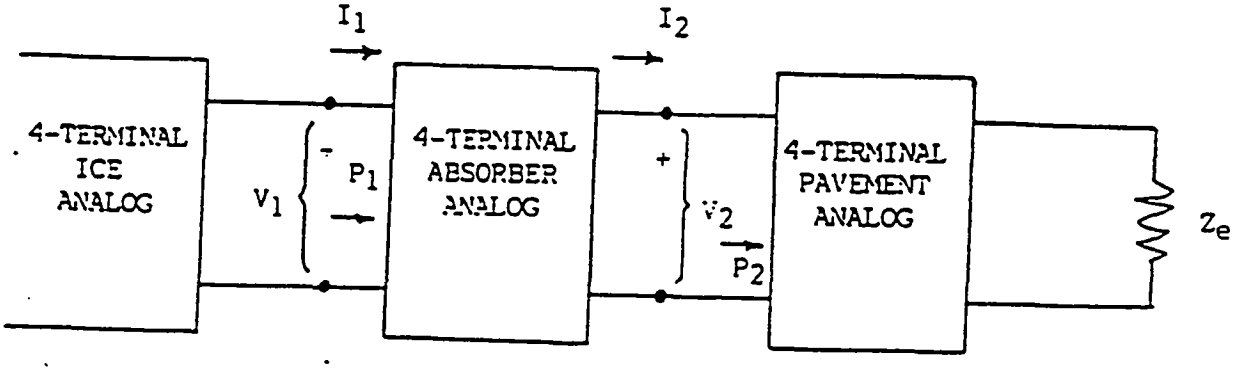

(b) Four-Terminal Network Analog

Figure 3. Accounting for the Absorbing Layer

$$Z_{FS}=\sqrt{\frac{\mu_o}{\epsilon_o}}=120\pi=377\,ohms$$

where ϵ_o and μ_o are the permittivity and permeability of free space. The magnitude of the voltage source will be determined by the powercapability of the applicator. If the available power (power into a matched load) is P_A, then the source voltage is

$$V_S=2\sqrt{P_A Z_{FS}}$$

The terminating impedance, Z_e, representing the earth should be obtainable from measured values of earth conductivity and complex dielectric constant. The same would be true of the pavement and ice strata. The parameters for representing the absorbing layer are discussed in connection with the materials problem.

The foregoing discussion has led to the representation of microwave propagation through the stratified media in terms of a cascade connection of four-terminal networks, one for each stratum, as indicated in Figure 4.

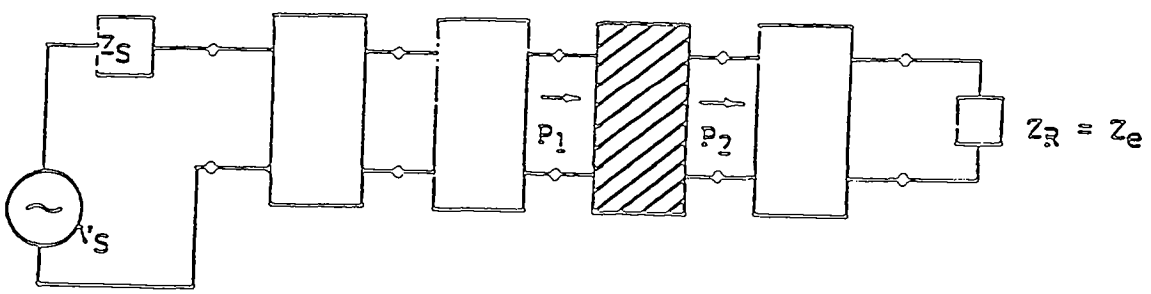

Figure 4. Cascaded Network Representation[4]

This configuration can be solved for the current and voltage at any terminal pair in

[4] The shaded network block represents the microwave absorber layer whose power dissipation is of interest.

terms of V_S, Z_S, ZR and the A, B, C, D parameters of each of the networks [1]. These parameters are related to propagation constant, γ, and characteristic impedance, Z_o, of the network through the following equations

$$A = D = \cosh(\gamma)$$

$$B = Z_o \sinh(\gamma)$$

$$C = \sinh(\gamma)/Z_o$$

The equality of A and D is due to the symmetry of the network (or transmission line segment) when viewed from either end. The propagation constant, γ, characterizes the propagation of voltages (or currents) through the network. It is complex, and is normally written as

$$\gamma = \alpha + j\beta$$

where α is the attenuation constant and β is the phase constant [1]. Recall that the four terminal network under discussion is the analog of one stratum in Figure 1. Therefore the γ for the network is the propagation constant for plane wave propagation in the stratum. The impedance, Z_o, has the usual meaning that the input impedance of the network terminated in Z_o is equal to Z_o. In terms of the wave propagation case, Z_o is the wave impedance of the medium. Von Hippel [2] gives the relationship between γ and Z_o and the electromagnetic parameters ϵ^* and μ^* of the propagation medium[5].

$$\gamma = j\omega\sqrt{\epsilon^*\mu^*}$$

$$Z_o = \sqrt{\frac{\mu^*}{\epsilon^*}}$$

The complex dielectric constant ϵ^* is expressed as

$$\epsilon^* = \epsilon' - j\epsilon''$$

---

[5] This expression for yields attenuation and phase shift per unit length of propagation path. The value for computing A, B, C, and D is equal to the per-unit , multiplied by the stratum thickness.

where ϵ' accounts for displacement current (in quadrature with applied field) and ϵ' accounts for dielectric loss, exhibited as a current component in phase with the applied field. The dielectric loss tangent is

$$\tan\delta_{\epsilon}=\frac{\epsilon''}{\epsilon'}$$

These relations can also be expressed in terms of a complex relative permittivity, K°,

$$K^{\circ}=\frac{\epsilon^{\circ}}{\epsilon_o}=K'-jK''$$

where ϵ_o is the permittivity of free space:

$$\epsilon_o=\frac{10^{-9}}{36\pi}\ farads/meter$$

The real part of ϵ° is related to the polarization of molecules, induced by the applied electric field. The imaginary part accounts for dielectric hysteresis loss as the polarized molecules rotate in the presence of an applied alternating electric field. The complex permeability, μ°, is similarly expressed as

$$\mu^{\circ}=\mu'-j\mu''$$

The real part, μ', accounts for magnetic polarization of the medium and μ' accounts for magnetic hysteresis loss. A magnetic loss tangent is defined by

$$\tan\delta_m=\frac{\mu''}{\mu'}$$

and a complex relative permeability can be defined as

$$K^{\circ}=\frac{\mu^{\circ}}{\mu_o}=K_m'-jK_m''$$

where μ_o is the permeability of free space:

$$\mu_o = 4\pi x\ 10^{-7}\ henry/meter$$

Thus, to determine the parameters of a given four terminal network of Figure 4 one needs to know the thickness of the stratum that is represented by the network, and the electromagnetic parameters of the material. These parameters are ϵ', ϵ'', μ', μ'' or alternately ϵ', μ', tan δ_e, tan δ_m.

Transient Heat Flow Problem

The microwave applicator injects a "pulse" of heat into the stratified medium. The pulse duration, probably of the order of a fraction of a second, corresponds to the passage of the moving applicator over a given point. During the pulse, the temperature of each point in the stratum rises in accordance with the amount of energy injected locally, and the energy flow from or to neighboring points. This can be described as a one-dimensional heat conduction problem, for the heat flow takes place in only the vertical dimension. Even though only one dimension is involved, it is a fairly complicated problem, for it involves a nonuniform vertical distribution of heat injection (from the solution of the microwave propagation problem). Moreover, it involves a phase change (ice to water) in the ice layer in contact with the pavement. That melt layer stays at constant temperature as heat energy flows into the layer to increase the melting. At the end of the heat input pulse, refreezing begins as heat energy flows out of the melt layer. Probably, with a layer of material at the top of the pavement that is highly absorbing, some rough approximations can be made to estimate the amount of ice melted and the time required to refreeze. Perhaps all heat injection outside the absorbing layer can be ignored. The ice layer and the pavement layer might both be treated as having infinite thickness. Even with these approximations, the numerical solution would probably require that the absorbing layer plus the nearby ice and pavement be modeled as a fairly large number of discrete cells. Specific heat, thermal conductivity and mass density values are needed for each of the materials described by the model.

The Materials Problem

Clearly, the microwave absorbing layer must be thin if the heat generated therein is to reach the melt zone quickly enough to contribute to melting rather than just a slow warming. For the sake of efficiency the layer should absorb a significant part of the energy from the microwave applicator. It seems unlikely that resistance heating can be depended on, conducting particles embedded in the paving surface need to be in contact with each other if significant conduction currents are to flow and produce energy dissipation. It seems more likely that either dielectric or magnetic hysteresis would have to supply the heating mechanism. Ferrite materials have been discussed [3, 4, 5, 6] as radar absorbing materials (RAM). As noted earlier, the attenuation constant, α, for a material is given by

$$\alpha = Re[\gamma] = Re[j\varpi\sqrt{\epsilon^*\mu^*}]$$

One of the more lossy materials appearing in the tables of reference [7] is $N_i = Z_n$ - cu Ferramic H. Its reported parameters for a frequency of 10 MHz[6] are:

$$K_m = 300$$

$$\tan \delta_m = 1.33$$

$$K_\epsilon = 550$$

$$\tan \delta_\epsilon = 5.5$$

$$\mu^* = \mu_o K_m (1 - j\tan\delta_m)$$

$$= \delta_o x300(1 - j\ 1.33)$$

$$\epsilon^* = \epsilon_o K_\epsilon (1 - j\tan\delta_\epsilon)$$

$$= \epsilon_o \times 550(1 - j5.5)$$

$$\epsilon^*\mu^* = \mu o \times 1.65 \times 10^5\ [10.76\exp(-j0.688)]$$

$$\gamma = j\varpi\sqrt{\epsilon^*\mu^*} = j\varpi\sqrt{\mu_o\epsilon_o}\,x\sqrt{1.775x10^6}\exp(-j0.344)$$

$$= j\varpi\sqrt{\mu_o\epsilon}x1330\,[0.941 - j0.337]$$

The value of

$$\sqrt{\mu_o\epsilon_o}$$

is just the reciprocal of the velocity of light.

$$\sqrt{\mu_o\epsilon_o} = \sqrt{\frac{10^{-16}}{9}} = \frac{1}{3X10^8}$$

Therefore α is given by

---

[6] The tables give no parameters for frequencies above 10 MHz. The above calculation is carried out only to illustrate the method of computing α.

$$\alpha = Re[\gamma] = \varpi X \frac{1330}{3X10^{8}} X(0.337)$$

$$= 1.49X10^{-6} \varpi nepers/m$$

at $\omega = 2\pi F = 2\pi$ X 10^7 rad/s the value of α is

$$\alpha_{10MHz} = 93.6 nepers/M$$

One neper is equivalent to 8.69 dB, so the attenuation constant is

$$\alpha_{10MHz} = 813 dB/M$$

or 8.13 dB for a layer 1 cm thick. The phase constant for the above material is

$$\beta = Im[\gamma] = \varpi x \frac{1330}{3x10^{8}} [-0.941]$$

$$= 4.17x10^{-6} \varpi rad/m$$

at 10 MHz we have

$$\beta = 4.17x10^{-6} x10^{-7} x2\pi x10^{7} = 262 rad/m$$

or 2.62 rad/cm. Thus the phase delay through a 1.0 cm layer of the material is

$$\phi = 2.62x \frac{180}{\pi} = 150°$$

The above example gives no information as to how the material would behave at microwave frequencies. However, if the microwave value of were equal to the value computed, a one-millimeter layer would produce only 0.81 dB of attenuation on a single

pass (only 17% of the energy would be absorbed).

References

1. Lepage, W.R. and S. Seely, General Network Analysis, McGraw-Hill, 1952.

2. Von Hippel, A.R., Dielectrics and waves, John Wiley & Sons, 1954.

3. Harmuth, H.F., Use of Ferrites for Absorbing Electromagnetic Waves, IEEE Transactions on Electromagnetic Compatibility, Vol. EMC-27, No. 2, May 1985, pp. 100 - 102.

4. Ruppin, R. Comments on "Use of Ferrites for Absorption of Electromagnetic Waves", IEEE Transactions on Electromagnetic Compatibility, Vol. EMC 28, No. 2, May 1986, pp. 111 - 112.

5. Thronton, B.S., Comments on "Use of Ferrites for Absorption of Electromagnetic Waves", IEEE Transactions on Electromagnetic Compatibility, Vol. EMC-28, No. 4, November 1986, p. 285.

6. Harmuth, H.F., On the Effect of Absorbing Materials on Electromagnetic Waves With Large Relative Bandwidth, IEEE Transactions on Electromagnetic Compatibility, Vol. EMC-25, No. 1, February 1983, pp. 32 - 39.

7. Giacoletto, L.J., Electronic Designer's Handbook, Second Edition, McGraw-Hill, 1977.

APPENDIX 2

Computation of Microwave Power Absorption

Figure A-1 gives two analogs for the plane-wave model of microwave propagation in a stratified medium. In the transmission line analog a voltage source, V_S, with source impedance Z_S drives a line consisting of four finite segments representing the air, ice, absorber and pavement strata. The pavement segment is attached to an infinite line representing the earth. Each segment has a characteristic impedance determined by the electromagnetic properties of the medium, and a length corresponding to he path length (thickness of the stratum).

In the network analog, each stratum is represented by the transmission matrix, sometimes referred t as the ABDC matrix, which relates output voltage and current to input voltage and current. If E_1 and E_2 are the input voltage and current, while E_2 and I_2 are the output voltage and current, then the network equations are

$$E_1 = AE_2 + BI_2$$

$$I_1 = CE_2 + DI_2$$

The equations in matrix form are

$$\begin{bmatrix} E_1 \\ I_1 \end{bmatrix} = [M] \begin{bmatrix} E_2 \\ I_2 \end{bmatrix}$$

This formulation is used because it permits the overall parameters of cascaded networks to be found by multiplication of the matrices of the individual networks. The elements of the matrix

$$m = \begin{bmatrix} A & B \\ C & C \end{bmatrix}$$

for a given stratum are given by

$$a = d = l\cosh(\gamma)$$
$$B = lZ_o \sinh(\gamma)$$
$$C = \frac{l}{Z_o} \sinh(\gamma)$$

In these equations, l is the path length (stratum thickness), Z_o is the characteristic impedance (wave impedance) of the medium, and γ is the propagation constant of the medium. These latter two parameters are related to the complex permittivity, ϵ^*, and the complex permeability, μ^*, of the medium

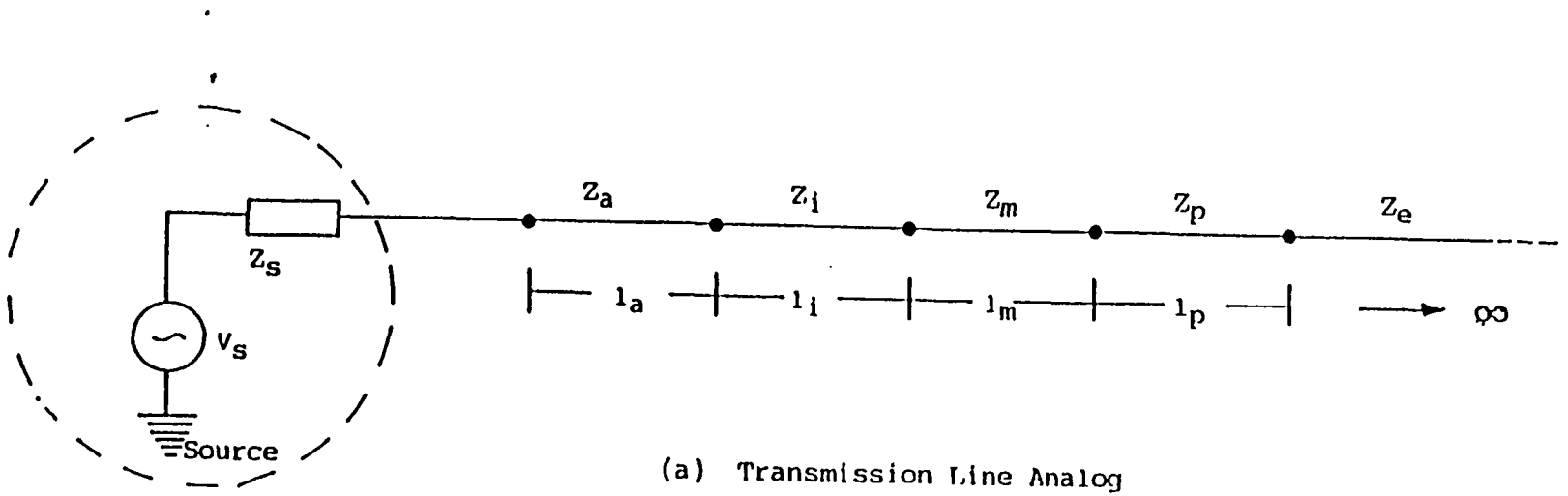

(a) Transmission Line Analog

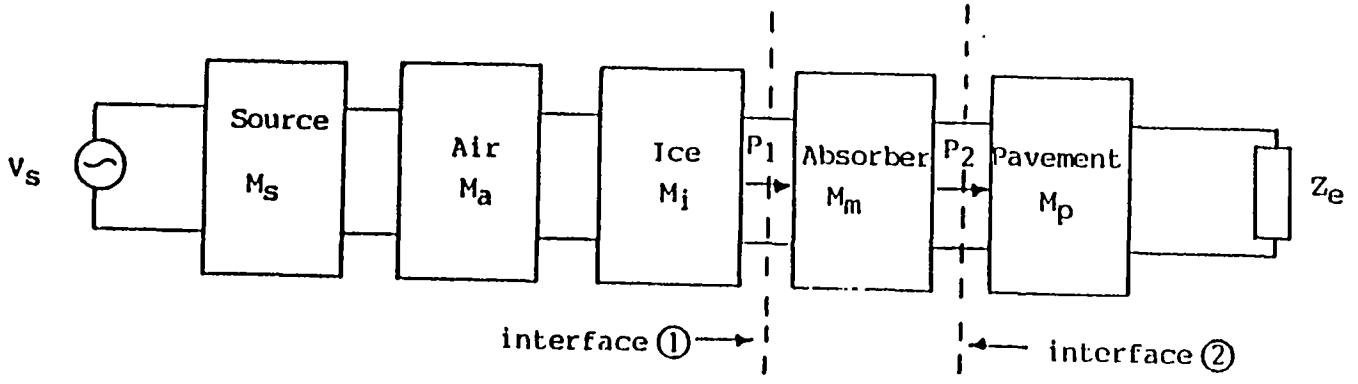

(b) Network Analog

Figure A-1. Models of Plane Wave Propagation in Stratified Medium

by[7]

$$Z_o=\sqrt{\mu^\circ/\epsilon^\circ}$$
$$\gamma=j\varpi\sqrt{\mu^\circ\epsilon^\circ}$$

Thus, to study microwave absorption by any stratum, the ABDC matrices for each stratum must be determined from the value of μ° and ϵ° for each material, at the operating frequency. As shown in Figure A-1, the source impedance is represented by the simple matrix

$$M_s=\begin{bmatrix}1 & Z_s\\ 0 & 1\end{bmatrix}$$

For calculations, Z_S was set equal to the wave impedance of free space (377 ohms).

The entity of interest is the power absorbed by the layer placed at the top of the pavement for the purpose of creating heat to disbond the ice. If E_1 and I_1 are the phasor voltage and current at interface 1 (the top surface of the absorber layer) then the power into the absorber is[8]

$$P_1 = E_1 I^\circ_1$$

Likewise, if E_2 and I_2 are the phasor voltage and current at interface 2, (the lower surface of the absorber layer) then the power leaving the layer is

$$P_2 = E_2 I^\circ_2$$

and the power absorbed is

$$\Delta P=P_1-P_2$$

---

[7] See, for example, Dielectrics and Waves, by A.R. von Hippel, John Wiley & Sons, 1954.

[8] The symbol I° represents the complex conjugate of I.

The power into the absorber is computed from the reduced equivalent network of Figure A-2.

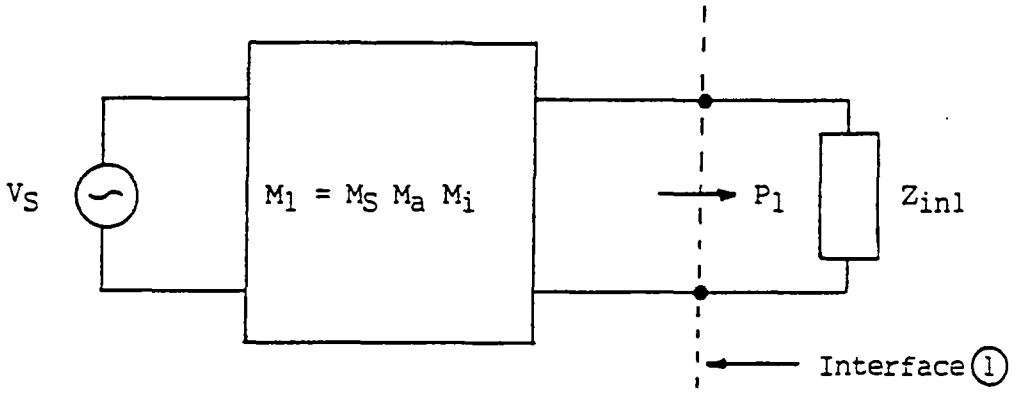

Figure A-2. Computation of P_1

The matrix M_1 is just the product of the matrices for the source impedance, the air stratum and the ice stratum. The power leaving the absorber is computed from the reduced network of Figure A-3,

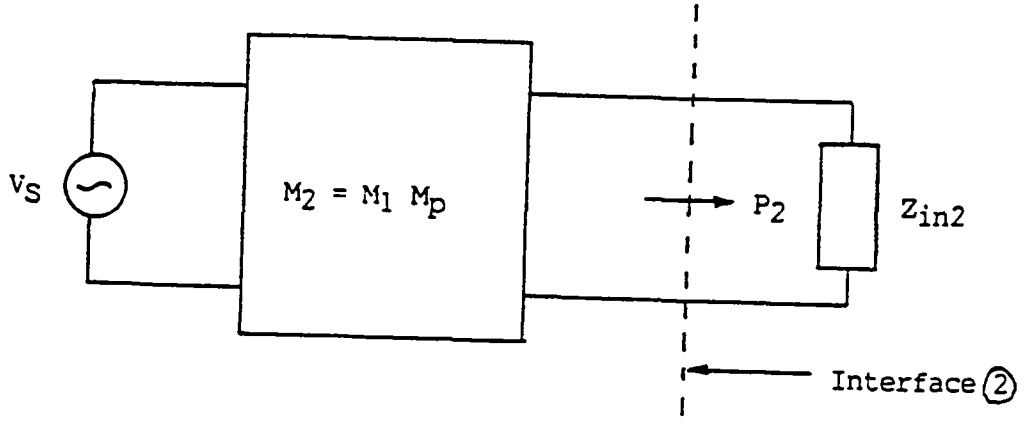

Figure A-3. Computation of P_2

The matrix M_2 is just the product of M_1 and the pavement matrix. It is easily shown that the impedance Z_{in2} (the impedance measured at interface 2, looking into the pavement) is given by

$$Z_{in2}=\frac{A_p Z_e+B_p}{C_p Z_e+D_p}$$

where Z_e is the characteristic impedance of the earth medium, and A_p, B_p, C_p, D_p are the elements of the pavement matrix. Likewise theimpedance Z_{in1} (the impedance at interface 1, looking into the top surface of the absorber) is given by

$$Z_{in1}=\frac{A_{mp} Z_e+B_{mp}}{C_{mp} Z_e+D_{mp}}$$

where A_{mp}, B_{mp}, C_{mp} and D_{mp} are the elements of the combined absorber/pavement matrix, M_{mp}.

$$M_{mp} = M_m M_p$$

Parameters of Baseline Model

A baseline model was established in which the microwave applicator surface was 10 cm above the surface of a 1.0 cm layer of ice. Under the ice was a 1.0 cm layer of absorber, consisting of coal/asphalt mix placed on a 10 cm layer of concrete. No ferromagnetic material was involved, so μ° is just equal to μ_o, the permeability of free space for all strata. The complex permittivity for any layer was then expressed in terms of relative dielectric constant, k_r, and the loss tangent, tan (δ), of the material of each stratum.

$$\epsilon^\circ=\epsilon_o k_r [1-j\tan(\delta)]$$

where ϵ_o is the permittivity of free space. The following table gives the strata parameters used for this baseline case.

Table A-1. Strata Parameters, Baseline Model

Stratum	Thickness (meters)	Relative Dielectric Constant	Loss Tangent
Air	0.10	1.0	0
Ice	0.01	3.2	0.001
Absorber	0.01	2.5	0.04
Pavement	0.10	4.0	0.01
Earth		10.0	0.10

For a unit voltage source (V_S = 1.0 volt) the computed powers are

$$P_1 = 5.68 \times 10^{-4} \text{ watt}$$

$$P_2 = 5.45 \times 10^{-4} \text{ watt}$$

$$\Delta P = 2.3 \times 10^{-5} \text{ watt}$$

Only about 4% of P_1 absorbed, so it is clear that modifications are essential in order to achieve more effective absorption of microwave power. Incidentally, P_1 proves to be a large fraction of P_{max} the power that the source could drive into a matched load (load impedance = Z_S = 377 ohms)

$$P_{max} = \frac{V^2_s}{4Z_s} = \frac{1}{4x377} = 6.63x10^{-4} watt$$

Thus, for our baseline model, the power into the absorber is 85% of the maximum power that could be delivered to a perfectly matched load (no reflections). Unfortunately most of the power passes on through the absorber.

With non-ferromagnetic material the absorption can be increased by increasing the layer thickness or by modifying the relative dielectric constant and the loss tangent. For moderate changes in thickness, the fraction of input power absorbed varies approximately linearly with thickness. This is not an acceptable approach, for power absorbed at appreciable depths is ineffective in contributing to melting.

Effect of Varying Absorber Parameters

The attenuation constant of a material can be shown to vary as the square root of the relative dielectric constant. Doubling the value of the relative dielectric constant from 2.5 to 5.0 in the model increases the absorption only from 4% to 6% of the value if P_1. (The value of P_1 drops from 85% to P_{max} to about 81% of P_{max}.

The attenuation constant of a material is a rather complicated function of loss tangent. As would be expected, a large increase in loss tangent produces more effective absorption. Ferrite materials have been shown to be very effective absorbers of microwave energy, and for that reason they have been incorporated into "radar absorbing material", sometimes called RAM, for reducing the detectability of military aircraft. Some ferrites have large values of relative dielectric constant and dielectric loss tangent[9]. To demonstrate the effectiveness of such a material, the baseline model was altered by giving the absorber the following parameters:

Relative dielectric constant = 100

Dielectric loss tangent = 10

Computations were carried out for four values of absorber layer thickness. The results are given in Table A-2.

Table A-2. Absorption by Highly Lossy Material

Absorber Layer Thickness	% of P_1 Absorbed	Value of P_1P_{max}
1.0 mm	60.2	0.98
2.0 mm	86.1	0.98
3.0 mm	95.3	0.98
1.0 cm	~100.0	0.98

Thus with only a 3 mm layer of this material, 95% of P_1 is absorbed. Moreover, P_1 is very nearly as great as the power that the source could drive into a perfectly matched load. A primary task then would be a search for a suitably lossy material. This is not a simple task, for most engineering applications call for low-loss dielectrics and low-loss ferrites. These are the materials for which parameter values can be found in the

[9] They may also have high relative permeability and high magnetic loss tangent, but we restrict consideration here to dielectric loss.

literature. Measurement of the electromagnetic parameters of materials at the operating frequency of interest is a complicated, time consuming process. Measurements of the return loss[10] from samples of materials applied to the flange of an open-ended waveguide were carried out at a frequency of 2.45 GHz. These measurements do not reveal the material parameters directly, for the field at the face of the material is not a uniform plane wave, but the measurements do give some feel for the relative lossiness of materials. For example, the return loss from a sample of Eccosorb 2.5 backed with an aluminum plate[11] was 11.4 dB. This means that only about 7% of the incident power was reflected, and so 93% of the incident energy is absorbed. Similar measurements on 1/4 inch thick slabs of coal/asphalt mix gave return loss values of about 3.5 dB. In this case 45% of the power was reflected. Of the remaining 55%, part would have been absorbed and part passed o through the outer face of the slab[12].

---

[10] The return loss is the level of the reflected power, compared to the level of power incident on the material.

[11] The material thickness was 0.085 inch.

[12] In the case of the metal-backed Eccosorb, the metal backing prevented any significant loss through the outer face.

Appendix 3

Network Analyzer Test Results (Return Loss in dB)

June 6, 1990 Anarec Microwave Tests

Sample No.	Description
20 log |r|* in dB	
1 -11.4	Ecosorb 2.5 backed with air aluminum plat.
2 - 5.3	Ecosorb 2.5 on top of PCC sample (6" x 4" high).
3 - 4.0	6" Asphalt sample, 1/2" thick w/sand added.
4 - 3.5	100% Carbon aggregate (5% binder), ~ 1/4" thick.
5 - 3.7	100% Carbon aggregate (15-20% binder), ~ 1/4" thick.
6 - 0.8	Ferrite 20%/Epoxy 80% ~ 1/8" thick w/alum backing.
7 - 4.3	PCC (6" dia. x 4" thick) only.
8 - 4.2	2 layers of ferrite on PCC sample.
9 - 0.3	Same as #6 except thicker epoxy 1/8" +.
10 - 5.7	Both samples 4 & 5 with #5 closest to flange.
11 - 6.4	Both samples 4 & 5 with #4 closest to flange.
12 - 3.5	2 layers of Ecosorb 2.5 backed with aluminum plate.

*Return loss = 20 log (|r|), where Γ = reflection coefficient.

Comments: Ecosorb 2.5 is tuned for 2.5 GHz, compare 1 and 12.

NOTE: All tests were run between 1.69 and 2.65 Hz.

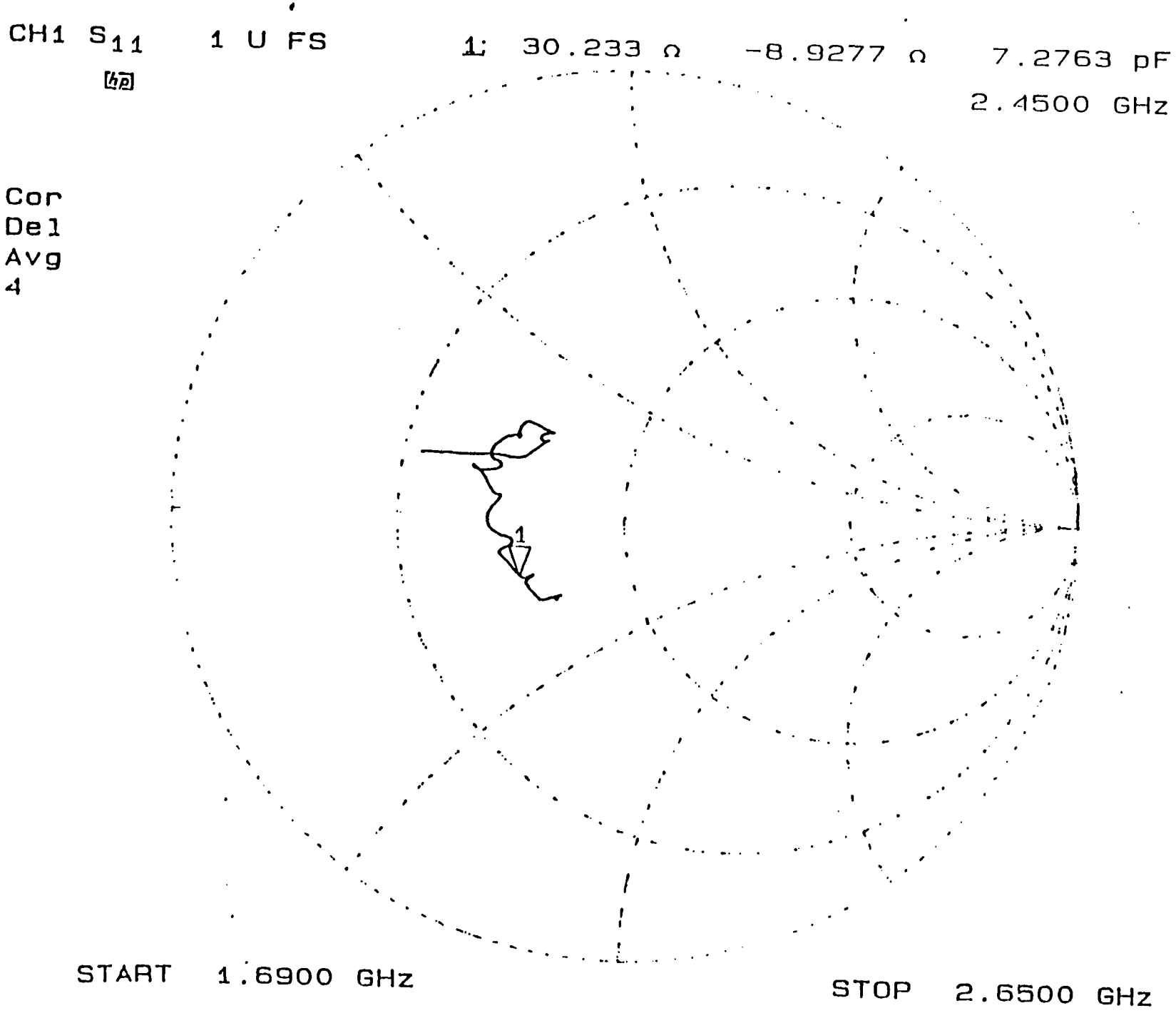
CH1 S11 1 U FS
1: 30.233 Ω -8.9277 Ω 7.2763 pF
2.4500 GHz
Cor
Del
Avg
4
1
START 1.6900 GHz
STOP 2.6500 GHz

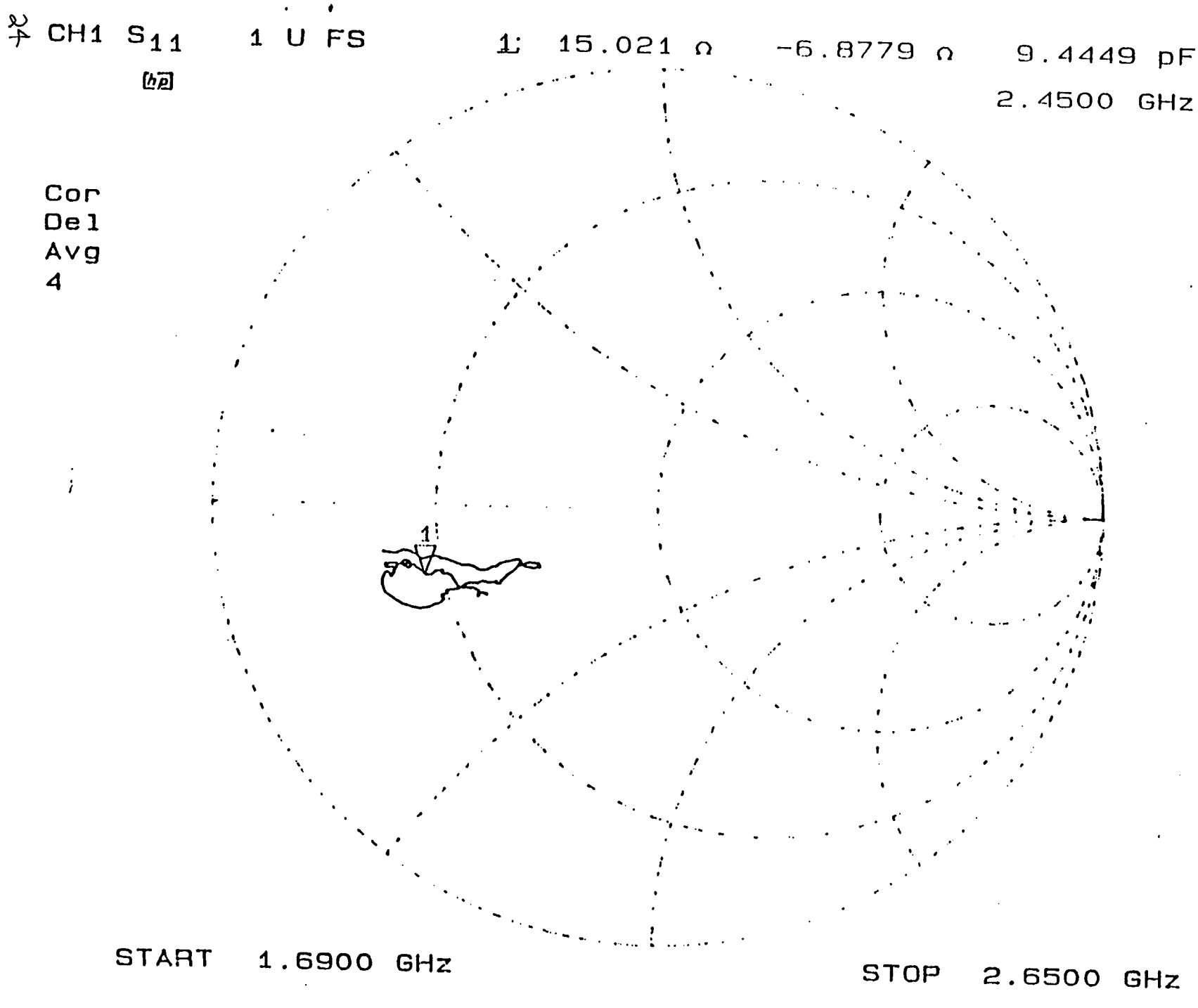
24 CH1 S11 1 U FS
1: 15.021 Ω -6.8779 Ω 9.4449 pF
2.4500 GHz
Cor
Del
Avg
4
1
START 1.6900 GHz
STOP 2.6500 GHz

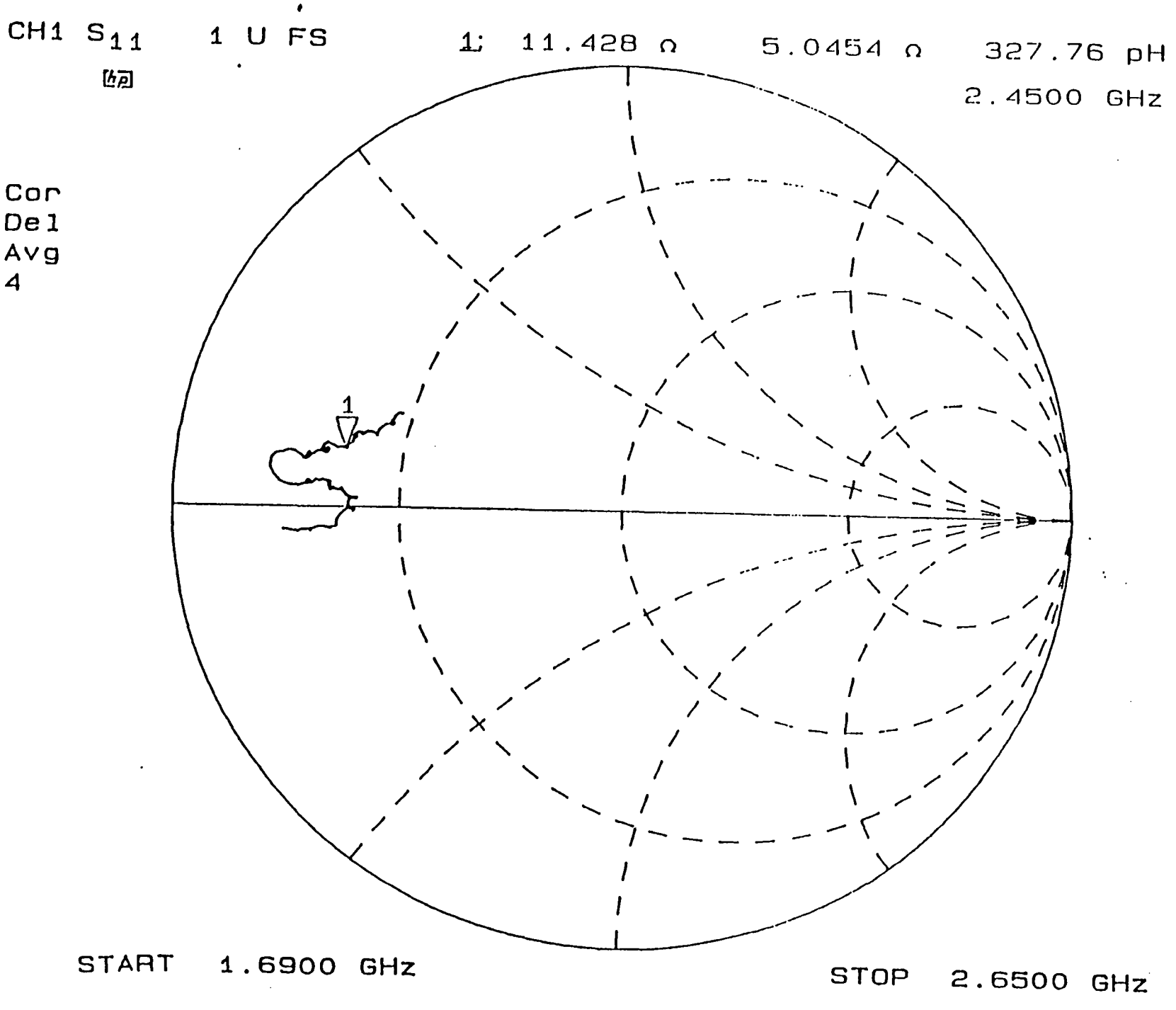
CH1 S11 1 U FS
1: 11.428 Ω 5.0454 Ω 327.76 pH
2.4500 GHz
Cor
Del
Avg
4
1
START 1.6900 GHz
STOP 2.6500 GHz

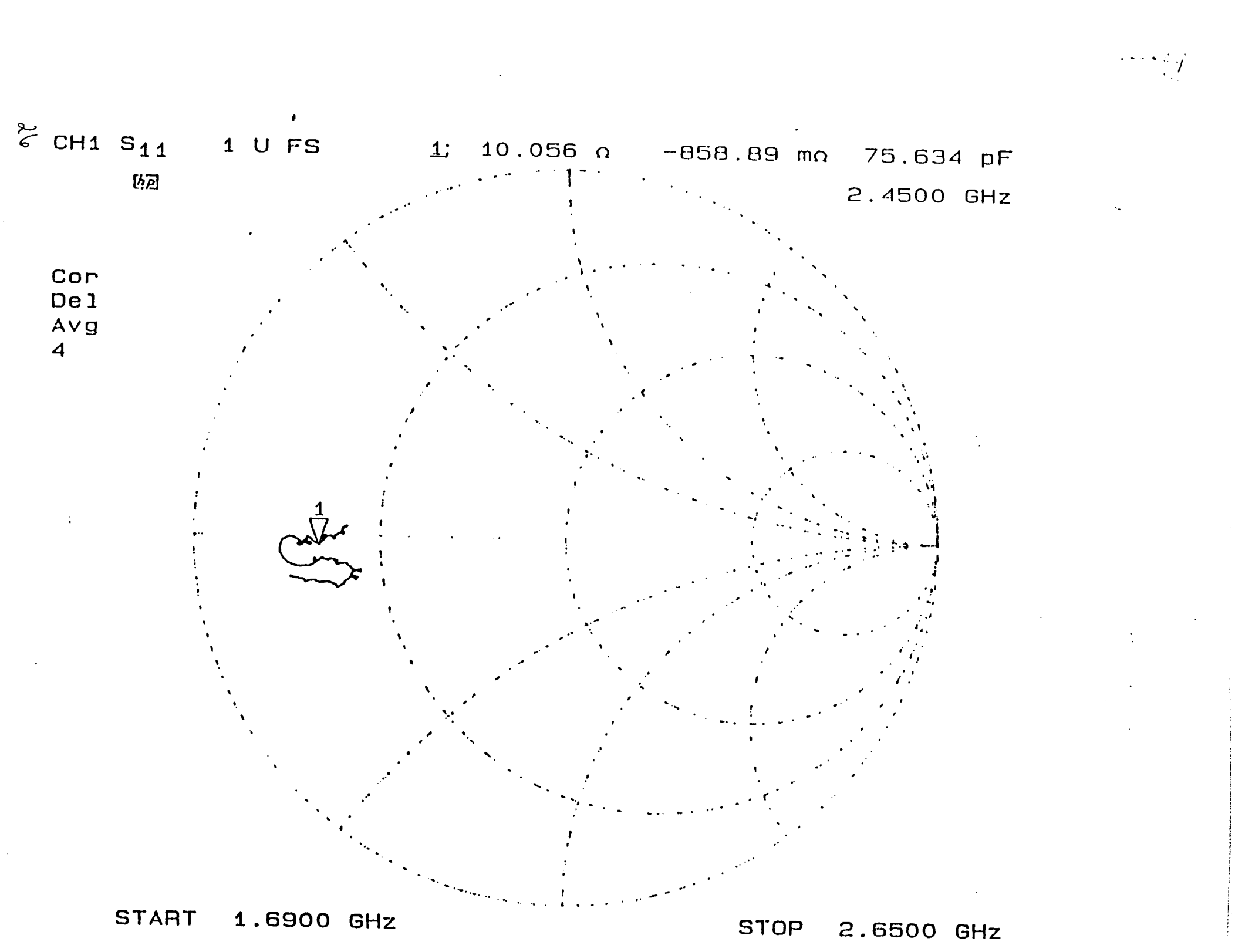
CH1 S11 1 U FS
1: 10.056 Ω -858.89 mΩ 75.634 pF
2.4500 GHz
Cor
Del
Avg
4
1
START 1.6900 GHz
STOP 2.6500 GHz

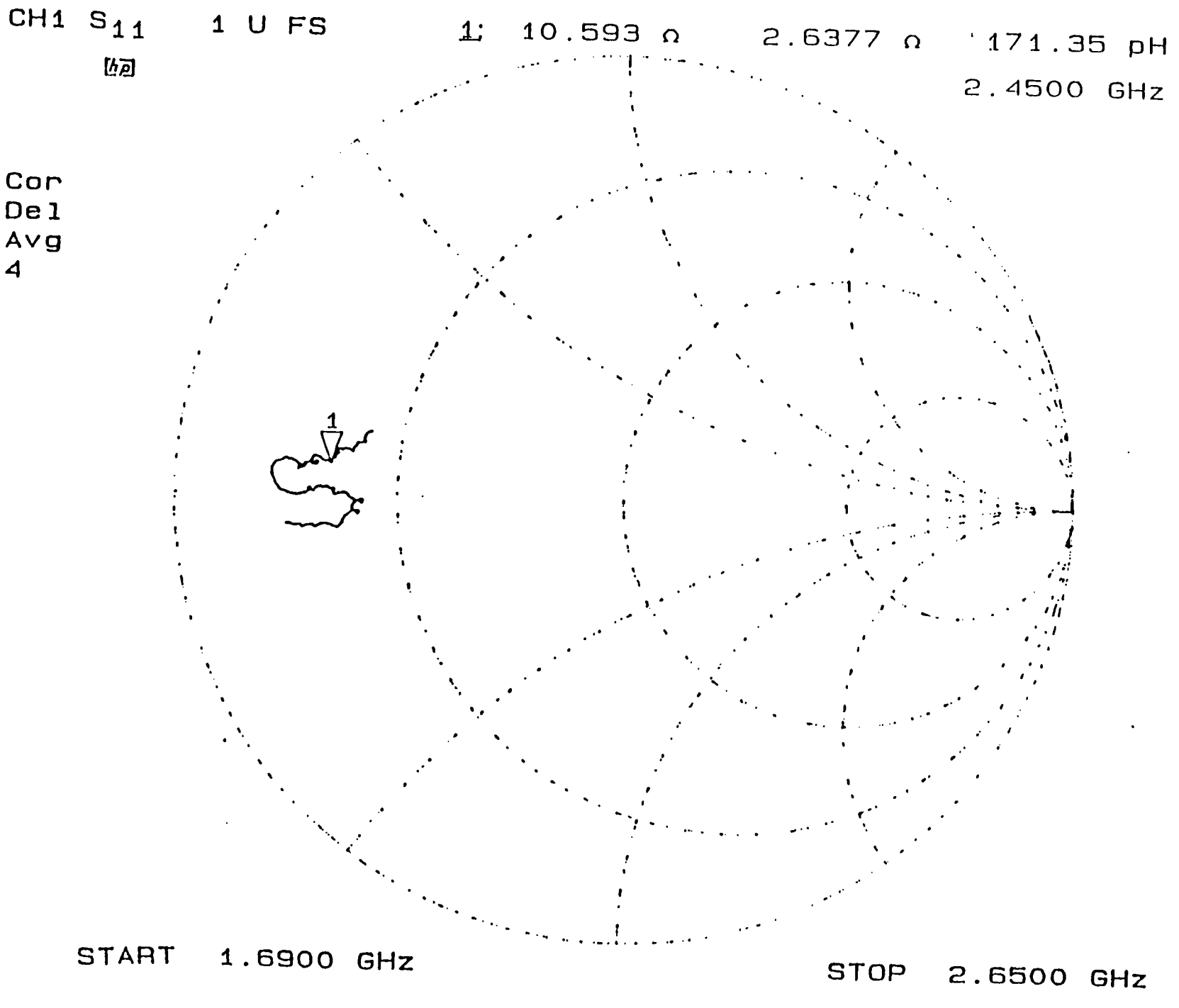
CH1 S11 1 U FS
1: 10.593 Ω 2.6377 Ω 171.35 pH
2.4500 GHz
Cor
Del
Avg
4
1
START 1.6900 GHz
STOP 2.6500 GHz

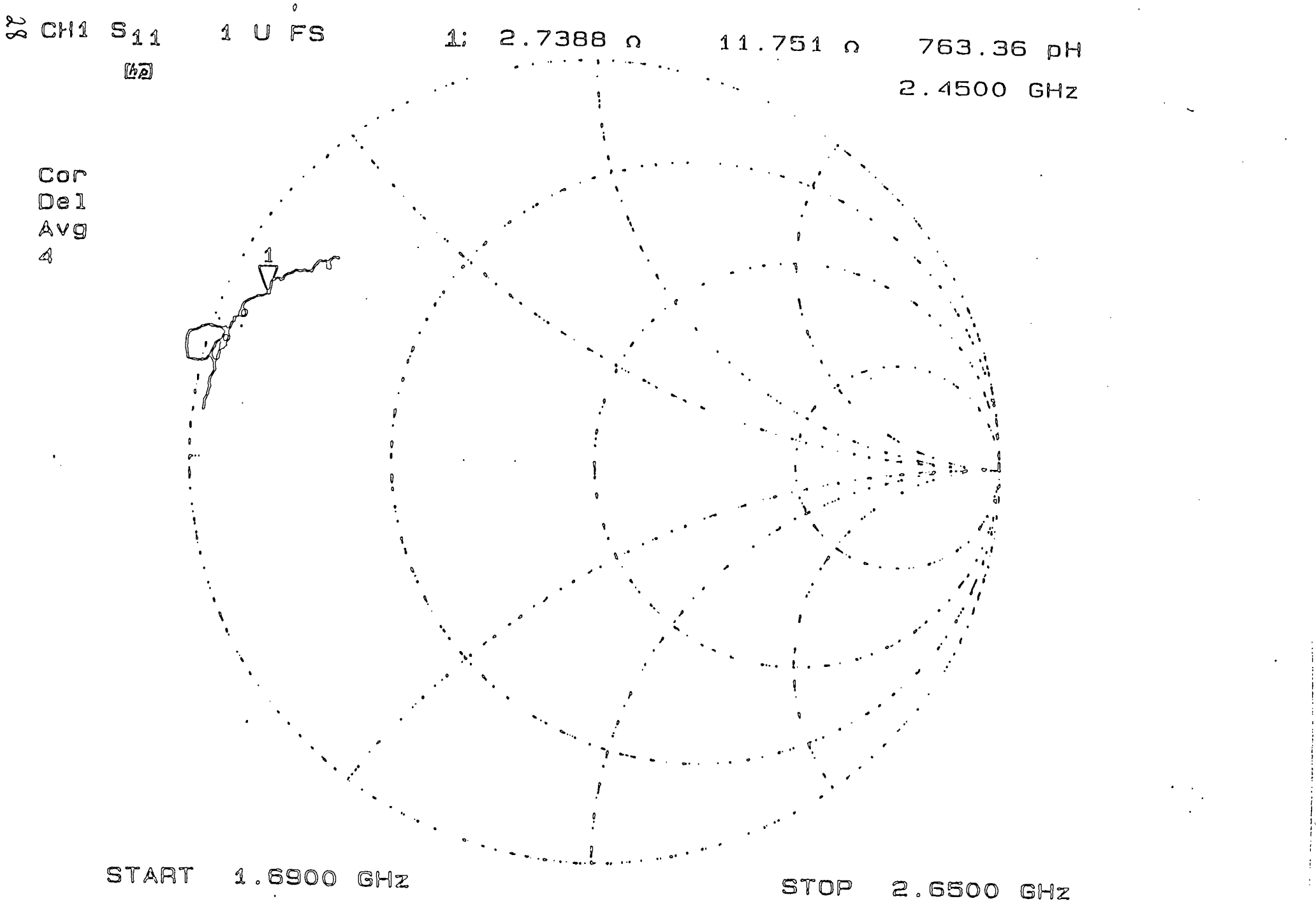
CH1 S11 1 U FS
1: 2.7388 Ω 11.751 Ω 763.36 pH
2.4500 GHz
Cor
Del
Avg
4
1
START 1.6900 GHz
STOP 2.6500 GHz

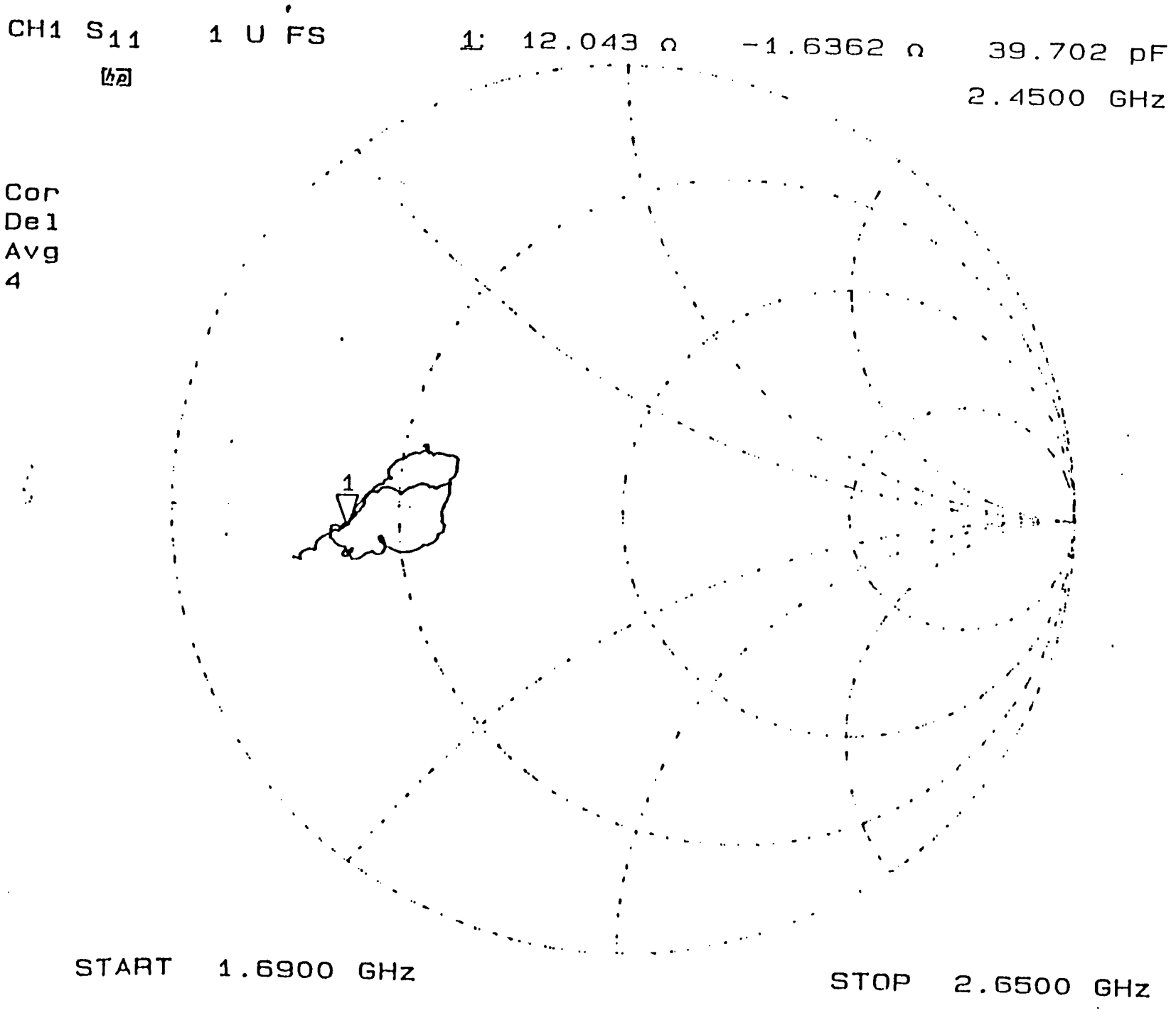
CH1 S11 1 U FS
1: 12.043 Ω -1.6362 Ω 39.702 pF
2.4500 GHz
Cor
Del
Avg
4
1
START 1.6900 GHz
STOP 2.6500 GHz

CH1 S_{11} 1 U FS

1: 11.896 Ω -1.9448 Ω 33.402 pF

2.4500 GHz

Cor
Del
Avg
4

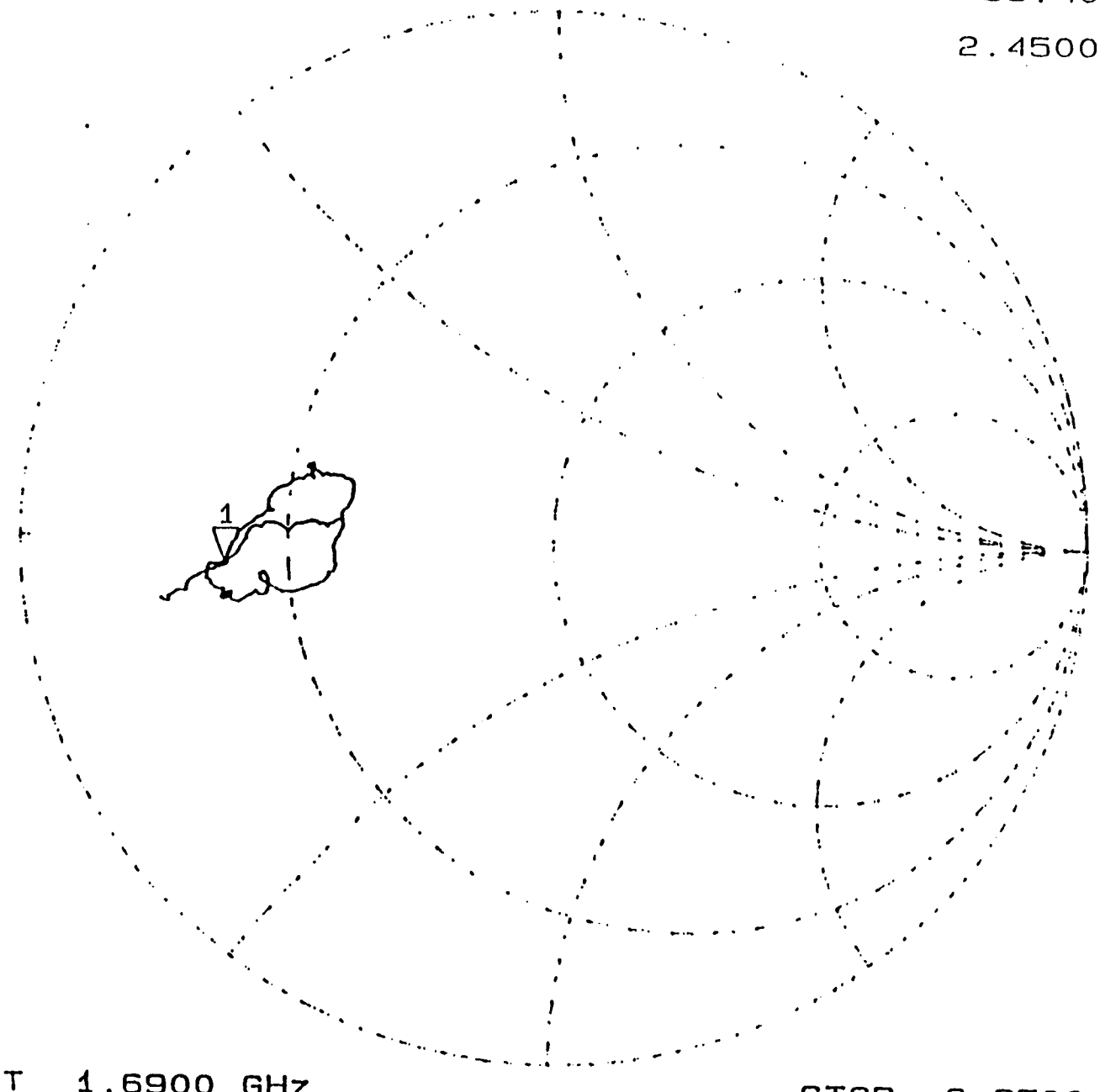

START 1.6900 GHz

STOP 2.6500 GHz

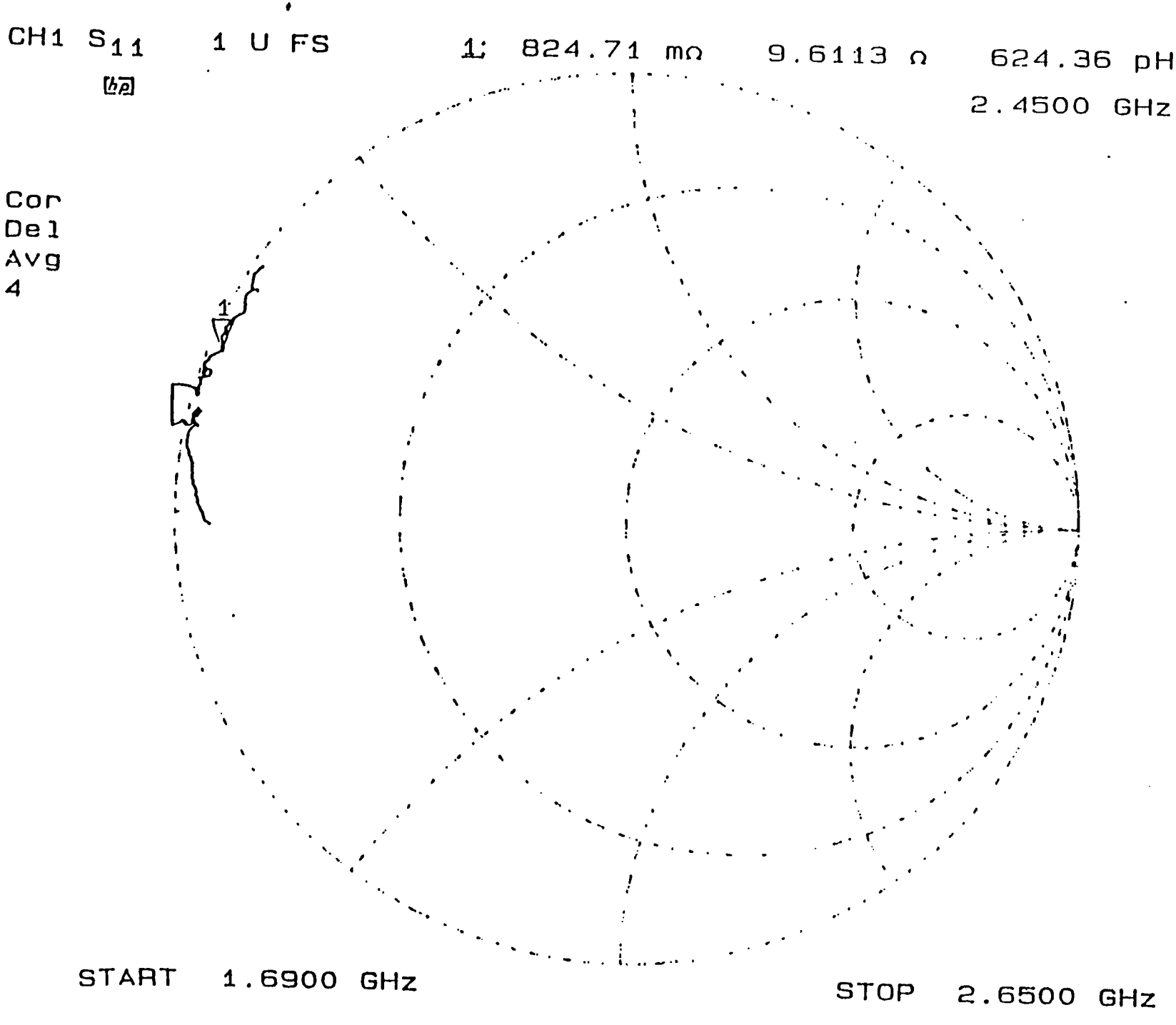
CH1 S11 1 U FS
1: 824.71 mΩ 9.6113 Ω 624.36 pH
2.4500 GHz
Cor
Del
Avg
4
START 1.6900 GHz
STOP 2.6500 GHz

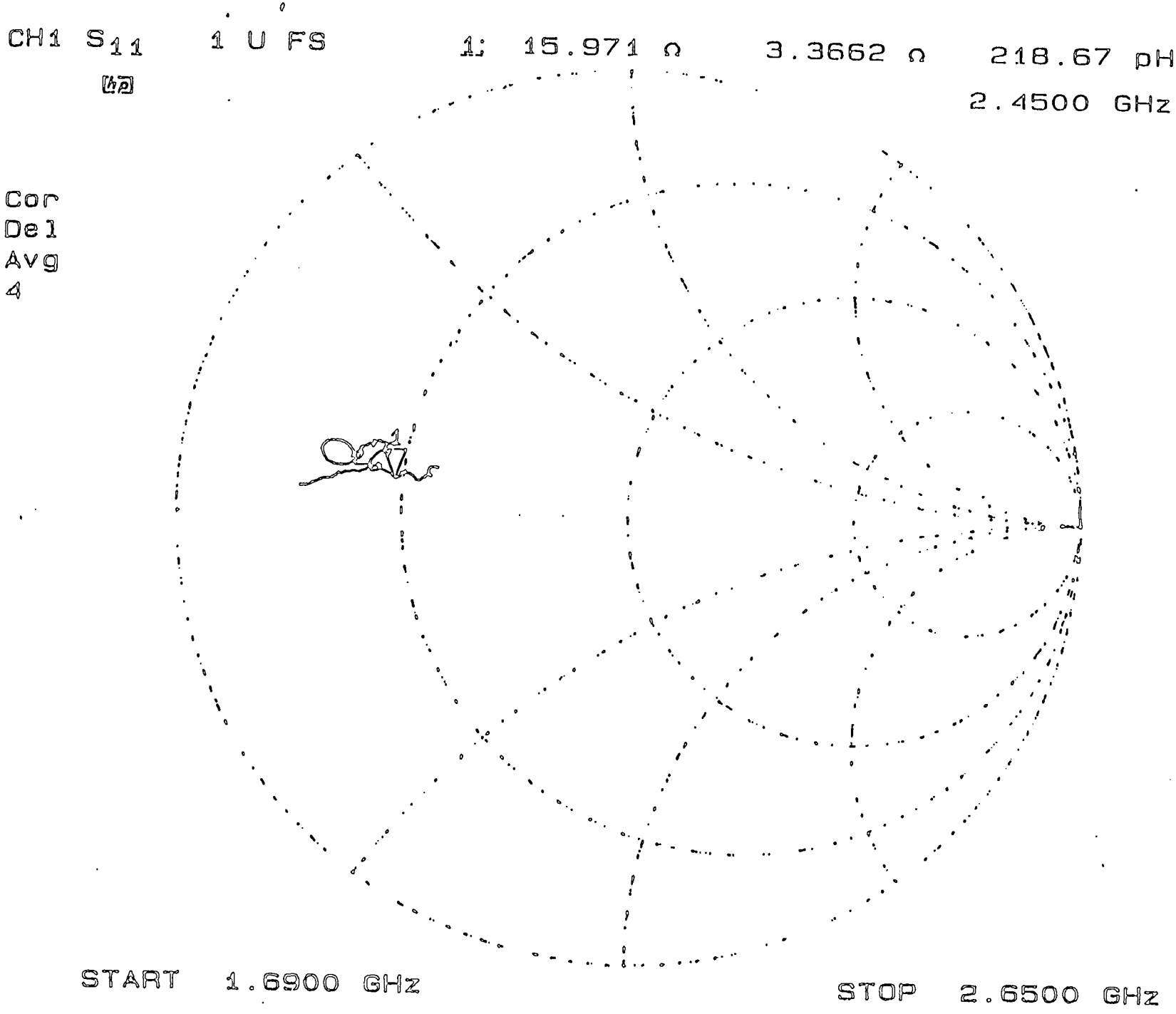
CH1 S11 1 U FS
1: 15.971 Ω 3.3662 Ω 218.67 pH
2.4500 GHz
Cor
Del
Avg
4
START 1.6900 GHz
STOP 2.6500 GHz

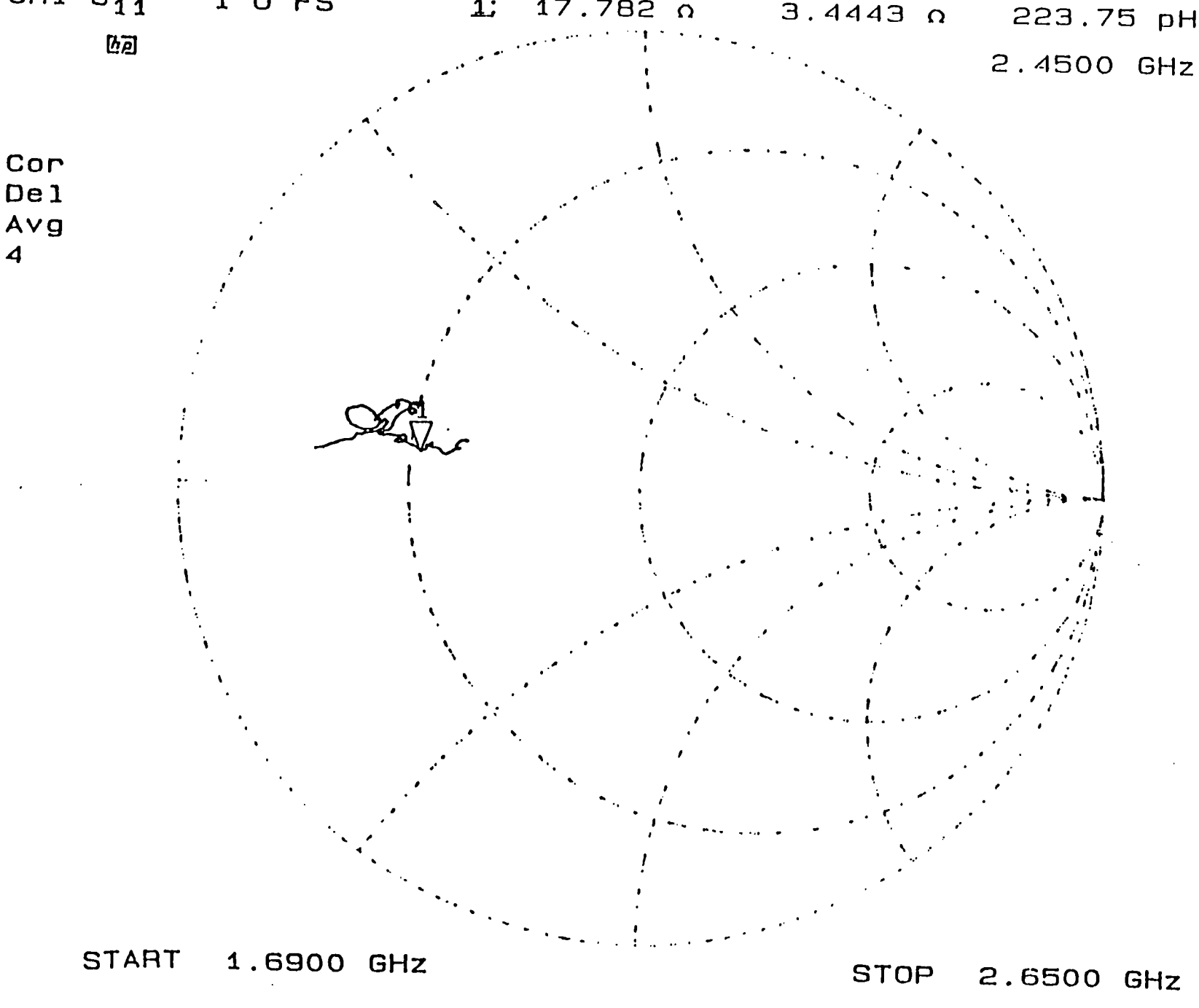
CH1 S11 1 U FS
1: 17.782 Ω 3.4443 Ω 223.75 pH
2.4500 GHz
Cor
Del
Avg
4
START 1.6900 GHz
STOP 2.6500 GHz

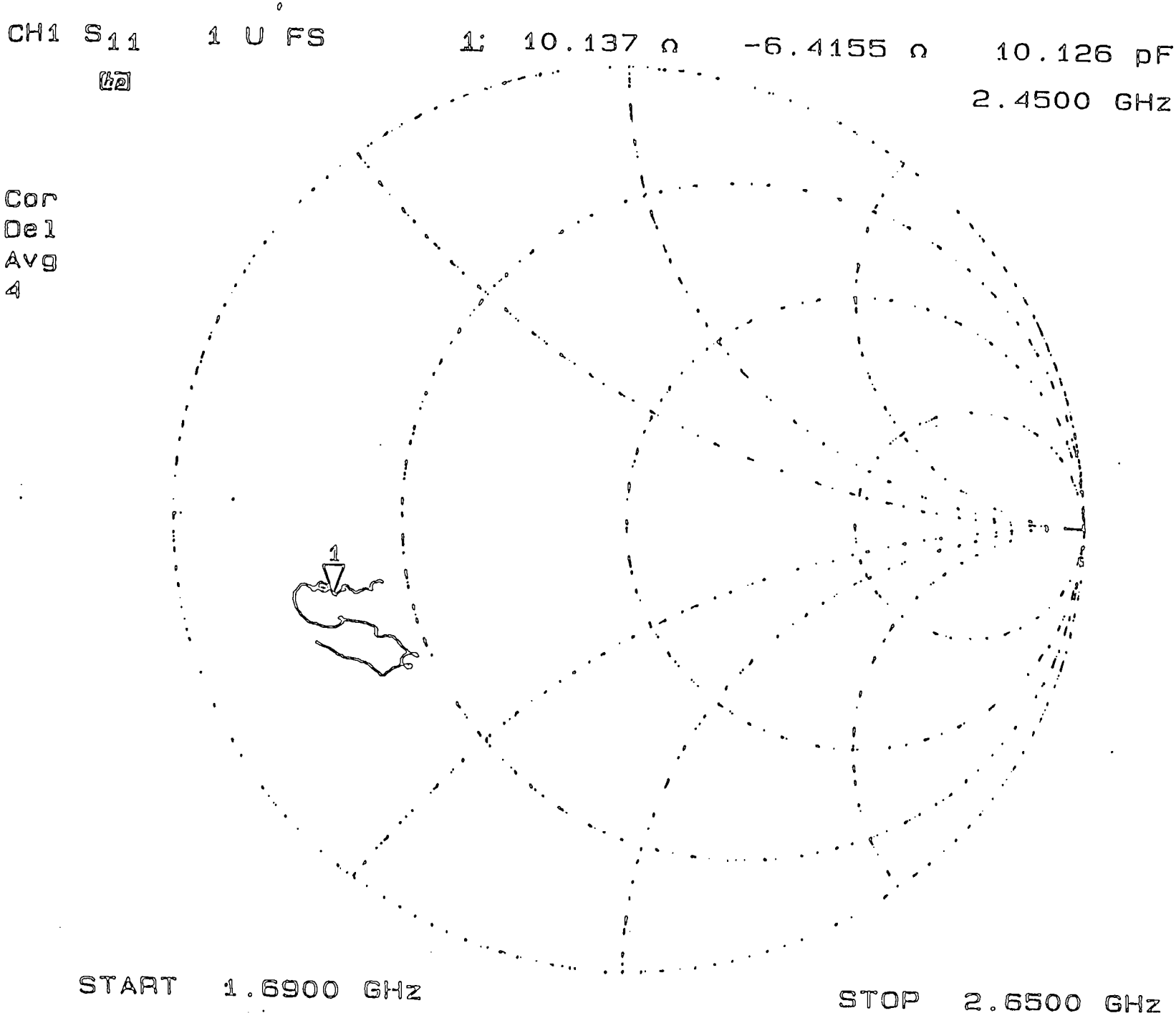
CH1 S11 1 U FS
1: 10.137 Ω -6.4155 Ω 10.126 pF
2.4500 GHz
Cor
Del
Avg
4
1
START 1.6900 GHz
STOP 2.6500 GHz

Appendix 4

STAINLESS STEEL BLADE

TEST NUMBER	COMMENT	VELOCITY DOWNLOAD	BLADE ANGLE	OVERALL MAX	OVERALL AVG	BEGIN MAX
99				66.98	14.7	66.98
100		0.1in/sec		29.39	13.85	29.39
101	Asphalt	150 lbf		34.55	8.72	34.54
102			15(SS)	37.55	7.01	37.55
103				21.9	10.23	18.38
104				38.04	12.23	38.05
			AVERAGE	38.07	11.12	37.48
			STAND DEV	14.06	2.74	14.77
118				78.97	20.61	78.97
119		1.0 in/sec		55.38	21.17	55.38
120	Asphalt	150 lbf		59.1	11.3	59.1
121			0(SS)	37.55	10.06	37.55
122				30.05	12.97	30.05
			AVERAGE	52.21	15.22	52.21
			STAND DEV	17.20	4.72	17.20
123				32.81	10.7	32.81
124		1.0 in/sec		26.91	9.8	26.91
125	Concrete	150 lbf		27.14	7.89	27.14
126			0(SS)	51.18	8.45	51.18
127				28.67	10.18	28.67
			AVERAGE	33.34	9.40	33.34
			STAND DEV	9.17	1.06	9.17
128				46.39	16.47	46.39
129		1.0 in/sec		58.97	13.95	58.97
130	Asphalt	150 lbf		46.54	21.04	46.54
131			30(SS)	29.15	10.27	29.15
132				56.27	20.29	56.27
			AVERAGE	47.46	16.40	47.46
			STAND DEV	10.46	4.01	10.46
133				30.43	9.64	30.43
134		1.0 in/sec		44.08	12.69	44.08
135	Concrete	150 lbf		41,93	10.96	41.93
136			30(SS)	27.89	13.23	27.89
137				31.2	11.07	31.2
			AVERAGE	35.11	11.52	35.11
			STAND DEV	6.58	1.29	6.58
149		0.1 in/sec		54.14	18.47	54.14
150	Asphalt	150 lbf		26.56	14.62	26.56
151			30(SS)	36.28	14.03	36.28
152				45.49	17.37	45.49
			AVERAGE	40.62	16.12	40.62
			STAND DEV	10.28	1.85	10.28
153		0.1 in/sec		30.11	12.67	30.11
155	Concrete	150 lbf		36	12.49	36
156			30(SS)	32.88	12.9	32.88
157				38.78	13.65	38.78
			AVERAGE	34.44	12.93	34.44
			STAND DEV	3.26	0.44	3.26

BEGIN AVG	MIDDLE MAX	MIDDLE AVG	END MAX	END AVG	MINIMUM	MAXIMUM	DEVIATION
23.99	21.81	12.82	16.42	7.61	140.4	153.1	12.7
12.68	27.62	17.99	22.75	10.86	148.2	179.4	31.2
10.69	20.25	10.71	13.78	4.84	148.8	180.2	31.4
6.16	15.73	9.6	11.84	5.27	149.1	197	47.9
9.02	21.9	13.32	15.08	8.31	148.8	197.8	49
16.3	20.47	12.14	14.93	8.35	150.9	197.8	46.9
13.14	21.30	12.76	15.80	7.54			
5.77	3.50	2.65	3.41	2.03			
25.59	24.68	16.71	51.77	20.26	151.5	181.3	29.8
22.89	18.68	16.21	40.29	24.47	149.3	169.9	20.6
16.77	19.39	11.47	11.93	6.48	152.3	189.7	37.4
16.35	18.75	10.87	14.46	3.87	130.6	201.1	70.5
15.71	20.94	10.56	23.39	12.88	149	184.3	35.3
19.46	20.49	13.16	28.37	13.59			
4.01	2.25	2.71	15.35	7.85			
12.62	15.1	10.45	13.19	9.33	149.9	193.8	43.9
14.05	15.61	10.61	10.17	5.88	149.6	169.9	20.3
12.59	20.07	9.22	13.65	2.65	149.9	184.8	34.9
11.64	15.38	7.71	12.02	6.36	147.4	206.2	58.8
15.77	17.16	9.02	15	6.35	151.5	184.5	33
13.33	16.66	9.40	12.81	6.11			
1.44	1.85	1.06	1.63	2.12			
20.22	31.14	17.93	21.72	11.75	131.2	153.9	22.7
24.29	17.16	11.87	11.65	6.91	96.7	174.8	78.1
28.78	22.03	17.67	21.83	17.63	144.7	164	19.3
14.81	14.86	9.61	12.33	6.97	150.7	169.1	18.4
26.53	30.12	16.64	27.87	18.53	149.9	162.9	13
22.93	23.06	14.74	19.08	12.36			
4.95	6.61	3.37	6.21	5.00			
13.3	16.08	11.38	13.06	4.82	145.2	184	38.8
16.14	17.66	14.02	14.49	8.38	152.8	191.9	39.1
17.97	16.18	11.31	16.08	4.6	150.9	194	43.1
19.51	17.84	12.57	17.43	8.5	151.2	191.9	40.7
16.05	16.55	13.33	12.17	4.61	151.5	195.6	44.1
16.59	16.86	12.52	14.65	6.18			
2.09	0.74	1.07	1.92	1.85			
29.62	20.91	14.89	16.36	11.23	150.4	184.5	34.1
17.65	23.62	16.49	15.68	9.82	152.3	220.6	68.3
19.95	24.28	17.14	21.23	5.27	152	197.6	45.6
21.54	24.6	16.7	18.79	14.01	151.2	203	51.8
22.19	23.35	16.31	18.02	14.05			
4.51	1.45	0.85	2.19	3.16			
15.36	20.69	13.85	17.22	8.93	149.1	187.8	38.7
18.66	21.1	12.8	15.39	6.24	151.2	188.1	36.9
18.18	19.25	13.29	13.11	7.43	150.9	194	43.1
21.99	20.49	13.42	11.63	5.82	150.9	207.9	57
18.55	20.38	13.34	14.34	7.11			
2.35	0.69	0.37	2.14	1.21			

TEST NUMBER	COMMENT	VELOCITY DOWNLOAD	BLADE ANGLE	OVERALL MAX	OVERALL AVG	BEGIN MAX
158				69.57	18.76	69.57
159		0.1 in/sec		109.5	13.04	109.5
160	Concrete	100 lbf		79.68	11.76	79.68
161			0(SS)	57.87	8.45	57.87
162				54.1	11.32	54.1
			AVERAGE	74.14	12.67	74.14
			STAND DEV	19.84	3.40	19.84
163				41.02	10.56	41.02
164		0.1 in/sec		61.26	14.05	61.26
165	Asphalt	100 lbf		127.02	10.18	127.02
166			0(SS)	59.86	9.64	59.86
167				171.82	19.62	171.82
			AVERAGE	92.20	12.81	92.20
			STAND DEV	49.34	3.74	49.34
168		0.1 in/sec		47.83	10.01	47.83
169		100 lbf		17.53	7.75	17.53
170	Asphalt		30(SS)	27.75	11.55	27.75
171				41.1	12.61	41.1
172				32.34	11.79	32.34
			AVERAGE	33.31	10.74	33.31
			STAND DEV	10.51	1.72	10.51
174		0.1 in/sec		39.51	14.41	39.51
175	Concrete	100 lbf		18.53	8.88	18.53
176			30(SS)	43.66	9.37	43.66
177				26.2	10.36	26.2
			AVERAGE	31.97	10.76	31.97
			STAND DEV	10.09	2.18	10.09
183				44.93	13.75	44.93
184		0.1 in/sec		64.51	17.54	64.51
185	Concrete	100 lbf		68.16	13.25	68.16
186			15(SS)	72.33	11.33	72.33
187				57.97	15.92	57.97
			AVERAGE	61.58	14.36	61.58
			STAND DEV	9.57	2.16	9.57
193				122.15	21.12	122.15
194		0.1 in/sec		171.17	37.42	171.17
195	Asphalt	200 lbf		116.51	24.05	116.51
196			0(SS)	105.63	20.95	105.63
197				113.06	15.48	113.06
			AVERAGE	125.70	23.80	125.70
			STAND DEV	23.35	7.35	23.35
198				125.7	22.99	125.7
199		0.1 in/sec		130.52	12.98	130.52
200	Concrete	200 lbf		80.49	20.05	80.49
201			0(SS)	156.73	21.95	156.73
202				109.12	23.3	109.12
			AVERAGE	120.51	20.25	120.51
			STAND DEV	25.18	3.81	25.18

BEGIN AVG	MIDDLE MAX	MIDDLE AVG	END MAX	END AVG	MINIMUM	MAXIMUM	DEVIATION
23.19	41.62	22.93	23.96	10.32	104.1	131.2	27.1
21.41	23.78	12.67	32.5	5.41	101.1	142	40.9
14.78	21.87	11.53	18.52	9.08	101.9	128.4	26.5
13.21	26.38	8.94	5.94	3.33	99.7	131.2	31.5
15.95	30.78	10.89	19.01	7.27	100	134.7	34.7
17.71	28.89	13.39	19.99	7.08			
3.89	7.03	4.92	8.63	2.51			
14.09	39.1	10.48	19.47	7.25	101.1	139.8	38.7
17.46	22.6	14.43	21.87	10.41	102.4	143.9	41.5
14.2	27.1	11.74	13.42	4.75	100.5	132	31.5
16.31	21.89	9.09	15.83	3.78	100.3	123.8	23.5
28.98	32.78	18.82	24.71	11.35	99.7	137.9	38.2
18.21	28.69	12.91	19.06	7.51			
5.54	6.50	3.44	4.06	2.99			
14.97	15.09	10.91	16.12	4.35	101.4	124.4	23
12.07	13.68	7.5	6.65	3.86	100.8	119.5	18.7
14.13	17.84	13.16	12.1	7.46	101.1	147.7	46.6
15.58	16.52	12.28	22.34	10.09	101.1	149.9	48.8
15.1	20.83	12.87	15.92	7.54	101.9	140.9	39
14.37	16.79	11.34	14.63	6.66			
1.24	2.45	2.07	5.17	2.30			
15.27	22.05	15.66	21.71	12.33	100.3	170.7	70.4
12.02	13.77	6.97	12.5	7.76	101.1	133.3	32.2
13.25	13.05	8.29	12.11	6.7	101.6	126	24.4
13.19	17.46	9.6	14.48	8.41	101.1	135.2	34.1
13.43	16.58	10.13	15.20	8.80			
1.17	3.57	3.33	3.86	2.13			
16.83	18.59	10.05	44.76	14.45	85.4	102.4	17
20.28	31.22	17.35	43.84	15.12	100.5	114	13.5
13.49	19.71	11.22	59.34	15.02	99.19	112.7	13.51
14.22	17.97	10.82	16.57	9.06	100	117.3	17.3
19.18	19.76	12.79	23.37	15.86	100.8	133.3	32.5
16.80	21.45	12.45	37.58	13.90			
2.66	4.93	2.61	15.54	2.46			
32.67	29.55	15.23	32.1	15.8	199.2	223.6	24.4
48.84	56.89	26.44	69.71	37.23	184	205.1	21.1
40.63	43.04	24.41	27.9	7.65	199.5	231.2	31.7
30.32	43.58	23.44	16.28	9.41	198.1	224.4	26.3
22.38	35.46	15.31	24.33	9.04	200.5	223.6	23.1
34.97	41.70	20.97	34.06	15.83			
9.05	9.19	4.75	18.57	11.07			
31.93	41.99	21.69	29.56	15.68	198.9	229.3	30.4
19.2	15.6	10.56	17.9	9.34	197.8	224.1	26.3
31.11	36.07	20.14	23.03	9.32	197.6	232.2	34.6
36.07	27.04	16.72	26.27	13.5	201.1	231.7	30.6
32.29	41.36	22.37	43.68	15.58	193	275.6	82.6
30.12	32.41	18.30	28.09	12.68			
5.72	9.97	4.33	8.69	2.85			

TEST NUMBER	COMMENT		VELOCITY DOWNLOAD	BLADE ANGLE	OVERALL MAX	OVERALL AVG	BEGIN MAX
208					52.66	14.85	52.66
209			0.1 in/sec		32.93	14.3	32.93
210	Concrete		150 lbf		44.6	14.02	44.6
211				15(SS)	61.36	21.02	61.36
212					44	16.85	44
				AVERAGE	47.11	16.21	47.11
				STAND DEV	9.50	2.60	9.50
	DIG-IN		0.1 in/sec				
213			250				
214	D-I	C	250	30(SS)			
215			300				
216	D-I	A	250	30(SS)			
217			300				
218	D-I	A	250	45(SS)			
219			300				
220	D-I	A	300	15(SS)			
222	D-I	A	250	0(SS)			
223			300				
224	D-I	A	250	15(SS)			
225			300				
226	D-I	C	250	15(SS)			
227			300				
228	D-I	C	250	0(SS)			
229			300				
	PRECONDITIONED						
230	100 lbf						
231	100		0.1 in/sec				
232	150	A	150 lbf				
233	150			30(SS)			
234	200						
235	100		0.1 in/sec				
236	100		150 lbf				
237	150	C		30(SS)			
238	150						
239	200						
240							
241			0.1 in/sec				
242	Asphalt		200 lbf				
243				30(SS)			
244							

BEGIN AVG	MIDDLE MAX	MIDDLE AVG	END MAX	END AVG	MINIMUM	MAXIMUM	DEVIATION
18.94	22.75	15.49	18.95	10.27	150.7	187	36.3
17.64	28.03	15.21	17.11	10.15	145	174	29
17.98	21.45	13.99	22.92	10.25	149.6	168	18.4
31.05	25	16.98	26.33	15.4	149.3	188.6	39.3
20.05	25.66	15.02	29.39	15.58	146.9	206.2	59.3
21.13	24.58	15.34	22.94	12.33			
5.03	2.30	0.96	4.54	2.58			

TEST NUMBER	COMMENT	VELOCITY DOWNLOAD	BLADE ANGLE	OVERALL MAX	OVERALL AVG	BEGIN MAX
245						
246		0.1 in/sec				
247	Concrete	200 lbf				
248			30(SS)			
249						
250				138.45	18.21	138.45
251		0.1 in/sec		88.7	12.33	88.7
252	Concrete	150 lbf		88.03	9.05	88.03
253			0(SS)	71.64	12.78	71.64
254				80.09	22.28	80.09
			AVERAGE	93.38	14.93	93.38
			STAND DEV	23.37	4.71	23.37
255				97.44	11.33	97.44
256		0.1 in/sec		38.84	12.6	38.84
257	Asphalt	150 lbf		48.9	13.73	48.9
258			0(SS)	157.51	12.84	157.51
259				50.52	11.67	50.52
			AVERAGE	78.64	12.43	78.64
			STAND DEV	44.35	0.86	44.35
260				79.88	23.05	79.88
261		0.1 in/sec		44.57	12.36	44.57
262	Asphalt	150 lbf		44.6	14.72	44.6
263			45(SS)	41.63	12.82	41.63
264				50.99	14.48	50.99
			AVERAGE	52.33	15.49	52.33
			STAND DEV	14.11	3.89	14.11
265				18.62	11.82	18.62
266		0.1 in/sec		24.23	14.25	24.23
267	Concrete	150 lbf		22.15	13.19	22.15
268			45(SS)	37.48	13.42	37.48
269				21.67	13.09	21.67
			AVERAGE	24.83	13.15	24.83
			STAND DEV	6.57	0.78	6.57
	PRECONDITIONED					
270	(300 lbf)			46.09	14.23	46.09
271		0.1 in/sec		27.76	12.99	27.76
272	Concrete	150 lbf		40.7	14.25	40.7
273			30(SS)	59.58	16.71	59.58
274				33.03	14.63	33.03
			AVERAGE	41.43	14.56	41.43
			STAND DEV	11.04	1.21	11.04
275				57.91	15.51	57.91
276		0.1 in/sec		43.31	14.73	43.31
277	Asphalt	150 lbf		72.74	16.08	72.74
278			30(SS)	62.17	13.84	62.17
279				54.96	13.68	54.96
			AVERAGE	58.22	14.77	58.22
			STAND DEV	9.59	0.93	9.59

BEGIN AVG	MIDDLE MAX	MIDDLE AVG	END MAX	END AVG	MINIMUM	MAXIMUM	DEVIATION
23.79	36.95	18.14	29.29	12.87			
11.74	30.79	13.99	32.79	11.21			
13.91	11.97	7.38	11.64	5.86	146.5	163.2	16.65
21.99	29.49	12.1	6.85	4.29	144.3	177.6	33.3
33.01	34.91	19.43	27.24	14.5	149.9	198.7	48.84
20.89	28.82	14.21	21.56	9.75			
7.60	8.85	4.33	10.32	3.98			
13.91	28.39	11.08	14.37	9.03	149.9	182.04	32.19
15.48	23.16	13.23	16.06	9.13	148.74	180.93	32.19
19.09	21.73	13.56	19.25	8.6	149.85	177.6	27.75
13.66	22.64	10.65	25.61	14.2	147.63	168.72	21.09
18.42	21.12	10.23	10.39	6.35	149.85	167.6	17.76
16.11	23.41	11.75	17.14	9.46			
2.26	2.59	1.37	5.11	2.58			
36.27	24.6	15.61	30.02	17.69			
15.75	17.65	11.63	15.19	9.83	149.85	174.3	24.42
17.7	21.5	15.08	20.04	11.49	150.95	184.26	33.3
17.18	19.55	13.66	16.91	7.82	150.96	179.82	28.86
18.82	17.52	14.24	16.75	10.56	148.74	186.48	37.74
21.14	20.16	14.04	19.78	11.48			
7.63	2.65	1.38	5.36	3.33			
13.24	16.7	12.91	13.43	9.38	150.96	204.24	53.28
14.2	18.43	15.77	17.49	12.78	149.85	194.25	44.4
15.35	16.83	13.48	17.58	10.83	149.85	192.03	42.18
17.73	17.07	14.08	14.92	8.63	149.85	200.91	51.06
16.47	17.31	13.37	16.82	9.56	149.85	206.46	56.61
15.40	17.27	13.92	16.05	10.24			
1.59	0.62	1.00	1.62	1.46			
17.7	21.59	16.05	17.17	9.08	149.85		
17.57	19.83	15.69	11.52	5.91	149.85		
15.23	25.02	17.66	17.03	9.89	149.85		
20.31	23.68	19.18	15.97	10.79	147.63		
17.03	23.22	17.44	20	9.57	148.74		
17.57	22.67	17.20	16.34	9.05			
1.63	1.79	1.25	2.75	1.67			
16.74	28.65	18.83	19.42	11.06	144.3		
18.47	22.85	15.85	15.29	10.03	152.1		
20.72	25.14	18.14	18.12	9.58	149.85	250.86	101.01
13.42	22.67	16.37	18.99	11.72	146.5	227.6	81.03
16.78	20.74	15.91	17.02	8.5	152.07	234.21	82.14
17.23	24.01	17.02	17.77	10.18			
2.39	2.71	1.23	1.49	1.13			

TEST NUMBER	COMMENT	VELOCITY DOWNLOAD	BLADE ANGLE	OVERALL MAX	OVERALL AVG	BEGIN MAX
	PRECONDITIONED					
280	(400 lbf)			27.29	14.34	27.29
281		0.1 in/sec		34.83	15.95	34.83
282	Asphalt	150 lbf		26.04	11.67	26.04
283			30(SS)	40.51	17.11	40.51
284				50.16	15.89	50.16
			AVERAGE	35.77	14.99	35.77
			STAND DEV	8.91	1.88	8.91
285		0.1 in/sec		27.05	13.56	27.05
286		150 lbf		61.67	16.6	61.67
287	Concrete		30(SS)	25.87	13.14	25.87
288				36.92	15.98	36.92
			AVERAGE	32.08	12.23	32.08
			STAND DEV	14.39	1.49	14.39
290				54.04	13.04	54.04
291		0.1 in/sec		42.59	18.87	42.59
292	Asphalt	200 lbf		37.99	15.6	37.99
293			30 SS	56.77	18.42	56.77
294				34.13	19.14	34.13
			AVERAGE	45.10	17.01	45.10
			STAND DEV	8.87	2.36	8.87
295				40.72	19.14	40.72
296		0.1 in/sec		27.5	14.98	27.5
297	Concrete	200 lbf		28.24	16.9	28.24
298			30 SS	65.8	18.4	65.8
299				32.33	16.3	32.33
			AVERAGE	38.92	17.14	38.92
			STAND DEV	14.24	1.48	14.24

BEGIN AVG	MIDDLE MAX	MIDDLE AVG	END MAX	END AVG	MINIMUM	DOWNLOAD MAXIMUM	DEVIATION
16.35	23.89	17.25	17.47	9.54			
21.29	19.98	14.27	20	12.49	153.18	228.66	75.48
14.02	17.93	11.07	17.36	10.06	145.41	199.8	54.39
20.38	24.94	17.26	20.3	13.82	149.85	240.87	91.02
18.53	26.69	19.23	23.74	10.08	150.96	235.32	84.36
18.11	22.69	15.82	19.77	11.20			
2.66	3.24	2.85	2.33	1.66			
15.78	22.83	15.39	21.14	9.63	150.96	224.22	73.26
23.36	21.12	14.76	21.02	11.93	149.85	222	72.15
15.51	18.74	12.96	18.4	11.03	149.85	209.79	59.94
23.43	20.63	13.6	15.24	11.16	149.85	206.46	56.61
16.15	17.31	11.91	15.63	9.08			
3.88	1.46	0.95	2.41	0.83			
20.84	20.58	12.96	8.08	5.58	197.58	249.8	52.2
25.76	23.19	19.12	19.41	11.98	199.8	280.8	81.03
16.96	23.93	17.83	20.43	12.09	196.5	276.4	79.9
21.69	25.19	19.79	22.5	13.89	202.02	281.9	79.9
21.34	26.35	21.07	23.24	15.13	199.8	298.6	98.8
21.32	23.85	18.15	18.73	11.73			
2.80	1.96	2.80	5.50	3.29			
19.33	25.91	21.32	29.35	16.82	199.8	300.8	101.01
18.85	20.66	15.68	17.03	10.56	199.8	273.1	73.3
16.98	26.89	20.35	24.07	13.41	199.8	289.7	89.9
26.31	23.23	18.65	17.63	10.4	200.9	276.4	75.5
21.79	22.41	16.25	16.83	11.06	199.8	272	72.2
20.65	23.82	18.45	20.98	12.45			
3.22	2.29	2.21	4.97	2.44			

MILD STEEL BLADE

TEST NUMBER	COMMENT	VELOCITY DOWNLOAD	BLADE ANGLE	OVERALL MAX	OVERALL AVG	BEGIN MAX
47				38.39	9.39	38.39
48				32.88	8.68	32.88
49	CONCRETE	0.1	0	27.45	7.66	27.45
50				26.71	8.02	26.71
51				37.84	9.42	37.84
54				41.85	6.85	41.85
				34.19	8.34	34.19
56				43.32	9.5	43.32
57				32.53	7.88	32.53
58	CONCRETE	0.1	30	19.17	6.68	19.17
59				18.6	11.01	18.6
60				16.17	7.48	16.17
61				16.05	4.66	16.05
62				25.49	8.64	25.49
				24.48	7.73	21.34
63				126.6	27.03	126.6
64				95.46	20.82	95.46
65	ASPHALT	0.1	0	102.2	27.01	102.24
66				51.95	21.72	51.95
67				98.66	27.51	98.66
68				101.6	22.54	101.6
				96.08	24.44	96.09
71				55.68	18.67	55.68
72				48.48	20.49	48.48
73	ASPHALT	0.1	45	29.89	19.32	29.89
74				60.81	19.31	60.81
75				37.42	21.53	37.42
				46.46	19.86	46.46
76				30.57	13.86	30.57
77				55.34	18.24	55.34
78	CONCRETE	0.1	45	76.04	23.63	76.04
79				72.55	18.24	72.55
80				50.5	19.21	50.5
81				55.71	18.18	55.71
82				44.36	21.71	44.36
83				59.08	19.87	59.08
84				38.73	20.31	38.73
				53.65	19.59	53.49
86				64.18	23.73	64.18
87				25.34	8.79	25.33
88	ASPHALT	0.1	30	29.12	9.97	29.12
89				29.45	12.21	29.45
90				27.28	11.2	27.09
				35.07	13.18	35.03

BEGIN AVG	MIDDLE MAX	MIDDLE AVG	END MAX	END AVG	MINIMUM	DOWNLOAD MAXIMUM	DEVIATION
18.37	14.45	7.81	5.53	1.84	148	187	39
18.07	16.96	7.79	8.73	0.53	149	194	45
13.58	11.87	7.23	7.2	2.35	148	191	43
13.79	16.64	8.11	7.33	2.36	148	188	40
15.58	14.42	7.42	10.56	5.46	150	198	48
11.24	20.53	9.11	5.27	0.34	149	197	48
15.11	15.81	7.91	7.44	2.15			
13.25	10.67	7.89	10.76	7.47	148	279	131
9.98	13.78	9.71	7.79	4.04	150	250	100
12.42	9.99	4.39	6.95	3.22	149	224	75
11.86	14.96	11.83	14.21	9.38	146	388	242
10.45	13.35	8.28	5.89	3.81	154	275	121
7.92	8.36	3.38	5.93	2.8	148	194	46
13.73	13.78	7.8	6.38	4.56	150	246	96
11.06	12.37	7.57	7.86	4.64			
38.18	41.54	28.59	28.66	14.73	149	219	70
41.94	31.62	15.13	15.05	6.07	147	241	94
37.51	38.03	28.02	29.37	15.93	153	279	126
32.48	33.45	20.75	20.56	12.29	150	222	72
40.24	51.21	26.24	28.62	16.52	143	230	87
29.65	48.21	23.3	23.89	14.97	148	207	59
36.67	40.68	23.67	24.36	13.42			
21.54	28.58	18.7	32.49	15.77	151	178	27
22.26	28.56	23.04	24.09	16.13	151	208	57
17.75	28.72	21.56	29.75	18.64	148	208	60
27.04	22.58	16.03	24.13	14.83	150	184	34
20	29.94	23.2	30.13	21.4	150	217	67
21.72	27.68	20.51	28.12	17.35			
19.1	18.42	12.4	14.88	10.25	150	198	48
24.8	23.31	15.88	18.39	14.25	150	214	64
31.95	29.14	22.35	26.23	16.85	148	235	87
25.88	27.91	17.09	16.97	11.97	147	209	62
21.81	33.31	22.01	21.49	13.95	149	234	85
21.03	27.93	20.58	17.2	13.07	151	213	62
28.51	33.1	22.63	20.5	14.21	149	257	108
25.66	29.12	20.09	20.13	14.05	151	195	44
25.79	28.6	20.27	22.65	15.03	149	230	81
24.78	29.99	20.45	19.82	13.71			
23.7	27.07	19.03	57.76	28.42	*		
13.48	18.78	9.39	14.58	3.65			
14.51	20.46	10.75	17.92	4.81			
11.73	24.11	16.59	18.82	8.3			
16.12	27.28	13.85	18.39	3.85			
15.91	23.54	13.92	25.49	9.81			

91				42.21	9.85	42.21
92				40.06	11.95	40.06
93	CONCRETE	0.1	15	33.04	16.6	33.04
94				33.84	8.74	33.84
95				54.83	15.8	54.83
96				38.66	12.75	38.66
97				57.08	9.86	57.08
98				46.99	9.83	46.99
				43.34	11.92	43.34
105				102.2	16.87	102.2
106				64	21.07	64
107	ASPHALT	1	0	40.35	18.6	40.35
108				34.58	9.89	34.58
109				48.97	13.87	48.97
				58.02	16.06	58.02
112				66.5	17.6	66.5
113				53.49	12	53.49
114	CONCRETE	1	0	55.68	13.87	55.68
115				97.29	13.1	97.29
116				31.52	14.91	31.52
117				61.02	18.49	61.02
				60.92	15.00	60.92
178				77.47	24.76	77.47
179				47.02	10.95	47.02
180	ASPHALT	0.1	15	64.66	15.86	64.66
181				49.44	13.21	49.44
182				39.74	13.68	39.74
				55.67	15.69	55.67

12.14	25.76	12.75	11.76	4.73	*		
17.25	14.17	11.12	13.56	7.65			
20.83	22.88	17.28	17.66	11.83			
14.05	16.64	12.23	7.59	0.16			
17.08	22.66	15.4	25.95	14.94			
19.47	20.83	12.73	20.63	6.23			
16.36	14.22	7.15	12.25	6.24			
9.77	26.68	11.45	21.53	8.27			
15.87	20.48	12.51	16.37	7.51			
25.25	22.46	15.74	22.08	9.98	140	159	19
32.25	32.32	21.35	27	10.75	151	178	27
22.7	30.3	18.46	34.62	14.91	150	160	10
12.11	17.68	11.59	11.16	6.25	150	166	16
22.97	20.12	12.15	15.52	7.64	150	184	34
23.056	24.576	15.858	22.076	9.906			
23.69	27.09	18	18.26	11.88	150	191	41
20.91	13.64	9.69	14.14	6.45	150	178	28
24.33	28.26	13.97	19.53	4.85	148	182	34
18.84	15.72	11.83	52.33	9.31	149	173	24
19.74	23.57	14.07	22.39	11.63	146	195	49
30.42	34.77	16.2	16.8	10.61	140	206	66
22.99	23.84	13.96	23.91	9.12			
32.37	43.14	22.26	36.66	19.84	101	147	46
13.91	24.37	11.95	14.26	7.15	100	123	23
18.75	25.83	17.41	21.87	11.52	97	137	40
13.19	23.44	15.15	21.95	11.29	101	129	28
16.77	22.41	13.56	20.05	10.8	101	125	24
19.00	27.84	16.07	22.96	12.12			

TEST NUMBER	COMMENT	VELOCITY DOWNLOAD	BLADE ANGLE	OVERALL MAX	OVERALL AVG	BEGIN MAX
310						
311		0.5 in/sec				
312	Asphalt	500 lbf		26.33	14.88	26.33
313			30 SS	35.04	14.86	35.04
314				28.28	15.67	28.28
			AVERAGE	22.41	11.35	22.41
			STAND DEV	13.34	6.56	13.34
315				33.46	11.37	33.46
316		0.5 in/sec		43.41	12.94	43.41
317	Concrete	500 lbf		34.11	14.51	34.11
318			30 SS	26.53	13.99	26.53
319				51.94	13.13	51.94
			AVERAGE	37.89	13.19	37.89
			STAND DEV	8.84	1.07	8.84
320				80.29	18.11	80.29
321		0.5 in/sec		94.94	14.84	94.94
322	Asphalt	500 lbf		37.91	15.84	37.91
323			00 SS	41.39	13.96	41.39
324				115.75	18.16	115.75
			AVERAGE	74.05	16.18	74.05
			STAND DEV	30.29	1.70	30.29
325				49.28	15.53	49.28
326		0.5 in/sec		37.61	14.07	37.61
327	Concrete	500 lbf		52.62	16.90	52.62
328			00 SS	42.58	14.42	42.58
329				53.06	13.85	53.06
			AVERAGE	47.03	14.95	47.03
			STAND DEV	6.02	1.13	6.02

BEGIN AVG	MIDDLE MAX	MIDDLE AVG	END MAX	END AVG	MINIMUM	DOWNLOAD MAXIMUM	DEVIATION
17.14	24.91	18.98	15.25	9.16	150.96	259.74	108.78
17.79	22.26	17.58	18.72	9.83	149.85	250.86	101.01
18.26	25.39	20.33	19.09	9.09	150.96	260.85	109.89
13.29	18.14	14.22	13.27	7.02			
7.69	10.54	8.27	7.81	4.06			
17.87	17.73	9.68	11.16	7.65	149.85	224.22	74.37
16.21	20.76	15.05	13.71	8.08	150.96	219.78	68.82
19.79	23.76	16.88	11.66	7.72	152.07	245.31	93.24
19.87	20.20	14.23	12.80	8.88	149.85	227.55	77.70
16.76	18.51	16.03	15.53	7.36	150.96	231.99	81.03
18.10	20.19	14.37	12.97	7.94			
1.51	2.10	2.51	1.56	0.52			
27.31	38.59	19.91	24.35	9.12	150.96	193.14	42.18
21.46	30.08	18.28	22.52	6.05	152.07	182.04	29.97
19.04	36.20	19.62	20.66	9.65	148.74	183.15	34.41
19.38	36.86	15.55	16.00	8.05	155.40	189.81	34.41
26.94	31.71	20.13	15.17	8.98	149.85	198.69	48.84
22.83	34.69	18.70	19.74	8.37			
3.61	3.24	1.70	3.60	1.27			
20.78	19.09	13.19	16.64	13.47	150.96	213.12	62.16
22.10	22.50	13.63	13.53	7.81	150.96	204.24	53.28
21.12	23.44	16.50	20.06	13.78	150.96	220.89	69.93
21.58	24.74	14.88	17.85	8.15	148.74	203.13	54.39
21.21	26.09	12.70	19.23	9.12	140.97	209.79	68.82
21.36	23.17	14.18	17.46	10.46			
0.45	2.37	1.37	2.29	2.62			